Modeling biological-physical feedback mechanisms in marine systems

Dissertation
zur Erlangung des Doktorgrades der Naturwissenschaften
im Fachbereich Geowissenschaften der Universität Hamburg

vorgelegt von
Sebastian Sonntag
aus
Reutlingen

Hamburg
2013

Als Dissertation angenommen vom Fachbereich Geowissenschaften
der Universität Hamburg

auf Grund der Gutachten von Prof. Dr. Inga Hense
und Prof. Dr. Carsten Eden

Hamburg, den 1. Juli 2013

Prof. Dr. Jürgen Oßenbrügge
Leiter des Fachbereichs Geowissenschaften

Abstract

The marine biosphere is an active and important component of the Earth system. Biologically induced changes in physical oceanic properties through phytoplankton cause potential positive and negative feedbacks. In particular, surface floating cyanobacteria can increase light absorption and the albedo at the ocean surface and decrease momentum input by wind.

In this thesis I study the feedbacks mediated by marine cyanobacteria on the physics of the upper ocean. Using the water column model GOTM, I set up a coupled biological-physical model to investigate local effects of the feedbacks on the mixed layer dynamics. Extending these one-dimensional studies, I use the general circulation model MITgcm and set up a three-dimensional coupled biological-physical model to study also non-local effects on the ocean circulation on a basin-wide scale.

I show that the absorption feedback by phytoplankton leads to a surface warming and a subsurface cooling. The temperature differences caused by cyanobacteria are more pronounced than those caused by other phytoplankton. The positive absorption and wind feedbacks mediated by cyanobacteria are stronger than the negative albedo feedback. Cyanobacteria mediate a local shallowing of up to 30% of the surface mixed layer due to the absorption feedback and of around 10% due to the wind feedback. By warming the ocean surface and shallowing the mixed layer cyanobacteria locally lead to environmental conditions promoting their own growth. Due to the circulation, colder subsurface waters can be transported and thus also lead to a surface cooling at other locations. Increased absorption by phytoplankton and cyanobacteria affects the meridional overturning circulation. Reduced surface wind stress mediated by cyanobacteria leads to a distortion of the subtropical gyre and to reduced subtropical downwelling and equatorial upwelling.

In a warmer environment the local effects of the absorption and the wind feedback are stronger than today. With increasing temperatures cyanobacteria shift northwards and lead to stronger effects of the biological-physical feedbacks in some regions, but weaker effects in other regions. Increasing temperatures might lead to a spread of cyanobacteria, if they are able to adapt to temperatures higher than 30°C, and thus a larger ocean region would be affected by the induced feedbacks. Yet, the model studies do not indicate a substantial increase in the area covered by cyanobacteria.

This thesis provides the first quantitative estimate of how surface floating cyanobacteria feed back on their physical environment. Overall, the results suggest that surface floating cyanobacteria and their feedbacks on light absorption and wind stress need to be taken into account in ocean models used for climate scenarios in order to capture changes in the dynamics of the upper ocean.

Contents

Chapter 1

Introduction

The dynamics of marine biota in the upper ocean is influenced to a large extent by the dynamics of the ocean surface and the light penetration. The current paradigm is that physics completely controls and, together with biochemical processes within the ecosystem, determines the spatial and temporal evolution of marine organisms. However, marine biota constitutes an important and active component of the global climate system. This active role of marine organisms in influencing their environment has been addressed and studied by assessing their effect on global biogeochemical cycles such as the carbon cycle (e.g. Denman *et al.*, 2007). Yet, the direct effects of marine biota on the physical environment have not received much attention and are far from being completely understood.

The Earth system consists of different subsystems like the atmosphere, hydrosphere, lithosphere, and biosphere. To understand the Earth as a system, it is not sufficient to study these subsystems separately. In fact, it is essential to understand the interactions between the Earth's interrelated subsystems. The understanding of these interactions is particularly crucial for studying the potential future evolution of the state of our planet. Earth system models are a valuable tool to investigate past, present, and future states of Earth and are used for projections of future climate. Although by far not all relevant processes are taken into account in these models, they are able to simulate realistic states of the Earth system. Yet, they might have this ability for the wrong reasons, since they do not consider all substantial interrelations between relevant subcomponents. When using Earth system models for projections, feedbacks between subsystems need to be taken into account. It is therefore of utmost importance to shed light on interrelations and feedbacks between subsystems of the Earth.

The aim of this thesis is to gain a better understanding of feedbacks between marine biota and the physics of the upper ocean.

1.1 | Marine biota in the Earth system

Marine ecosystems The marine ecosystem can be described as the system of all living marine organisms and their interaction with the environment. These interactions are sometimes rather direct, relatively well known and straightforward to describe quantitatively, but more often they are not known in detail or hardly possible to measure or it is just not feasible to describe all the involved mechanisms. Light and nutrients are two fundamental factors which are of particular importance for marine ecosystems. One of the key biological components within the marine system is phytoplankton. These passively drifting or wandering organisms are small, primarily microscopic, algae that carry out photosynthesis. They are the drivers of biogeochemical cycles and as primary producers form the basis of the marine food web. That is, the absorption of solar energy by photosynthetic pigments like chlorophyll enables them to convert inorganic material into new organic compounds. The links from this primary production to higher trophic levels are provided via the food web.

Marine cyanobacteria Cyanobacteria are an important group of phytoplankton and are also known as blue-green algae. Cyanobacteria are found in almost all aquatic habitats. Probably the most abundant cyanobacterium in the open ocean is *Trichodesmium* (e.g. Capone *et al.*, 1997). These microorganisms are able to generate gas vacuoles to control their buoyancy. By floating to the surface they can build very large surface mats with high concentrations of matter. Since they are diazotrophs, which means that they are able to fix atmospheric nitrogen gas (N_2) into a more usable form, they can grow without external sources of fixed nitrogen (e.g. Zehr, 2011). Throughout this thesis, I will refer to surface buoyant N_2-fixing cyanobacteria species when speaking of cyanobacteria.

Cyanobacteria are a major component of the global nitrogen cycle and are responsible for a large part of the nitrogen input into the marine system. They influence the nitrogen availability for other phytoplankton and thereby affect the whole marine ecosystem (e.g. Gruber and Sarmiento, 1997; Karl *et al.*, 2002). Cyanobacteria are widely found in tropical and subtropical ocean regions with low nutrient levels (e.g. Capone *et al.*, 1997). They are most abundant in conditions of stable stratification of the water column, can tolerate temperatures between 20 and 34°C (LaRoche and Breitbarth, 2005) and have high optimal temperatures for growth (Stal, 2009). Because of their ability to fix N_2 they have an advantage compared to other phytoplankton that depend on the supply of nutrients. Since in the open ocean this nutrient supply is realized through upwelling of water from deeper layers or strong vertical mixing, cyanobacteria benefit from calm, stably stratified conditions. By floating to the surface, cyanobacteria have an additional benefit compared to other phytoplankton in the competition for light.

Cyanobacteria are expected to expand their range in the future under globally increasing temperatures (Breitbarth *et al.*, 2007; Paerl and Huisman, 2008) and increasing stratification (Doney, 2006). Since increases in carbon dioxide levels also can promote nitrogen fixation by cyanobacteria, their influence on the global nitrogen cycle can be

expected to increase even more at future higher carbon dioxide levels (e.g. Hutchins *et al.*, 2007). Collectively, cyanobacteria are suggested to be one of the "winners" of future anthropogenic climate change (Hutchins *et al.*, 2009).

Biological-physical interactions in marine systems The interactions between marine biota and the environment can be divided into a biogeochemical and a physical part (Figure 1.1): The biogeochemical part is mediated by marine organisms taking up and releasing chemical substances. Marine organisms are thus a key component of global biogeochemical cycles, which are an integral part of the climate system. The physical part is mediated by marine organisms altering the optical and mechanical properties of the ocean. The optical properties can be altered by changes in the ocean surface albedo (e.g. Holligan *et al.*, 1983) and the absorptivity (e.g. Sathyendranath *et al.*, 1991). Mechanical properties in the ocean can be changed by surface mats of biogenic matter, affecting the surface wind drag of the ocean (e.g. Deacon, 1979), and also by the generation of turbulence in the ocean by swimming animals (e.g. Huntley and Zhou, 2004). Changes in the ocean surface albedo and in the absorptivity of the seawater have a direct effect on light penetration and heat redistribution and thereby affect the water temperature. Changes in the surface wind drag lead to altered turbulent mixing by breaking surface waves and additional generation of turbulence affect the mixing in the ocean interior. These changes in temperature and mixing have an impact on ocean stratification and mixed layer dynamics and also can lead to altered circulation patterns. Since the physical properties in turn affect the dynamics of marine biota, several positive or negative feedback loops can emerge.

In this thesis I investigate biological-physical interactions with a focus on feedback loops within the marine system. In particular, I study the influence of cyanobacteria on their environment by modeling the optical and mechanical impacts on the ocean system. A detailed survey on studies about general direct effects of marine biota on its physical environment is given in Appendix B.

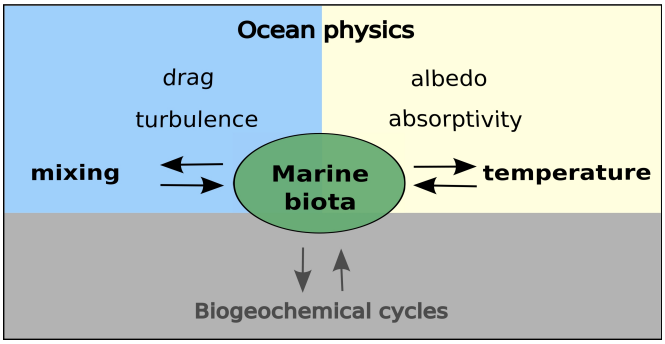

Figure 1.1.: Mechanisms and processes involved in feedbacks between marine biota and ocean physics.

1.2 | Biological-physical feedbacks involving cyanobacteria

Marine organisms can influence upper ocean properties and alter light absorption, the ocean surface albedo, and turbulent mixing by wind. These modifications in absorption, albedo and wind mixing due to cyanobacterial mats at the ocean surface (Figure 1.2) may induce other changes that feed back positively or negatively on cyanobacteria.

Absorption feedback The absorption of solar energy in the ocean is dominated by the absorption by seawater itself. The variability in absorption and the radiative transfer in the upper layers of the open ocean is controlled primarily by phytoplankton pigment concentrations (e.g. Smith and Baker, 1978; Lewis *et al.*, 1990). Even though the effects of light absorption by marine phytoplankton on their physical environment have been investigated quite intensively in the last years using models of different complexity and with different regional or thematic focus (e.g. Oschlies, 2004; Manizza *et al.*, 2005; Wetzel *et al.*, 2006; Löptien *et al.*, 2009; Patara *et al.*, 2012), the magnitude of the resulting effects is not unequivocal. The specific role of cyanobacteria leading to higher sea surface temperature and thus to more favorable conditions for cyanobacteria growth has been studied in a shallow water environment, where the life cycle of cyanobacteria is assumed to play an important role (Hense, 2007). In the open ocean, cyanobacteria are involved in the following absorption feedback loop (Figure 1.3):

The expected increase of sea surface temperatures (SST) in many parts of the world ocean will very likely lead to enhanced stratification and decreased concentration of nutrients like nitrate in the surface mixed layer (Doney, 2006). This will lead to beneficial environmental conditions for cyanobacteria, since these do not depend on the supply of elemental nitrogen, but are able to fix dissolved molecular atmospheric nitrogen (Zehr, 2011), prefer relatively high temperatures (Breitbarth *et al.*, 2007; Paerl and Huisman, 2008) and have high optimal temperatures for growth (Stal, 2009). The higher abundances of cyanobacteria at the ocean surface will lead to increased light absorption which may lead to higher sea surface temperatures (Capone *et al.*, 1998) thereby closing this positive feedback loop.

Albedo feedback The ocean surface albedo is defined as the ratio of upward to downward short-wavelength radiation right above the sea surface and is influenced by the sun zenith angle and the ratio of diffuse and direct sunlight. Surface floating marine organisms can alter the total amount of solar radiation entering the ocean (e.g. Holligan *et al.*, 1983; Tyrrell *et al.*, 1999). The magnitude and the direction of the effect is species-dependent (Jin *et al.*, 2004), i.e., how much light can enter the water depends on the color of the organisms located at the surface. Cyanobacteria are part of the following albedo feedback loop (Figure 1.3):

An increase in cyanobacteria will likely lead to an increased ocean surface albedo (Kahru *et al.*, 1993) allowing less light to penetrate the ocean. This decrease of so-

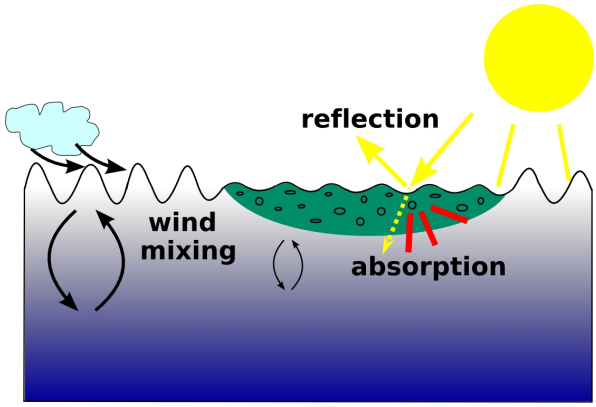

Figure 1.2.: Cyanobacterial surface mats alter the reflection and absorption of sunlight as well as the mixing induced by wind.

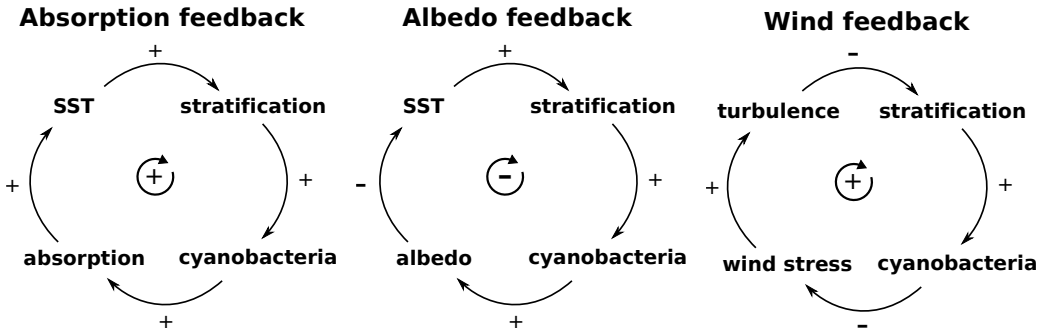

Figure 1.3.: Positive absorption feedback, negative albedo feedback, and positive wind feedback induced by cyanobacteria.

lar radiation in the water will decrease sea surface temperatures providing a negative feedback, counteracting the positive absorption feedback mechanism.

Wind feedback Turbulent mixing in the upper ocean is influenced by the fluxes of momentum, heat and freshwater across the air-sea interface and the mechanical properties of the ocean surface. The viscosity of the seawater at the ocean surface can be increased by surface floating marine organisms leading to a reduction of momentum input by wind and of turbulent mixing in the water (Hutchinson and Webster, 1994). Cyanobacteria are part of the following wind feedback loop (Figure 1.3):

Increasing abundances of cyanobacteria might lead to a decrease in turbulence levels, since the organisms build up large surface mats (Carpenter and Capone, 1992) that may decrease the momentum input from the atmosphere by wind (Deacon, 1979). Decreased turbulence will lead to less mixing and stronger stratification leading to higher sea surface temperatures resulting in a positive feedback.

In addition to these feedback mechanisms, which are described here in a one-dimensional local way, also indirect, non-local effects potentially providing feedbacks can occur. Local changes in temperature for instance can also lead to altered currents and circulation patterns having an effect on the stratification at a different location. These feedbacks need to be considered in a three-dimensional framework.

1.3 | Research questions and thesis structure

This thesis is one step to a better understanding how climate change induced alterations in the phytoplankton community composition to one with increased abundance of positively buoyant species feed back on the climate locally as well as on regional and global scales. Within this context I focus my studies on the direct effects of biology on physics, which potentially affect the climate system, and do not focus on indirect effects through changes of the biogeochemical cycles leading to biological-physical feedbacks.

The particular direct effects of marine phytoplankton on their physical environment that I study in this thesis are mediated by changes in absorption, albedo, and wind mixing. Throughout this work, with the term *feedback* I will also refer to the effect of phytoplankton on a physical property and not only to the corresponding closed feedback loop. The absorption feedback is mediated by absorbing pigments within all phytoplankton, but can have different effects depending on the distribution of a phytoplankton group. The albedo and the wind feedback, however, are only mediated by mat-building surface buoyant cyanobacteria.

The questions I specifically address in this work, are

- How do different distributions of phytoplankton groups affect the temperature structure of the upper ocean via the absorption feedback?
- What are the relative magnitudes of the effects mediated by the absorption, the albedo, and the wind feedback due to cyanobacteria?
- How do the different feedbacks influence the ocean surface mixed layer thickness locally?
- What are the non-local effects of the different feedbacks through and on ocean circulation?
- What are potential changes in the effects of the feedbacks in the future?

These questions are answered using two different model frameworks: a one-dimensional water column model and a three-dimensional basin-wide configuration.

In Chapter 2, I present experiments for the one-dimensional water column model addressing the relative magnitude of the feedbacks, the local effects on the temperature structure and mixed layer thickness, and the corresponding effects in a warming scenario.

In Chapter 3, I present experiments for the three-dimensional general circulation model addressing local as well as non-local regional and basin-wide effects of the feedbacks on the mixed layer dynamics and circulation patterns.

In Chapter 4, I address the feedbacks in three-dimensional warming scenario model simulations studying the effect of a changing phytoplankton community in response to higher temperatures and the resulting impacts on ocean physics.

Chapter 5 gives conclusions and perspectives of this work.

Technical remark While this introduction and Chapter 5 are written in the first person singular, Chapters 2, 3, and 4 are written in the first person plural.

Chapter 2

Quantification of local biological-physical feedbacks

Parts of the study presented in this chapter are published in Sonntag and Hense (2011).

In this chapter the modeling studies within a one-dimensional water column framework are described and the results are presented and discussed. For the conceptual studies presented here we use idealized biological models and idealized forcings of the physical model. The aim is to quantify the different local effects of different phytoplankton groups on the upper ocean.

In the first three sections of this chapter we describe the specific physical and biological model setups as well as the implementation of the biological-physical feedback mechanisms. (Underlying mathematical formulations, assumptions and numerical approaches used in coupled biological-physical ocean models are presented in Appendix A.) In Section 2.4 we describe and analyze the results of a control simulation and the model simulations including the biological-physical feedbacks. In Sections 2.5 and 2.6 we evaluate our model results and discuss the dependence on the specific model setup. Section 2.7 describes and analyzes simulations with and without the feedbacks in a warming scenario. In this scenario we study the effect of a changing phytoplankton community in response to higher temperature forcing in the model and the resulting impacts on ocean physics. We close this chapter with a section summarizing and discussing the main results and drawing conclusions from these model studies in a water column framework investigating the one-dimensional local biological-physical feedback mechanisms between phytoplankton and the physical environment.

2.1 | Physical model setup

We use the one-dimensional water column model General Ocean Turbulence Model (GOTM) as a framework for the hydrodynamics of the ocean with atmospheric boundary conditions as well as for the coupling of biology and physics. As cyanobacteria occur in oligotrophic ocean regions in low latitudes, we set up a scenario for a low-latitude region. We use a configuration of the physical model similar to the one described in Hense and Quack (2009). This scenario is set up for the Cape Verde region, located at about 16°N, 25°E, and uses observed and analyzed climatological mean atmospheric data from this region to drive the physical model. Initial temperature and salinity profiles are taken from WOA01 monthly objectively analyzed means (see Conkright *et al.*, 2002). For the calculation of momentum, heat and freshwater fluxes we use climatological monthly means of daily mean values of 10 m-wind velocities, 2 m-air temperature, air pressure and dew point temperature as well as cloud cover and precipitation from ERA40 reanalysis (Uppala *et al.*, 2005). In order to prescribe a meteorological forcing data set every 6 hours, we interpolate linearly between the climatological monthly mean values. We repeat the same meteorological forcing every model year. For the calculation of the fluxes we use the bulk formulae according to Fairall *et al.* (1996) and the calculation of long-wave back radiation is done according to Clark *et al.* (1974). The annual and daily cycle of the solar irradiance at the ocean surface is calculated from the geographical location via astronomical formulae and from cloud cover values according to Rosati and Miyakoda (1988). Furthermore, the local ocean surface albedo is calculated from the angle of inclination according to Payne (1972).

For the mean flow part of the model we use a constant external pressure gradient, which is interpreted as a surface elevation gradient, set to zero. Also the internal pressure gradients are set to zero. Furthermore, we start from zero initial velocities.

To account for horizontal effects and to get a stable annual cycle, we include a small relaxation term for temperature θ and salinity S to their initial values in the whole water column except for the upper 100 m with a time constant of $\tau_\theta = \tau_S = 1$ year. The depth of the water column is set to 700 m with a vertical resolution of 1 m. The timestep is set to 1 h. The values of the additional parameters for the physical part of the model chosen for this study are given in the appendix in Tables A.1 and A.2. The model framework GOTM and the specific parameterizations which we use in our studies are presented in the appendix A.2.

2.2 | Biological model setup

To study the impact of phytoplankton on the physical environment, we set up an idealized biological model. The biological model describes a nitrogen-based system of phytoplankton, a nutrient, and detritus. Depending on the parameters two different phytoplankton key groups are described, differing in growth rates, the dependence of growth on temperature, on light, and on nutrients as well as in buoyancy.

One group is nutrient dependent and neutrally buoyant (describing, e.g., picophytoplankton or picocyanobacteria), the other group is nutrient independent and positively buoyant (describing buoyant N_2-fixing cyanobacteria like, e.g., *Trichodesmium*). The growth of both groups is light-limited. Cyanobacteria growth is assumed to be nutrient-independent, since we refer to cyanobacteria that are able to fix atmospheric N_2. We do not consider potential growth limitation by micro-nutrients like phosphorus or iron, which might occur regionally (e.g. Sohm *et al.*, 2008). We rather aim at simulating conditions allowing for cyanobacteria blooms to occur. Altogether this biological model is a rather simple one, which is in a similar minimalistic form also implemented in Earth system models. However, it includes the elements most relevant for our studies.

For our model simulations we will use two different systems of equations for the source and sink dynamics of the biological state variables. One system describes the dynamics of picophytoplankton and the other system describes the dynamics of cyanobacteria. The equations describing the dynamics of the biological state variables are given by

$$\partial_t P = \mu_P \left(I_{\mathrm{PAR}}, N\right)\, P - \delta\, P \tag{2.1}$$

$$\partial_t C = \mu_C \left(I_{\mathrm{PAR}}, T\right)\, C - \delta\, C - w_C\, \partial_z C \tag{2.2}$$

$$\partial_t N = \omega\, D - \mu_P \left(I_{\mathrm{PAR}}, N\right)\, P \tag{2.3}$$

$$\partial_t D = \delta\, P + \delta\, C - \omega\, D - w_D\, \partial_z D \tag{2.4}$$

Here, $P = P\,(z,t)$, $N = N\,(z,t)$, $D = D\,(z,t)$, and $C = C\,(z,t)$ are the concentrations of the picophytoplankton, nutrient, detritus, and cyanobacteria, respectively, depending on the vertical coordinate z and the time coordinate t. For the system describing the dynamics of picophytoplankton we set $C = 0$, and for the system describing the dynamics of cyanobacteria we set $P = 0$.

The autonomous vertical upward motion of cyanobacteria is described by the constant vertical velocity w_C, the sinking of detritus is described by the constant vertical velocity w_D. The constant mortality rate is assumed to be the same for both phytoplankton species groups and is denoted by δ, the constant remineralization rate is denoted by ω. The growth rate μ_P of picophytoplankton depends on the irradiance $I_{\mathrm{PAR}}(z,t)$ of the photosynthetically active radiation (PAR) and the concentration of nutrients N, whereas the growth rate μ_C of cyanobacteria depends on $I_{\mathrm{PAR}}(z,t)$ and temperature $T = T(z,t)$. The temperature which we use here to calculate the growth rate μ_C is the temperature calculated in the physical part of the model. This calculated temperature is the potential temperature and not the in-situ temperature, which would be needed for a proper calculation of μ_C. However, compared to the uncertainty in measured values for the dependence of μ_C on temperature, the difference between potential and in-situ temperature is negligible in the relevant depth and temperature range.

We use no-flux boundary conditions at the surface and at the bottom for P, C, N, and D. In the cyanobacteria model, we account for denitrification by adding a sink term in the equation for the detritus concentration D in the bottom layer. This sink term equals the vertically integrated nitrogen fixation rate by cyanobacteria.

Note that equation 2.2 for the cyanobacteria model is decoupled from equations 2.3 and 2.4, since cyanobacteria do not take up the nutrient N. That is, we only describe growth, mortality, and buoyancy of cyanobacteria, sinking and remineralization of detritus and denitrification, but do not explicitly model the nitrogen uptake by cyanobacteria. In contrast, the system of equations for the picophytoplankton model is closed with respect to the sources and sinks. In the numerical experiments which will be described later, we use either the system of equations for picophytoplankton or the system of equations for cyanobacteria, i.e., we either describe a system only containing picophytoplankton or only containing cyanobacteria in the biological model.

Light limitation is modeled by a so-called photosynthetic irradiance (PI) curve first proposed by Smith (1936) and very widely used also today in ecosystem models:

$$l_i^I(I_{\mathrm{PAR}}) := \frac{\alpha\, I_{\mathrm{PAR}}}{\left(\mu_i^{\max 2} + \alpha^2 {I_{\mathrm{PAR}}}^2\right)^{1/2}} \tag{2.5}$$

Here, α is a constant parameter describing the initial slope of the PI curve, I_{PAR} is the irradiance of the photosynthetically available radiation, and $\mu_i^{\max}$ is the constant maximum growth rate of species group i, picophytoplankton ($i = P$) or surface buoyant nitrogen fixing cyanobacteria ($i = C$).

Limitation by nutrients is described by a hyperbolic function l_N, which was proposed by Caperon (1967) and since it has the same form as the Michaelis-Menten equation describing enzyme kinetics is also referred to by the same name, and reads

$$l_N(N) := \frac{N}{k_N + N} \tag{2.6}$$

with a constant parameter k_N specifying the half-saturation of nutrients.

For the temperature limitation function l_T a modified Gaussian function is used:

$$l_T(T) := \exp\left(-\frac{(T - T_{\mathrm{opt}})^4}{(T_1 - T_2 \operatorname{sgn}(T - T_{\mathrm{opt}}))^4}\right), \tag{2.7}$$

where T_{opt}, T_1 and T_2 describe the optimal temperature for cyanobacteria growth and the distribution around this optimum. These three parameters are assumed to be constant. The function and the parameter values we use here agree with the observed temperature dependence of growth of N_2-fixing cyanobacteria (Breitbarth *et al.*, 2007).

The actual growth rate of phytoplankton then is calculated by taking the product of the maximum growth rate and the limiting functions for the growth of the respective phytoplankton species group:

$$\mu_P = \mu_P^{\max}\, l_P^I\, l_N \tag{2.8}$$

$$\mu_C = \mu_C^{\max}\, l_C^I\, l_T \tag{2.9}$$

The initial conditions at time t_0 for the biological state variables are given as homogeneous profiles for phytoplankton, nutrients and detritus, i.e. $P(z, t_0) = C(z, t_0) = P_0$, $N(z, t_0) = N_0$, and $D(z, t_0) = D_0$.

The parameter values for the biological part of the model are given in Table 2.1.

α	=	$0.03\,\mathrm{m^2\,W^{-1}d^{-1}}$	T_{opt}	=	$28\,^{\circ}\mathrm{C}$
ω	=	$0.008\,\mathrm{d^{-1}}$	T_1	=	$5.5\,^{\circ}\mathrm{C}$
δ	=	$0.05\,\mathrm{d^{-1}}$	T_2	=	$1\,^{\circ}\mathrm{C}$
$\mu_P^{\max}$	=	$0.5\,\mathrm{d^{-1}}$	w_D	=	$-20\,\mathrm{m\,d^{-1}}$
$\mu_C^{\max}$	=	$0.25\,\mathrm{d^{-1}}$	P_0	=	$5\cdot10^{-3}\,\mathrm{mmol\,N\,m^{-3}}$
w_C	=	$0.5\,\mathrm{m\,d^{-1}}$	N_0	=	$40\,\mathrm{mmol\,N\,m^{-3}}$
k_N	=	$0.3\,\mathrm{mmol\,N\,m^{-3}}$	D_0	=	$1\cdot10^{-5}\,\mathrm{mmol\,N\,m^{-3}}$

Table 2.1.: Parameter values for the biological part of the model in the one-dimensional studies using GOTM.

2.3 | Coupling of physics and biology

In the coupled biological-physical model the growth and vertical distribution of phytoplankton depend on the physics and also the physics depends on the phytoplankton distribution. Thus our model studies include a two-way coupling of biology and physics. This coupling is mediated by changes in light absorption by both phytoplankton species as well as in surface albedo and surface wind stress changes by cyanobacteria.

The altered light attenuation and corresponding temperature changes due to absorption by biological matter is referred to as the absorption feedback. The effect of cyanobacteria on the surface reflectance, i.e., the albedo of the ocean surface, is referred to as the albedo feedback. A third feedback mechanism involves the alteration of the surface wind drag coefficient by cyanobacteria at the ocean surface. This reduction of the momentum input into the ocean by wind due to cyanobacterial mats is implemented as a reduced wind stress and is referred to as the wind feedback. In the following we describe the parameterizations of the three different biological-physical feedback mechanisms in the model.

2.3.1 | Absorption feedback

From the shortwave solar irradiance only the term describing the blue-green part of the light spectrum is used to calculate the irradiance of the photosynthetically available radiation I_{PAR}, i.e.,

$$I_{\mathrm{PAR}}(z,t) := I_0(t)\,(1-a)\,\exp\left(k_{\mathrm{w}}z\right)\,B(z,t)\,, \tag{2.10}$$

where $I_0(t)$ is the irradiance of the incoming solar shortwave radiation at the surface at time t, $(1-a)$ is the fraction that is photosynthetically usable, k_{w} is the constant absorption coefficient for seawater for this part of the spectrum, and

$$B\left(z,t\right) := \exp\left[k_{\mathrm{bio}}\int_0^z c\left(z',t\right)\,dz'\right] \tag{2.11}$$

is the bioturbidity. By including this bioturbidity here the effect of self-shading by phytoplankton is taken into account. The parameter k_{bio} is the constant absorption

coefficient of absorbing pigments within particulate matter, which is described here as the concentration $c := P + D$ or $c := C + D$, i.e. the sum of the concentrations of picophytoplankton or cyanobacteria, respectively, and detritus.

The attenuation of the shortwave irradiance I with depth is given by

$$I(z,t) = I_0(t)\, a\, \exp\left(k_{w'} z\right) + I_{\mathrm{PAR}}(z,t)\,, \tag{2.12}$$

where the first term describes the attenuation of the red part of the spectrum, specified by a constant absorption coefficient $k_{w'}$. The parameters k_w, $k_{w'}$ and a are taken from Paulson and Simpson (1977), who provide values for the parameters for different types of oceanic water that are classified according to Jerlov (1968). We use parameter values (see Table A.1) describing clear open ocean Jerlov Type I waters. For the parameter k_{bio} a value comparable to the ones used in many other studies (e.g. Hense, 2007) is chosen. To assess the sensitivity of the model to the choice of this parameter, we perform additional model experiments with different parameter values for k_{bio}, which are described in Section 2.6.

Warming of water by light absorption of phytoplankton is included as an internal source of heat through a term proportional to $\partial_z I$ in the temperature equation, thereby providing the feedback from biology to physics through altering the absorption of light.

2.3.2 | Albedo feedback

The ocean surface albedo is coupled to the cyanobacteria concentration in the top layer. That is, we compute the total ocean surface albedo α at time t according to

$$\begin{aligned} \alpha(t) &= \alpha_{\mathrm{phys}}(t) + \alpha_{\mathrm{bio}}(t) \\ \text{with} \qquad \alpha_{\mathrm{bio}}(t) &= \min\left[\alpha_{\mathrm{bio}}^{\max}, \beta\, C(z=0,t)\right]\,, \end{aligned}$$

where $\alpha_{\mathrm{phys}}(t)$ is the ocean surface albedo calculated in the physical part of the model, β and $\alpha_{\mathrm{bio}}^{\max}$ are constant parameters, and $C(z=0,t)$ is the cyanobacteria concentration in the top layer at time t. The parameter $\alpha_{\mathrm{bio}}^{\max}$ is extracted from observed data from Kahru *et al.* (1993), who measured a maximum increase of the ocean surface albedo due to surface cyanobacteria by 0.02 compared to the surrounding water. We assume that this maximum increase due to cyanobacteria is reached for a cyanobacteria surface concentration of $10\,\mathrm{mmol\,N\,m^{-3}}$ and thus set $\alpha_{\mathrm{bio}}^{\max} = 0.02$ and $\beta = 0.002\,\mathrm{m^3(mmol\,N)^{-1}}$.

To assess the sensitivity of the model to the choice of these parameters, we perform additional model experiments with different parameter values, which are described in Section 2.6.

2.3.3 | Wind feedback

The surface wind stress is coupled to the cyanobacteria concentration in the top layer. We assume that the surface wind stress is reduced by cyanobacteria at the ocean surface,

leading to the altered surface wind stress

$$\begin{aligned} \vec{\tau}(t) &= \vec{\tau}_{\mathrm{phys}}(t)\, r_{\mathrm{bio}}(t) \\ \text{with} \qquad r_{\mathrm{bio}}(t) &= \max\left[r_{\mathrm{bio}}^{\max}, (1 - \delta\, C(z=0,t))\right] , \end{aligned}$$

where $\vec{\tau}_{\mathrm{phys}}(t)$ is the surface wind stress calculated in the physical part of the model, δ and $r_{\mathrm{bio}}^{\max}$ are constant parameters, and $C(z=0,t)$ is the cyanobacteria concentration in the top layer at time t. The parameter $r_{\mathrm{bio}}^{\max}$ is taken from observations by Deacon (1979), who reports that biological surface films reduce the drag coefficient by a factor of up to three as compared to the open sea. We assume that cyanobacterial surface films (Sieburth and Conover, 1965) or mats are comparable to those reported by Deacon (1979) and that the maximum decrease by a factor of three is reached for a cyanobacteria surface concentration of $20\,\mathrm{mmol\,N\,m^{-3}}$. Thus, we set $r_{\mathrm{bio}}^{\max} = 0.33$ and $\delta = 0.033\,\mathrm{m^3(mmol\,N)^{-1}}$.

To assess the sensitivity of the model to the choice of these parameters, we perform additional model experiments with different parameter values, which are described in Section 2.6.

Note that the surface wind stress is used in two different parts of the model: As an upper boundary condition in the horizontal momentum equations and for the vertical turbulent momentum flux. Thus, a change in the surface wind stress leads to changes in the horizontal velocities and in the vertical turbulent mixing, which both lead to changes in the depth of the mixed layer. In the one-dimensional model studies described in this chapter, we will not separate these two different pathways, but will focus on the net effect of cyanobacteria surface mats on the dynamics of the surface mixed layer.

2.4 | Numerical experiments and results

To assess the biological-physical feedbacks in the system we conduct six different numerical experiments. The first four experiments are run with buoyant N_2-fixing cyanobacteria behavior, one of which does not include any feedback from biology to physics (CYA0), one including the absorption feedback only (CYA1), one including the absorption and the albedo feedback (CYA2), and one including the absorption, the albedo, and the wind drag feedback (CYA3). The other two experiments are run with picophytoplankton behavior, one without any feedback (PIC0) and one with the absorption feedback included (PIC1). The model state becomes stable with a repeating annual cycle after a spin-up of several years. In the following we describe the results of the simulations for a period of one year after the spin-up phase.

The diurnal and annual cycle of the incoming solar short wave irradiance and the annual cycle of the 10 m-wind velocity and the 2 m-air temperature are shown in Figure 2.1.

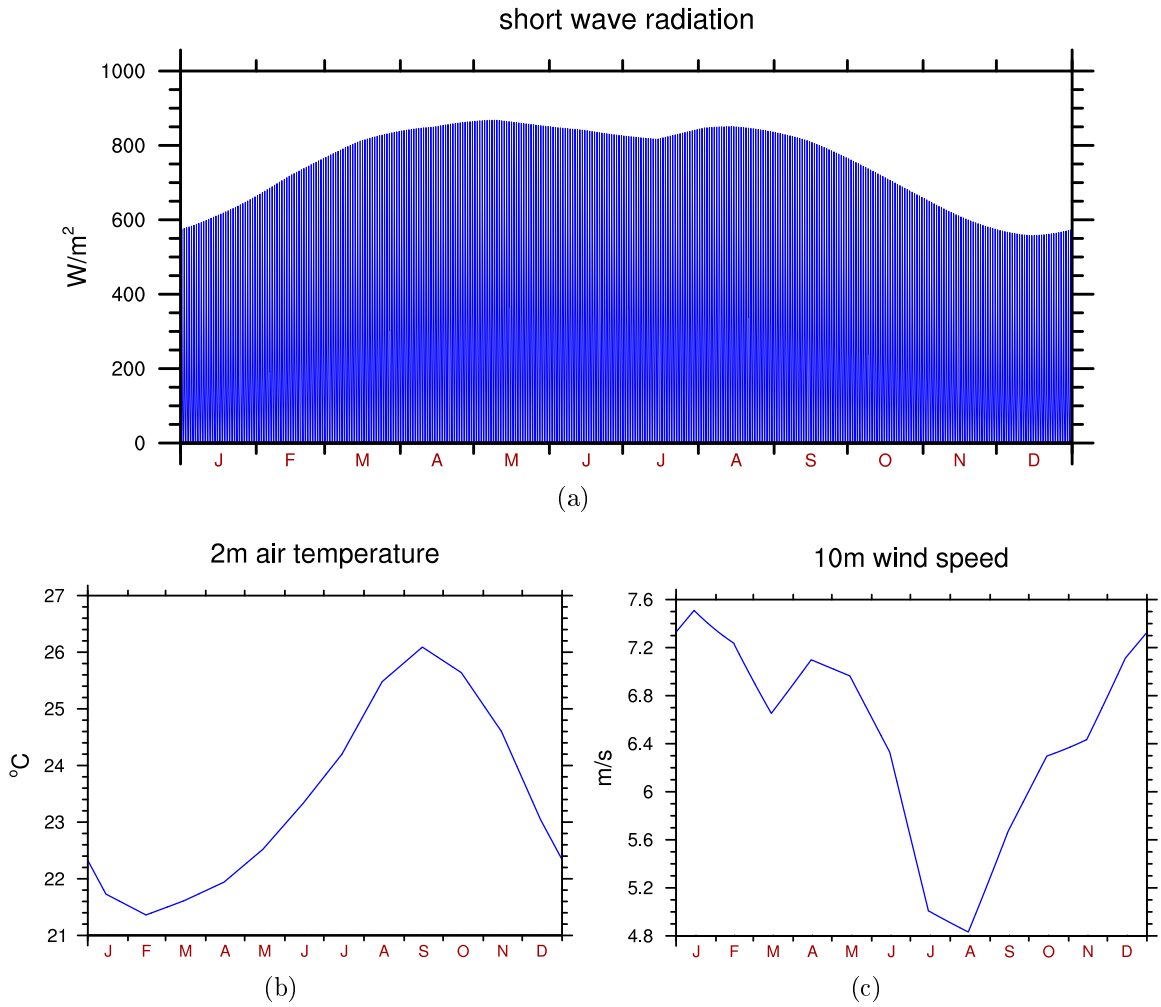

Figure 2.1.: Incoming short wave irradiance calculated from time, latitude, longitude, and fractional cloud cover (a), the 2 m-air temperature (b), and the 10 m-wind velocity (c) from linearly interpolated climatological monthly means from ERA40 reanalysis for the Cape Verde scenario.

2.4.1 | Control simulation

In the course of a year the surface layers warm up in spring due to increasing solar radiation. Maximum temperature occurs in summer (August) leading to a relatively shallow surface mixed layer. With decreasing solar irradiance and increasing mixing by wind in fall, the surface layers cool again and the annual cycle restarts (Figure 2.2). Since the warming of water due to absorption by phytoplankton pigments is not included in experiments CYA0 and PIC0, the temperature distribution is identical for both experiments.

Buoyant cyanobacteria accumulate in the surface layers in summer when the energy supply by sunlight is high and mixing is low (Figure 2.3 (a)). Picophytoplankton show a very different distribution. They build a subsurface bloom extending from spring to fall (Figure 2.3 (b)). This subsurface bloom, which is also often referred to as deep chlorophyll maximum, is formed where the concentration of nutrients and availability of light is just large enough to allow for a net growth of phytoplankton.

As expected, our model results for the physical variables and for the picophytoplankton concentrations are very similar to the results by Hense and Quack (2009) showing reasonable vertical structure of the variables compared to observations. Observed vertically integrated concentrations of neutrally buoyant picophytoplankton reach $45\,\mathrm{mmol\,N\,m^{-2}}$ (converted from data by Liu *et al.* (1997), see Section 2.5), which is in agreement with our model results (see also Figure 2.6 (d)). The typical profile of picophytoplankton showing a subsurface maximum is also reflected by the model. Observed concentrations of buoyant cyanobacteria like *Trichodesmium* within surface blooms can vary significantly (e.g. Carpenter and Capone, 1992; Westberry and Siegel, 2006). Values corresponding to surface concentrations of around $10\,\mathrm{mmol\,N\,m^{-3}}$ and even higher than $1000\,\mathrm{mmol\,N\,m^{-3}}$ (converted from data by (Capone *et al.*, 1998) as well as Carpenter and Capone (1992) and references therein, respectively, as described in Section 2.5) have been reported. Thus, the cyanobacteria abundances of 8–$27\,\mathrm{mmol\,N\,m^{-3}}$ for the maximum surface concentrations simulated by our model (see also Figure 2.6 (a)) are in a plausible range.

2.4.2 | Absorption feedback

By absorbing light at different depths in the water column, different distributions of phytoplankton have different direct effects on the temperature distribution, which can be seen in the results of the experiments including the absorption feedback (Figure 2.4). Differences in the phytoplankton distributions between experiments CYA1 and PIC1 result in higher temperatures at the surface and lower temperatures below the surface for positively buoyant as compared to neutrally buoyant phytoplankton at times when surface concentrations are high (Figure 2.4 (c)). That is, in experiment CYA1 an earlier and stronger surface warming as well as a weaker subsurface warming in spring and summer and a stronger surface cooling in fall can be seen in the model results. The simulated temperature differences reach $0.5\,^{\circ}\mathrm{C}$ at the surface and more than $-2\,^{\circ}\mathrm{C}$

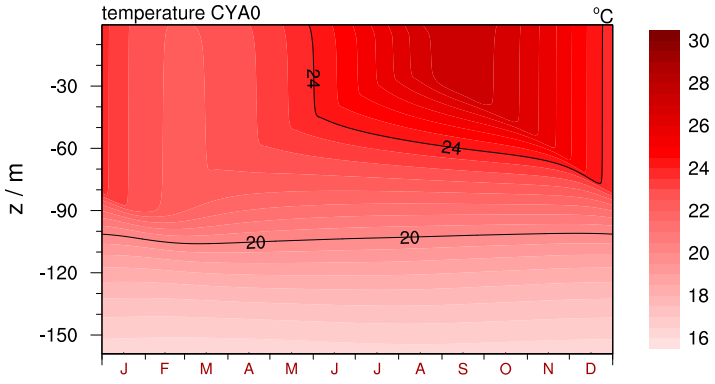

Figure 2.2.: Temperature in the upper part of the water column from January to December in experiment CYA0 and PIC0.

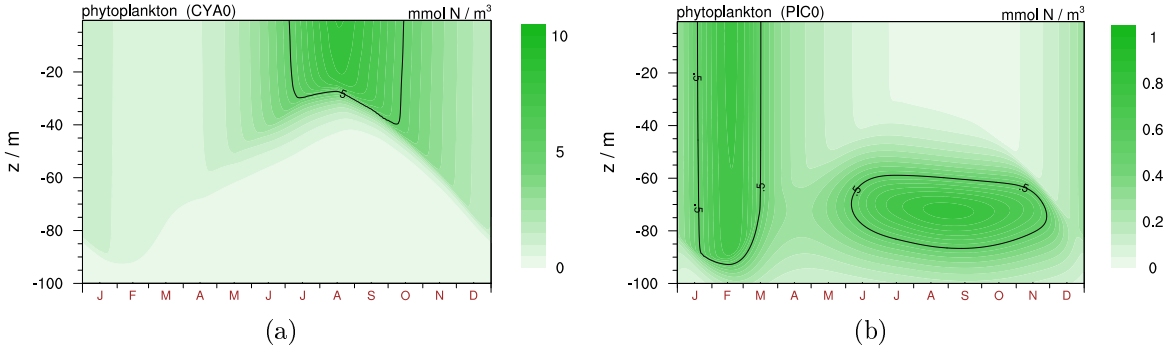

Figure 2.3.: Phytoplankton concentrations in the upper part of the water column from January to December in experiment CYA0 (a) and PIC0 (b).

subsurface.

The warming of the surface waters and a corresponding shallowing of the mixed layer (Figure 2.7 (a)) lead to higher phytoplankton concentrations in experiment CYA1 as compared to experiment CYA0 (Figure 2.6 (a) and (c)). The concentration of phytoplankton in experiment PIC1 changes only very little as compared to experiment PIC0 (Figure 2.6 (b) and (d)), since nitrogen availability instead of temperature regulates the seasonal dynamics of picophytoplankton.

These results indicate that the organisms' behavior, particularly whether they are floating at the surface (cyanobacteria) or passively drifting (picophytoplankton), play an important role in the temperature distribution and the dynamics of the surface mixed layer. Higher surface temperatures due to enhanced light absorption by surface buoyant cyanobacteria establish conditions promoting their own growth, providing a positive feedback loop within the system, which is in agreement with the study by Hense (2007).

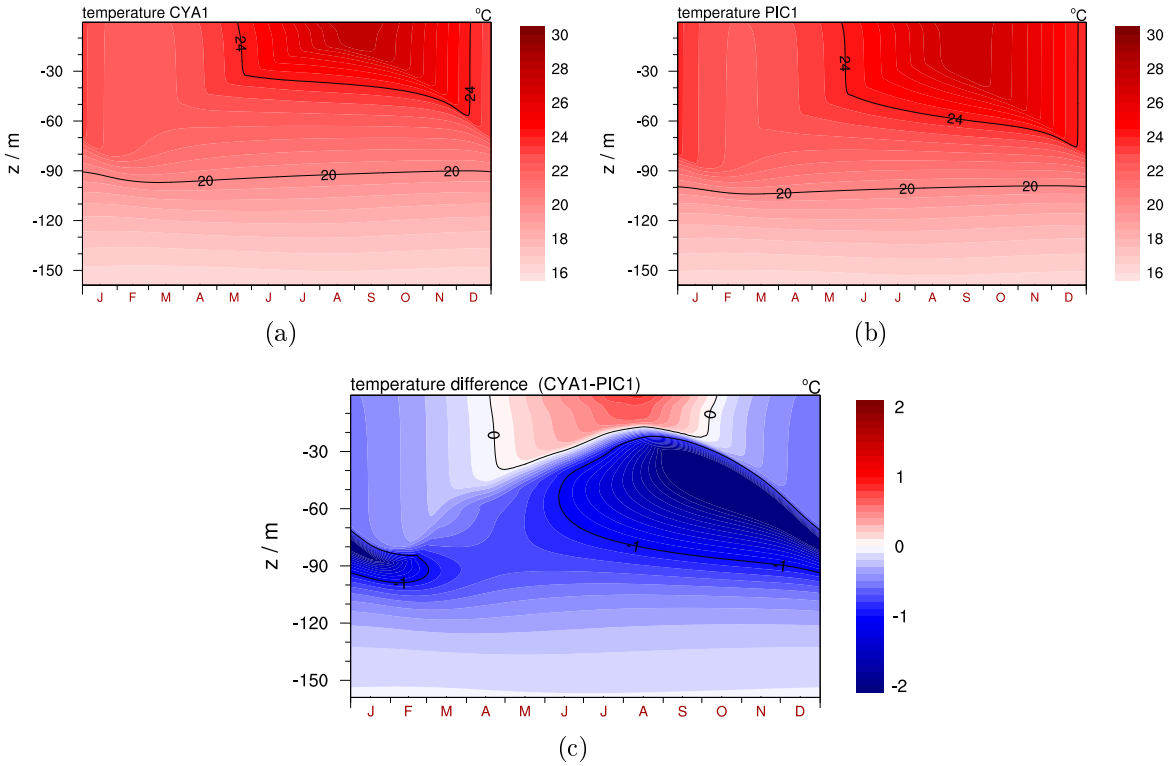

Figure 2.4.: Temperature in experiment CYA1 (a) and in experiment PIC1 (b) as well as the temperature difference between experiments CYA1 and PIC1 (c) in the upper part of the water column from January to December.

2.4.3 | Albedo and wind feedback

The temperature differences between experiments CYA2, including the feedback processes via changes in absorption and albedo, and PIC1 show a similar pattern as the differences between the experiments including the absorption feedback only. However, including the additional albedo feedback leads to slightly less pronounced temperature differences (Figure 2.5 (a)). That is, the additional effect of altered albedo reduces the magnitude of the absorption feedback, but cannot compensate for it, leaving the net feedback effect a positive one. The phytoplankton concentration is only slightly affected by the altered surface albedo in experiment CYA2 (Figure 2.6 (a) and (c)).

Including the additional feedback via decreased surface wind drag results in further changes in the temperature distribution. The stronger surface warming, the weaker sub-surface warming, and the stronger cooling in fall are all even more pronounced when including the additional wind feedback in the model (Figure 2.5 (b)).

As in the case of the absorption feedback, the higher surface temperatures promote the growth of surface buoyant phytoplankton (Figure 2.6 (a) and (c)). Also the seasonal cycle of the mixed layer depth is affected strongly by the wind feedback (Figure 2.7 (a)). Due to decreased momentum transfer from the atmosphere to the ocean leading to decreased vertical mixing a substantial shallowing of the mixed layer during summer can be seen.

In the experiments involving the neutrally buoyant phytoplankton species the mixed layer depth is affected only very slightly by including the absorption feedback (Figure 2.7 (b)).

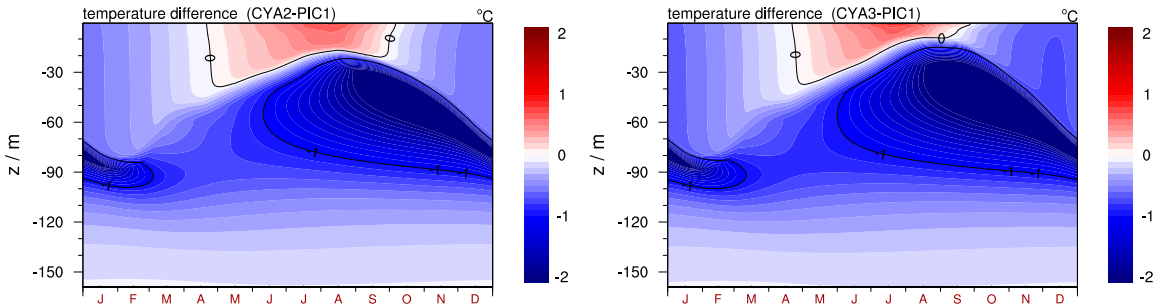

Figure 2.5.: Temperature difference between experiments CYA2 and PIC1 (a) and CYA3 and PIC1 (b) in the upper part of the water column from January to December.

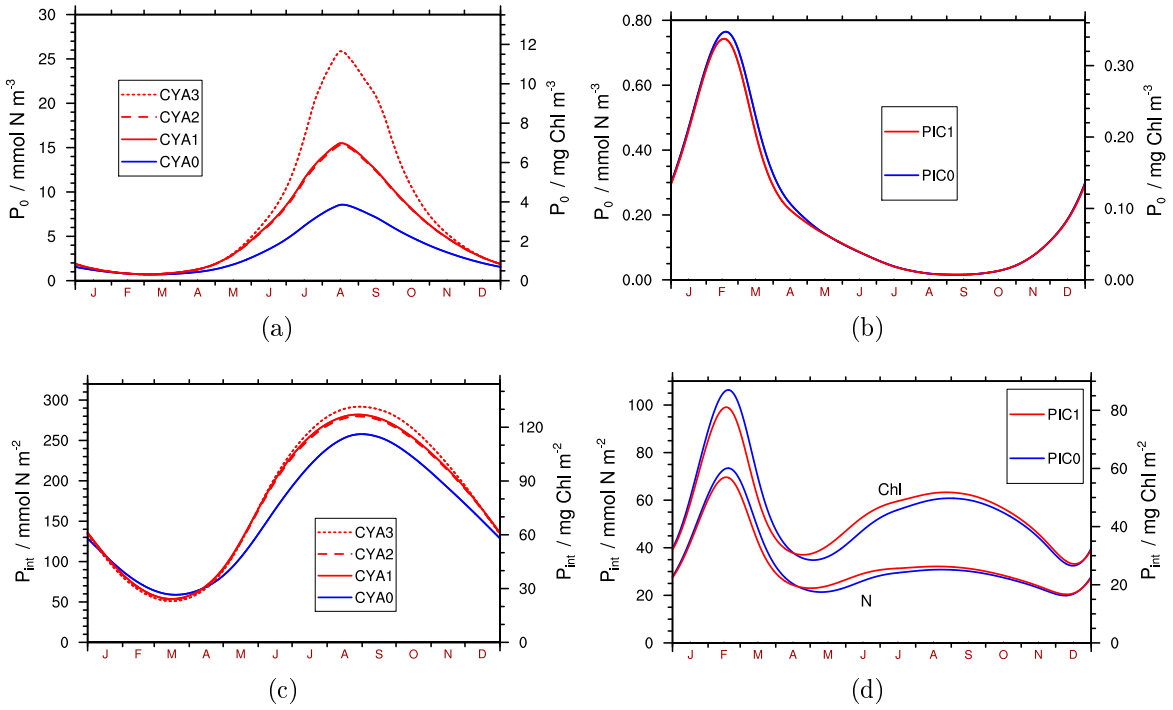

Figure 2.6.: Phytoplankton concentrations P_0 in the top layer in experiments CYA0, CYA1, CYA2, and CYA3 (a) and in experiments PIC0 and PIC1 (b) as well as vertically integrated phytoplankton concentrations $\mathrm{P}_{\mathrm{int}}$ in experiments CYA0, CYA1, CYA2, and CYA3 (c) and in experiments PIC0 and PIC1 (d). The conversion from the model unit for phytoplankton concentrations to chlorophyll (Chl) contents is done using a fixed N:Chl ratio for the buoyant cyanobacteria and a depth-dependent N:Chl ratio for the picophytoplankton.

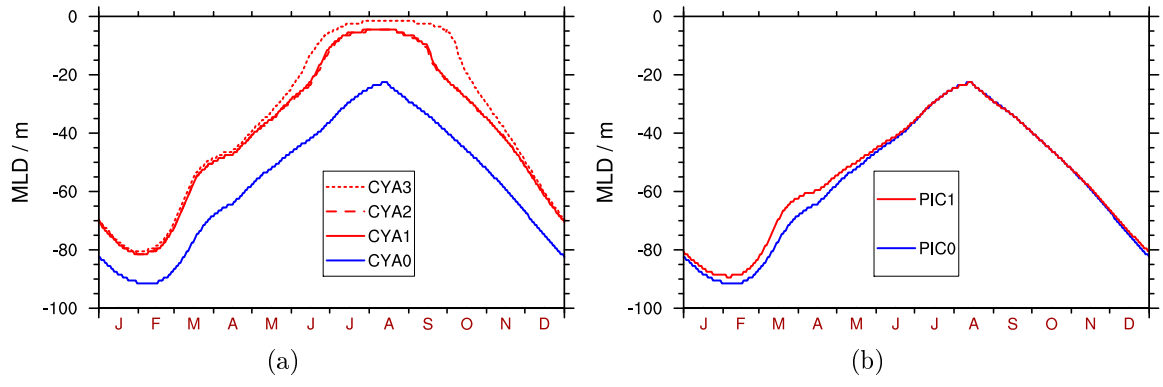

Figure 2.7.: Mixed layer depths (MLD) in experiments CYA0, CYA1, CYA2, and CYA3 (a) and in experiments PIC0 and PIC1 (b), calculated from a temperature criterion with $\Delta T = 0.2\,^{\circ}\mathrm{C}$.

2.5 | Quantitative evaluation of the biological results

In the analysis of the model results we argue that the modeled cyanobacteria surface concentrations are in a reasonable range. We arrive at this conclusion

1) from bloom concentrations of surface buoyant cyanobacteria in the Baltic Sea, where values for the dominant buoyant N_2-fixing cyanobacteria of $6\,\mathrm{mg\,FW\,l^{-1}}$ at $20\,^\circ\mathrm{C}$ in the upper 10 m for the time period 1979 to 1993 have been reported (Wasmund, 1997). This measured concentration corresponds to a value of about $8\,\mathrm{mmol\,N\,m^{-3}}$, assuming that $1\,\mathrm{mg\,FW\,l^{-1}}$ corresponds to $110\,\mu\mathrm{g\,C\,l^{-1}}$ and using the Redfield-ratio $\mathrm{C:N} = 6.625$ for the conversion into nitrogen units.

and 2) from tropical open ocean observations of the N_2-fixing buoyant cyanobacteria species *Trichodesmium*, which typically occurs in the upper 5 to upper 15 m of the ocean (Carpenter *et al.*, 2004; Capone *et al.*, 2005). The concentrations within the bloom can vary significantly (e.g. Carpenter, 1983; Carpenter and Capone, 1992; Westberry and Siegel, 2006). In surface slicks in the Arabian Sea, the concentrations could reach 17,000 trichomes $\mathrm{l^{-1}}$ (Capone *et al.*, 1998). This concentration corresponds to about $12\,\mathrm{mmol\,N\,m^{-3}}$, assuming a value of 10 ng N per trichome. However, concentrations even higher than $1000\,\mathrm{mmol\,N\,m^{-3}}$ in the upper 0.5 m have been reported (see Carpenter and Capone (1992) and references therein; assuming the conversion factors mentioned above).

The annually averaged and vertically integrated concentrations for picophytoplankton simulated by our model are in the order of $40\,\mathrm{mmol\,N\,m^{-2}}$. This agrees well with observed values for the dominant picophytoplankton/picocyanobacteria species *Prochlorococcus* of up to 6.74×10^9 cells (Liu *et al.*, 1997) or $45\,\mathrm{mmol\,N\,m^{-2}}$, assuming a value of 53 fg C per cell (Campbell *et al.*, 1997) and the Redfield-ratio.

For the surface buoyant nitrogen fixing cyanobacteria, our model simulates maximum values for the vertically integrated concentration of up to $300\,\mathrm{mmol\,N\,m^{-2}}$ and surface concentrations of up to $27\,\mathrm{mmol\,N\,m^{-3}}$. These model results are compatible with the observed values mentioned above.

The conversion of the modeled phytoplankton concentration in units of nitrogen to chlorophyll content is done using measurements from Carpenter *et al.* (2004) for the buoyant cyanobacteria and using a depth dependent carbon to chlorophyll ratio as motivated by Hense and Beckmann (2008) for the picophytoplankton / picocyanobacteria. Carpenter *et al.* (2004) measured 21 ng Chl per colony and $1.17\,\mu\mathrm{g\,N}$ per colony as well as 38 ng Chl per colony and $0.82\,\mu\mathrm{g\,N}$ per colony of buoyant cyanobacteria. These values correspond to an average value of $0.45\,\mathrm{mg\,Chl\,(mmol\ N)^{-1}}$, i.e., we do the conversion of cyanobacteria concentrations C according to

$$\mathrm{Chl}(z,t) = 0.45\,\mathrm{mg\,Chl\,(mmol\,N)^{-1}}\,C(z,t)\,. \tag{2.13}$$

Following Hense and Beckmann (2008) we use the conversion of picophytoplankton

concentrations P according to

$$\mathrm{Chl}(z,t) = \frac{12R}{r(z)}\,\mathrm{mg\,Chl\,(mmol\,N)^{-1}}\,P(z,t)\,, \tag{2.14}$$

where R is the Redfield-ratio $R = \mathrm{C:N} = 6.625$,

$$r(z) = r_{min} + \gamma\,\exp(z/d) \tag{2.15}$$

is the C:Chl ratio, $r_{min} = 25$ is the minimum C:Chl ratio, and $\gamma = 150$ and $d = 40\,\mathrm{m}$ are parameters adjusted to fit the mean observational and modeled C:Chl ratios in Hense and Beckmann (2008).

2.6 | Sensitivity of the model

2.6.1 | Sensitivity to parameterization of the feedbacks

To study the sensitivity of our model to the parameterization of the different feedbacks, we perform additional model simulations with different parameter values in the corresponding feedback parameterizations. For all three feedbacks we perform simulations with a weak, a medium, and a strong feedback, and for the albedo and the wind feedback we perform additional simulations with an extreme feedback strength. The different parameter values used for the sensitivity studies are given in Table 2.2. The relationships between cyanobacteria surface concentration and biologically induced ocean surface albedo increase as well as surface wind stress decrease for the different parameter sets are shown in Figure 2.8.

feedback	parameter	value small	value medium	value large	value extreme	unit
absorption	k_{bio}	0.02	0.03	0.04		$\mathrm{m^2\,(mmol\,N)^{-1}}$
albedo	$\alpha_{\mathrm{bio}}^{\mathrm{max}}$	0.02	0.02	0.02	0.1	
	β	0.0004	0.002	0.01	0.01	$\mathrm{m^3(mmol\,N)^{-1}}$
wind	$r_{\mathrm{bio}}^{\mathrm{max}}$	0.33	0.33	0.33	0.1	
	δ	0.013	0.033	0.066	0.09	$\mathrm{m^3(mmol\,N)^{-1}}$

Table 2.2.: Parameter values for the absorption, albedo, and wind feedback experiments (medium) and for the corresponding sensitivity experiments describing a small, large, and extreme feedback strength.

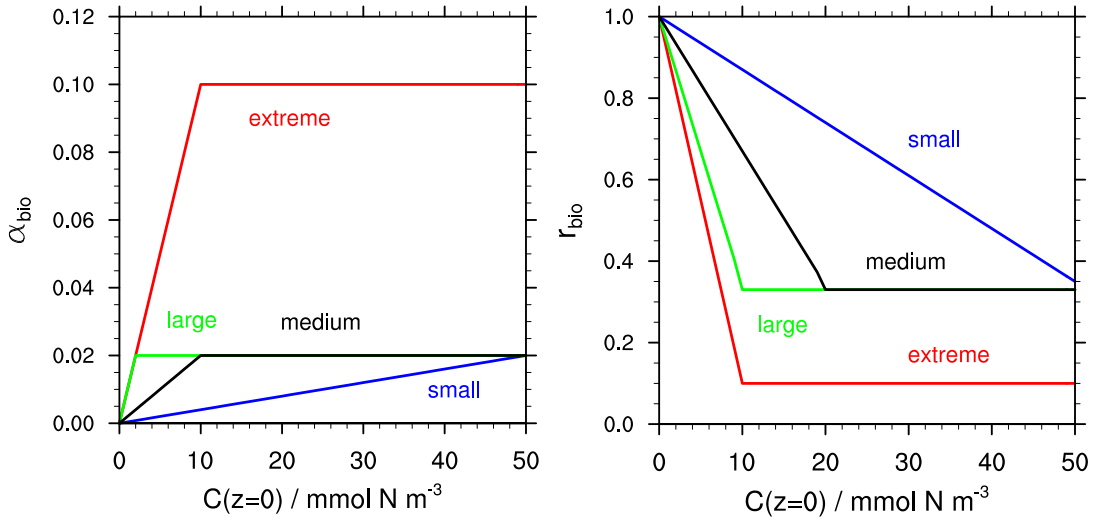

Figure 2.8.: Relationship between cyanobacteria surface concentration $\mathrm{C}(\mathrm{z}=0)$ and ocean surface albedo increase α_{bio} (left) and surface wind stress reduction r_{bio} (right) for the different sets of parameters representing small, medium, large, and extreme effects of the biologically induced feedbacks.

Absorption feedback sensitivity

In addition to the experiment CYA1, we perform model experiments also including the absorption feedback only, but using different parameter values for the absorption coefficient k_{bio} of absorbing biological matter. The mixed layer depths resulting from the different model experiments do not show any differences for the different parameter values (Figure 2.9 (a)). This might seem surprising, since a higher (lower) value of k_{bio} should lead to more (less) absorption in the layers where cyanobacteria are present and therefore also to a shallower (deeper) mixed layer. However, the parameter k_{bio} also affects the amount of light which is available for the growth of cyanobacteria. A higher (lower) value leads to less (more) available light and therefore reduced (increased) cyanobacteria growth and reduced (increased) cyanobacteria concentrations (Figure 2.9 (b)). From the model results we conclude that these lower (higher) cyanobacteria concentrations compensate the effect of higher (lower) specific absorption and subsequent stronger (weaker) warming in such a way that the sensitivity in the resulting temperature field and mixed layer depth to the value chosen for the parameter k_{bio} is essentially negligible.

Albedo feedback sensitivity

As described in Section 2.4, the effect of the albedo feedback on the mixed layer depth is very small in the model experiments. When including the albedo feedback only (experiment CYAALB), the changes in the mixed layer depth compared to the experiment CYA0 without including any feedbacks are negligible (Figure 2.10 (a)). The additional sensitivity model simulations with the albedo feedback show that even with an ex-

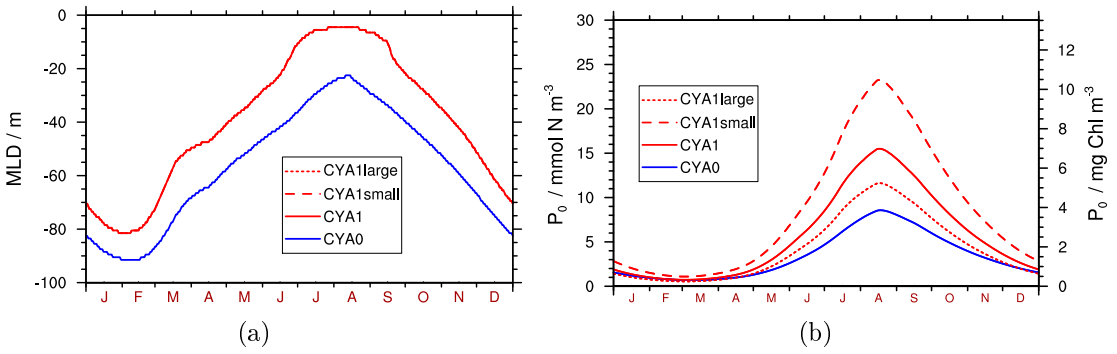

Figure 2.9.: (a) Mixed layer depths (MLD) and (b) cyanobacteria surface concentrations of the sensitivity model experiments for the absorption feedback. MLDs are calculated from a temperature criterion with $\Delta T = 0.2\,^{\circ}\mathrm{C}$.

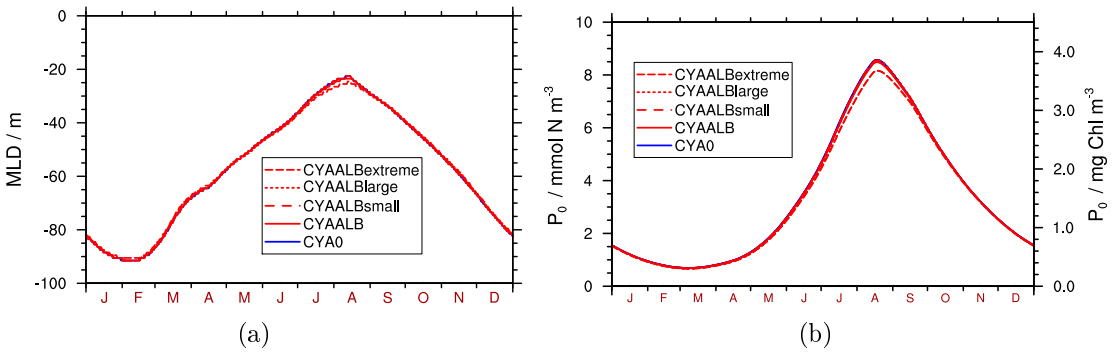

Figure 2.10.: (a) Mixed layer depths (MLD) and (b) cyanobacteria surface concentrations of the sensitivity model experiments for the albedo feedback. MLDs are calculated from a temperature criterion with $\Delta T = 0.2\,^{\circ}\mathrm{C}$.

treme assumption for the strength of the albedo feedback, the effect of including this feedback is negligible. As for the absorption feedback, there are two competing effects of changing the parameter values describing the relationship between ocean surface albedo increase and cyanobacteria surface concentration. If the effect of cyanobacteria on albedo increase is assumed to be stronger (weaker), the amount of available light for heating the water is reduced (increased), which would lead to a cooling (warming) of the surface layers and a deeper (shallower) mixed layer. At the same time, however, also less (more) light is available for cyanobacteria growth, leading to lower (higher) cyanobacteria surface concentrations and thus to a reduced (enhanced) albedo increase and therefore less deepening (less shallowing) of the mixed layer. Yet, for the albedo feedback, neither the effect on the mixed layer depth, nor on the cyanobacteria surface concentration (Figure 2.10 (b)) is sensitive to the changes in the feedback parameter in the range of values chosen here.

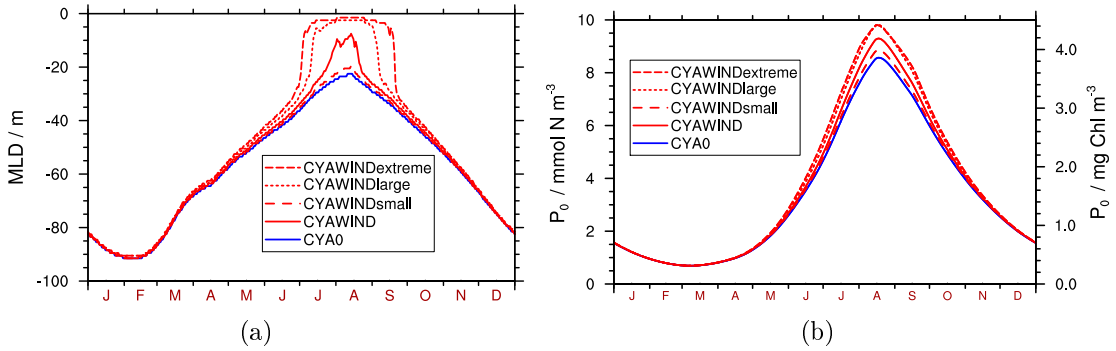

Figure 2.11.: (a) Mixed layer depths (MLD) and (b) cyanobacteria surface concentrations of the sensitivity model experiments for the wind feedback. MLDs are calculated from a temperature criterion with $\Delta T = 0.2\,^{\circ}\mathrm{C}$.

Wind feedback sensitivity

To assess the sensitivity of our model on the parameter values used for the wind feedback parameterization, we perform model experiments including the wind feedback only (experiment CYAWIND) and additional model experiments with different parameter values describing the strength of the wind feedback. The model is sensitive in the resulting mixed layer depths to a certain extent to the choice of the parameter values (Figure 2.11 (a)). A stronger (weaker) dependence of the surface drag reduction on the cyanobacteria surface concentration leads to less (more) turbulent mixing and thus to a shallower (deeper) mixed layer. Also the cyanobacteria surface concentrations in summer are sensitive to the choice of the parameter values used for the wind feedback parameterization to a certain extent (Figure 2.11 (b)). A higher (lower) value leads to slightly higher (lower) cyanobacteria surface concentrations in summer. In contrast to the absorption and the albedo feedbacks, the wind feedback does not affect cyanobacteria growth via light availability, but via changes in temperature, which are mediated by the effect of the feedback. That is, using a stronger (weaker) dependence of the surface drag reduction on the cyanobacteria surface concentration does not have a direct effect on cyanobacteria concentrations, but an indirect one via less (more) mixing and thus higher (lower) surface temperatures and therefore increased (decreased) growth. This amplification of enhanced cyanobacteria growth, however, seems to be rather limited in the model, since the cyanobacteria surface concentrations only differ slightly between the different model sensitivity experiments.

2.6.2 | Sensitivity to the atmospheric forcing

In our model studies we use climatological monthly means of daily mean values for the atmospheric forcing of the water column model. We interpolate linearly between the monthly mean values and thus do not take into account any short term variability in the forcing data. To assess the impact of short term variability in the forcing on our model

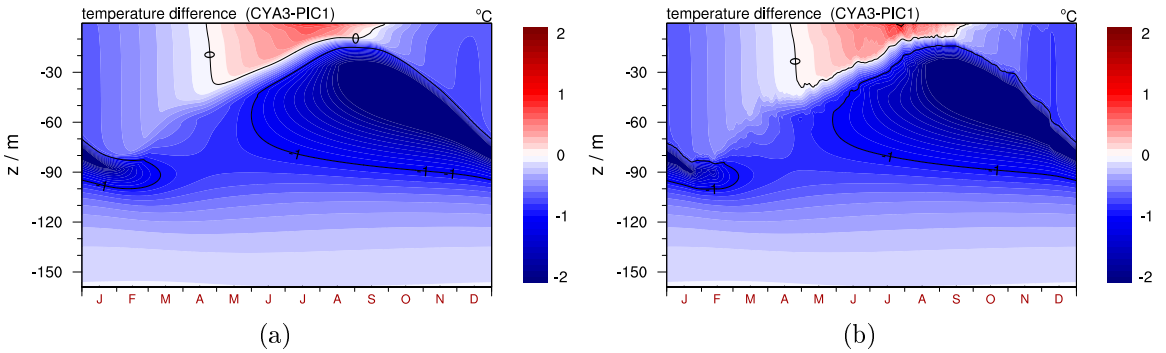

Figure 2.12.: Temperature differences between experiments CYA3 and PIC1 with monthly mean (a) and 6-hourly mean (b) atmospheric forcing.

results, we compare our model results to results from model runs with climatological 6-hourly mean atmospheric forcing including short term variability.

Since we are interested in the impact of biological processes on ocean physics, we calculate the differences in the results between model runs with and without the biologically induced feedbacks for both types of atmospheric forcing. The corresponding temperature differences (Figure 2.12) are qualitatively and quantitatively very similar for both forcing types. Thus, in order to assess the potential impact of biological disturbances on ocean physics on a climatological time scale, high frequency forcing is not essential.

2.7 | Warming scenario

Since cyanobacteria are expected to benefit from higher temperatures, we use our model setup to study the effect of a warming induced by higher atmospheric temperatures on cyanobacteria growth and the resulting changes in the effects of the different feedbacks. We use the same model setup as described in the previous sections, except for an altered temperature forcing, and repeat the previous model experiments with this altered forcing. The air temperature forcing is shifted by 3 K (Figure 2.13) to simulate higher atmospheric temperatures.

Again four experiments are run with buoyant N_2-fixing cyanobacteria behavior, one of which does not include any feedback from biology to physics (CYA0WARM), one including the absorption feedback only (CYA1WARM), one including the absorption and the albedo feedback (CYA2WARM), and one including the absorption, the albedo, and the wind feedback (CYA3WARM). In addition, two experiments are run with picophytoplankton behavior, one without any feedback (PIC0WARM) and one with the absorption feedback included (PIC1WARM). As in the previous model experiments, the model state becomes periodically stable after a spin-up of several years.

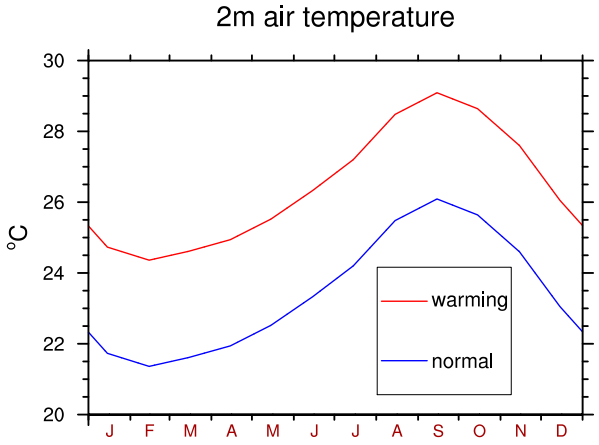

Figure 2.13.: The 2 m-air temperature from linearly interpolated climatological monthly means from ERA40 reanalysis for the present-day Cape Verde scenario (normal) and the same values shifted by 3 K used for the warming scenario (warming)

2.7.1 | Control simulation

Due to the higher air temperatures, the temperature in the upper part of the water column is altered in the warming scenario compared to the present-day Cape Verde scenario (Figure 2.15). Temperatures are generally higher in the upper 150 m of the water column with an increase of up to 1.5 °C in the surface layers.

The warming of the upper water column leads to altered growth conditions for cyanobacteria, since their growth rate depends on temperature (Figure 2.14). The higher temperatures lead to a decreased range in depth and time of the cyanobacteria's growth limitation, i.e., the phase of temperatures being high enough not to strongly limit the cyanobacteria growth in the upper water column is increased (Figure 2.16 (a)-(b)).

The reduced cyanobacteria growth limitation by temperature leads to altered cyanobacteria concentrations in the upper water column (Figure 2.16 (c)-(e)). Although the increased temperatures do not lead to increased maximum cyanobacteria concentration, cyanobacteria grow earlier in the year leading to higher values in the upper layers in spring and to higher annually integrated concentrations in the warming scenario compared to the present-day Cape Verde scenario.

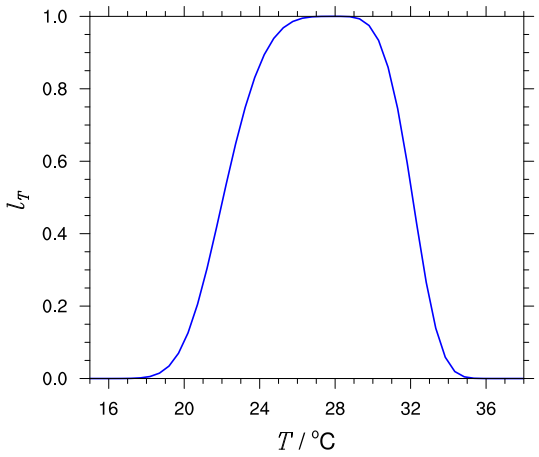

Figure 2.14.: Temperature limitation function $l_T(T)$ of cyanobacteria growth.

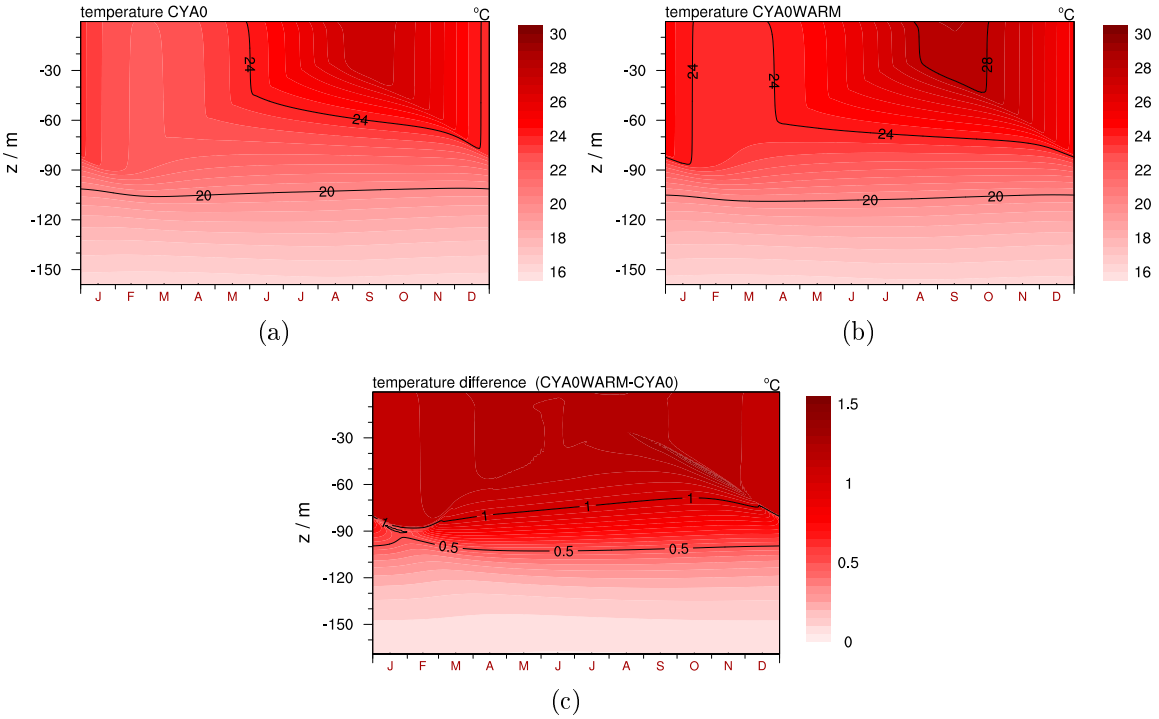

Figure 2.15.: Temperature in the upper part of the water column from January to December in experiment CYA0 for the Cape Verde scenario (a) and in experiment CYA0WARM for the warming scenario (b), and the corresponding temperature difference between experiments CYA0WARM and CYA0 (c).

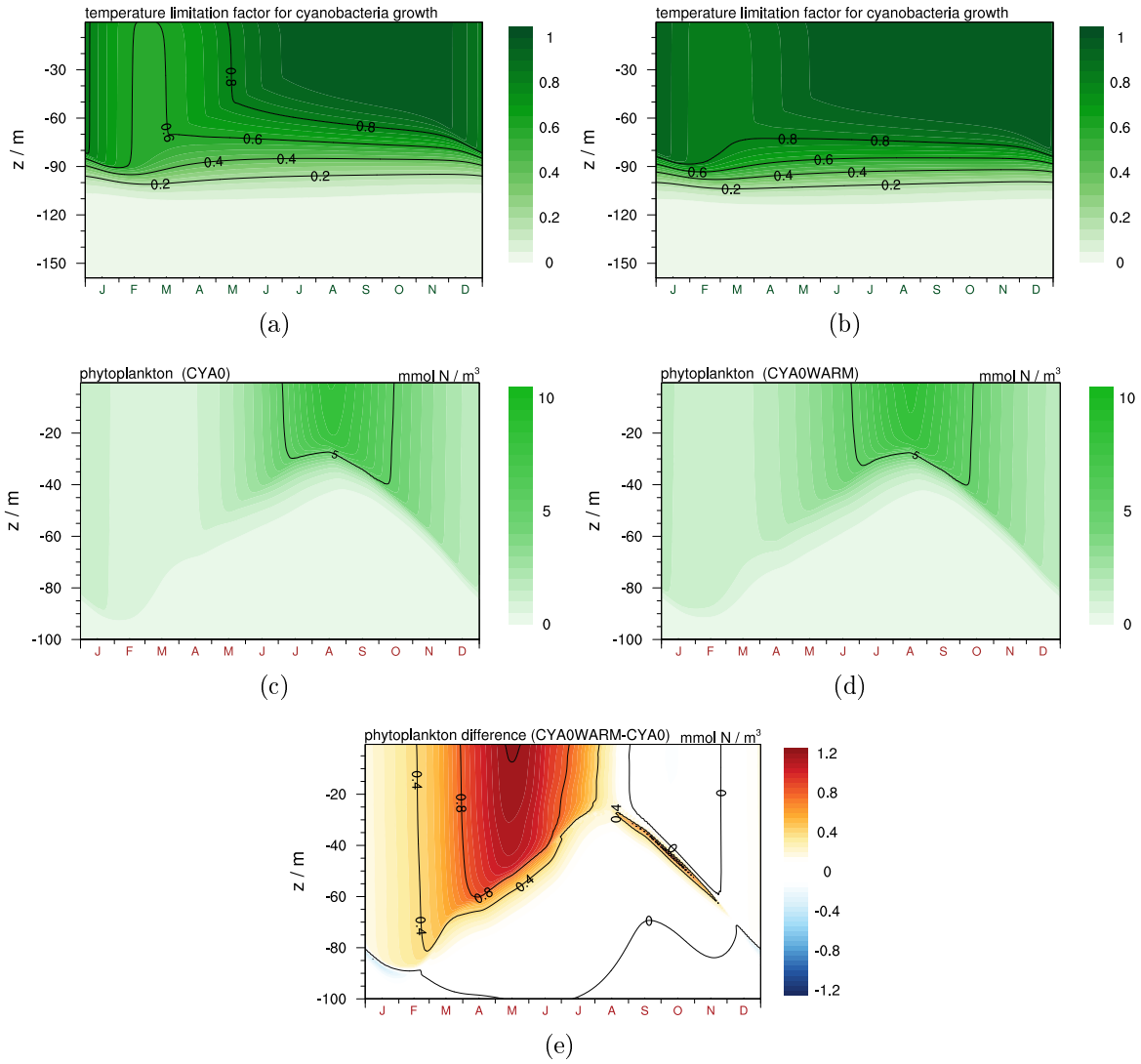

Figure 2.16.: Temperature limitation factor l_T of the cyanobacteria growth rate in experiments CYA0 (a) and CYA0WARM (b) as well as phytoplankton concentrations in experiments CYA0 (c) and CYA0WARM (d) as well as the difference between experiments CYA0WARM and CYA0 (e) in the upper part of the water column from January to December.

2.7.2 | Effect of the feedbacks

The altered cyanobacteria concentrations due to the increased temperature forcing also lead to different effects of the biological-physical feedbacks. Including the absorption feedback leads to a slightly earlier surface warming and to a subsurface cooling that is slightly stronger and penetrating deeper in the warming scenario compared to the present-day Cape Verde scenario (Figure 2.17). The small effect of including the additional albedo feedback is comparable in the warming scenario and in the present-day Cape Verde scenario in the sense that the surface warming due to the absorption feedback is only slightly reduced by the albedo feedback (Figure 2.18). Including the additional wind feedback leads to an enhanced subsurface cooling in the warming scenario compared to the present-day Cape Verde scenario (Figure 2.19).

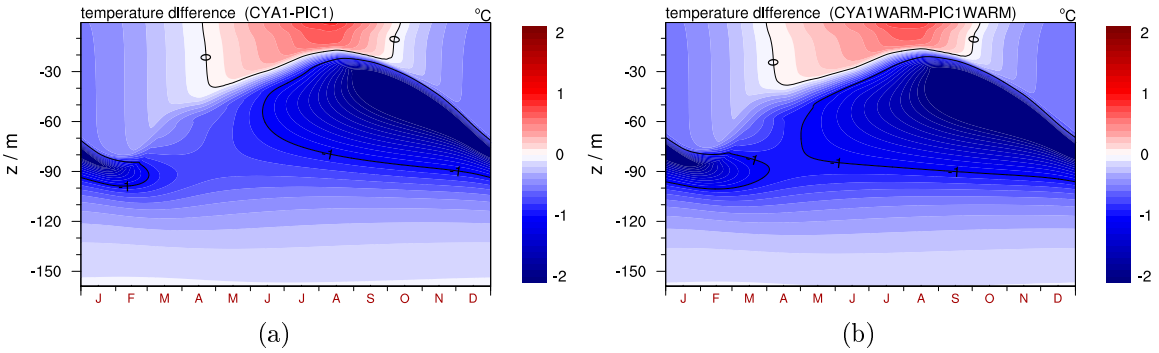

Figure 2.17.: Temperature difference in the upper part of the water column from January to December between experiments CYA1 and PIC1 (a) and between experiments CYA1WARM and PIC1WARM (b).

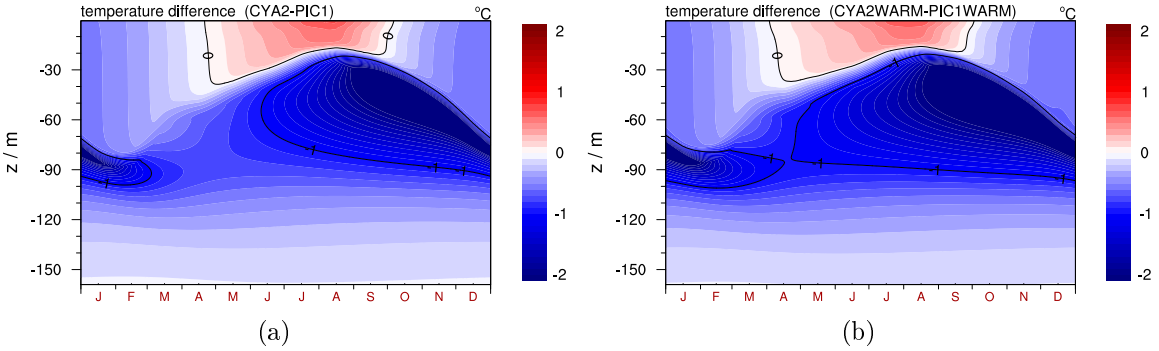

Figure 2.18.: Temperature difference in the upper part of the water column from January to December between experiments CYA2 and PIC1 (a) and between experiments CYA2WARM and PIC1WARM (b).

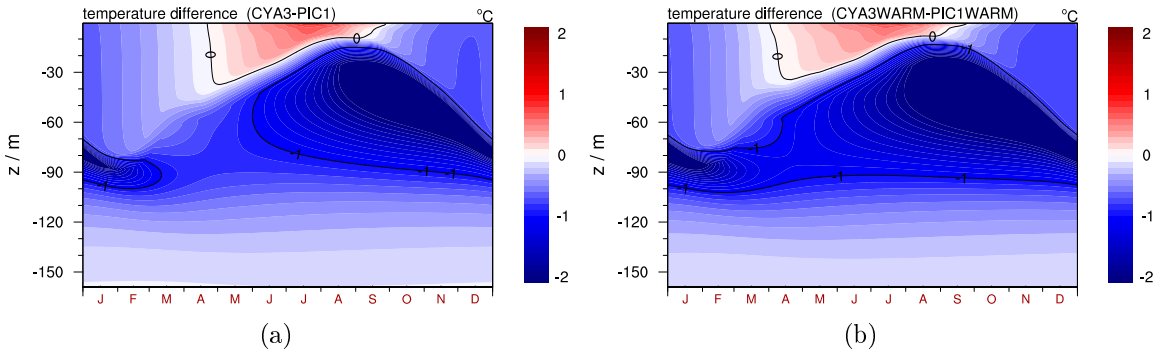

Figure 2.19.: Temperature difference in the upper part of the water column from January to December between experiments CYA3 and PIC1 (a) and between experiments CYA3WARM and PIC1WARM (b).

As in the present-day Cape Verde scenario, also in the warming scenario including the different biological-physical feedbacks leads to altered cyanobacteria concentrations (Figure 2.20). The increase in the cyanobacteria surface concentrations and in the vertically integrated concentrations when including the absorption feedback is similar in the warming scenario and in the present-day Cape Verde scenario in the maximum values. However, the increase in cyanobacteria concentrations due to the absorption feedback starts earlier in the year. Including the additional albedo feedback has a negligible effect on the cyanobacteria concentrations in both scenarios. In contrast, the increase of cyanobacteria due to the additional wind feedback starts earlier in the year, reaches slightly increased maximum values, and results in higher annually integrated values in the warming scenario compared to the present-day Cape Verde scenario.

The changes in the effects of the biological-physical feedbacks in the warming scenario also affect the mixed layer depth (Figure 2.21). The shallowing of the mixed layer due to the absorption feedback is stronger in spring in the warming scenario compared to the present-day Cape Verde scenario. Including the albedo feedback has a negligible effect on the mixed layer depth in both scenarios. The wind feedback leads to an additional shallowing of the mixed layer which is more pronounced in spring leading to a prolonged period of a shallow mixed layer in the warming scenario compared to the present-day Cape Verde scenario.

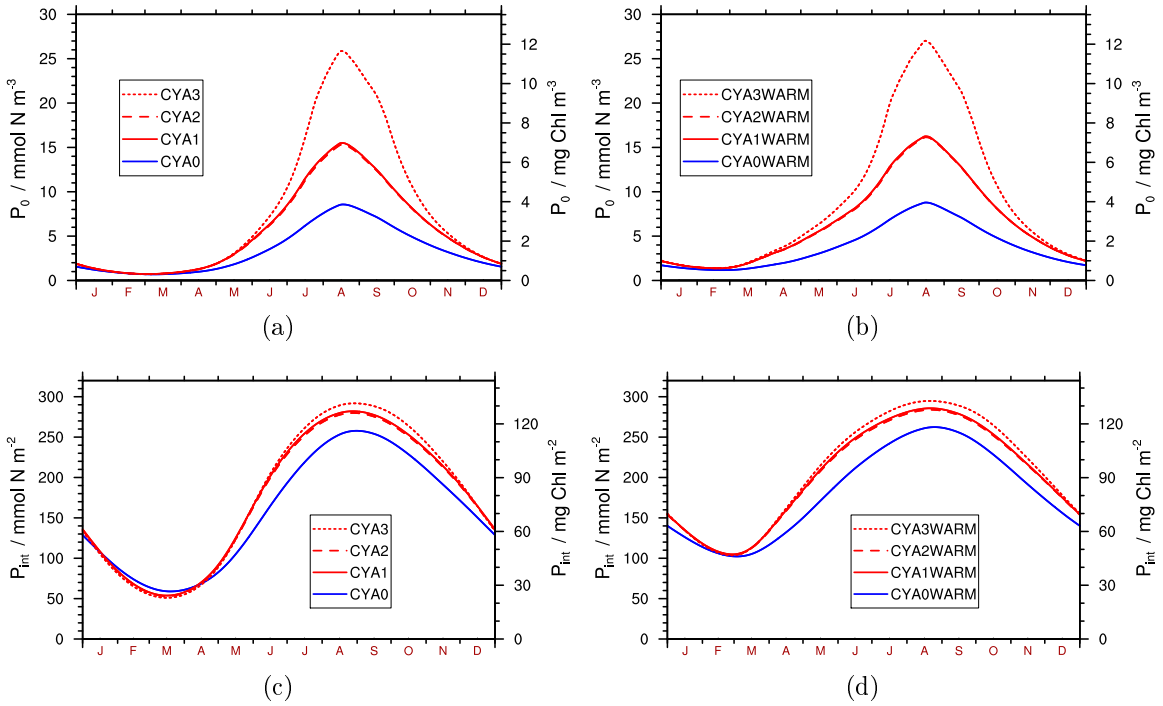

Figure 2.20.: Cyanobacteria concentrations P_0 in the top layer in experiments CYA0, CYA1, CYA2, and CYA3 (a) and in experiments CYA0WARM, CYA1WARM, CYA2WARM, and CYA3WARM (b), as well as vertically integrated cyanobacteria concentrations $\mathrm{P}_{\mathrm{int}}$ in experiments CYA0, CYA1, CYA2, and CYA3 (c) and in experiments CYA0WARM, CYA1WARM, CYA2WARM, and CYA3WARM (d). The conversion from the model unit for phytoplankton concentrations to chlorophyll (Chl) contents is done using a fixed N:Chl ratio.

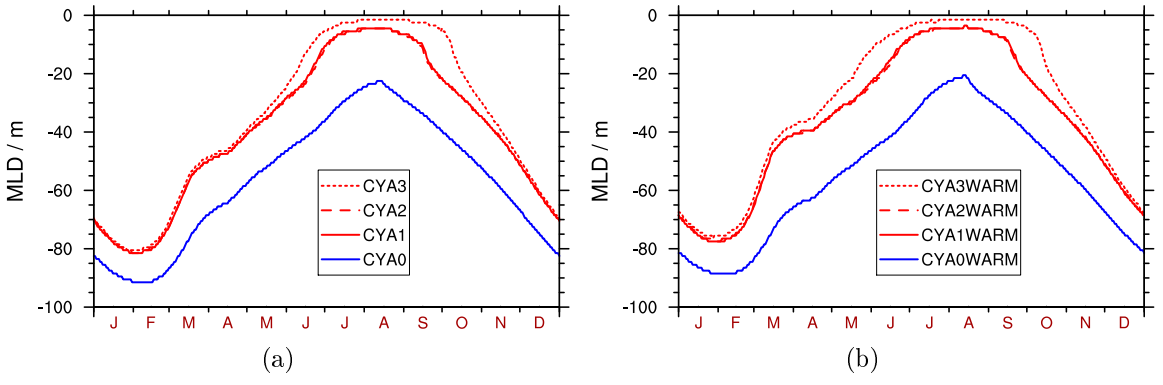

Figure 2.21.: Mixed layer depths (MLD) for all experiments including cyanobacteria for the Cape Verde scenario (a) and for the warming scenario (b), calculated from a temperature criterion with $\Delta T = 0.2\,^{\circ}\mathrm{C}$.

2.8 | Summary, discussion and conclusions

The results of our one-dimensional model study show that the absorption and the wind feedback lead to a faster and stronger warming of the surface layers and a weaker subsurface warming in spring and summer and a stronger cooling in fall. The absorption feedback leads to an increase in summer sea surface temperature of up to 1°C, while the albedo feedback induces a decrease in the surface temperature of only about 0.1°C. In addition, the absorption feedback leads to a doubling of the maximum cyanobacteria surface concentrations, while the albedo feedback effect on cyanobacteria surface concentrations is almost negligible. Furthermore, the absorption and the wind feedback lead to a shallowing of the mixed layer with a maximum decrease in the summer mixed layer depth of about 20 m. The albedo feedback, in contrast, affects the mixed layer depth only to a very small extent. These results suggest that the positive absorption feedback and the wind feedback have stronger effects on upper ocean physics than the negative albedo feedback. Thus, the overall feedback effect of the surface floating phytoplankton to sea surface temperature is a positive one.

Buoyant cyanobacteria actually drive two different positive feedback mechanisms, one via increased light absorption in the surface layers and one via wind drag reduction. Both these feedbacks lead to higher surface temperatures as well as reduced turbulent mixing which both lead to a benefit for buoyant cyanobacteria (as also suggested by, e.g., Jöhnk *et al.*, 2008). Thus, buoyant cyanobacteria create environmental conditions promoting their own growth and providing a competitive advantage over non-buoyant phytoplankton species.

While changes in the absorption of light by phytoplankton have been included in previous model studies, the additional effects of altered ocean surface albedo and surface wind drag were assessed here for the first time in a fully coupled biological-physical numerical model. Our parameterization of the coupling of the surface albedo and the wind stress to phytoplankton surface concentrations needs to be seen as a first quantitative estimate. Further quantitative measurements in the field are needed to get more confidence in the magnitude of the simulated effects. Yet, the sensitivity studies concerning the parameterizations of the different feedbacks show that the model results are quite robust for a reasonable range of assumed feedback strengths.

Our results suggest that in oceanographic regions with sufficient abundances of buoyant cyanobacteria these organisms will have substantial effects on upper ocean dynamics. These open ocean regions include the tropical and subtropical Atlantic and Pacific, as well as the Arabian Sea. The biological changes in the physical oceanic surface properties due to surface buoyant cyanobacteria might increase in the future, since an 11% areal increase in the potential geographic distribution of cyanobacteria due to future changes in sea surface temperatures may occur, if they adapt to temperatures higher than 30°C (Breitbarth *et al.*, 2007).

Concerning the effect of potential future increases in atmospheric temperatures, the warming scenario model results suggest that the period of favorable growth conditions

for cyanobacteria will be prolonged and that the effects of the absorption and the wind feedback on upper ocean physics will be even stronger in a warmer environment.

Our study allows to investigate in detail the various feedback loops and constitutes an elucidating example of a small system with already several feedback loops between biology and physics. Our results indicate potential consequences of a shift in the phytoplankton community composition to one dominated by cyanobacteria. Besides already observed changes in nitrogen cycling (e.g. Karl, 1999) additional effects like a prolonged growth period of cyanobacteria and direct effects on ocean physics like a prolonged period with high sea surface temperatures and a relatively shallow mixed layer can be expected. As noted already for example by Strutton and Chavez (2004), chlorophyll variability can have substantial effects on mixed layer dynamics and needs to be taken into account in physical ocean models. As our study suggests that marine biological feedbacks will have an impact on the mixed layer dynamics, model simulations of climate change scenarios should stop to ignore the fundamental changes in surface ocean biota.

Chapter 3

Quantification of local and non-local biological-physical feedbacks

We have described and analyzed the biological-physical feedback mechanisms in a one-dimensional local way so far. Yet, also indirect, non-local effects potentially providing feedback loops can occur in the upper ocean. The biologically induced effects on temperature distribution and mixed layer dynamics might be even stronger in a three-dimensional environment due to lateral advection caused by horizontally inhomogeneous phytoplankton concentration (as proposed, e.g., by Burchard *et al.*, 2006). Contrarily, the local effects of the biological-physical feedback mechanisms might be reduced due to horizontal processes, which cannot be resolved in a one-dimensional water column model. Non-local effects on upper ocean structure and dynamics and on the general circulation need to be studied in a model environment that can simulate the three-dimensional structure and circulation of the ocean. Therefore, we study the effects of including biological-physical feedback mechanisms also in a three-dimensional model framework. The aim is to quantify the local and non-local biologically induced feedback effects.

In the first three sections of this chapter we describe the specific physical and biological model setups as well as the implementation of the biological-physical feedback mechanisms in the three-dimensional model framework. (Underlying mathematical formulations, assumptions and numerical approaches used in coupled biological-physical ocean models are presented in Appendix A.) In Sections 3.4 to 3.7 we describe and analyze the results of a control simulation and the model simulations including the biological-physical feedbacks. We close the chapter with a section summarizing and discussing the main results and drawing conclusions from the three-dimensional model simulations.

3.1 | Physical model setup

Within the MIT general circulation model framework (MITgcm, Marshall *et al.*, 1997) we set up an idealized physical ocean model covering the North Atlantic coupled to a simplified biological model, which is suited to study the biologically induced impacts on ocean circulation and mixed layer dynamics in a controllable and conceptual yet quantitative way.

The physical model setup is based on the Boussinesq, incompressible hydrostatic primitive equations finite-volume model in z-coordinates, as described in the appendix A.3. We use a rigid lid and a linear equation of state without taking into account salinity changes. The model domain is a closed rectangular sector with an extent of 2560 km in meridional and 5120 km in zonal direction. We use a Cartesian grid on a β-plane with fixed z-levels and choose the Coriolis parameter and its meridional gradient such that the model domain ranges from about 10°N to 55°N. The bottom topography is flat and the depth of the basin is 900 m. Figure 3.1 shows a schematic depiction of the model domain. The horizontal resolution is 80 km and the vertical resolution is 2 m in the upper 20 m and gradually coarser from top to bottom with 40 levels in total. We apply no-slip conditions at the bottom boundary and free-slip conditions at the lateral boundaries. The additional parameter values used in the physical model part are given in the appendix in Table A.3.

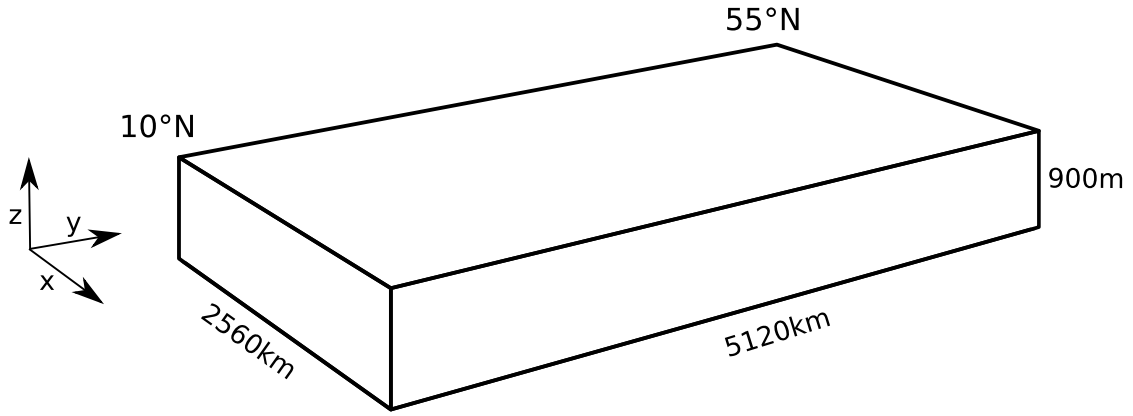

Figure 3.1.: Schematic depiction of the ocean sector model domain used in the MITgcm model setup.

We use the Redi scheme (Redi, 1982) and Gent-McWilliams parameterization (Gent and Mcwilliams, 1990; Gent *et al.*, 1995) for isopycnal mixing with the parameters and settings summarized in Table A.4 and the turbulent-kinetic-energy-based mixed layer closure scheme by Gaspar *et al.* (1990) for the vertical mixing with the parameters given in Table A.5. In addition, we use constant lateral and vertical background eddy viscosities and constant vertical background tracer diffusivities. Since the employed advection scheme is rather diffusive, we set the lateral and biharmonic tracer diffusivities to zero.

Physical model forcing

At the ocean surface we apply an idealized temperature and wind forcing. The heat flux between atmosphere and ocean is parametrized using a dynamic term for the long wave radiation and a prescribed term for the short wave radiation. The dynamic long wave radiation term is provided by restoring the model sea surface temperature to a prescribed idealized climatological annual cycle of temperature through a Haney-type restoring (Haney, 1971). This linearized formulation of the surface heat budget describes the interaction with an atmosphere with infinite heat capacity. Thus, this description allows for a response of the heat flux to changes in the sea surface temperature calculated by the model and represents a physically plausible flux correction. The restoring coefficient in the linearized heat flux has typical values of about $50\,\mathrm{W\,m^{-2}K^{-1}}$. This coefficient (divided by the density and specific heat of water and the thickness of the upper model layer) determines the restoring timescale used in the temperature equation of the model.

The prescribed idealized restoring temperature is zonally constant, but meridionally varying and includes an annual cycle as shown in Figure 3.2 (a). The annual and daily cycle of the solar short wave irradiance at the ocean surface is calculated from the geographical location via astronomical formulae and locally constant cloud cover values according to Brock (1981) and Reed (1977). Figure 3.2 (b) shows the solar irradiance at the ocean surface at local noon. Furthermore, the local ocean surface albedo is calculated from the geographical location and the angle of solar inclination according to Briegleb *et al.* (1986). In addition, we prescribe an idealized constant zonal wind stress with meridional variation based on observed northern hemisphere pattern, as shown in Figure 3.2 (c). The same temperature, light, and wind forcing is repeated every model year for all model simulations.

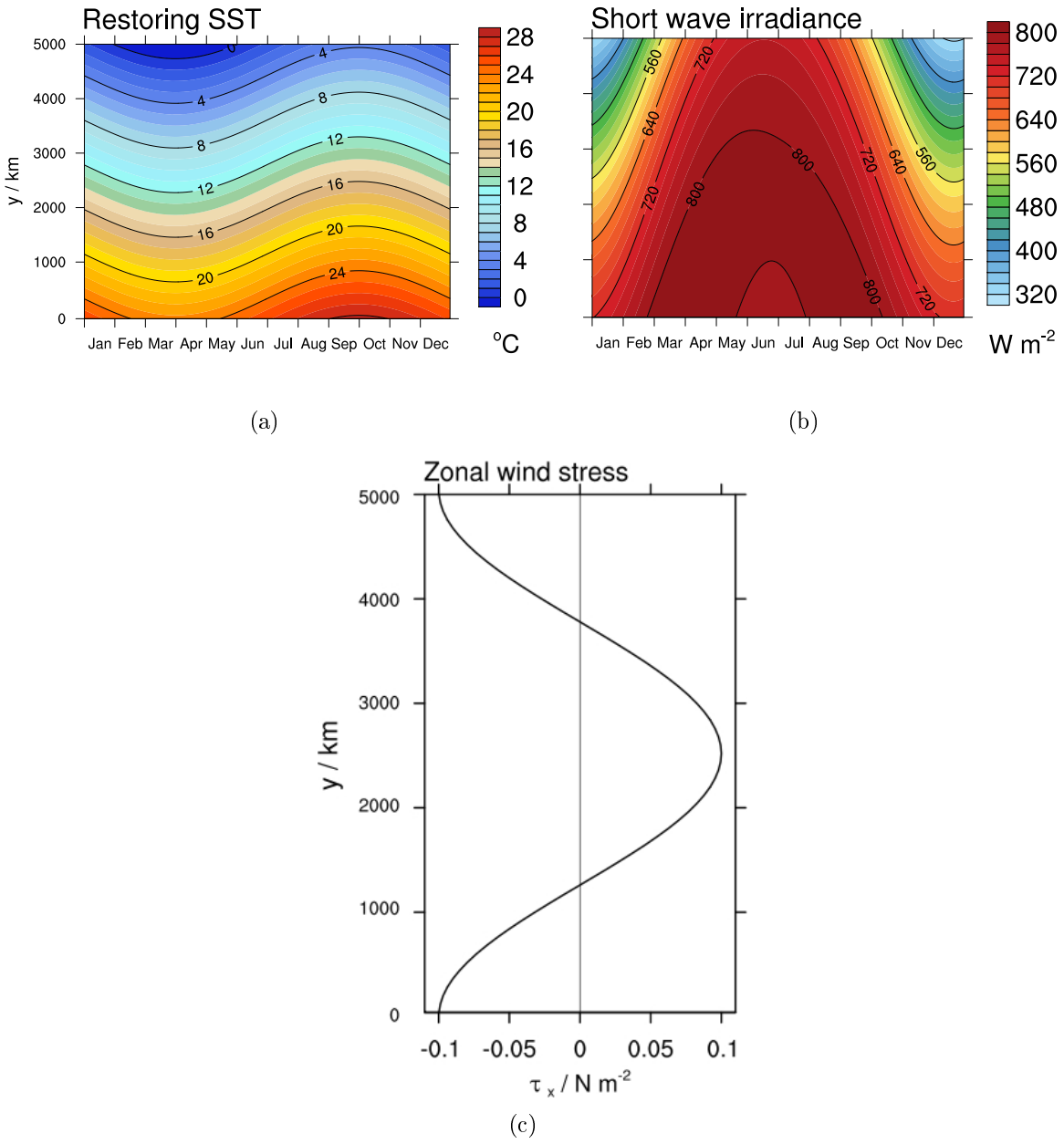

Figure 3.2.: Annual cycle of the restoring sea surface temperature (a), the solar irradiance at local noon (b), and the idealized constant zonal wind stress forcing τ_x (c) used in the MITgcm model setup.

3.2 | Biological model setup

The physical ocean model velocities and diffusivities are used to redistribute the biological tracers within the ocean. Additional redistribution comes from biological sources and sinks. In the following we describe the biological model, which we implement in the MITgcm framework. The dynamics for the concentration of all biological tracers $\mathcal{C}$ is given by

$$(\partial_t + \vec{v} \cdot \nabla)\,\mathcal{C} = \left(K_{\mathrm{h}}^{\mathrm{bio}}\,\partial_{xx} + K_{\mathrm{h}}^{\mathrm{bio}}\,\partial_{yy} + K_{\mathrm{v}}^{\mathrm{bio}}\,\partial_{zz}\right)\mathcal{C} + \mathcal{Q}_{\mathcal{C}} \tag{3.1}$$

where $K_{\mathrm{h}}^{\mathrm{bio}}$ and $K_{\mathrm{v}}^{\mathrm{bio}}$ are the horizontal and the vertical biological tracer diffusivities and the term $\mathcal{Q}_{\mathcal{C}}$ represents sources and sinks of the biological tracer $\mathcal{C}$. The parameter values for the diffusivities are given in the appendix in Table A.3.

The biological model describes a system of two different phytoplankton species groups named phytoplankton and cyanobacteria, respectively. Analogous to the biological model used in the one-dimensional studies described in Chapter 2, the phytoplankton group has a nutrient-limited growth rate and the cyanobacteria group has a temperature-limited growth rate and is positively buoyant. The model consists of a system of equations for the concentrations P, C, N, D_{S}, and D_{L} of phytoplankton, cyanobacteria, nutrients (dissolved inorganic nitrogen), and two pools of detritus – one pool with a short and one pool with a long remineralization length scale – respectively. All concentrations are expressed in nitrogen units. The sources and sinks are given by

$$\mathcal{Q}_P = \mu_P\,P - \delta_P\,P \tag{3.2}$$

$$\mathcal{Q}_C = \mu_C\,C - \delta_C\,C - w_C\,\partial_z C \tag{3.3}$$

$$\mathcal{Q}_N = \omega_{\mathrm{S}}\,D_{\mathrm{S}} + \omega_{\mathrm{L}}\,D_{\mathrm{L}} - \mu_P\,P \tag{3.4}$$

$$\mathcal{Q}_{D_{\mathrm{S}}} = \beta_P\delta_P\,P + \beta_C\delta_C\,C - \omega_{\mathrm{S}}\,D_{\mathrm{S}} - w_{D_{\mathrm{S}}}\,\partial_z D_{\mathrm{S}} \tag{3.5}$$

$$\mathcal{Q}_{D_{\mathrm{L}}} = (1-\beta_P)\,\delta_P\,P + (1-\beta_C)\,\delta_C\,C - \omega_{\mathrm{L}}\,D_{\mathrm{L}} - w_{D_{\mathrm{L}}}\,\partial_z D_{\mathrm{L}} - \gamma\,D_{\mathrm{L}} \tag{3.6}$$

with the growth functions

$$\begin{aligned}\mu_P &= \mu_P\,(I_{\mathrm{PAR}}, N)\\ &= \mu_P^{\max}\,\frac{\alpha\,I_{\mathrm{PAR}}}{\left(\mu_P^{\max 2} + \alpha^2 {I_{\mathrm{PAR}}}^2\right)^{1/2}}\,\frac{N}{k_N + N}\end{aligned} \tag{3.7}$$

$$\begin{aligned}\mu_C &= \mu_C\,(I_{\mathrm{PAR}}, T)\\ &= \mu_C^{\max}\,\frac{\alpha\,I_{\mathrm{PAR}}}{\left(\mu_C^{\max 2} + \alpha^2 {I_{\mathrm{PAR}}}^2\right)^{1/2}}\,\exp\left[-\frac{(T-T_{\mathrm{opt}})^4}{(T_1 - T_2\,\mathrm{sgn}\,(T-T_{\mathrm{opt}}))^4}\right]\end{aligned} \tag{3.8}$$

The photosynthetically available radiation I_{PAR} is calculated as a fixed fraction q_{PAR} of the local solar irradiance. The temperature T is the local potential temperature calculated by the physical model. The values and meanings of the constants used in the biological model are given in Table 3.1.

The limiting functions in the growth rates μ_P and μ_C are the same that are used in the biological model for the one-dimensional framework described in Chapter 2. In particular, for the functional relationship between growth rate and solar radiation we use the one which was first proposed by Smith (1936) and for the dependence of the growth rate on nutrient concentrations we use the hyperbolic function proposed by Caperon (1967). For the temperature dependence of the growth rate μ_C we use a modified Gaussian function describing the optimal temperature for cyanobacteria growth and the distribution around this optimum, which is in agreement with the observed temperature dependence of growth of N_2-fixing cyanobacteria (Breitbarth *et al.*, 2007). The temperature which we use here to calculate the growth rate μ_C is the temperature calculated in the physical part of the model. This calculated temperature is the potential temperature and not the in-situ temperature, which would be needed for a proper calculation of μ_C. However, compared to the uncertainty in measured values for the dependence of μ_C on temperature, the difference between potential and in-situ temperature is negligible in the relevant depth and temperature range.

$\mu_P^{\max}$	=	0.5	d^{-1}	phytoplankton maximum growth rate
$\mu_C^{\max}$	=	0.25	d^{-1}	cyanobacteria maximum growth rate
α	=	0.03	$\mathrm{m^2 W^{-1} d^{-1}}$	initial slope of P-I curve
k_N	=	0.3	$\mathrm{mmol\,N\,m^{-3}}$	half-saturation constant for N uptake
δ_P	=	0.05	d^{-1}	phytoplankton mortality rate
δ_C	=	0.05	d^{-1}	cyanobacteria mortality rate
$\beta_P = \beta_C$	=	0.5		fractionation of detritus pools
w_C	=	1.0	$\mathrm{m\,d^{-1}}$	cyanobacteria vertical velocity
ω_S	=	0.1	d^{-1}	remineralization rate of detritus described by D_S
ω_L	=	0.01	d^{-1}	remineralization rate of detritus described by D_L
w_{D_S}	=	-10	$\mathrm{m\,d^{-1}}$	vertical velocity of detritus described by D_S
w_{D_L}	=	-10	$\mathrm{m\,d^{-1}}$	vertical velocity of detritus described by D_L
γ	=	0.0095	d^{-1}	denitrification/deposition rate
T_opt	=	28	°C	cyano growth optimum temperature
T_1	=	5.5	°C	cyano growth temp. window parameter
T_2	=	1	°C	cyano growth temp. window parameter
q_PAR	=	0.43		PAR fraction of irradiance

Table 3.1.: Values and meanings of the parameters used in the biological model part in the MITgcm model setup.

3.3 | Coupling of physics and biology

The coupling between the biological and the physical model part is implemented as a two-way interaction. The physical model calculates velocity, temperature, and light fields, which are passed to the biological model and are used to redistribute the biological tracers and to calculate the source and sink terms in the biological equations. In addition, the biological tracers affect the light field via attenuation in the water and reflection at the ocean surface, thereby feeding back to the temperature field.

Analogous to the one-dimensional model studies presented in Chapter 2, the altered light attenuation and corresponding temperature changes due to absorption by biological matter is referred to as the absorption feedback. The effect of biological matter on the surface reflectance, i.e., the albedo of the ocean surface, is referred to as the albedo feedback, and the alteration of the surface wind drag coefficient by cyanobacteria at the ocean surface, implemented as a reduced wind stress, is referred to as the wind feedback. The parameterizations of the three different biological-physical feedback mechanisms in the three-dimensional model framework are implemented analogously to the model described in Chapter 2.

3.3.1 | Absorption feedback

The incoming solar short wave irradiance is absorbed and attenuated by the seawater and by biological matter thus leading to less available light in deeper water layers. At a given location (x, y), the attenuated local irradiance I at depth z and time t is calculated as

$$I(x,y,z,t) = I_0(x,y,t)\left[a\exp\left(k'_{\mathrm{w}}z\right) + (1-a)\exp\left(k_{\mathrm{w}}z\right)\exp\left(k_{\mathrm{bio}}\int_0^z c(x,y,z',t)\mathrm{d}z'\right)\right], \tag{3.9}$$

where $c := P + C + D_{\mathrm{L}} + D_{\mathrm{S}}$ is the sum of the concentrations of phytoplankton, cyanobacteria, and detrital matter, I_0 is the incoming solar short wave irradiance at the surface, the parameters k'_{w}, and k_{w} are absorption coefficients for seawater, and a is a dimensionless weighting parameter. This parametrization is the same that is used in the water column model in Chapter 2, except for the concentration c taking into account the additional biological compartments. Also analogous to the studies in Chapter 2, the parameters are taken according to Jerlov water type I, which describes the background open ocean clear seawater, and the specific absorption coefficient for biological matter is set to $k_{\mathrm{bio}} = 0.03\,\mathrm{m}^2\,(\mathrm{mmol\,N})^{-1}$. The local irradiance I is then used for the calculation of local phytoplankton growth as well as for the source term proportional to $\partial_z I$ in the temperature equation to account for local warming by light absorption.

To assess the sensitivity of the model to the choice of the parameter k_{bio}, we perform additional model experiments analogous to the one-dimensional model experiments with the parameter values given in Table 2.2.

3.3.2 | Albedo feedback

The ocean surface albedo at a given location is coupled to the cyanobacteria concentration in the top layer at that location. That is, we compute the total ocean surface albedo α at location (x, y) at time t according to

$$\alpha(x,y,t) = \alpha_{\text{phys}}(x,y,t) + \alpha_{\text{bio}}(x,y,t) \tag{3.10}$$

$$\text{with} \quad \alpha_{\text{bio}}(x,y,t) = \min\left[\alpha_{\text{bio}}^{\max}, \beta\, C(x,y,z=0,t)\right] , \tag{3.11}$$

where $\alpha_{\text{phys}}(t,x,y)$ is the local ocean surface albedo calculated in the physical part of the model from the geographical location and the angle of solar inclination according to Briegleb *et al.* (1986), β and $\alpha_{\text{bio}}^{\max}$ are constant parameters, and $C(x,y,z=0,t)$ is the cyanobacteria concentration in the top layer at location (x,y) at time t. This parametrization and also the values for the parameters are the same that are used in Chapter 2.

To assess the sensitivity of the model to the choice of these parameters, we perform additional model experiments analogous to the one-dimensional model experiments with the different sets of parameter values given in Table 2.2 and illustrated in Figure 2.8.

3.3.3 | Wind feedback

The surface wind stress at a given location is coupled to the cyanobacteria concentration in the top layer at that location. We assume that the surface wind stress is reduced by cyanobacteria at the ocean surface, leading to the altered surface wind stress

$$\vec{\tau}(x,y,t) = \vec{\tau}_{\text{phys}}(x,y)\, r_{\text{bio}}(x,y,t) \tag{3.12}$$

$$\text{with} \quad r_{\text{bio}}(x,y,t) = \max\left[r_{\text{bio}}^{\max}, (1-\delta\, C(x,y,z=0,t))\right] , \tag{3.13}$$

where $\vec{\tau}_{\text{phys}}$ is the prescribed surface wind stress and δ and $r_{\text{bio}}^{\max}$ are constant parameters. Again, this parametrization and also the values for the parameters are the same that are used in Chapter 2.

To assess the sensitivity of the model to the choice of these parameters, we perform additional model experiments analogous to the one-dimensional model experiments with the different sets of parameter values given in Table 2.2 and illustrated in Figure 2.8.

As also stated in Chapter 2, the surface wind stress is used in two different parts of the model: As an upper boundary condition in the horizontal momentum equations and for the vertical turbulent momentum flux. Thus, a change in the surface wind stress leads to changes in the horizontal velocities and in the vertical turbulent mixing, which both lead to changes in the depth of the mixed layer. To separate these two different pathways in the three-dimensional model setup described here, we perform additional model experiments which are discussed in Section 3.8.

3.4 | Control simulation

To assess the effects of the different biological-physical feedback mechanisms we perform a control simulation with the biological-physical model without taking into account the effects of biology on physics. The physical model part in this case only acts as a driver of the biological model part. We initialize the physical model from a state at rest with a homogeneous temperature field. After a spin-up phase of 600 model years with the physical model part alone we perform a spinup run with the coupled biological-physical model for another 500 model years. After this spinup phase both the physical and the biological system are in a quasi steady state with a repeating annual cycle. In the following we describe the results of this control simulation after the spinup phase.

General circulation

The prescribed wind forcing produces the expected western-intensified double-gyre structure (Figure 3.3) with a cyclonic gyre in the northern part of the model domain, corresponding to the North Atlantic sub-polar gyre, and an anticyclonic gyre in the southern part of the model domain, corresponding to the North Atlantic subtropical gyre. These surface currents, which do not show a seasonal cycle because of the constant wind stress, together with the thermal forcing produce the surface temperature field with a strong positive north-south temperature gradient and a pronounced seasonal cycle (Figure 3.4). The western surface current in the southern part of the ocean basin flows northward until about the middle of the basin before it turns eastwards flowing to the north-eastern corner of the basin (Figure 3.5, left), where the warmer water masses lose heat to the atmosphere and deep water formation takes place. This surface current, transporting heat from lower to higher latitudes, corresponds to the Gulf Stream system in the North Atlantic. In the deeper layers the newly formed deep water gets transported from the north-eastern corner of the basin first westwards and then southwards by a deep western-boundary current to the southern border of the basin (Figure 3.5, right), where it gets upwelled again. The structure of the overturning circulation is visualized in the zonally integrated meridional overturning streamfunction (Figure 3.6) showing the net transport northward at the surface and southward at the bottom as well as upwelling across a large part of the ocean basin and downwelling at the northern boundary of the basin. In addition, there are two shallow wind-driven overturning cells, reflecting the near surface upwelling in the sub-polar gyre and at the southern boundary as well as the downwelling in the subtropical gyre.

In general, the circulation is consistent with previously published idealized models (e.g. Follows *et al.*, 2002) and resembles the general structure of the North Atlantic Ocean. Deviations from a more realistic setup mainly originate from the idealized geometry and the size of the ocean basin as well as from the idealized forcing. The strength of the meridional overturning circulation, for example, is substantially weaker in our idealized setup compared to observations of the Atlantic Ocean because of the smaller extent of our ocean basin in zonal direction.

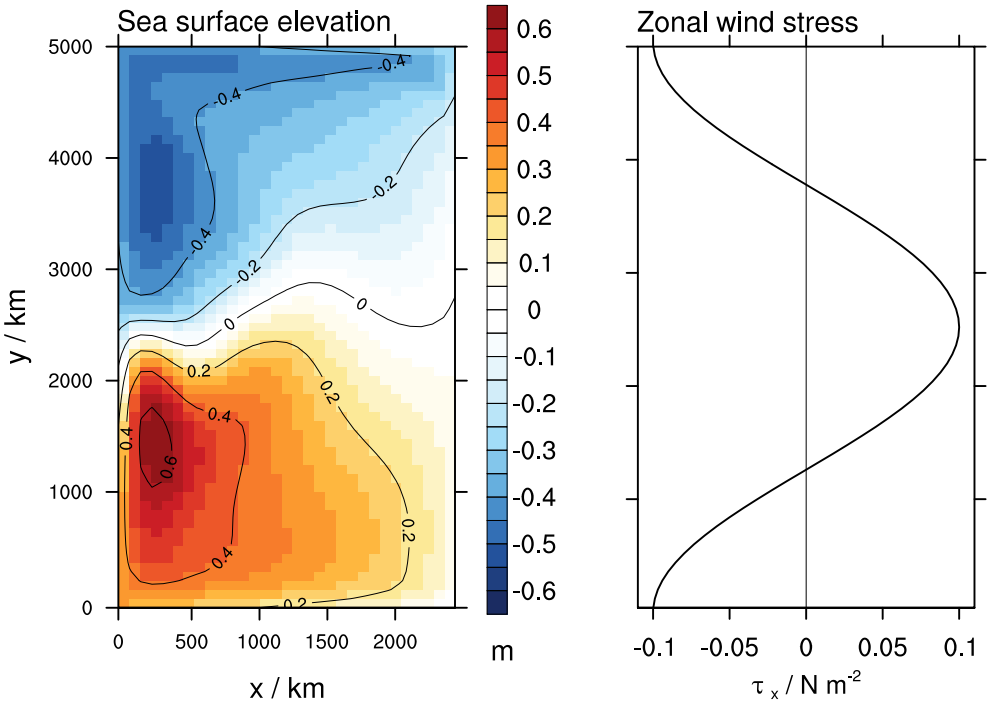

Figure 3.3.: Sea surface elevation in the control simulation (left) and the constant zonal wind stress forcing (right).

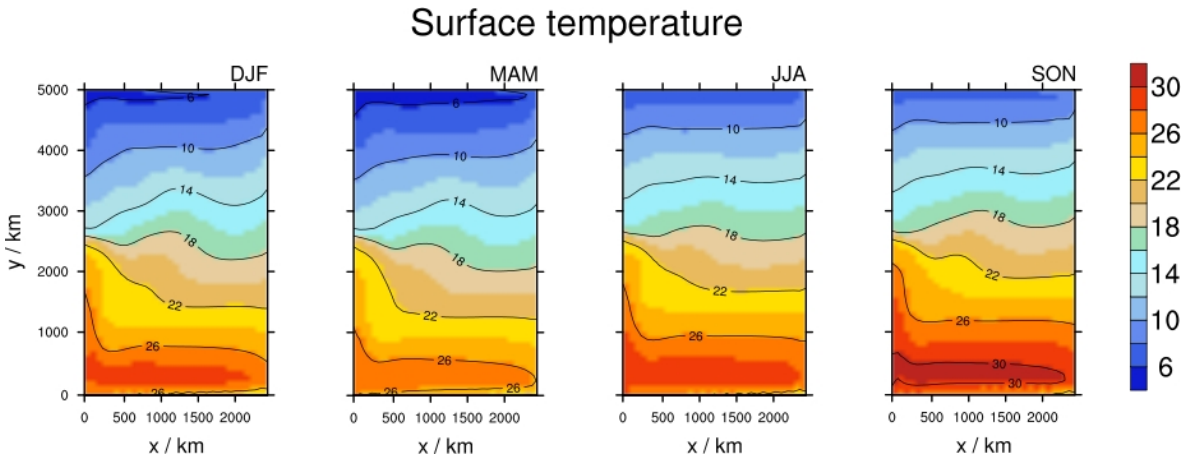

Figure 3.4.: Seasonal mean surface temperature in winter (DJF), spring (MAM), summer (JJA), and fall (SON) in the control simulation.

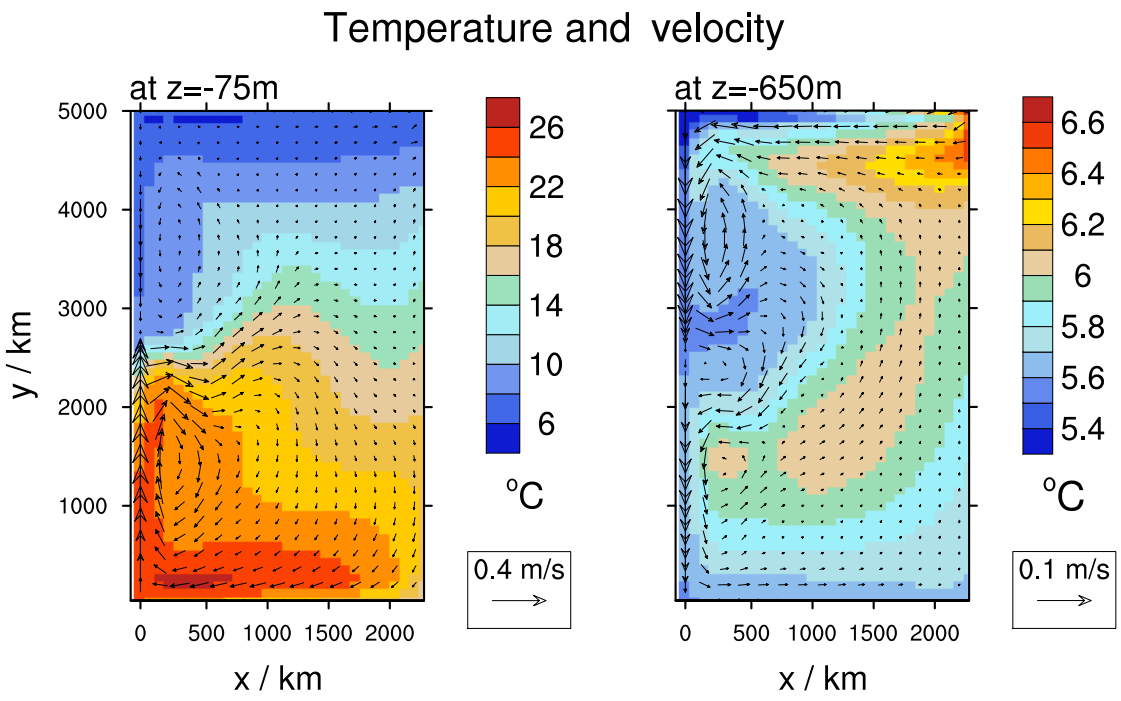

Figure 3.5.: Annual mean temperature and velocities at 75 m depth and 650 m depth in the control simulation.

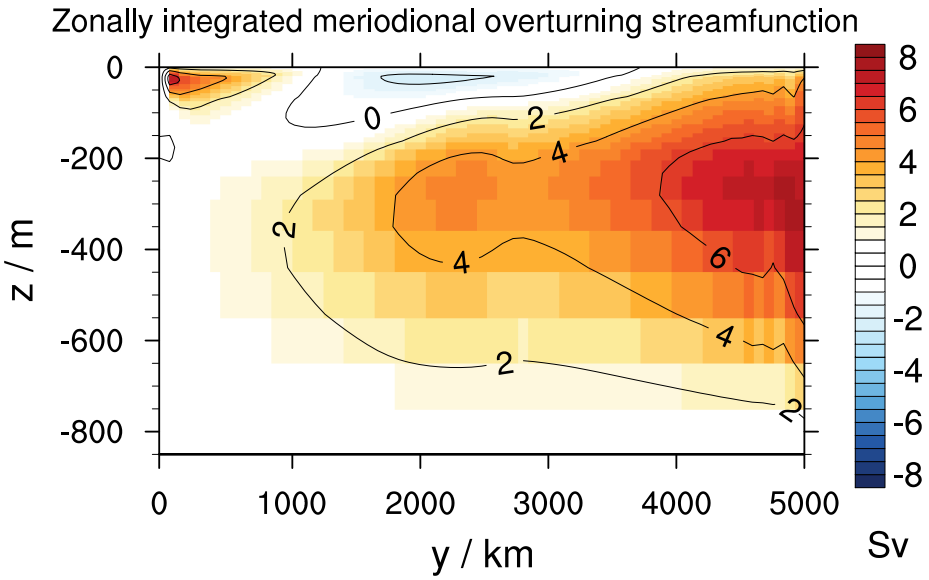

Figure 3.6.: Annual mean zonally integrated meridional overturning streamfunction in the control simulation.

Temperature structure and mixed layer dynamics

In the southern part of the ocean basin, the surface mixed layer, which is defined by a density-based criterion following Kara *et al.* (2000) throughout our studies in the three-dimensional framework, is rather shallow with a strong thermal stratification (Figure 3.7 and Figure 3.8). In the region corresponding to the subtropics, the mixed layer depth varies between around 60 m in winter and around 20 m in summer. At the southern boundary of the ocean basin, the upper ocean stratification is broken due to upwelling of colder water. In the northern part of the basin, the mixed layer depth is larger than 200 m in winter and fall in a large region at the northern boundary with a deep mixing down to the bottom of the basin directly at the northern boundary during the whole year. Additionally, the thermocline is deepened due to Ekman pumping in the northwestern part of the subtropical gyre, while colder water is lifted up via Ekman suction in the subpolar gyre, with the largest effect on the mixed layer depth in this region in summer and fall.

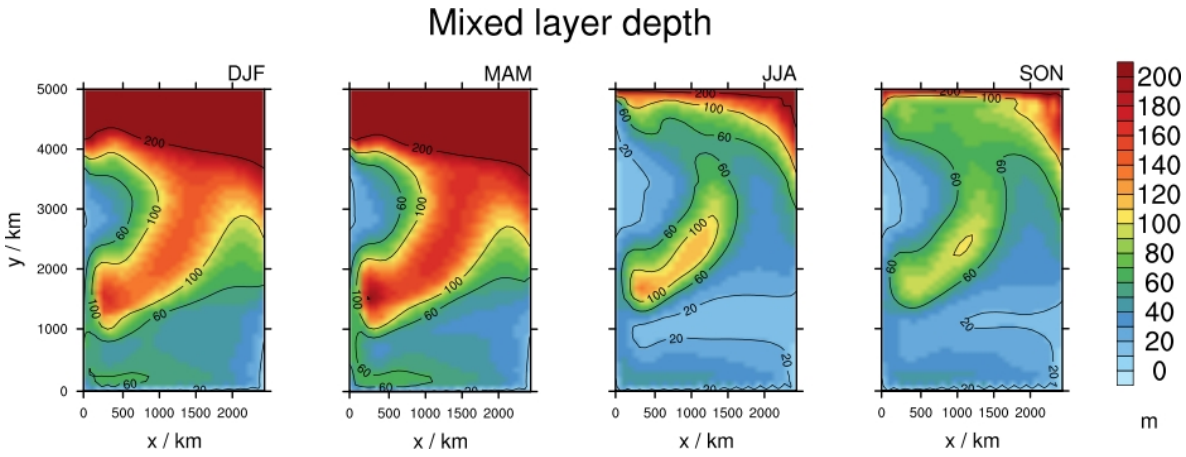

Figure 3.7.: Seasonal mean mixed layer depths, calculated via a density-based criterion following Kara *et al.* (2000), in the control simulation.

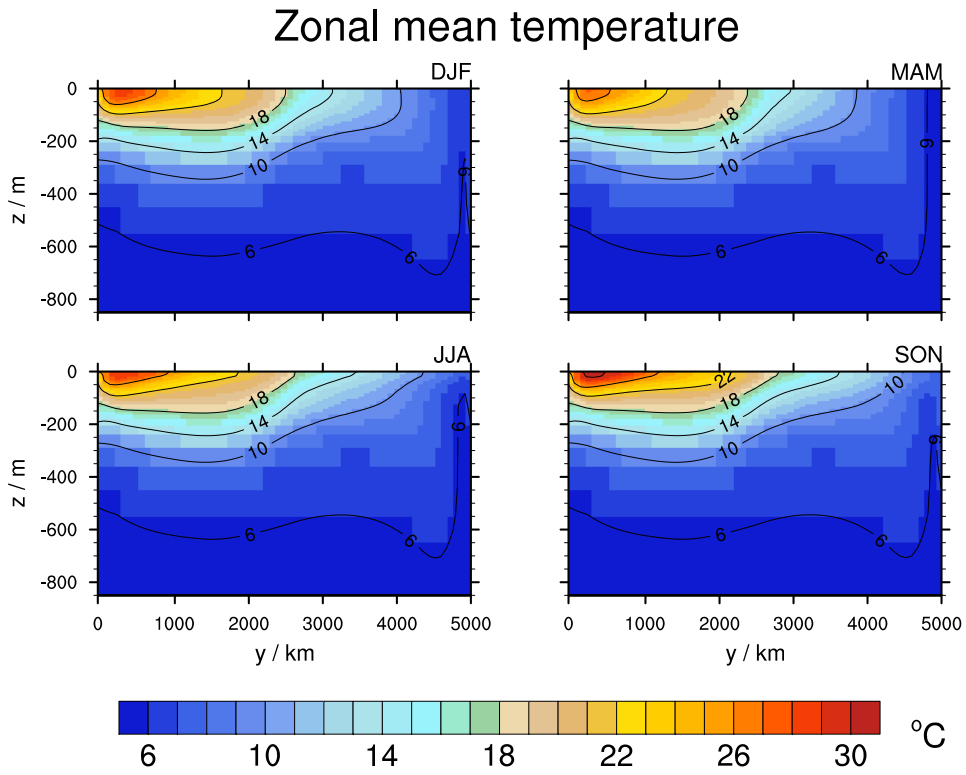

Figure 3.8.: Seasonal zonal mean temperature in the control simulation.

Biological variables

For the coupled biological-physical model simulations, the phytoplankton and cyanobacteria fields are initialized with horizontally homogeneous concentrations of $0.2\,\mathrm{mmol\,N\,m^{-3}}$ in the upper 300 m and $10^{-6}\,\mathrm{mmol\,N\,m^{-3}}$ below. The two detritus fields are initialized with a homogeneous concentration of $10^{-4}\,\mathrm{mmol\,N\,m^{-3}}$ and the initial nutrient field is horizontally homogeneous and vertically follows the profile as shown in Figure 3.9.

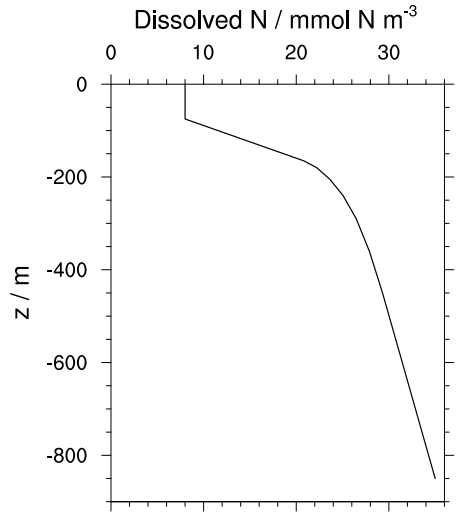

Figure 3.9.: Initial nutrient concentration profile. Horizontally, the initial nutrient field is homogeneous.

After the spinup phase the modeled phytoplankton surface concentrations (Figure 3.10, top) show relatively high values at the southern boundary of the ocean basin during the whole year. This persistent bloom is due to upwelling of nutrients to the surface in the Ekman cell in this region (Figure 3.13) and the availability of light all year long. Another area of high phytoplankton concentrations can be seen in the subpolar gyre. Here, nutrients are not limiting the growth of phytoplankton substantially, since they are upwelled due to Ekman suction to the surface in winter and spring (Figure 3.13). The highest phytoplankton surface concentrations can be found in the northern part of the ocean basin in summer. Here, nutrients and light are also hardly limiting the growth of phytoplankton. This surface bloom at the northern boundary of the ocean basin, however, only occurs in summer and early fall, since light levels are lower in winter and nutrients get depleted at the surface in fall and get mixed up again in winter and spring (Figure 3.13). In the subtropical region, phytoplankton surface concentrations are relatively low, since not enough nutrients are available at the surface because of the strong stratification and the Ekman pumping leading to downwelling. An additional reason for the low phytoplankton surface concentrations is the light shading by cyanobacteria. Cyanobacteria come in high concentrations in the southern part of the subtropical region during the whole year (Figure 3.10, bottom)

and, since they are surface buoyant, have an advantage in the competition for light compared to phytoplankton. Since cyanobacteria are not limited by nutrient availability at all in the model, they can grow even in the nutrient depleted surface layers of the subtropical region. The reason why cyanobacteria growth is restricted to the southern region of the ocean basin is their temperature dependent growth rate, which is too low further north, because temperatures are too low. Cyanobacteria are not present at the southern boundary of the ocean basin, but phytoplankton can grow there, since the actual growth rate is higher for phytoplankton than for cyanobacteria. The reason for this is twofold: 1) temperatures exceed the optimum temperature for cyanobacteria growth, and 2) the nutrient limitation for phytoplankton is weak in these nutrient replete conditions.

The vertical structure of the phytoplankton and cyanobacteria concentration is shown in Figure 3.12. Zonally averaged, both phytoplankton and cyanobacteria concentrations have their maximum at the surface, but phytoplankton is distributed over the upper 60-90 m, whereas cyanobacteria are restricted to the upper 20-30 m due their positive buoyancy and the relatively shallow mixed layer in the subtropical region.

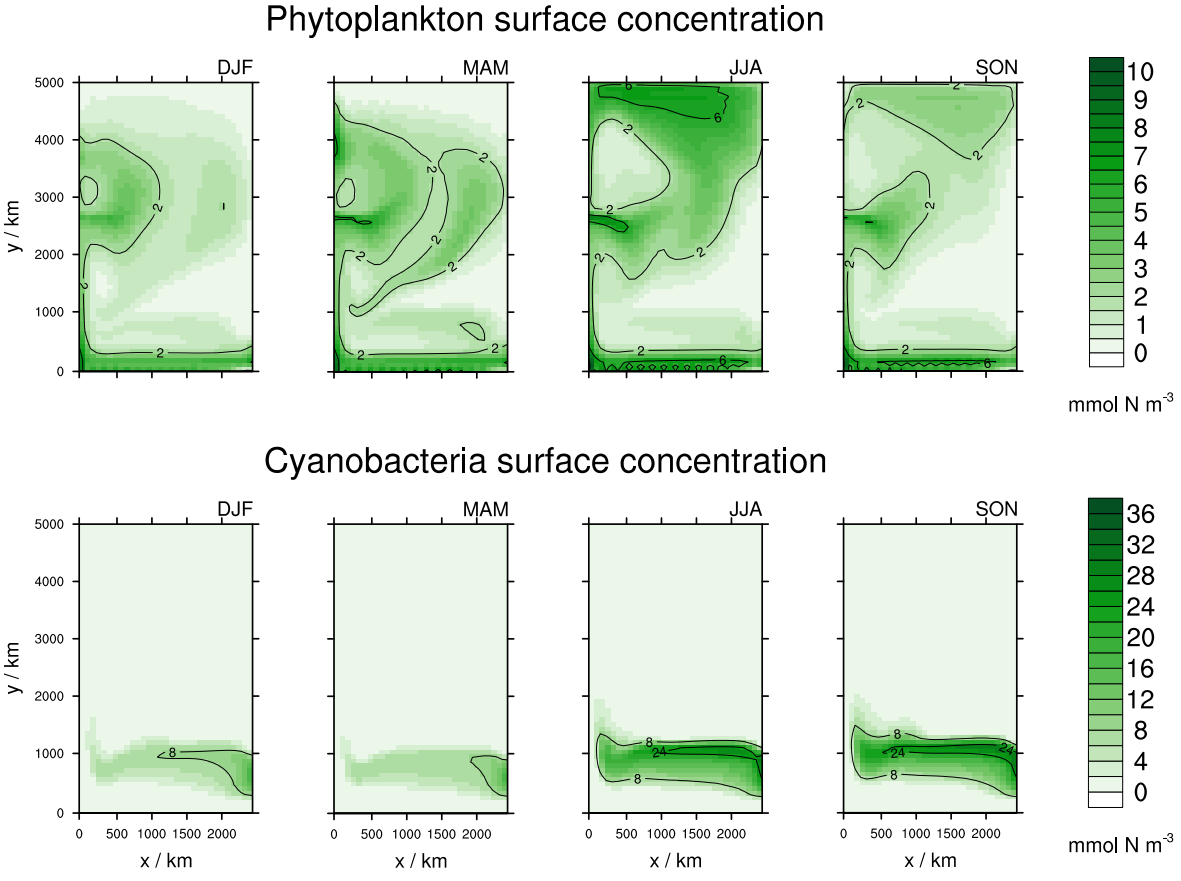

Figure 3.10.: Seasonal mean phytoplankton and cyanobacteria surface concentrations in the control simulation.

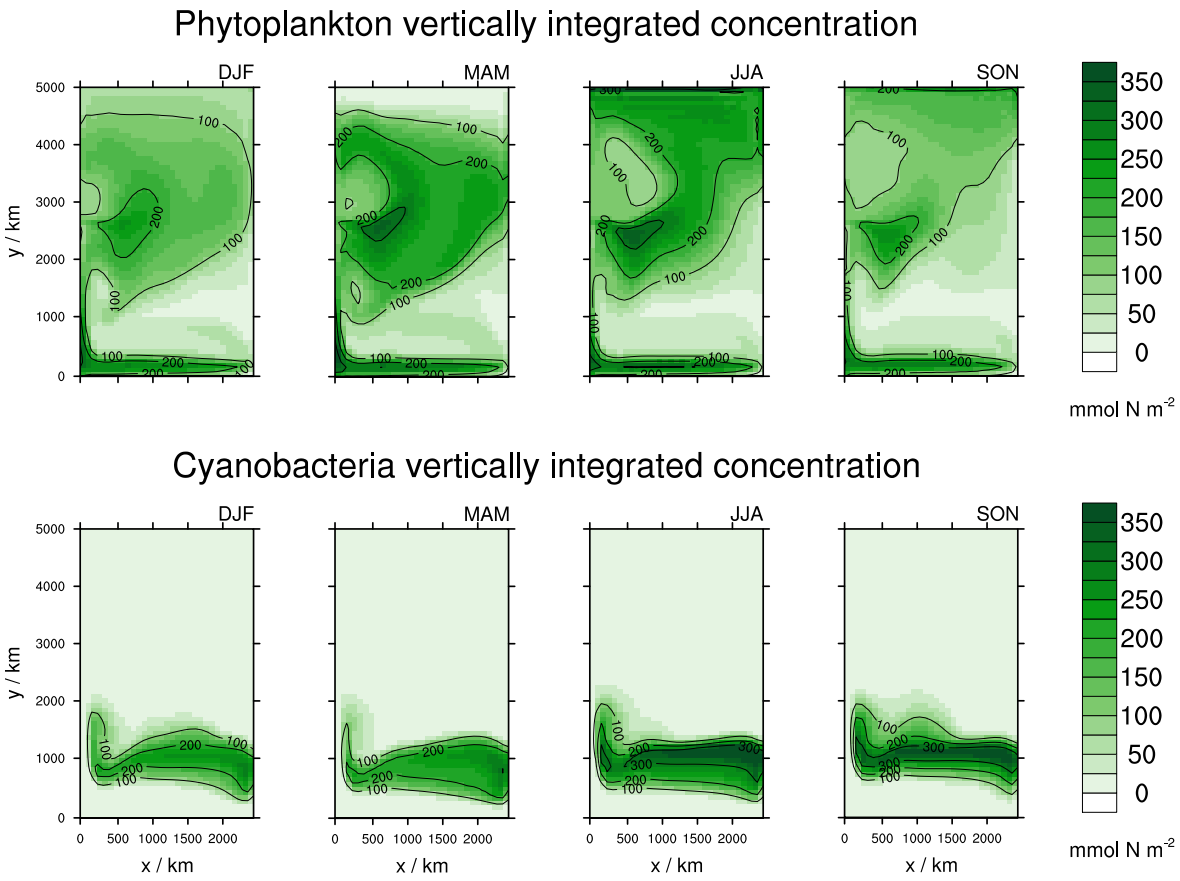

Figure 3.11.: Seasonal mean vertically integrated phytoplankton and cyanobacteria concentrations in the control simulation.

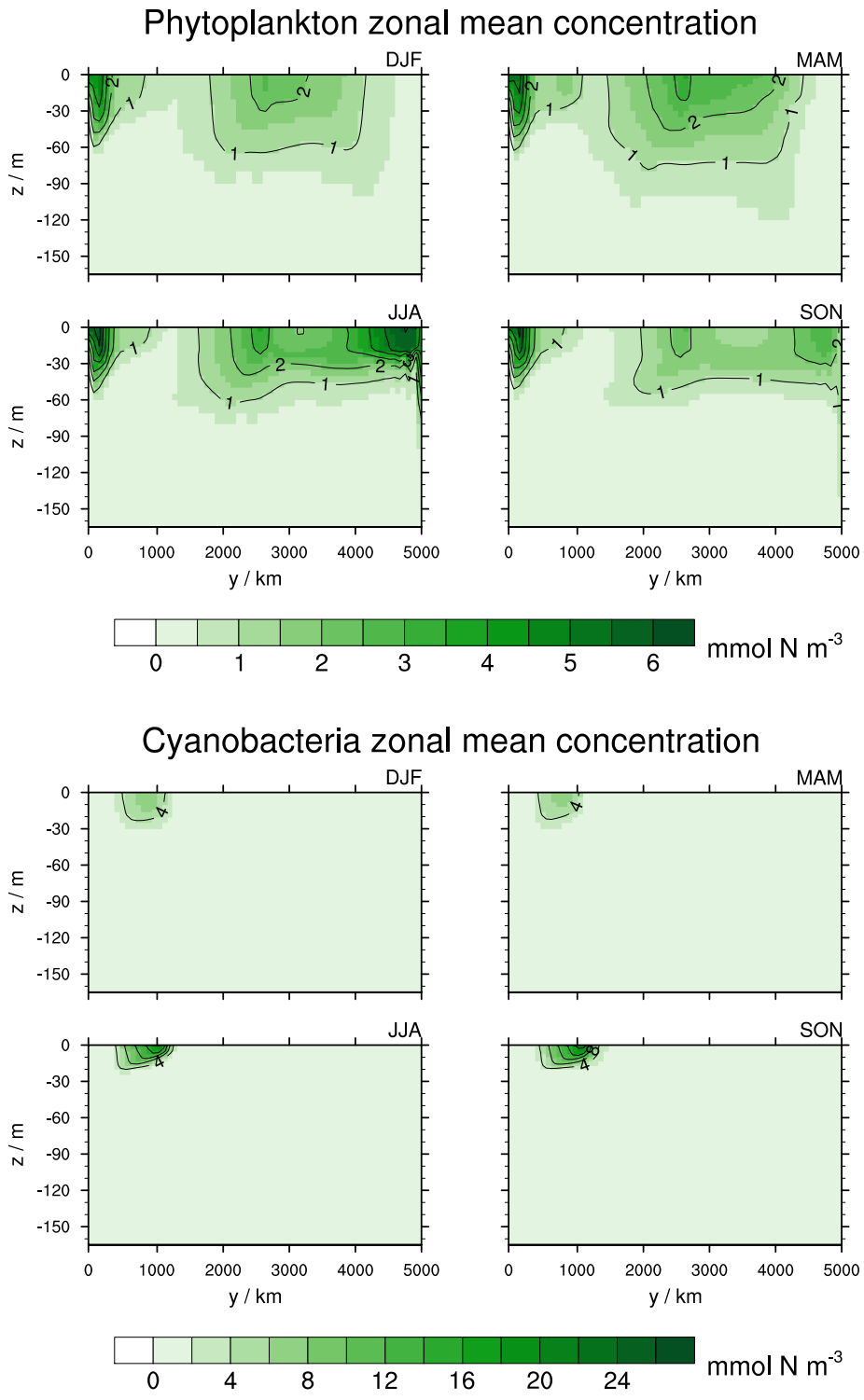

Figure 3.12.: Seasonal zonal mean phytoplankton and cyanobacteria concentrations in the control simulation.

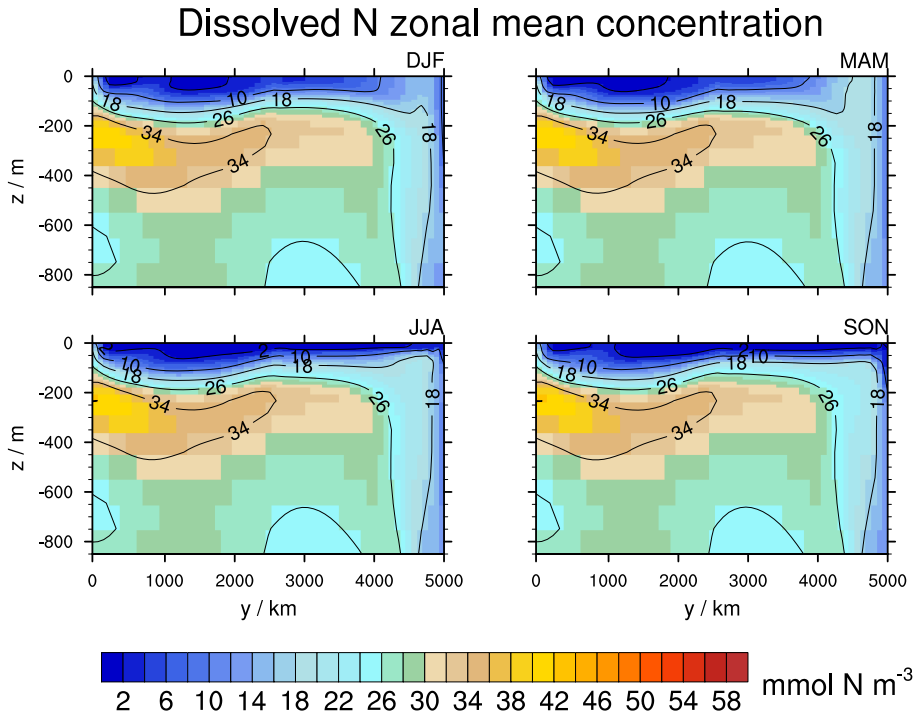

Figure 3.13.: Seasonal zonal mean nutrient concentrations in the control simulation.

3.5 | Quantitative evaluation of the biological results

To assess the magnitude of the biological-physical feedbacks, we aim to simulate the main characteristics of the phytoplankton and cyanobacteria dynamics, with reasonable concentrations and a reasonable spatial and seasonal pattern, using a minimalistic, yet process-based prognostic model which dynamically links phytoplankton and cyanobacteria to their physical environment.

Phytoplankton

The spatial pattern of highest phytoplankton concentrations in the northern part of the ocean basin and at the southern boundary as well as low phytoplankton concentrations in the region between compares well with the structure found in the North Atlantic Ocean (e.g. McClain *et al.*, 2004). The pronounced seasonal cycle of the modeled phytoplankton concentrations in the northern part of the ocean basin with a maximum in late spring/early summer is comparable to the observed phytoplankton dynamics in the North Atlantic. In this region, surface concentrations of chlorophyll (Chl) regularly reach 3 mg Chl m^{-3} in spring (McClain *et al.*, 2004), corresponding to 1.5–6.8 mmol N m^{-3}, assuming a Chl:C mass ratio between 40 and 180 (Sathyendranath

et al., 2009) and the Redfield molar C:N ratio of 6.625. The modeled phytoplankton surface concentrations of up to 6 mmol N m^{-3} at the northern boundary of the ocean basin are thus in a reasonable range. The modeled relatively high phytoplankton surface concentrations at the southern boundary of the ocean basin with maximum concentrations in summer are comparable to the phytoplankton distribution in the Atlantic equatorial upwelling region. The maximum surface chlorophyll concentrations in this upwelling region are around 1 mg Chl m^{-3} (McClain *et al.*, 2004), corresponding to 0.5–2.3 mmol N m^{-3}, assuming the above conversion factors. The model thus overestimates phytoplankton concentrations in this region, with summer mean maximum values of up to 6 mmol N m^{-3}, which can be explained by boundary effects or a too high nutrient availability in the model. The model region north of this boundary region is comparable with the oligotrophic subtropical North Atlantic, where very low phytoplankton concentrations are found. The observed surface values of around 0.05 mg Chl m^{-3} (McClain *et al.*, 2004), corresponding to 0.025–0.115 mmol N m^{-3}, are comparable to the phytoplankton surface concentrations simulated by the model with values below 0.5 mmol N m^{-3} in large parts of the ocean basin between 1000 and 2000 km north of the southern boundary.

Also the vertically integrated phytoplankton concentrations of up to 300 mmol N m^{-2} simulated by our model are in a reasonable range, compared to observed values of up to 180 mg Chl m^{-2} found by, e.g., Lochte *et al.* (1993), corresponding to about 100–400 mmol N m^{-2}. Yet, one needs to remember that the conversion of chlorophyll to the phytoplankton nitrogen content is not straightforward, which we account for here by assuming a large range of possible values for the Chl:C ratio, since the chlorophyll content of phytoplankton is highly variable (e.g. Geider, 1987) and also the Redfield C:N ratio is not constant (e.g. Geider and La Roche, 2002).

Concerning the vertical distribution of phytoplankton, in regions with strong and deep vertical mixing as well as in upwelling regions, modeled phytoplankton is distributed in the upper 60 to 120 m of the ocean with highest concentrations at the surface, whereas in stratified oligotrophic ocean regions, simulated phytoplankton concentrations form a subsurface maximum. These different vertical distributions compare well with observed profiles of phytoplankton in the North Atlantic (e.g. Marañón *et al.*, 2000).

Cyanobacteria

The spatial distribution of cyanobacteria simulated in our model agrees with the reported distribution of the surface buoyant nitrogen fixing cyanobacteria species *Trichodesmium*, which is generally restricted to low latitude oligotrophic ocean regions and rarely occurs at higher latitudes with water temperatures below 20 °C (Breitbarth *et al.*, 2007). The vertical distribution with highest concentrations at the surface, the large scale horizontal distribution pattern with the geographical restriction to the region north of the equatorial region, but south of the central subtropical gyre, as well as the seasonal cycle with maximum abundances in fall as simulated by our model are

found in satellite-based studies (Westberry and Siegel, 2006; Bracher *et al.*, 2009) and model studies (Gregg and Casey, 2007; Hood *et al.*, 2004) in the tropical and subtropical North Atlantic. Observed concentrations of *Trichodesmium* within surface blooms vary significantly (e.g. Carpenter and Capone, 1992; Westberry and Siegel, 2006; Luo *et al.*, 2012) and have been compiled and also compared to model results by, e.g., Hood *et al.* (2004) and more recently by Monteiro *et al.* (2010). Values of 2000–20,000 trichomes l^{-1} have been reported (e.g. Capone *et al.*, 1998; Tyrrell *et al.*, 2003; Carpenter *et al.*, 2004), corresponding to cyanobacteria concentrations of 1.4–14 mmol N m^{-3}, assuming a value of 10 ng N per trichome (Carpenter *et al.*, 2004). The maximum of this range of reported values for the North Atlantic is about a factor of 2 lower compared to the maximum surface concentrations of cyanobacteria of up to 25 mmol N m^{-3} simulated by our model. Yet, also very dense surface accumulations of cyanobacteria with up to $38–44 \times 10^6$ trichomes l^{-1} (Devassy *et al.*, 1978; Kromkamp *et al.*, 1997, for the Arabian Sea) have been reported, corresponding to up to 27,000–32,000 mmol N m^{-3}, assuming the conversion factor mentioned above. Thus, the cyanobacteria surface abundances simulated by our model are in a plausible range.

The simulated vertically integrated cyanobacteria concentrations with maximum values around 300 mmol N m^{-2} are higher compared to maximum values observed by, e.g., Carpenter *et al.* (2004), of up to 230 mmol N m^{-2}. Yet, as with the conversion of the phytoplankton chlorophyll content, also the nitrogen content of cyanobacteria is varying and it is this difficult to compare modeled values in units of nitrogen with measured values of numbers of cells, trichomes, or colonies.

3.6 | Perturbation experiments including feedbacks

Using the final state of the control simulation as initial state, we perform model simulations with the coupled biological-physical model, now taking into account also the effects of biology on physics. To assess the feedback mechanisms separately, we first switch on the three effects via absorption, albedo, and wind changes in separate model simulations. After an additional spin-up phase of 600 model years with the coupled model including the respective feedbacks, both the physical and the biological system reach a new quasi steady state with a repeating annual cycle. In the following we describe and analyze the results of the different perturbation experiments after the spinup phase with respect to the resulting differences to the control simulation.

3.6.1 | Absorption feedback

Effects on temperature

Since phytoplankton and cyanobacteria concentrations are highest at the surface in almost all regions of the ocean basin, the direct local effect of taking into account the absorption feedback is a surface warming due to absorption by biological matter. Since higher light absorption at the surface leads to less available light below the surface at a certain location, also a surface cooling at a different location can result due to the circulation. Figure 3.14 shows the surface temperature difference between the experiment including the absorption feedback (ABS) and the control simulation (CTRL).

In experiment ABS, seasonal mean surface temperatures are higher by up to 0.6 °C in summer compared to CTRL in the subtropical region where cyanobacteria are present in high concentrations. Also in the northern part of the ocean basin, during summer, when phytoplankton surface concentrations are highest, surface temperatures are higher (by up to 0.2 °C) in ABS compared to CTRL. During the whole year, at the southern boundary as well as at the western boundary, between 1600 and 2600 km north of the southern boundary, and in winter, in the part of the ocean basin north of the subtropical region, surface temperatures are lower by up to 0.4 °C in ABS compared to CTRL.

Below the surface layers, the temperature differences between the experiment ABS and CTRL are negative everywhere (Figure 3.15), since less light is available due to increased surface absorption. The strongest subsurface cooling of up to 1 °C in the zonal mean temperature occurs at a depth of around 60 m, below a depth of 200 m this cooling is less than 0.4 °C. In these deeper layers, the cooling effect is less pronounced, since the solar irradiance available for heating is very low here also without taking into account the attenuation by biological matter. Yet, negative temperature differences between ABS and CTRL occur down to the bottom of the ocean basin because the total amount of solar energy available for heating is reduced in experiment ABS. The heating of the surface layers cannot compensate for the subsurface cooling because of the increased heat loss to the atmosphere in the model. The surface cooling in experiment ABS compared to CTRL (Figure 3.14) is due to colder subsurface water that is upwelled to the surface.

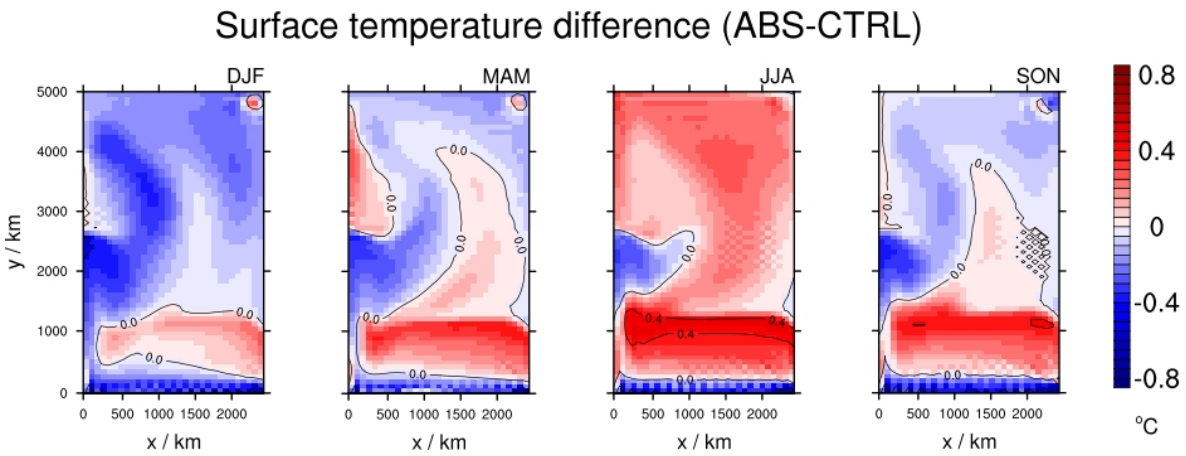

Figure 3.14.: Seasonal mean surface temperature differences between experiments ABS and CTRL.

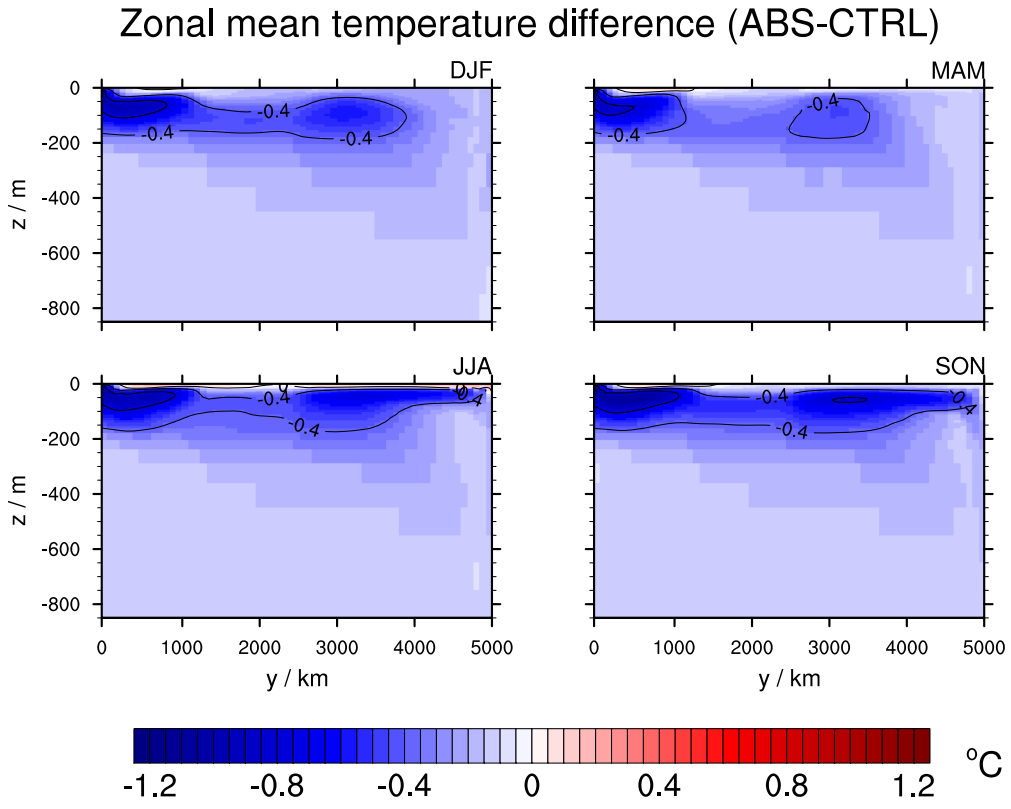

Figure 3.15.: Seasonal zonal mean temperature differences between experiments ABS and CTRL.

Effects on mixed layer dynamics and circulation

In experiment ABS, mixed layer depths are generally smaller almost everywhere in the ocean basin compared to experiment CTRL (Figure 3.16). In the subtropical region in winter and spring, the mixed layer is up to 30 m shallower in ABS compared to CTRL due to the biologically induced surface warming via absorption. The absolute reduction of the mixed layer depth in the subtropics is stronger in the western part of the ocean basin, since in the eastern part the mixed layer is very shallow already in experiment CTRL. In the northern part of the ocean basin, the mixed layer depth decrease is most pronounced in spring and summer and reaches more than 60 m. Only in winter this northern region is characterized by a deeper mixed layer in experiment ABS compared to CTRL.

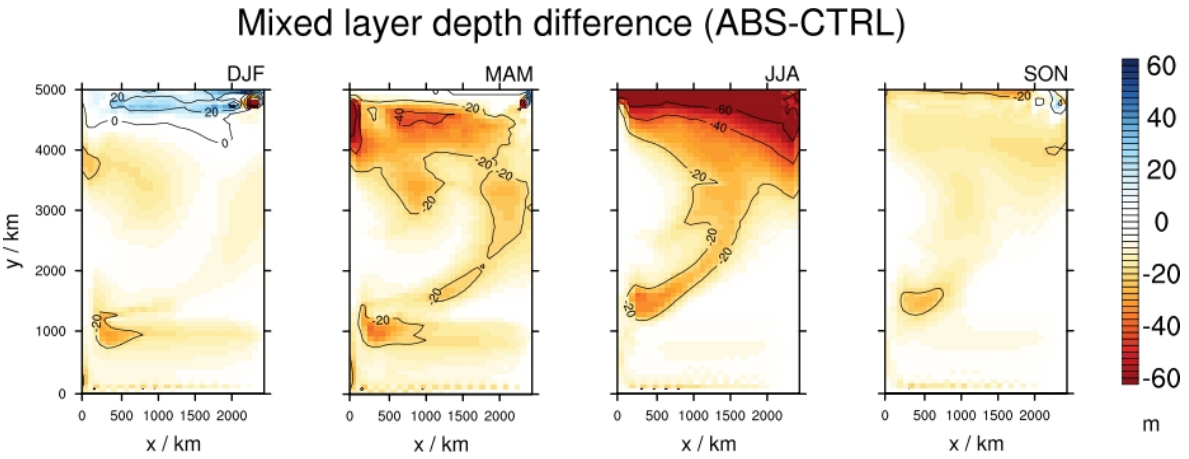

Figure 3.16.: Seasonal mean mixed layer depth differences between experiments ABS and CTRL.

Also the general circulation is affected by including the absorption feedback in the model. While the horizontal circulation is affected only very slightly (not shown), the meridional overturning streamfunction is reduced by up to 0.3 Sv in summer in the northern part of the ocean basin in experiment ABS compared to CTRL (Figure 3.17). In addition, the wind driven shallow surface overturning cell close to the southern boundary is increased by up to 0.4 Sv in ABS compared to CTRL throughout the year.

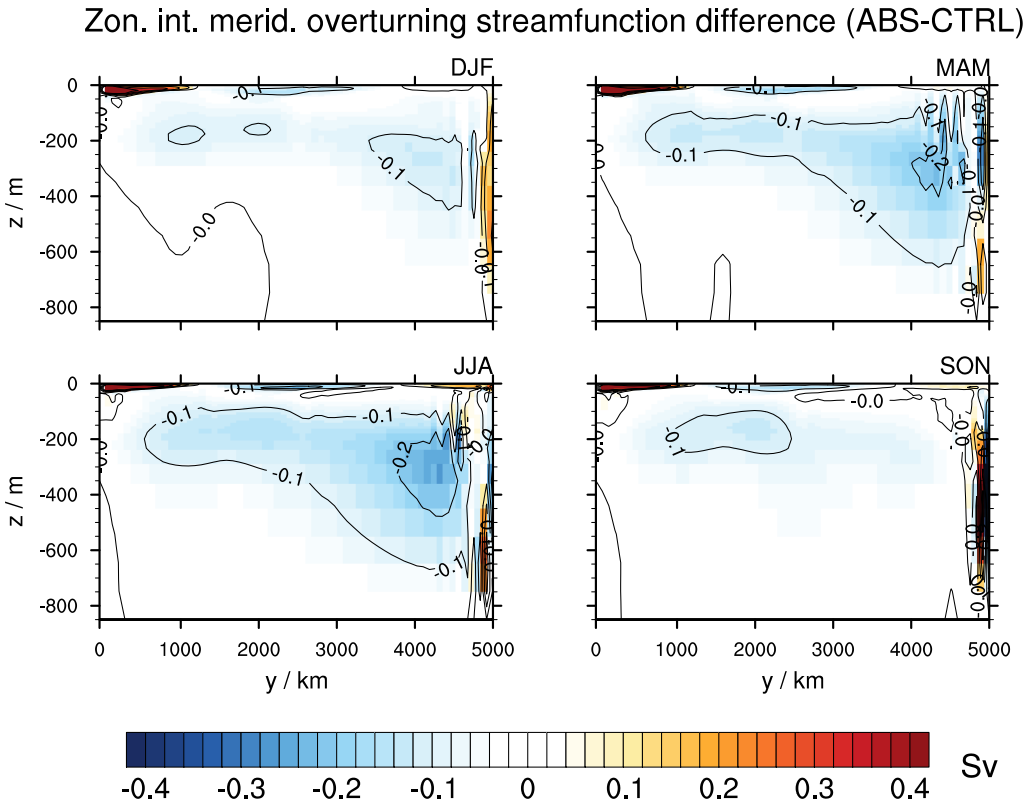

Figure 3.17.: Seasonal mean zonally integrated meridional overturning streamfunction differences between experiments ABS and CTRL.

Secondary effects on biological components

The changes in the temperature field and in upper ocean dynamics due to the absorption feedback lead to secondary effects on the biological tracers, since their dynamics and distribution depends on the model physics, thereby closing the feedback loop between biology and physics.

In experiment ABS, the phytoplankton surface concentrations are generally higher everywhere in the ocean basin compared to experiment CTRL (Figure 3.18). At the southern boundary of the ocean basin, these increases in the seasonal mean phytoplankton surface concentrations are around 1–2 mmol N m^{-3} during the whole year, corresponding to a relative change of about 30 % compared to experiment CTRL. In the northern part of the ocean basin, these increases are seasonally varying, with maximum values of up to 2 mmol N m^{-3}. Also the cyanobacteria surface concentrations are increased in experiment ABS compared to CTRL in the subtropical region, where cyanobacteria grow. The increase in the seasonal mean cyanobacteria surface concentration is as high as 14 mmol N m^{-3} in fall, corresponding to a relative change of about 50 % compared to experiment CTRL.

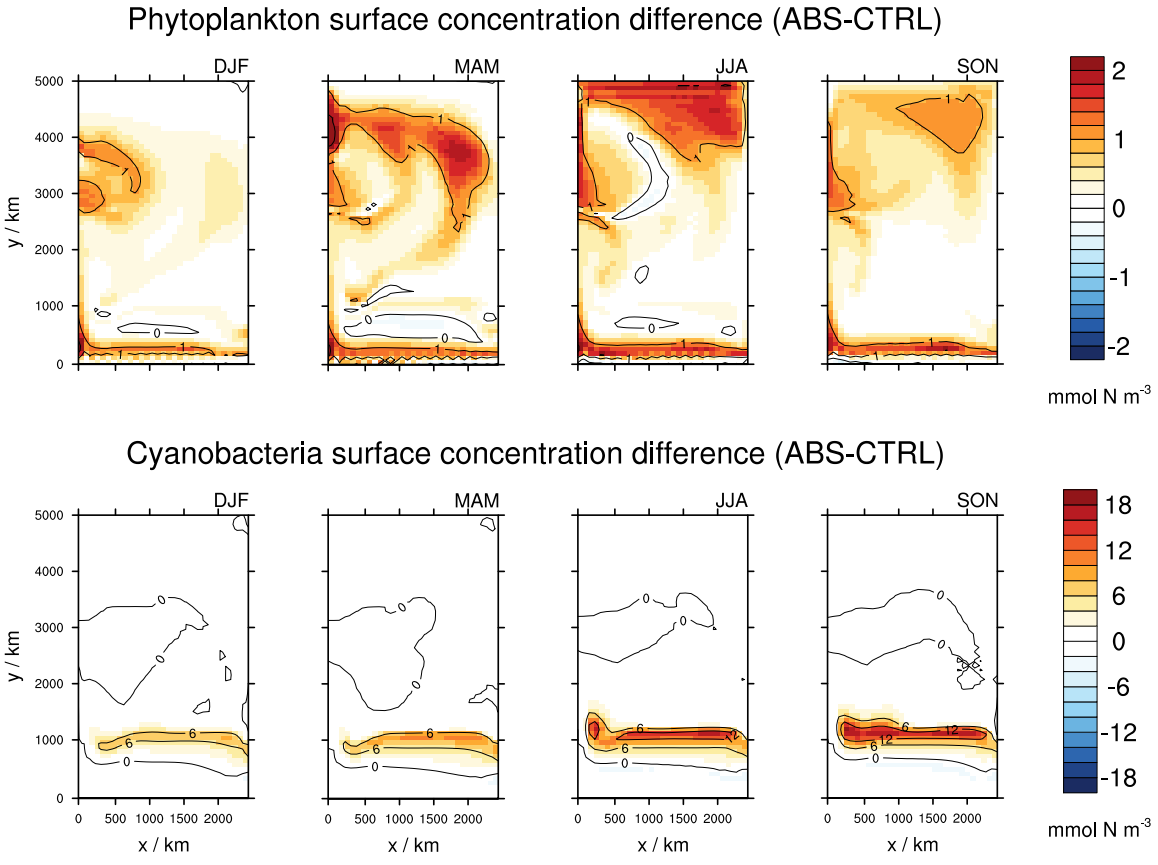

Figure 3.18.: Seasonal mean phytoplankton and cyanobacteria surface concentration differences between experiments ABS and CTRL.

The increases in phytoplankton and cyanobacteria surface concentrations in experiment ABS seem to be due to higher net growth of the organisms in the model. Yet, the vertically integrated concentrations show that the total amount of phytoplankton and cyanobacteria in a certain water column is increased in some regions, but decreased in other regions in experiment ABS compared to CTRL (Figure 3.19). For phytoplankton, the vertically integrated concentrations are decreased directly at the southern boundary of the ocean basin and increased in a strip between the southern boundary and the subtropical region. That is, the amount of phytoplankton close to the southern boundary is increasing, but part of the increased surface concentrations is explained by a northward shift of the phytoplankton bloom. In the subtropical region, the vertically integrated phytoplankton concentrations are reduced because of an even stronger dominance of cyanobacteria in this region in experiment ABS. In a large region in the northern part of the ocean basin, vertically integrated phytoplankton concentrations are decreased in summer. The vertically integrated cyanobacteria concentrations are increased in the northern part of the subtropical region, but decreased in the southern part, indicating a shift of the cyanobacteria bloom closer to the surface and northward.

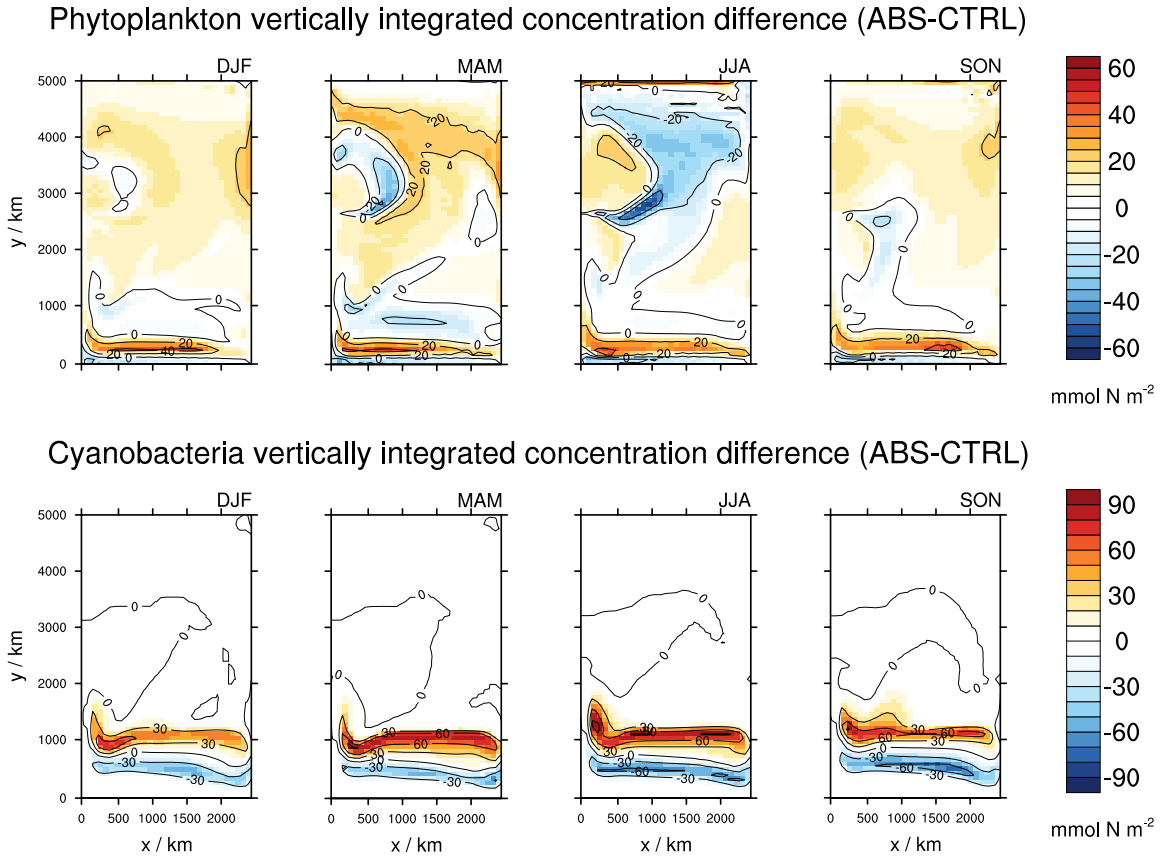

Figure 3.19.: Seasonal mean phytoplankton and cyanobacteria vertically integrated concentration differences between experiments ABS and CTRL.

3.6.2 | Albedo feedback

Since the albedo feedback only depends on the cyanobacteria surface concentrations, the direct local effect of taking into account the ocean surface albedo increase by cyanobacteria is a surface cooling due to increased reflectance of solar radiation. This surface cooling in the experiment including the albedo feedback (ALB) in the subtropics where cyanobacteria surface concentrations are highest reaches 0.1 °C compared to experiment CTRL (Figure 3.20). The wind induced shallow overturning cell at the southern boundary of the ocean basin leads to a slight subsurface cooling between the southern boundary and the subtropical region up to a depth of around 120 m in experiment ALB (Figure 3.21). The mixed layer depths are barely affected by including the albedo feedback in the model almost everywhere in the ocean basin (Figure 3.20).

The general circulation as well as the biological components in the model are also barely affected by including the albedo feedback (not shown).

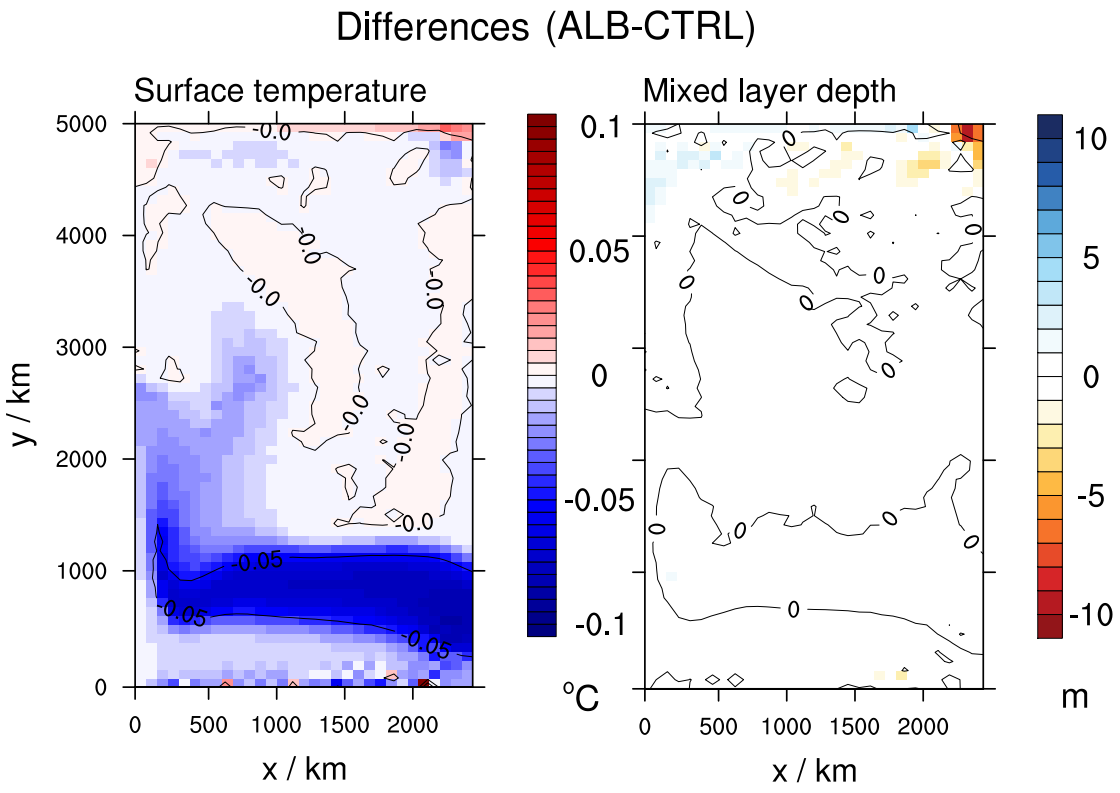

Figure 3.20.: Annual mean surface temperature and mixed layer depth differences between experiments ALB and CTRL.

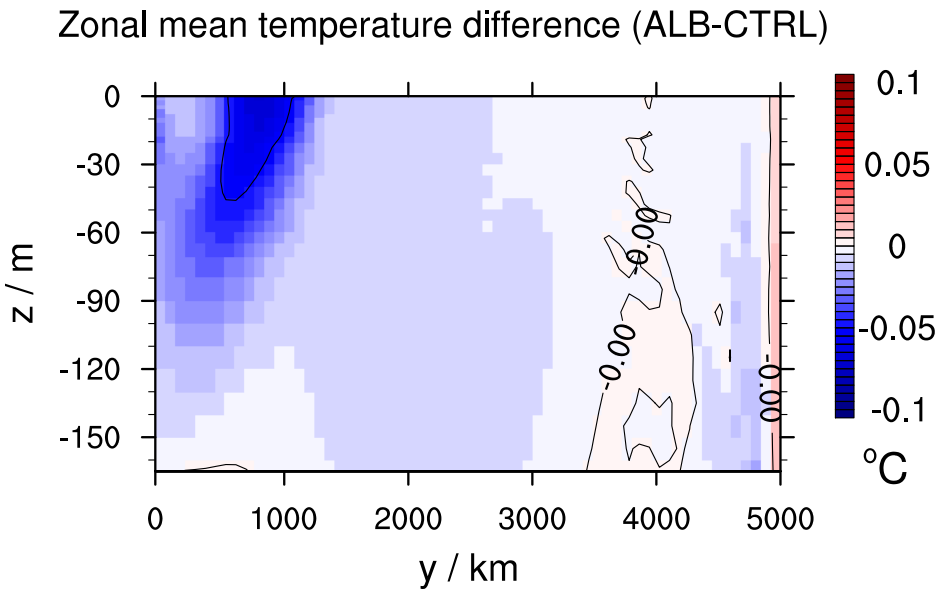

Figure 3.21.: Annual zonal mean temperature differences between experiments ALB and CTRL.

3.6.3 | Wind feedback

In experiment WIND we include the wind feedback in the model, leading to a reduction of the wind stress proportional to the local surface cyanobacteria concentration. The prescribed wind stress only has a zonal component and is constant over time, but varying meridionally (Figure 3.22, left). In experiment WIND the magnitude of this prescribed wind stress is reduced in the subtropical region where cyanobacteria occur (Figure 3.22, right).

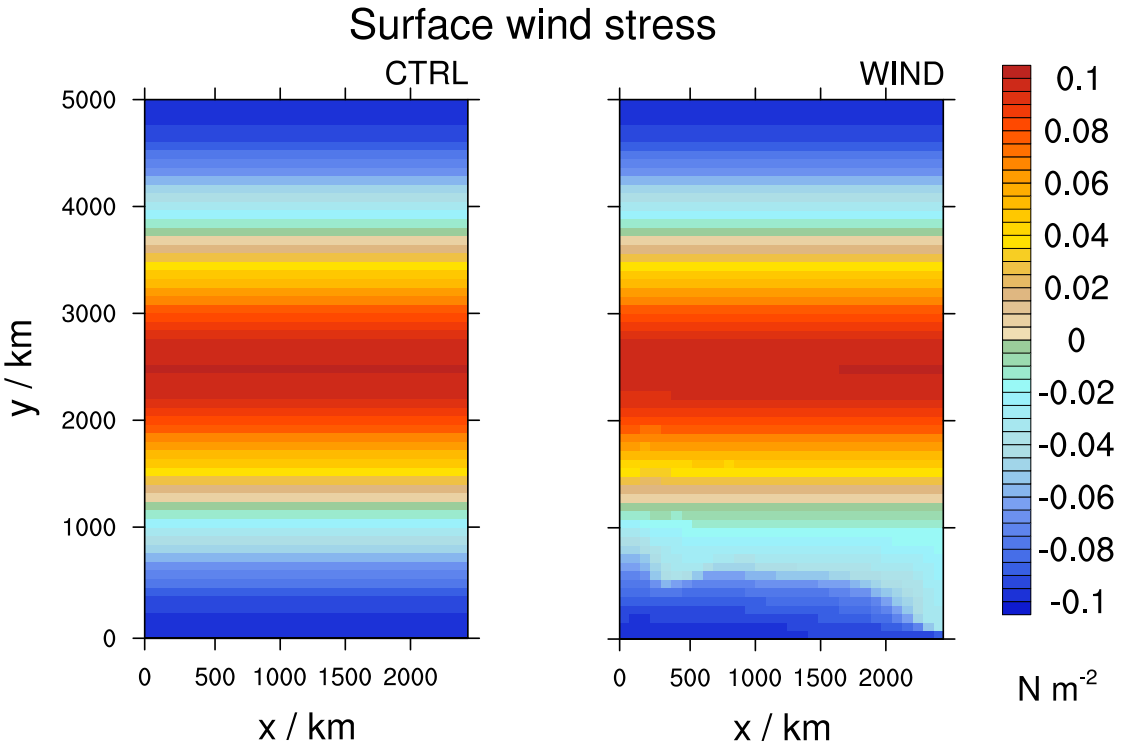

Figure 3.22.: Annual mean surface wind stress in experiments CTRL and WIND.

The absolute reduction of the surface wind stress magnitude in experiment WIND is strongest in the southern part of the subtropical region at the eastern boundary of the ocean basin, since cyanobacteria concentrations are highest and the magnitude of the surface wind stress is higher here than further north within the subtropical region (Figure 3.23, left). The surface wind stress magnitude reduction is as high as 0.01 to $0.03\,\mathrm{N\,m^{-2}}$ in most parts of the subtropical region and reaches up to $0.06\,\mathrm{N\,m^{-2}}$. In relative terms, the surface wind stress reduction in experiment WIND is at least 30%, and reaching more than 60% in summer and fall, of the original surface wind stress magnitude in most parts of the subtropical region (Figure 3.23, right). The reduction of the surface wind stress never reaches more than 66%, since we assume that this is the maximum reduction due to cyanobacteria.

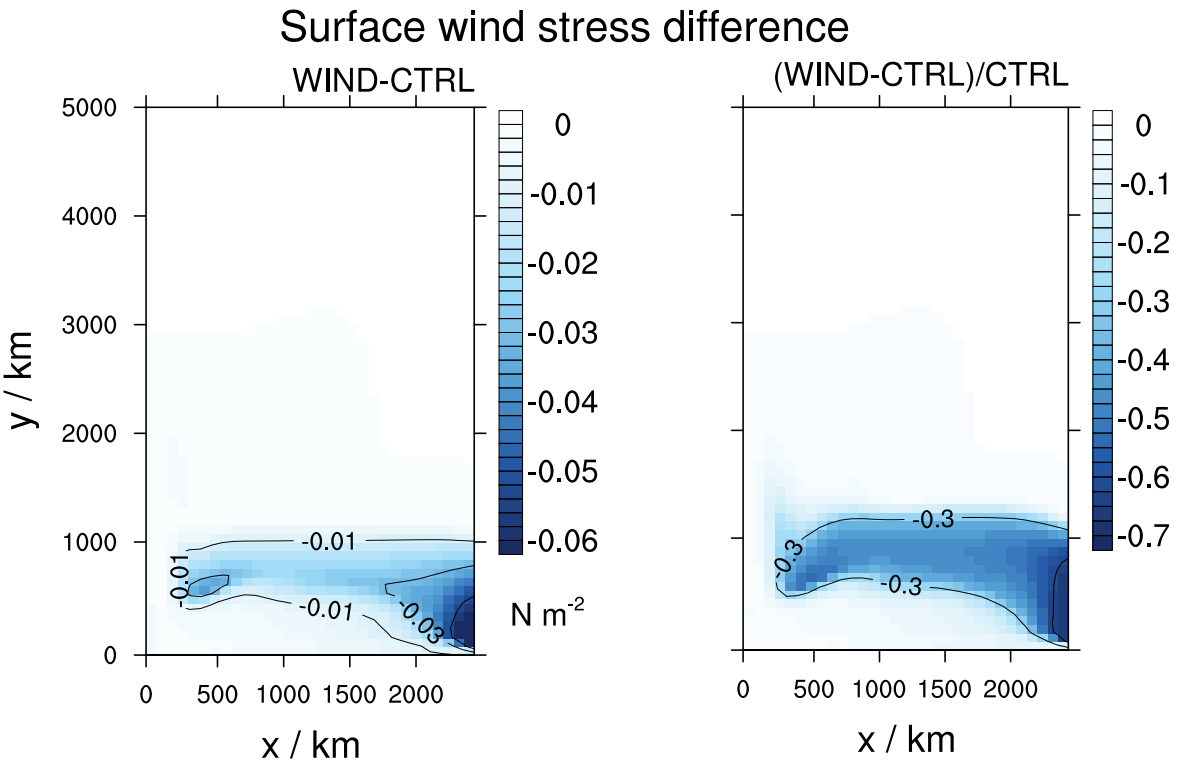

Figure 3.23.: Annual mean surface wind stress magnitude differences (left) and relative differences (right) between experiments WIND and CTRL.

The wind-driven subtropical gyre gets distorted in experiment WIND compared to CTRL (Figure 3.24) due to the altered surface wind stress in the subtropical region. The maximum sea surface elevation in the anticyclonic gyre is decreased and the whole gyre is shifted to the west.

The reduced wind stress in experiment WIND leads to a reduced wind-driven downwelling in the subtropical region and a confinement of the upwelling at the southern boundary of the ocean basin closer to the boundary (Figure 3.26). These changes in the circulation lead to higher zonal mean temperatures in the upper 400 m between the southern boundary and the subtropical region due to decreased upwelling of colder waters from deeper layers as well as to lower zonal mean temperatures in the upper 400 m in the subtropical region due to decreased downwelling of warmer surface water (Figure 3.25).

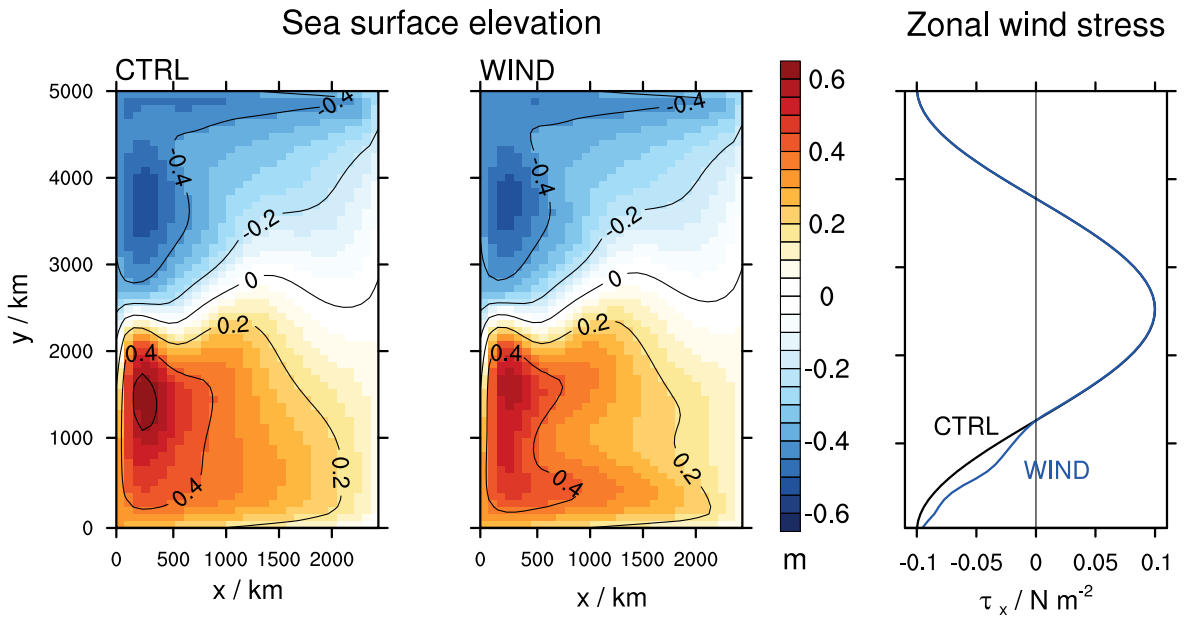

Figure 3.24.: Annual mean sea surface elevation in experiments CTRL and WIND and the corresponding zonally averaged zonal surface wind stress.

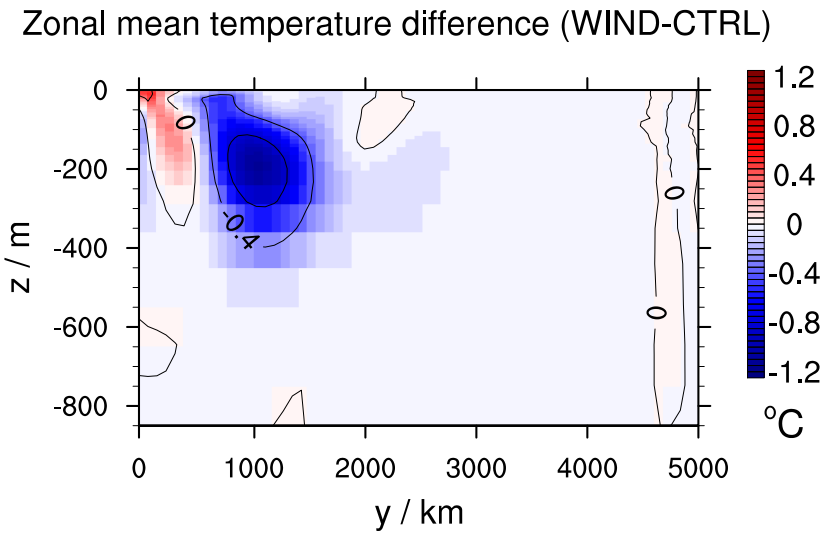

Figure 3.25.: Annual zonal mean temperature differences between experiments WIND and CTRL.

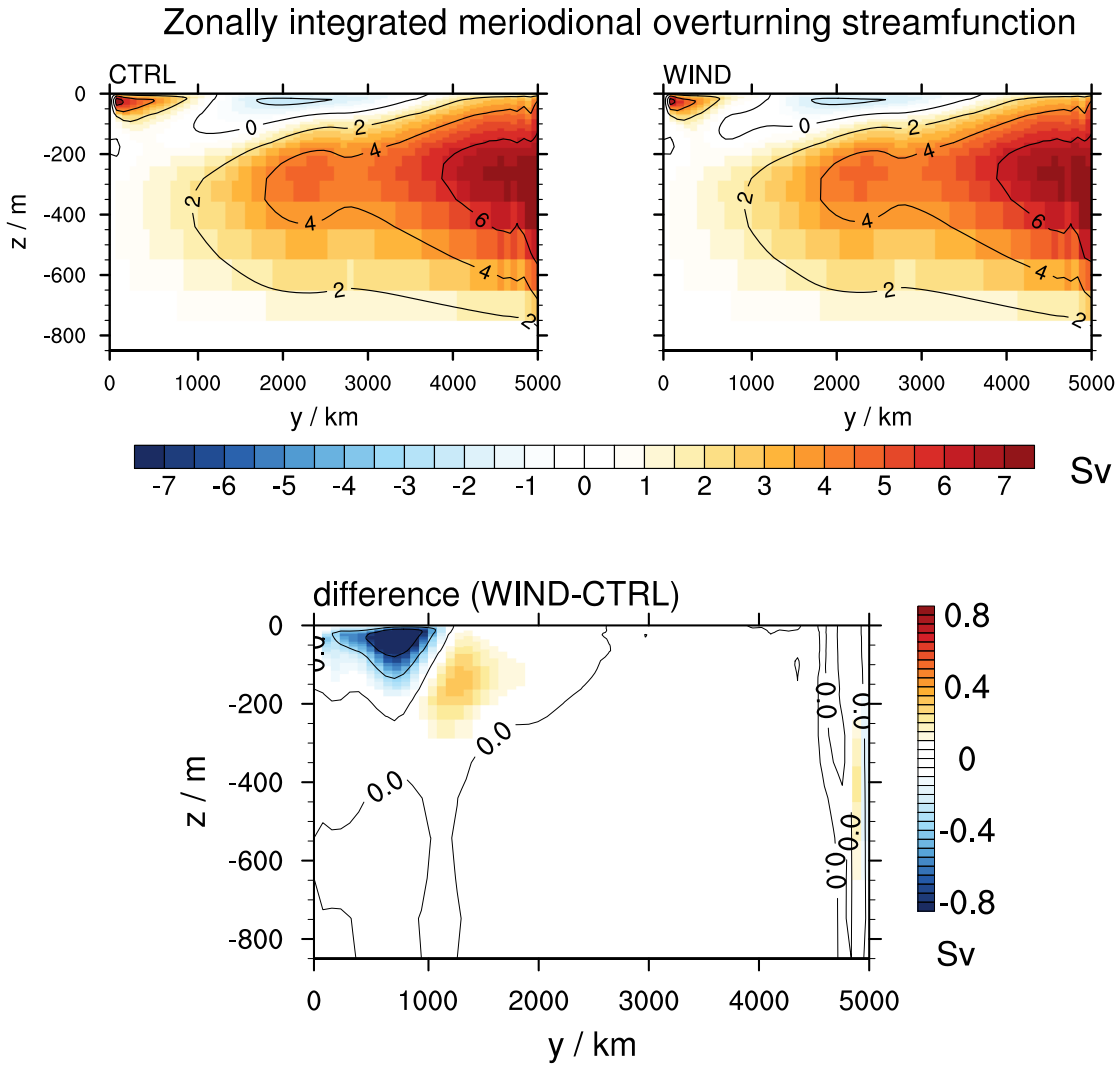

Figure 3.26.: Annual mean zonally integrated meridional overturning streamfunction in experiments CTRL and WIND and the difference between experiments WIND and CTRL.

The changes in the circulation and the temperature field induced by the wind feedback lead to similar secondary effects on the biological components in the model as the changes induced by the absorption feedback. Phytoplankton concentrations are increased in a strip at the southern boundary of the subtropical region as well as at the western boundary in the subtropical region, but decreased at the southern boundary of the ocean basin, in experiment WIND compared to CTRL (Figures 3.27 and 3.28, left). Cyanobacteria concentrations are increased in the southern subtropical region, in the southeastern corner of the ocean basin, and at the southern boundary of the ocean basin, but decreased near the western boundary in the subtropical region, in experiment WIND compared to CTRL (Figures 3.27 and 3.28, right). The westward shift of the subtropical gyre and the decreased downwelling in the subtropical region lead to the increases in the phytoplankton concentrations due to reduced growth limitation by nutrients and a subsequent decrease of the cyanobacteria concentration near the western boundary in the subtropical region. Due to the reduced upwelling at the southern boundary of the ocean basin, phytoplankton concentrations decrease because of more pronounced growth limitation by nutrients, leading to higher cyanobacteria concentrations.

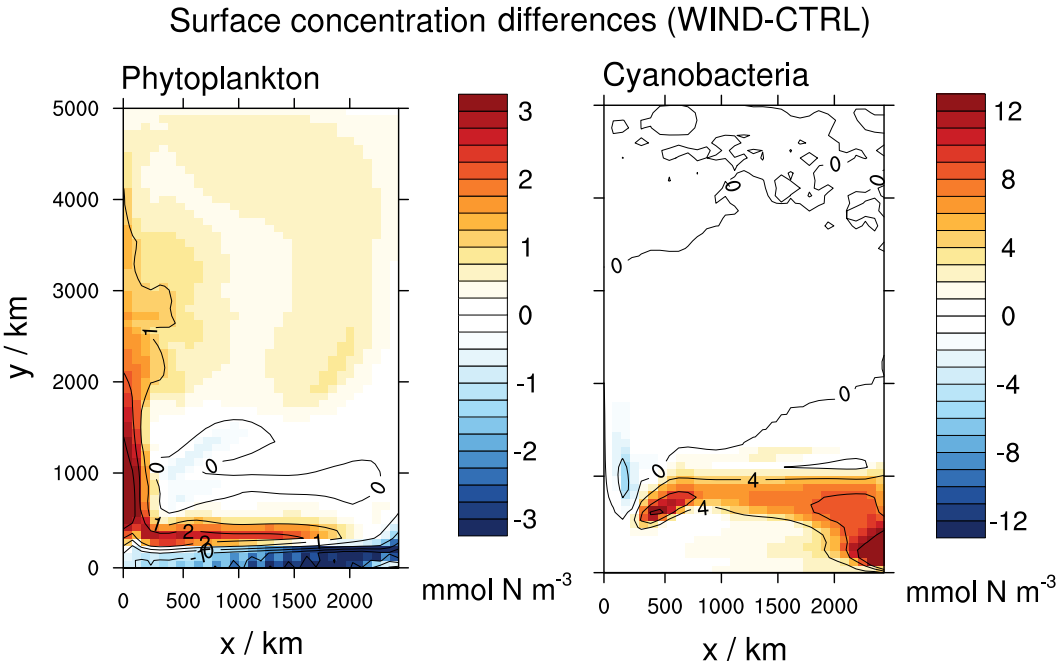

Figure 3.27.: Annual mean phytoplankton and cyanobacteria surface concentration differences between experiments WIND and CTRL.

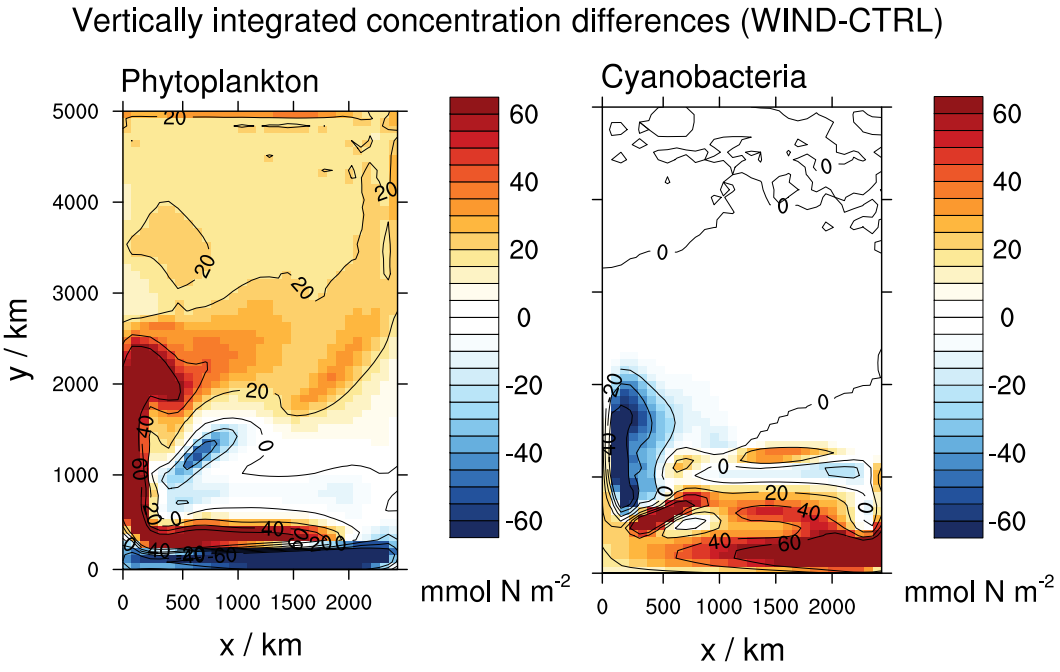

Figure 3.28.: Annual mean phytoplankton and cyanobacteria vertically integrated concentration differences between experiments WIND and CTRL.

3.6.4 | Basin-wide and regional mean effects of the feedbacks

In order to further assess the effects of the different feedbacks, we perform two additional model simulations. In the model experiment ABSALB we include the absorption and the albedo feedback together and in experiment ABSALBWIND we additionally include the wind feedback. In the following we compare the results of these two experiments and experiment ABS with the control experiment CTRL.

In experiment ABS the basin mean temperature is reduced by $0.19 - 0.22\,°C$ during the whole year compared to experiment CTRL (Figure 3.29 (a)). This cooling effect has its minimum in spring and its maximum in fall. The additional effect of the albedo feedback on the basin mean temperature is a very slight cooling, but additionally taking into account the wind feedback leads to an overall cooling of $0.31\,°C$ in the annual mean, again with a minimum in spring and a maximum in fall. The annual cycle of the basin mean surface temperature is slightly shifted backwards in time in experiment ABS compared to experiment CTRL, with an earlier cooling in fall and an earlier warming in spring (Figure 3.29 (b)). This shift is due to the additional warming by phytoplankton and cyanobacteria in experiment ABS and results in basin mean surface temperatures being lower from October to April and higher in the rest of the year in experiment ABS than in CTRL. These surface warming and cooling effects reach $0.17\,°C$ and $-0.14\,°C$, respectively. In experiment ABSALB the mean surface temperature is slightly shifted to lower values compared to experiment ABS, resulting in a slightly stronger cooling and a slightly weaker warming. In experiment ABSALBWIND the cooling effect is even more pronounced and the warming effect is restricted to a shorter period of time with a higher and later maximum compared to experiment ABS.

The different feedbacks also lead to different subsequent effects in the biological model components. Including the absorption feedback leads to a decrease in June and July and an increase in the rest of the year in the basin mean phytoplankton concentration (Figure 3.29 (a)). The additional albedo feedback leads to a decrease and the additional wind feedback leads to an increase during the whole year in the basin mean phytoplankton concentration. The decrease due to the albedo feedback is similarly strong during the whole year, whereas the increase due to the wind feedback is most pronounced in mid summer and least pronounced in spring. Concerning cyanobacteria, the absorption feedback leads to an increase in the basin mean cyanobacteria concentration, which is most pronounced in late spring, whereas the albedo feedback leads to a reduction of the basin mean cyanobacteria concentration which is similarly strong during the whole year (Figure 3.29 (b)). The wind feedback leads to an increase of the basin mean cyanobacteria concentration which is most pronounced in spring.

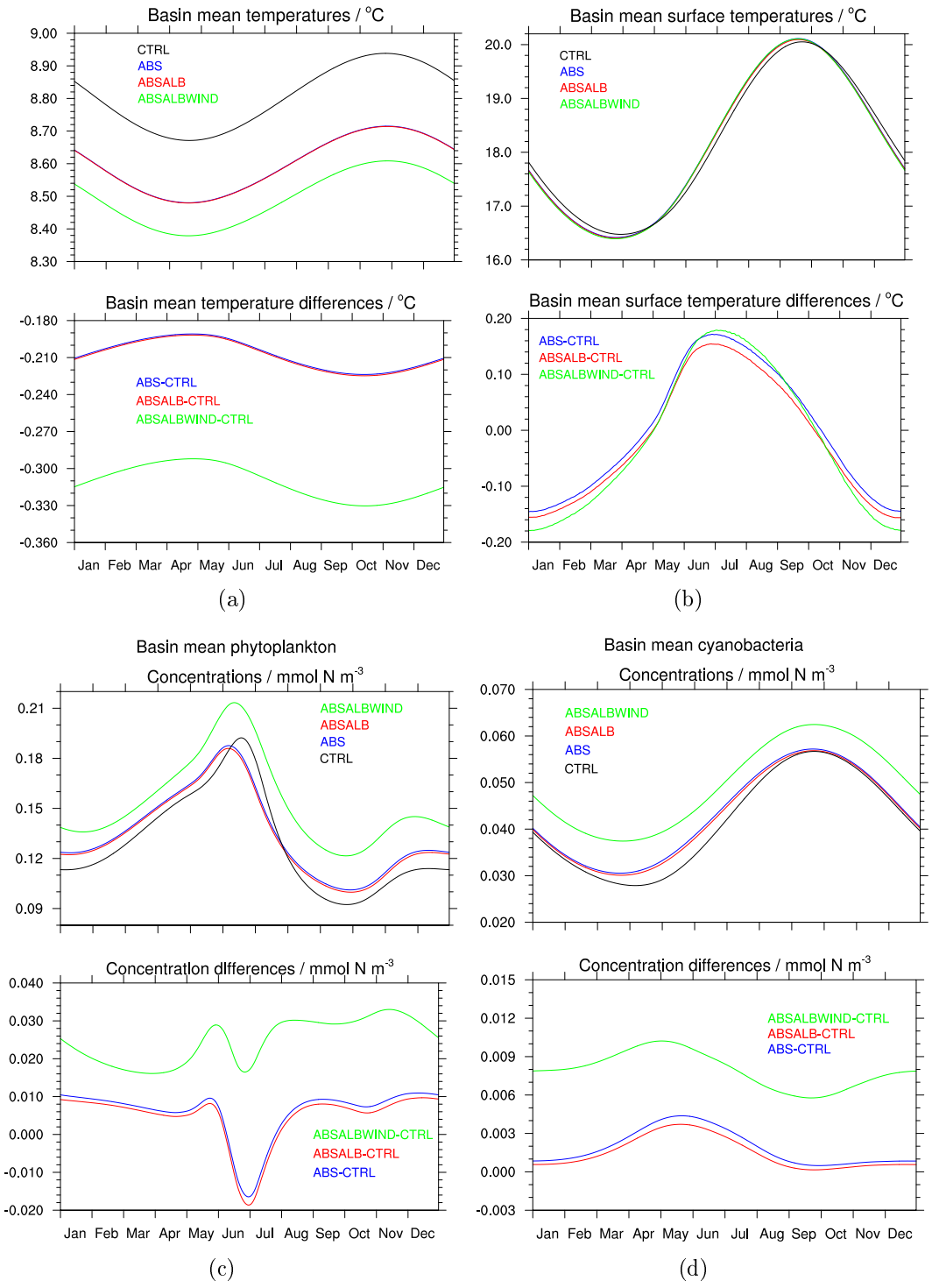

Figure 3.29.: Basin mean temperatures (a), surface temperatures (b), phytoplankton (c), and cyanobacteria (d) concentrations and the differences of experiments ABS, ABSALB and ABSALBWIND compared to CTRL.

To study the regionally different effects of the different feedbacks, we define two regions of interest: the equatorial region, ranging from the southern boundary 240 km north, and the subtropical region, ranging from 240 km to 1440 km north.

In the equatorial region, the mean surface temperature is around 0.3 °C lower in experiment ABS and in experiment ABSALB than in CTRL (Figure 3.30 (a)). In experiment ABSALBWIND the equatorial mean surface temperature is comparable to the one in CTRL in winter and spring, but higher than in CTRL in summer and fall. This means that the absorption feedback has a cooling effect on the equatorial mean surface temperature, the albedo feedback has almost no effect, and the wind feedback has a warming effect, which is most pronounced in summer and fall.

In the subtropical region, the effect of the absorption feedback on the mean surface temperature has a strong seasonal cycle (Figure 3.30 (b)). In experiment ABS the subtropical mean surface temperature is comparable to the one in experiment CTRL in winter, but is up to 0.3 °C higher than in CTRL in summer. In experiment ABSALB the subtropical mean surface temperature difference to CTRL follows the one in ABS, but is going from −0.04 °C in winter to 0.24 °C in summer. In experiment ABSALBWIND the seasonal cycle of the subtropical mean surface temperature difference to CTRL is even more pronounced, going from −0.1 °C in winter to 0.25 °C in summer, and the period of positive temperature difference is shorter. This means that the absorption feedback has a warming effect on the subtropical mean surface temperature, which is most pronounced in summer, the albedo feedback has a cooling effect, and the wind feedback has an additional cooling effect in winter leading to a shorter warming period in summer.

The surface warming effect in the subtropical region and the surface cooling effect in the equatorial region in experiment ABS are due to the increased absorption by cyanobacteria in the subtropical region leading to warmer surface waters and a colder subsurface waters that are then upwelled in the equatorial region. The surface cooling effect in the subtropical region and the surface warming effect in the equatorial region in the experiment including the wind feedback are due to the reduction of the wind-driven downwelling in the subtropical region and the upwelling in the equatorial region. The effect of the albedo feedback is locally limited to a cooling in the subtropical region.

Through direct changes in vertical momentum input by wind and indirect changes via the altered temperature field, also the mixed layer depth (MLD) is affected in regionally different ways by the biological-physical feedbacks.

In the equatorial region, the MLD follows a seasonal cycle with highest values of around 40 m in spring and lowest values of around 20 m in early fall in experiment CTRL (Figure 3.30 (c)). In experiments ABS and ABSALB the equatorial mean MLD is reduced during the whole year compared to experiment CTRL with reductions between 20% in winter and 32% in summer. In experiment ABSALBWIND this reduction is only slightly stronger in spring and summer and slightly weaker from October to December.

In the subtropical region, the MLD follows a seasonal cycle which is more pronounced

than in the equatorial region, reaching highest values of around 60 m in late winter and lowest values of around 20 m in late summer in experiment CTRL (Figure 3.30 (d)). As in the equatorial region, also in subtropical region experiments ABS and ABSALB show a reduction of the equatorial mean MLD during the whole year compared to experiment CTRL with reductions between 19% in winter and 33% in late spring. Experiment ABSALBWIND shows an even stronger reduction of the subtropical mean MLD, with reductions between 36% in winter and 45% in late spring, but the seasonal differences are less pronounced than in ABS and ABSALB.

The reduction of the MLD in the subtropical region due to the absorption feedback are due to the surface warming and subsurface cooling caused by cyanobacteria in this region, leading to an upward shift of the thermocline. The additional reduction of the subtropical MLD by the wind feedback is due to the reduced wind stress by cyanobacteria leading to less vertical mixing and reduced downwelling in this region. In the equatorial region, the reduction of the MLD due to the absorption feedback is due to the cooling effect by upwelled colder subsurface water, which is less pronounced at the surface than subsurface and thus leads to a shallower mixed layer in this region. Since the albedo feedback only leads to a slight surface cooling in the subtropical region, it has almost no effect on the subtropical and the equatorial mean MLD.

The different biological-physical feedbacks also have regionally different effects on the phytoplankton and cyanobacteria concentrations. The absorption feedback leads to an increase in the phytoplankton surface concentrations by about 10–15% in the equatorial region (Figure 3.31 (a)) and by about 20–30% in the subtropical region (Figure 3.31 (b)) during the whole year. Including the absorption feedback also leads to an increase in the cyanobacteria surface concentrations by about 22–32% in the subtropical region (Figure 3.31 (d)), whereas it has a negligible effect on the cyanobacteria surface concentrations in the equatorial region (Figure 3.31 (c)). The albedo feedback reduces the phytoplankton and the cyanobacteria surface concentrations very slightly in both regions. The wind feedback leads to a decrease in the phytoplankton surface concentrations by about 40–70% in the equatorial region (Figure 3.31 (a)) and an increase by about 30–70% in the subtropical region (Figure 3.31 (b)), whereas the cyanobacteria surface concentration is increased in the equatorial region by a factor of around 30 (Figure 3.31 (c)) and by around 40–70% in the subtropical region (Figure 3.31 (d)).

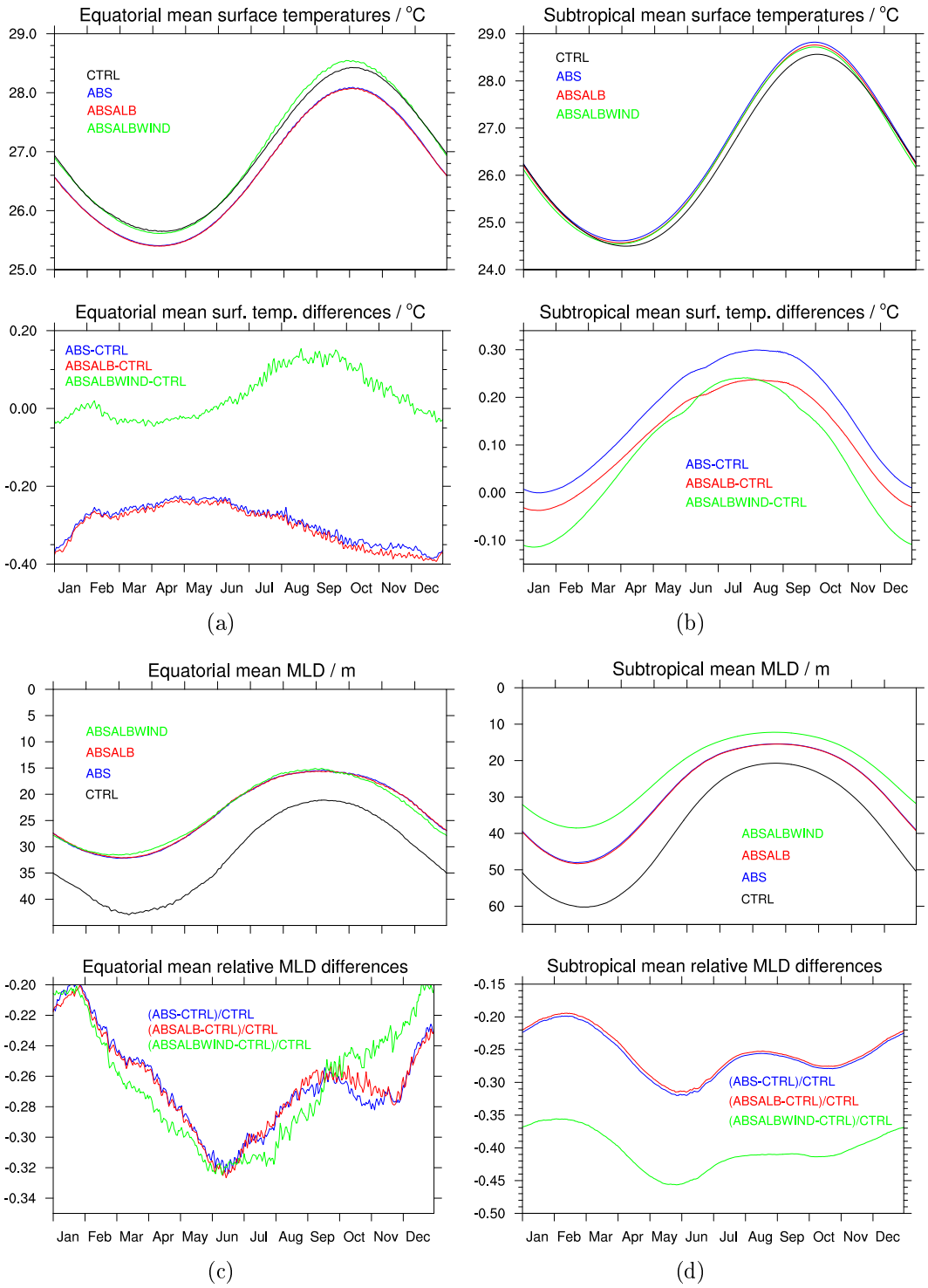

Figure 3.30.: Equatorial (a) and subtropical (b) mean surface temperatures and the corresponding mixed layer depths (MLD) (c)-(d) as well as the differences of experiments ABS, ABSALB and ABSALBWIND compared to CTRL.

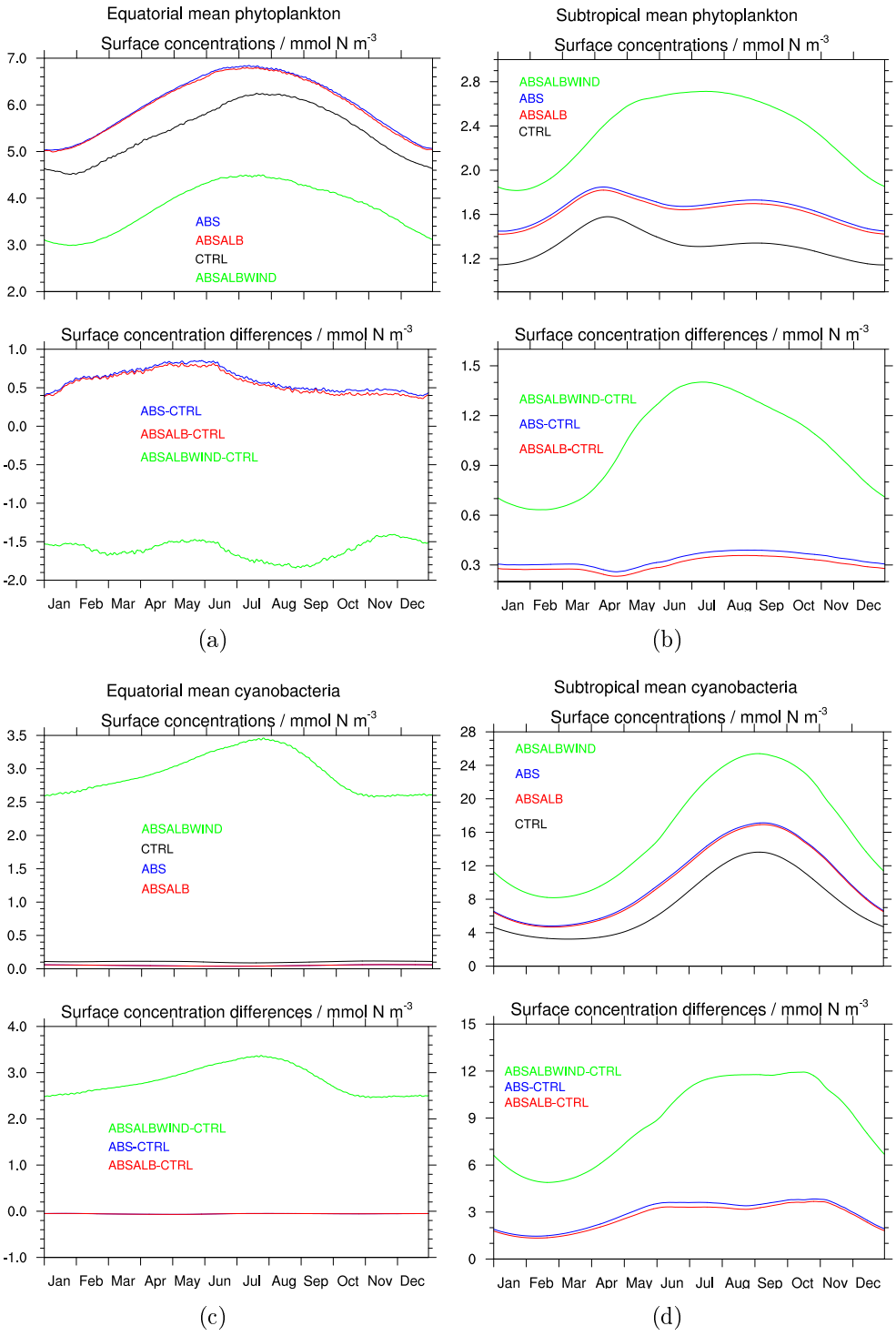

Figure 3.31.: Equatorial (a) and subtropical (b) mean surface phytoplankton concentrations and the corresponding cyanobacteria concentrations (c)-(d) as well as the differences of experiments ABS, ABSALB and ABSALBWIND compared to CTRL.

3.7 | Sensitivity to parameterization of the feedbacks

To study the sensitivity of our model to the parameterization of the different feedbacks we perform additional model simulations with different parameter values in the corresponding parameterizations. For all three feedbacks we perform simulations with a weak, a medium, and a strong feedback, and for the albedo and the wind feedback we perform additional simulations with an extreme feedback strength.

The different parameter values used for the sensitivity studies are the same as for the one-dimensional model studies presented in Chapter 2 and are given in Table 2.2. The relationships between cyanobacteria surface concentration and biologically induced ocean surface albedo increase as well as surface wind stress decrease for the different parameter sets are shown in Figure 2.8.

To study the sensitivity of the model to the choice of parameter values in the feedback parameterizations, we calculate for all experiments the annual mean temperature of the basin mean $\overline{T}$, of the basin surface mean $\overline{T}_{\text{surf}}$, of the equatorial surface mean $\overline{T}_{\text{equat}}$, and of the subtropical surface mean $\overline{T}_{\text{subtr}}$, as well as the annual mean mixed layer depths averaged over the equatorial region $\overline{M}_{\text{equat}}$ and over the subtropical region $\overline{M}_{\text{subtr}}$. These values as well as the corresponding values of the control experiment CTRL and the respective differences $\Delta\overline{T}$, $\Delta\overline{T}_{\text{surf}}$, $\Delta\overline{T}_{\text{equat}}$, $\Delta\overline{T}_{\text{subtr}}$, $\Delta\overline{M}_{\text{equat}}$, and $\Delta\overline{M}_{\text{subtr}}$ between the perturbation experiments including the feedbacks and experiment CTRL are shown in Table 3.2 and Table 3.3.

The sensitivity in the basin mean temperature $\overline{T}$ to the choice of parameter values in the absorption and the albedo feedback is essentially negligible compared to the wind feedback sensitivity, where the different parameter values lead to a spread in the resulting basin mean temperatures with annual mean cooling effects between 0.01 °C and 0.18 °C compared to experiment CTRL. The basin mean surface temperature $\overline{T}_{\text{surf}}$ shows a very low sensitivity of the model to the choice of parameter values in the absorption and the wind feedbacks, but a stronger sensitivity with respect to the albedo feedback parameterizations.

In the equatorial and the subtropical region, the sensitivity in the annual mean surface temperatures $\overline{T}_{\text{equat}}$ and $\overline{T}_{\text{subtr}}$ as well as of the mixed layer depths $\overline{M}_{\text{equat}}$ and $\overline{M}_{\text{subtr}}$ to the choice of parameter values is lowest in the absorption feedback, moderate in the albedo feedback, and strongest in the wind feedback, with the exception of the extreme albedo feedback leading to a cooling more than twice as high as the medium albedo feedback in the subtropical region.

exp.	strength	$\overline{T}$	$\Delta\overline{T}$	$\overline{T}_{\text{surf}}$	$\Delta\overline{T}_{\text{surf}}$
CTRL		8.80		18.13	
ABS	small	8.60	-0.20	18.13	0.00
	medium	8.60	-0.20	18.13	0.00
	large	8.60	-0.20	18.13	0.00
ALB	small	8.80	0.00	18.13	0.00
	medium	8.80	0.00	18.12	-0.01
	large	8.80	0.00	18.11	-0.02
	extreme	8.79	-0.01	18.07	-0.06
WIND	small	8.79	-0.01	18.13	0.00
	medium	8.73	-0.07	18.13	0.00
	large	8.70	-0.10	18.13	0.00
	extreme	8.62	-0.18	18.13	0.00

Table 3.2.: Sensitivity of the annual mean basin mean temperature and basin mean surface temperature to the parametrization of the absorption, albedo, and wind feedback describing small, medium, large, and extreme feedback strengths.

exp.	strength	$\overline{T}_{\text{equat}}$	$\Delta\overline{T}_{\text{equat}}$	$\overline{T}_{\text{subtr}}$	$\Delta\overline{T}_{\text{subtr}}$	$\overline{M}_{\text{equat}}$	$\Delta\overline{M}_{\text{equat}}$	$\overline{M}_{\text{subtr}}$	$\Delta\overline{M}_{\text{subtr}}$
CTRL		26.93		26.38		31.7		39.1	
ABS	small	26.64	-0.29	26.55	0.17	23.4	-8.3	29.3	-9.8
	medium	26.64	-0.29	26.55	0.17	23.4	-8.3	29.2	-9.9
	large	26.64	-0.29	26.55	0.17	23.4	-8.3	29.2	-9.9
ALB	small	26.93	0.00	26.37	-0.01	31.7	0.0	39.1	0.0
	medium	26.92	-0.01	26.34	-0.04	31.7	0.0	39.1	0.0
	large	26.91	-0.02	26.32	-0.06	31.6	-0.1	39.2	0.1
	extreme	26.86	-0.07	26.17	-0.21	31.0	-0.7	39.4	0.3
WIND	small	27.00	0.07	26.37	-0.01	32.2	0.5	37.4	-1.7
	medium	27.31	0.38	26.35	-0.03	31.5	-0.2	34.0	-5.1
	large	27.62	0.69	26.33	-0.05	31.2	-0.5	31.6	-7.5
	extreme	28.47	1.54	26.31	-0.07	26.1	-5.6	28.7	-10.4

Table 3.3.: Sensitivity of the annual mean equatorial and subtropical mean surface temperatures and mixed layer depths to the parametrization of the absorption, albedo, and wind feedback describing small, medium, large, and extreme feedback strengths.

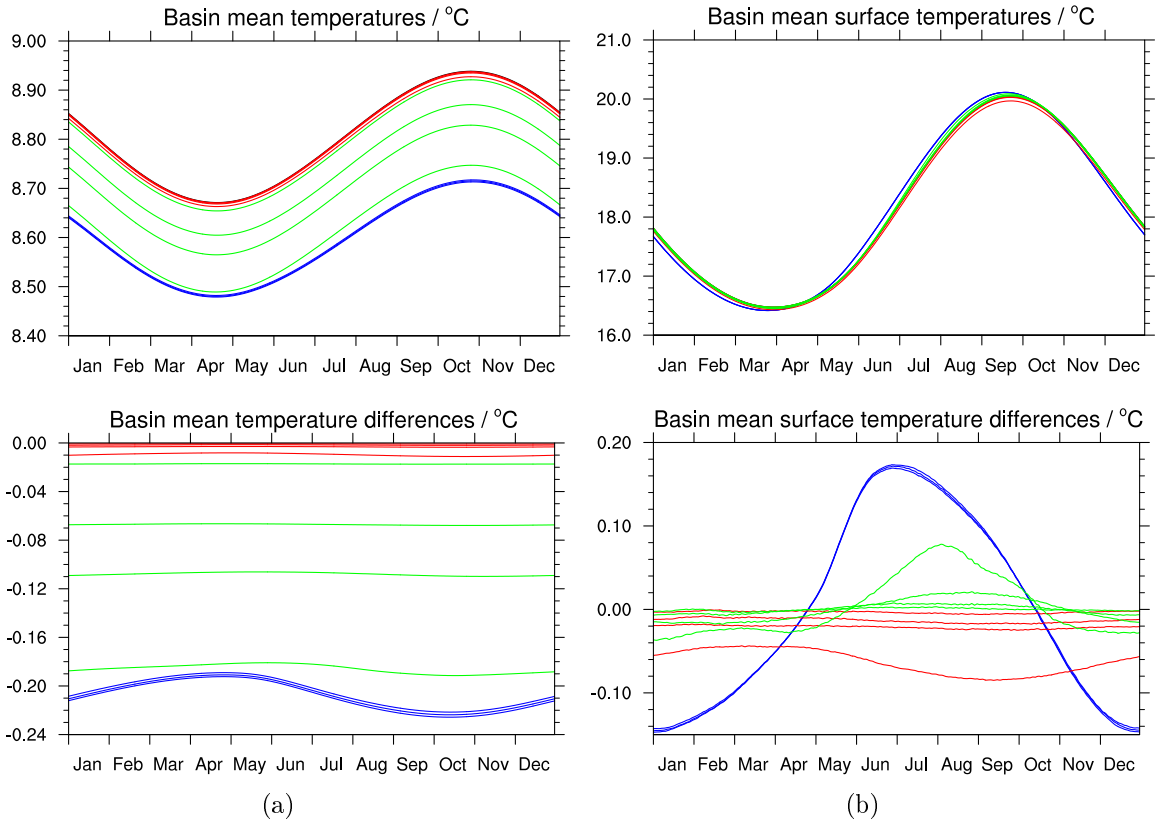

Figure 3.32.: Basin mean temperature (a) and basin mean surface temperature (b) and the corresponding differences for experiments ABS (blue), ALB (red) and WIND (green) compared to CTRL (black) for the different feedback parameter values.

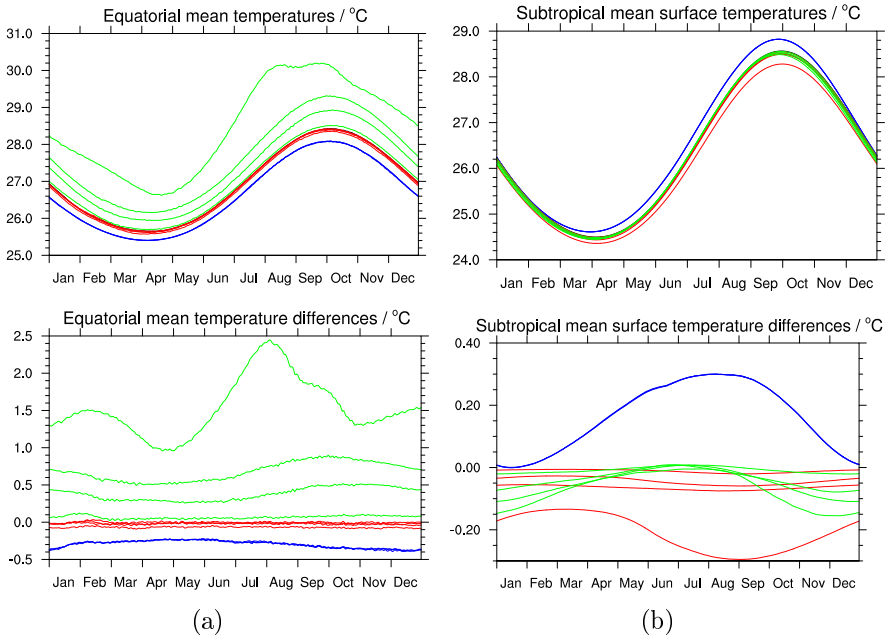

Figure 3.33.: Equatorial (a) and subtropical (b) mean surface temperature and the corresponding differences for experiments ABS (blue), ALB (red) and WIND (green) compared to CTRL (black) for the different feedback parameter values.

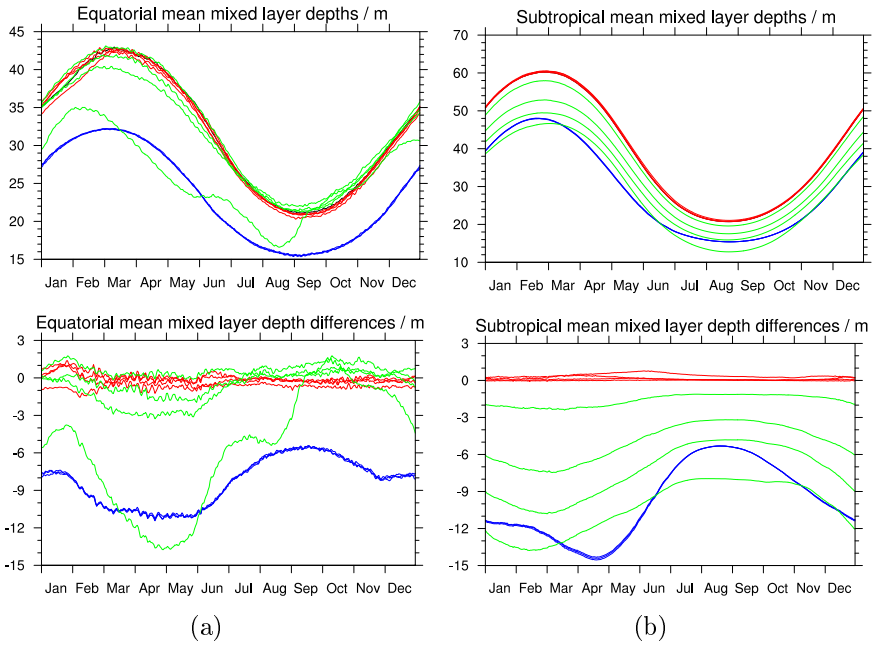

Figure 3.34.: Equatorial (a) and subtropical(b) mean mixed layer depths and the corresponding differences for experiments ABS (blue), ALB (red) and WIND (green) compared to CTRL (black) for the different feedback parameter values.

3.8 | Separation of the two different pathways of the wind feedback

Since in our model setup the surface wind stress is used both as an upper boundary condition in the horizontal momentum equations and for the vertical turbulent momentum flux, a change in the surface wind stress due to cyanobacteria leads to changes in the horizontal velocities and in the vertical turbulent mixing, which both lead to changes in the depth of the mixed layer. To separate these two different pathways in the three-dimensional model setup, we perform two additional model experiments: In one experiment, which we call WINDMOM, the reduction of the surface wind stress is only taken into account in the upper boundary condition for the horizontal momentum equations. In another experiment, which we call WINDTURB, the reduction of the surface wind stress is only taken into account in the upper boundary condition for the vertical turbulent kinetic energy. In the experiment WIND, which is described and analyzed in Section 3.6, the reduction of the surface wind stress due to cyanobacteria is included in both parts of the model.

In the experiment WINDMOM, the shallowing of the mixed layer due to surface cyanobacteria is comparably strong as in experiment WIND, whereas in experiment WINDTURB the mixed layer depth is affected only very little (not shown). In experiment WINDTURB the very small effect of the wind stress reduction due to cyanobacteria also leads to very small changes in the cyanobacteria surface concentrations, whereas in experiments WIND and WINDMOM the cyanobacteria surface concentrations are substantially higher than in experiment CTRL. Thus, also the wind stress reduction due to cyanobacteria is smaller in experiment WINDTURB than in experiments WIND and WINDMOM. Yet, this smaller wind stress reduction can only partly explain the much smaller effect of the wind stress reduction on the mixed layer depth in experiment WINDTURB compared to WIND and WINDMOM.

These results indicate that the effect of cyanobacteria at the ocean surface on the mixed layer depth is largely due to the reduction of the horizontal momentum input. Since the corresponding magnitudes of the two different pathways might depend on model specific details, e.g., on the used parameterization schemes, future studies might focus on this aspect to further analyze the separation of the pathways.

3.9 | Summary, discussion and conclusions

The three-dimensional model studies presented in this chapter show how ocean physics and biology influence each other through local and non-local effects mediated by physical-biological feedbacks in the model. For the first time, the specific feedbacks mediated by marine cyanobacteria through ocean surface albedo increase and wind stress reduction have been studied here in a three-dimensional ocean model. We have investigated these feedbacks together with the altered light absorption by phytoplankton and cyanobacteria in a dynamically coupled three-dimensional ecosystem-ocean general circulation

model simulating conditions comparable to the North Atlantic.

3.9.1 | Summary of the feedback effects

The local effect of the absorption feedback is a surface warming in the northern part of the ocean basin during summer due to absorption by phytoplankton and in the subtropical region during the whole year due to cyanobacteria. The increased absorption at the surface leads to less available light subsurface and thus to a subsurface cooling. Due to the changed thermal structure, the absorption feedback leads to a shallower mixed layer in the northern part of the ocean basin as well as in the subtropical region. Non-local effects of the absorption feedback include a surface cooling, for example in the equatorial region, where colder subsurface waters are upwelled. Also the circulation is affected by the absorption feedback, with the meridional overturning circulation being reduced in the northern part and increased in the surface overturning cell close to the southern boundary.

The albedo feedback locally has the effect of a cooling at the surface and reaching also deeper layers in the subtropical region, whereas non-local effects are very weak.

The local effect of the wind feedback is a warming in the equatorial region and a cooling in the subtropical region due to changes in the wind-driven circulation leading also to a shallowing of the mixed layer in the subtropical region. Due to the wind feedback, the wind-driven subtropical gyre gets distorted with a decrease in the maximum sea surface elevation in the anticyclonic gyre and a westward shift of the whole gyre; downwelling is reduced in the subtropical region, and the upwelling at the southern boundary of the ocean is confined closer to the boundary.

Overall, the biological-physical feedbacks have substantial effects on the upper ocean temperature structure, on the mixed layer dynamics, and on circulation patterns.

Due to the shallower mixed layer and the surface warming, the absorption feedback leads to an increase of locally up to 30% in the phytoplankton concentrations and up to 50% in the cyanobacteria concentrations, whereas the effect of the albedo feedback on the phytoplankton and cyanobacteria concentrations is rather weak. Due to the wind feedback, the phytoplankton concentrations decrease by up to 70% in the equatorial region, but increase by up to 70% in the subtropical region, whereas cyanobacteria concentrations increase by a factor of around 30 in the equatorial region and by up to 70% in the subtropical region. These changes in the phytoplankton and cyanobacteria concentrations due to the wind feedback are explained by the reduced subtropical downwelling and equatorial upwelling leading to locally less or more pronounced phytoplankton growth limitation and subsequently to a less or more pronounced competitive advantage of cyanobacteria over phytoplankton.

3.9.2 | Discussion and conclusions

The increased light absorption in the surface layers and the decreased wind stress due to cyanobacteria lead to higher surface temperatures as well as reduced turbulent mixing, providing positive feedback mechanisms. The negative feedback mechanism via increased surface albedo of cyanobacteria is a lot weaker compared to the positive absorption and wind feedbacks. Cyanobacteria locally create environmental conditions that promoting their own growth. However, the absorption and the wind feedback also have non-local effects leading to a surface cooling and less pronounced growth limitation of phytoplankton, and thus to less beneficial conditions for cyanobacteria.

The effect of increased light absorption at the surface by phytoplankton leading to surface warming and subsurface cooling has been described and studied in several model studies in the last years. The results of our model studies concerning the magnitude of the temperature differences induced by absorption due to phytoplankton are in the range of previously published studies. (An overview is given in Appendix B.) The models that were used in these studies included ocean general circulation models as well as fully coupled Earth system models with both prescribed or interactive biological components. Yet, these model studies have not explicitly included surface buoyant cyanobacteria and their special characteristics in providing biological-physical feedbacks.

The effects of altered ocean surface albedo and surface wind drag were assessed here for the first time in a fully coupled biological-physical ocean general circulation model. While further quantitative measurements in the field are needed to get more confidence in the magnitude of the simulated effects, the sensitivity studies concerning the parameterizations of the different feedbacks show that the model results are quite robust in a certain range of assumed feedback strengths. The details of the model results might be affected by the idealized nature of our physical and biological model setup. Less idealized atmospheric forcings and boundary conditions of the physical model part and also less idealized parameterizations of the phytoplankton and cyanobacteria model might affect the details of our model results. Yet, our results suggest that buoyant cyanobacteria have substantial effects on upper ocean dynamics.

Our coupled biological-physical ocean general circulation model study allows to investigate in detail the local and non-local effects of the different feedbacks mediated by surface buoyant cyanobacteria. Our study suggests that marine biological feedbacks affect the ocean's temperature structure, mixed layer dynamics, and circulation patterns. Climate scenario model simulations should therefore start to incorporate changes in surface ocean biota.

Chapter 4

Biological-physical feedbacks in a warming scenario

In the previous chapter, we have studied the local and non-local biological-physical feedback mechanisms in a three-dimensional model framework. We have seen that cyanobacteria driven feedbacks can have substantial effects on the mixed layer dynamics and circulation patterns. In this chapter, we describe and analyze simulations with and without the feedbacks in a warming scenario. In this scenario we study the effect of a changing phytoplankton community in response to higher temperature forcing in the model and the resulting impacts on ocean physics. The aim is to quantify potential changes in the effects of the feedbacks in the future.

In the first section of this chapter, we describe the model setup, which is the same as the one used in the previous chapter, but with an altered temperature forcing. In Section 4.2 we describe and analyze the results of a control simulation using this altered forcing, and in Section 4.3 we include the biological-physical feedbacks in the model and analyze the effects of the feedbacks in this warming scenario. We close the chapter with a section drawing conclusions from the three-dimensional warming scenario model simulations.

4.1 | Model setup

Since cyanobacteria are expected to benefit from higher temperatures, we use our model setup to study the effect of a warming induced by higher forcing temperatures on the cyanobacteria distribution and the resulting changes in the effects of the different feedbacks. We use the same biological model setup and the same parameterizations for the coupling of physics and biology, as described in Sections 3.2 and 3.3. We also use the same physical model setup as described in Section 3.1, except for an altered temperature forcing, and repeat the model experiments described in Sections 3.4 and

3.6 with this altered forcing. In order to simulate a projected increase in sea surface temperatures, we increase the surface restoring temperature homogeneously by 3 °C (Figure 4.1).

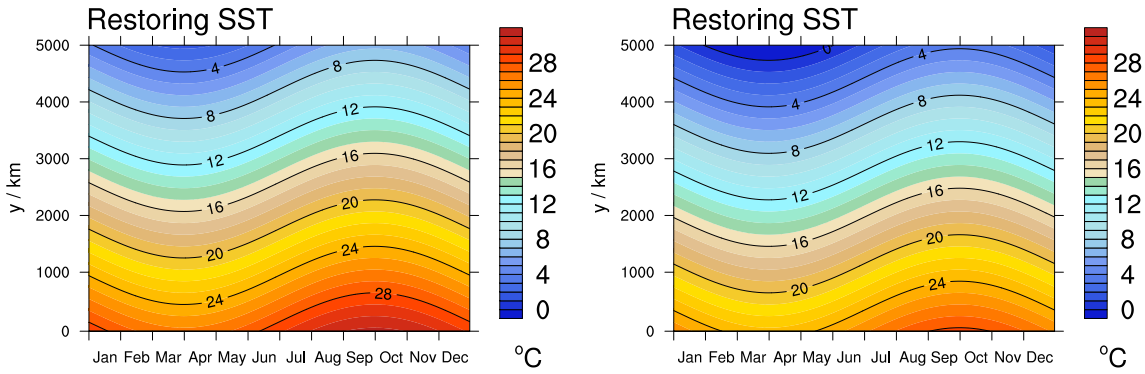

(a) (b)

Figure 4.1.: Annual cycle of surface restoring temperature in the warming scenario (a) and in the present-day case (b).

4.2 | Control simulation

In the following, we describe the differences between the control simulation without including any feedbacks in the model for the warming scenario, which we call CTRL*, and experiment CTRL for the present-day case, which is described in Section 3.4.

The altered temperature forcing in the warming scenario leads to a shift of the sea surface temperature in experiment CTRL* that follows the shift in the restoring surface temperature very closely. That is, the surface temperature field has a strong positive north-south gradient and a pronounced seasonal cycle in both scenarios, while the temperature field is increased by 3 °C almost completely homogeneously in experiment CTRL*. The mixed layer dynamics is almost identical in both scenarios, with a rather shallow mixed layer in the southern part of the ocean basin, less pronounced stratification at the southern boundary due to upwelling, and a larger mixed layer depth in the northern part of the basin. Figure 4.2 shows the annual mean surface temperatures and mixed layer depths in experiments CTRL and CTRL* as well as the corresponding differences.

Also the vertical temperature structure is almost identical in the two scenarios (Figure 4.3) with the only difference of an almost completely homogeneous shift of the temperature field by 3 °C. This shift of the temperature field is also reflected in the annual cycle of the basin mean temperature and the basin mean surface temperature (Figure 4.4).

Since the wind forcing is not changed, also the warming scenario simulation shows the western-intensified double-gyre structure with a cyclonic gyre in the northern part and an anticyclonic gyre in the southern part of the model domain. The surface and deep currents and the overturning structure are also almost identical in the two scenarios (not shown).

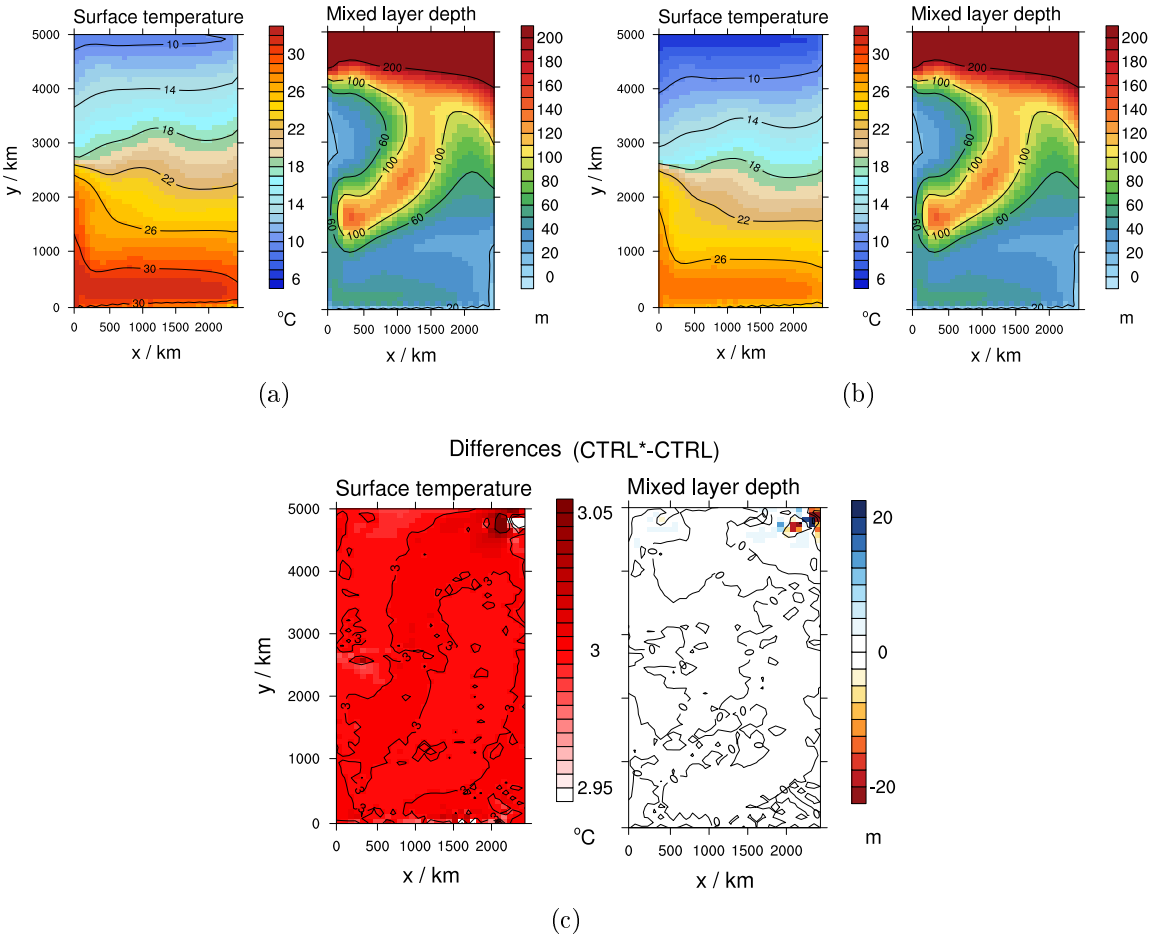

Figure 4.2.: Annual mean surface temperature and mixed layer depth in the warming scenario control simulation CTRL* (a) and in the present-day scenario control simulation CTRL (b) as well as the corresponding differences between experiments CTRL* and CTRL (c).

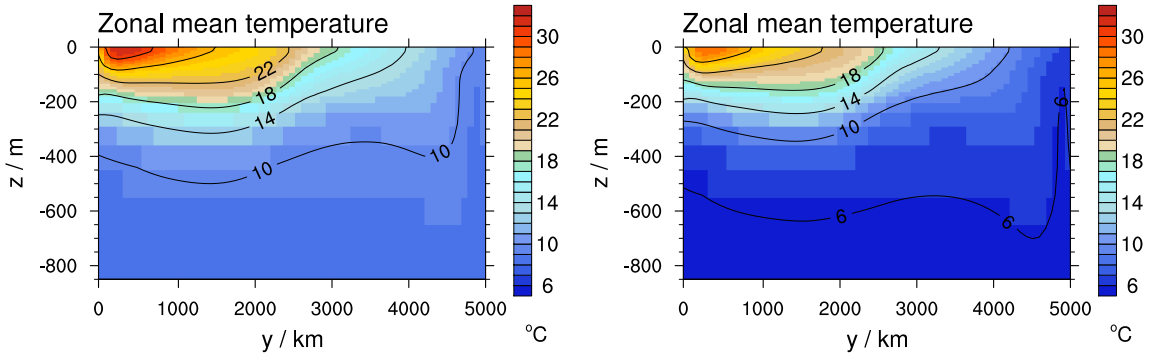

(a) (b)

Figure 4.3.: Annual zonal mean temperature in the warming scenario control simulation CTRL* (a) and in the present-day scenario control simulation CTRL (b).

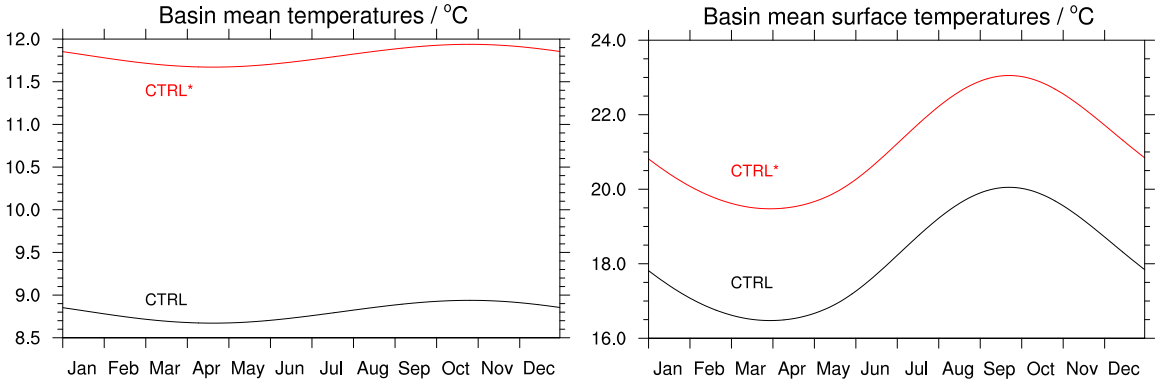

(a) (b)

Figure 4.4.: Basin mean temperatures (a) and basin mean surface temperatures (b) in the warming scenario control simulation CTRL*, in the present-day scenario control simulation CTRL.

Biological variables

Due to the higher temperatures in the warming scenario, the conditions for cyanobacteria growth are altered, since their growth rate depends on temperature. The size of the region where cyanobacteria growth at the surface is limited by temperature generally decreases in the warming scenario compared to the present-day case (Figure 4.5). The surface area where temperatures do not limit cyanobacteria growth extends more to the north in the warming scenario compared to the present-day case. However, the surface temperatures increase beyond the temperature optimum for cyanobacteria growth near the southern boundary of the ocean basin in the warming scenario. This increase leads to a regional growth limitation north of the southern boundary upwelling region, which is most pronounced in fall.

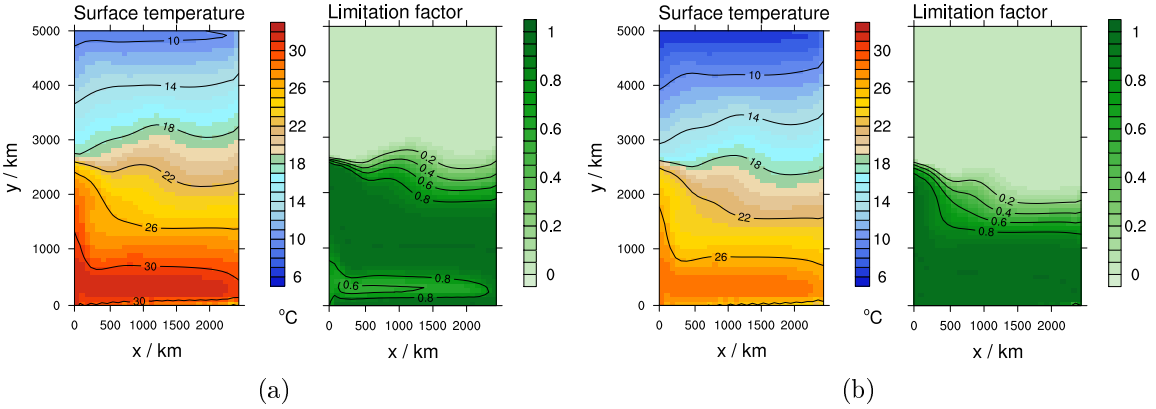

Figure 4.5.: Annual mean surface temperature and the temperature limitation factor for cyanobacteria growth in the warming scenario control simulation CTRL* (a) and in the present-day scenario control simulation CTRL (b).

In response to the altered growth conditions, the surface distribution of cyanobacteria is changed in experiment CTRL* compared to CTRL (Figure 4.6). The region where cyanobacteria occur at the surface spreads northward and increases in its size. In particular in summer, the area covered by cyanobacteria is larger and the maximum cyanobacteria surface concentrations are higher in experiment CTRL* compared to experiment CTRL. In fall, the region covered by cyanobacteria is similarly large in both experiments, but is shifted to the north in experiment CTRL* compared to CTRL. Also the vertically integrated concentrations of cyanobacteria are increased in the warming scenario (Figure 4.7), especially in spring and summer. In fall and winter, the cyanobacteria distribution is rather shifted northward than actually increased in experiment CTRL* compared to CTRL.

The distribution of phytoplankton in the warming scenario follows a similar surface pattern as in the present-day scenario (Figure 4.6). Yet, phytoplankton surface concentrations are slightly increased or decreased regionally. Although phytoplankton growth does not depend on temperature in our model, their growth is affected by the

altered temperature field in indirect ways. Since the input of nitrogen into the system is affected by cyanobacteria growth, the nutrient availability for phytoplankton changes with the cyanobacteria distribution. In addition, cyanobacteria affect the light availability for phytoplankton via shading. Thus, if the cyanobacteria distribution is altered, also the phytoplankton distribution changes.

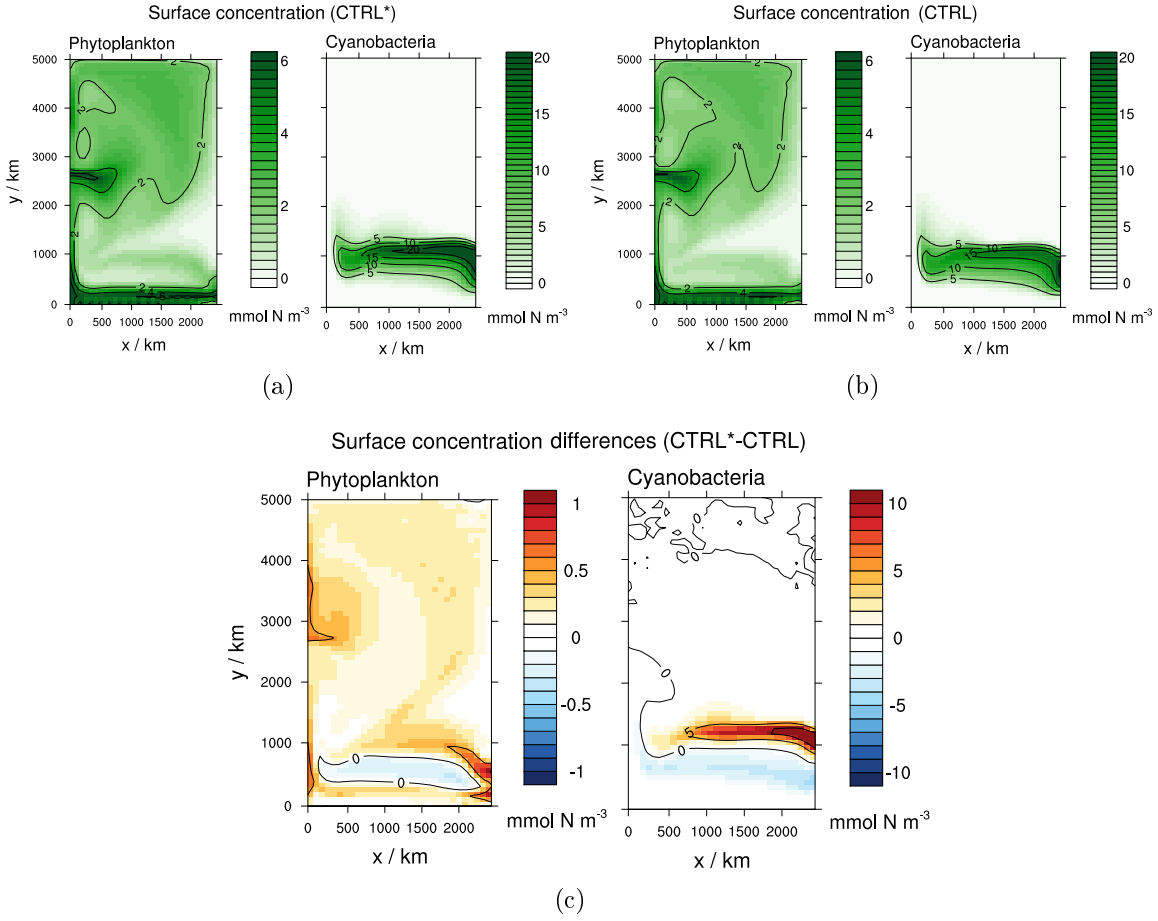

Figure 4.6.: Annual mean phytoplankton and cyanobacteria surface concentrations in the warming scenario control simulation CTRL* (a) and in the present-day scenario control simulation CTRL (b) as well as the corresponding differences between experiments CTRL* and CTRL (c).

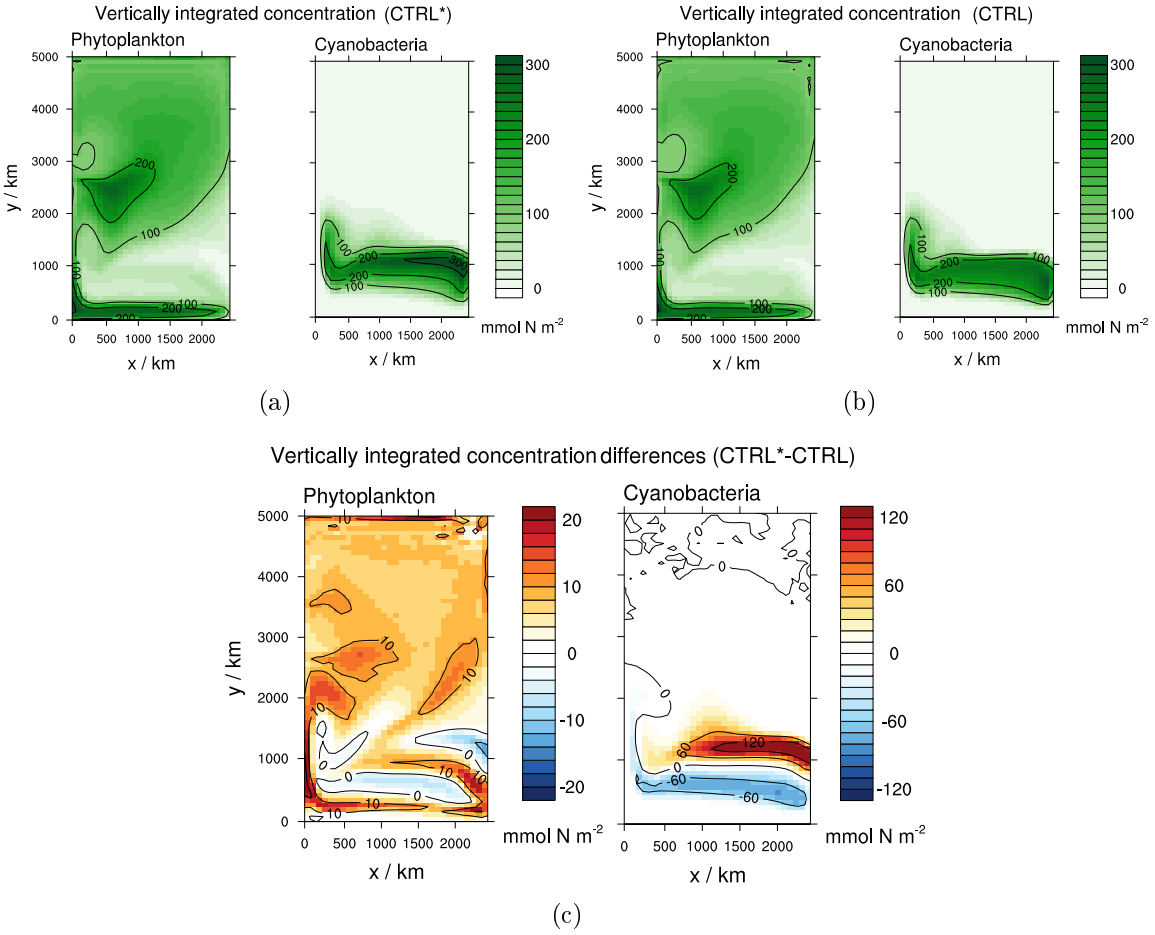

Figure 4.7.: Annual mean phytoplankton and cyanobacteria vertically integrated concentrations in the warming scenario control simulation CTRL* (a) and in the present-day scenario control simulation CTRL (b) as well as the corresponding differences between experiments CTRL* and CTRL (c).

A comparison of the basin mean and basin surface mean cyanobacteria concentrations between experiment CTRL* and CTRL shows that the annual cycle of the mean cyanobacteria concentration is shifted in the warming scenario (Figure 4.8 (a)-(b)). Due to the higher temperatures in the warming scenario the threshold of the cyanobacteria concentration to allow significant growth is exceeded earlier in the year. In the basin mean concentrations, the minimum value is larger and occurs about two months earlier and the maximum value is slightly lower and also occurs about two months earlier in experiment CTRL* than in CTRL. Furthermore, the largest increase in the basin mean cyanobacteria concentration in experiment CTRL* compared to CTRL occurs in late May, whereas the largest decrease occurs in October. In the basin mean surface concentrations, the shift of the minimum and maximum concentrations is about one month, the largest increase occurs in late June and the largest decrease occurs in October.

The annual cycle of the phytoplankton basin mean and basin surface mean concentrations is very similar in both scenarios (Figure 4.8 (c)-(d)) with slightly higher concentrations during the whole year in experiment CTRL* compared to CTRL. The increase in the phytoplankton basin mean and basin surface mean concentrations is highest in July.

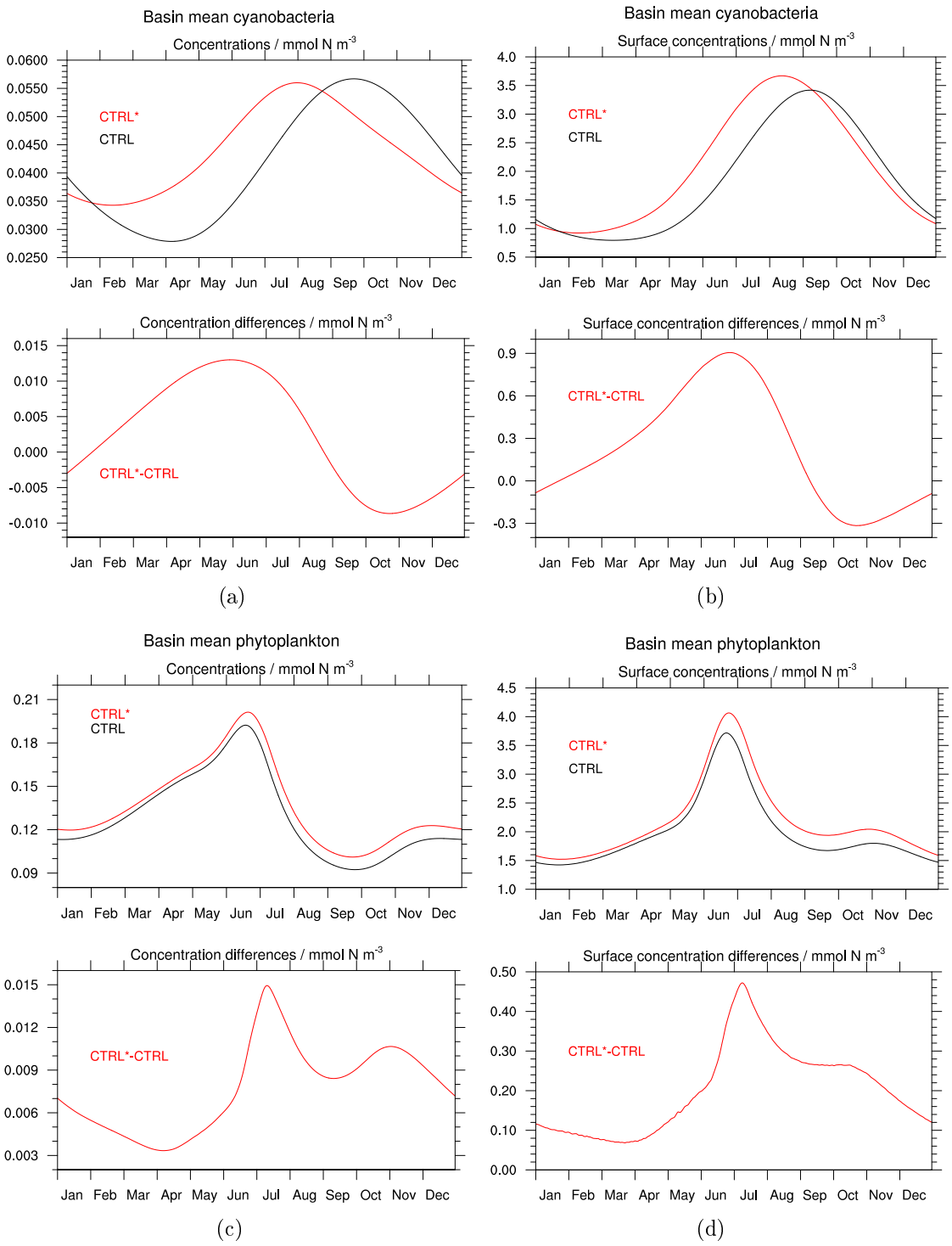

Figure 4.8.: Cyanobacteria basin mean (a) and basin surface mean (b), phytoplankton basin mean (c) and basin surface mean (d) concentrations and the corresponding differences of experiments CTRL* and CTRL.

4.3 | Effects of the feedbacks

Analogous to the present-day scenario model experiments described in Section 3.6, we perform simulations with the coupled biological-physical model taking into account the effects of biology on physics also in the warming scenario. In the following we describe and analyze the results of these perturbation experiments with respect to the differences to the control simulation in the warming scenario as well as to the differences in the corresponding differences in the present-day case.

4.3.1 | Absorption feedback

Effects on physical components

Taking into account the absorption feedback leads to similar effects on the surface temperature and the mixed layer depth in the warming scenario and in the present-day case (Figure 4.9 (a)-(b)). The direct local effect of a surface warming and the indirect effect of a surface cooling due to the circulation can be observed in both scenarios. Yet, in the warming scenario experiment including the absorption feedback (experiment ABS*), the surface warming is stronger by about 0.2 °C in the northern part of the subtropical region, whereas the surface warming is reduced by up to 0.1 °C in the southern part of the subtropical region (Figure 4.9 (c)). These differences can be explained by the increase and northward shift of the cyanobacteria in the warming scenario. The shallowing of the mixed layer in the subtropical region due to the absorption feedback of high cyanobacteria surface concentrations is also more pronounced in the warming scenario. The mixed layer depth decrease in the subtropical region by including the absorption feedback is locally stronger by about 10 m in the warming scenario.

Also below the surface layers, the temperature differences between experiment ABS* and CTRL* and between experiments ABS and CTRL are similar (Figure 4.10 (a)-(b)). Yet, in the warming scenario the subsurface cooling is locally more pronounced by up to 0.2 °C (Figure 4.10 (c)). The effects of the absorption feedback on the surface and deep currents and the overturning structure are also almost identical in the two scenarios (not shown).

Secondary effects on biological components

The different effects of the absorption feedback on temperature and upper ocean dynamics in the two scenarios also lead to different secondary effects on the biological components (Figure 4.11). In the warming scenario, the increase in the phytoplankton surface concentrations is higher in the northern part of the ocean basin and north of the southern boundary and lower in the subtropical region. The increase in the cyanobacteria surface concentrations is stronger in the northern part of the subtropical region and reduced in the southern part of the subtropical region in fall in the warming scenario compared to the present-day case.

The different effects of the absorption feedback in the two scenarios on the vertically integrated concentrations of phytoplankton partly reflect the differences in the

effect on the surface concentrations (Figure 4.12). Yet, the absorption feedback leads to a stronger increase in the vertically integrated phytoplankton concentration in the southern subtropical region, where phytoplankton replace cyanobacteria, and a stronger decrease in the northern subtropical region, where cyanobacteria replace phytoplankton. These shifts in the regional dominance between phytoplankton and cyanobacteria are due to the different surface temperatures in the two scenarios, with suboptimal temperatures for cyanobacteria growth in the southern subtropical region and more favorable temperatures for cyanobacteria growth in the northern subtropical region in the warming scenario. The increase in the vertically integrated cyanobacteria concentrations is stronger in the northern subtropical region in the warming scenario, especially in spring. In fall, however, this increase as well as the decrease in the southern part of the subtropical region are less pronounced in the warming scenario.

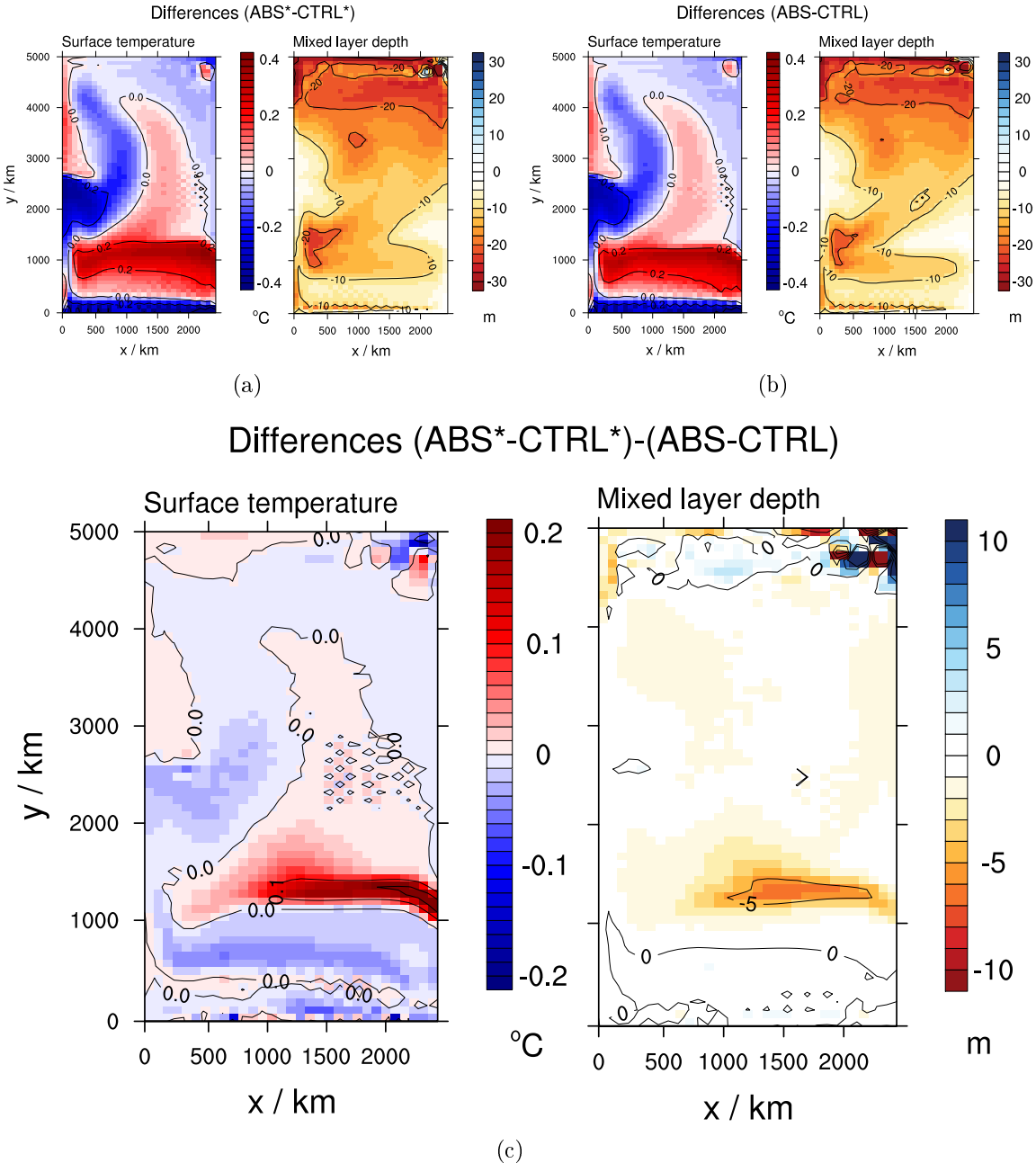

Figure 4.9.: Annual mean surface temperature and mixed layer depth differences between experiment ABS* and CTRL* in the warming scenario (a) and between experiment ABS and CTRL in the present-day scenario (b) as well as the corresponding differences between the differences (ABS*-CTRL*) and (ABS-CTRL) (c).

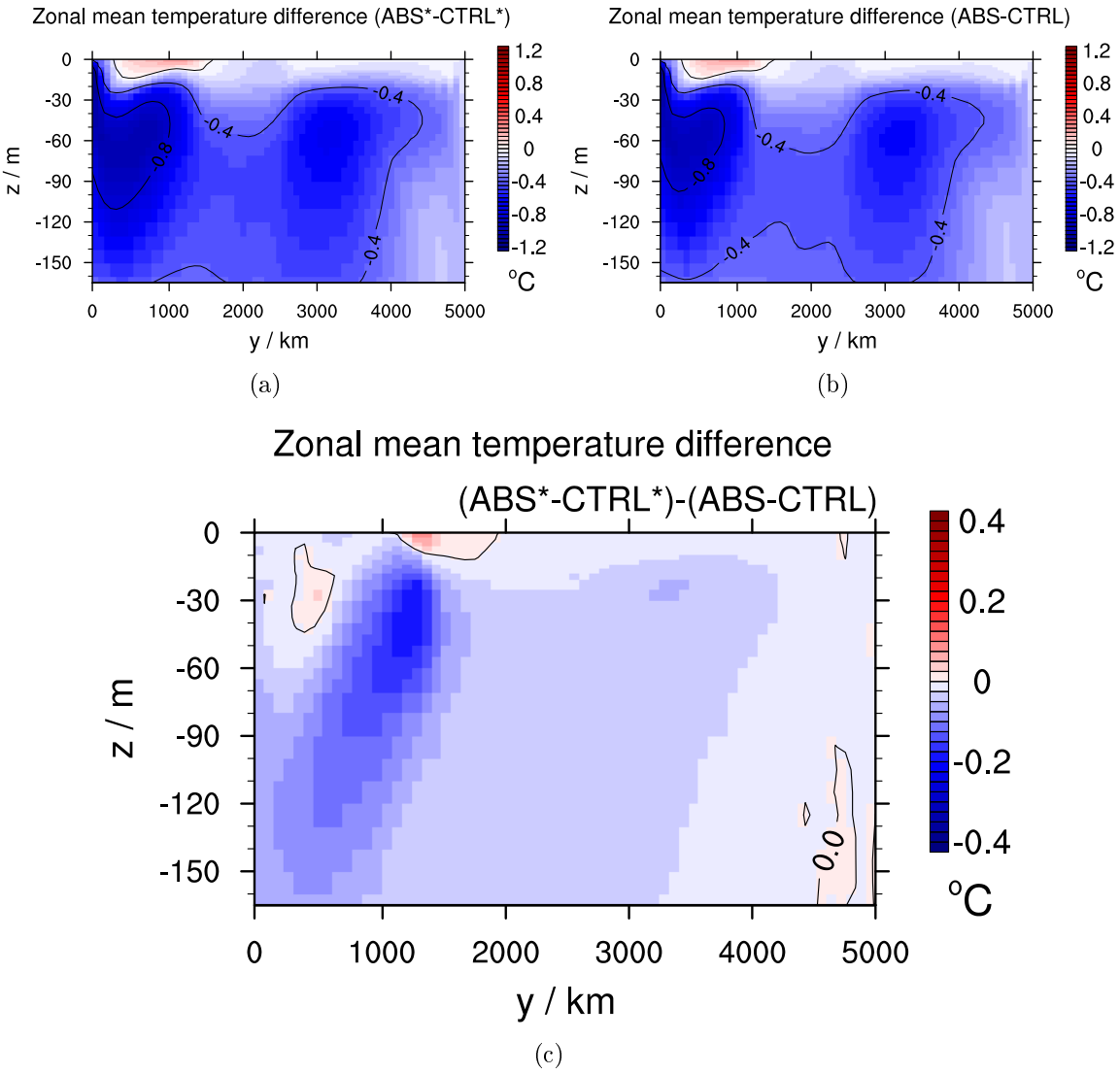

Figure 4.10.: Annual zonal mean temperature differences between experiment ABS* and CTRL* in the warming scenario (a) and between experiment ABS and CTRL in the present-day scenario (b) as well as the corresponding differences between the differences (ABS*-CTRL*) and (ABS-CTRL) (c).

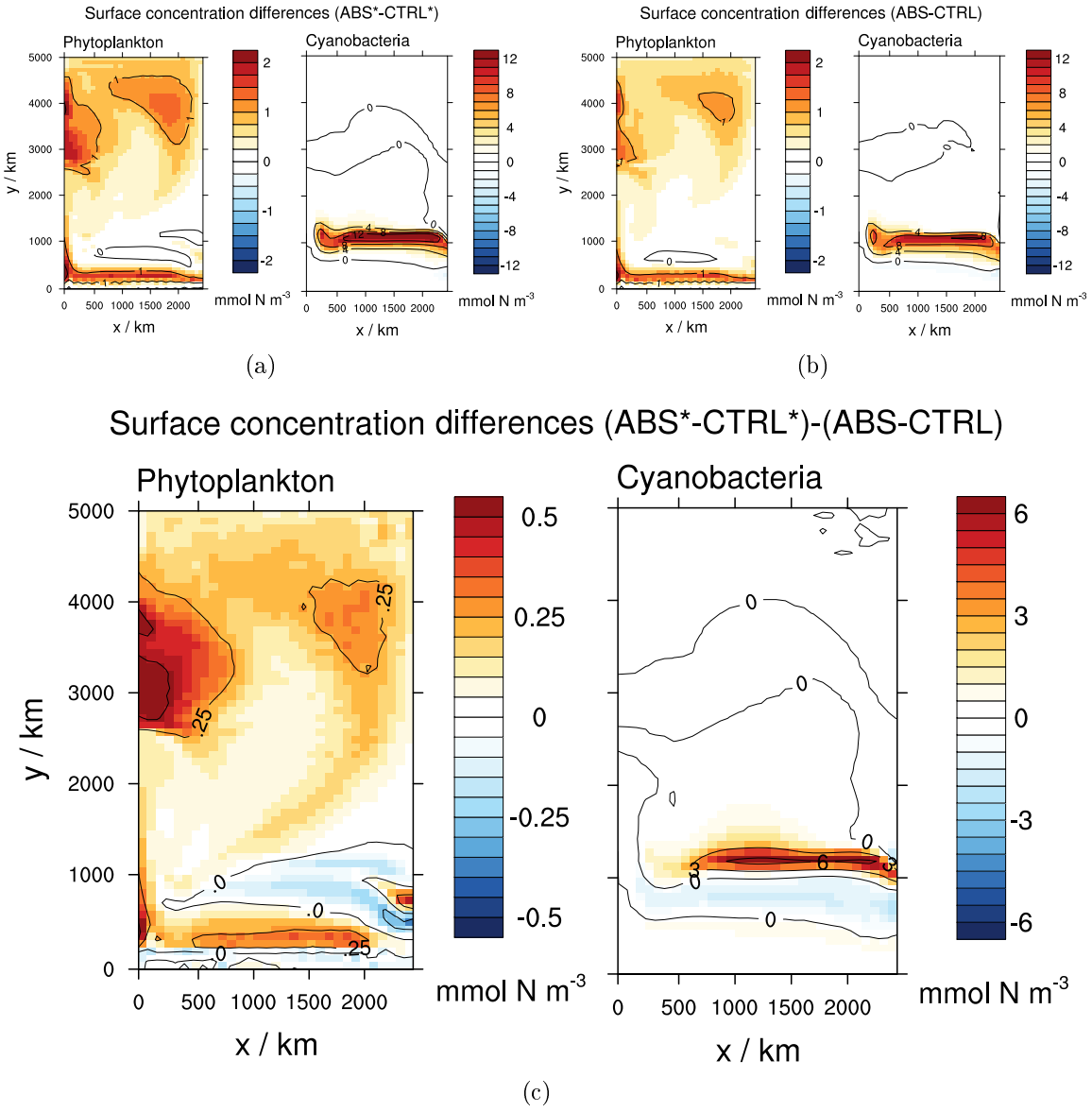

Figure 4.11.: Annual mean phytoplankton and cyanobacteria surface concentration differences between experiment ABS* and CTRL* in the warming scenario (a) and between experiment ABS and CTRL in the present-day scenario (b) as well as the corresponding differences between the differences (ABS*-CTRL*) and (ABS-CTRL) (c).

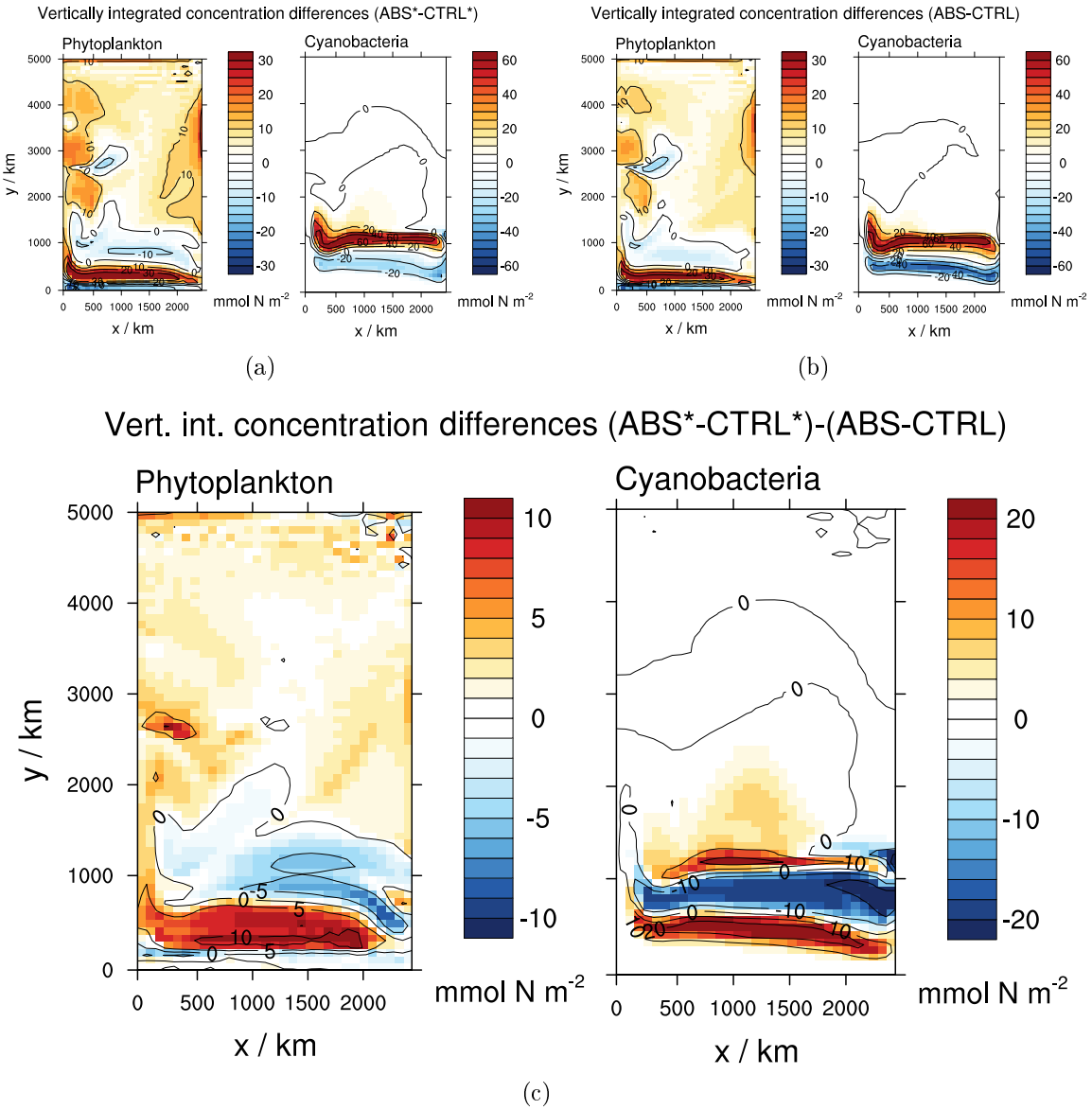

Figure 4.12.: Annual mean phytoplankton and cyanobacteria vertically integrated concentration differences between experiment ABS* and CTRL* in the warming scenario (a) and between experiment ABS and CTRL in the present-day scenario (b) as well as the corresponding differences between the differences (ABS*-CTRL*) and (ABS-CTRL) (c).

4.3.2 | Albedo feedback

The direct local effect of taking into account the ocean surface albedo increase by cyanobacteria is a surface cooling due to increased reflectance of solar radiation. This surface cooling in the subtropics where cyanobacteria surface concentrations are highest reaches 0.1 °C in both scenarios (Figure 4.13) (a)-(b)). Yet, in the warming scenario experiment including the albedo feedback (experiment ALB*), the northward shift of the cyanobacteria leads to an increased cooling effect in the northern part of the subtropical region and a decreased cooling in the southern part of the subtropical region (Figure 4.13 (c)).

The subsurface cooling in the subtropical region due to the wind induced shallow overturning cell at the southern boundary of the ocean basin is similar in both scenarios. Yet, due to the northward shift of the cyanobacteria in the warming scenario, this subsurface cooling is less pronounced in the southern part and more pronounced in the northern part of the subtropical region (Figure 4.14).

The mixed layer depths are barely affected by including the albedo feedback in the model almost everywhere in the ocean basin in both scenarios (Figure 4.13). Also the weak effect of including the albedo feedback on the general circulation and on the biological components is similar in both scenarios (not shown).

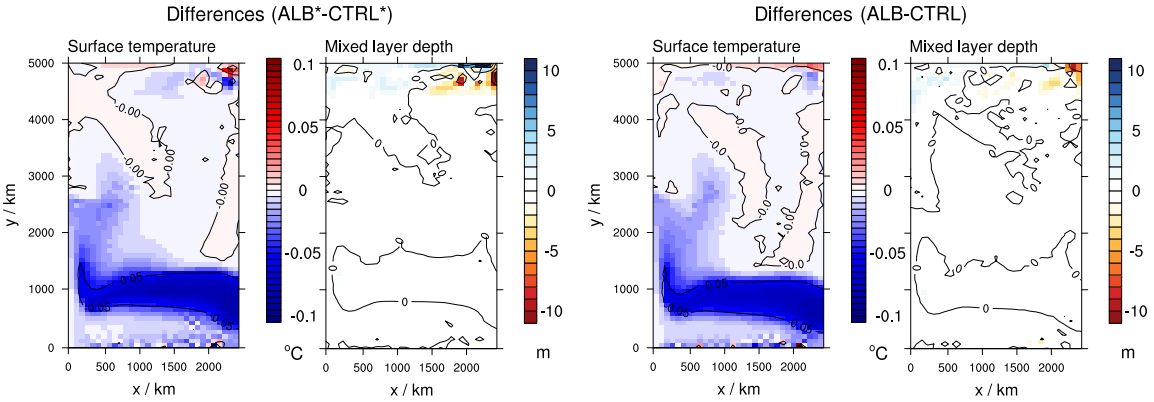

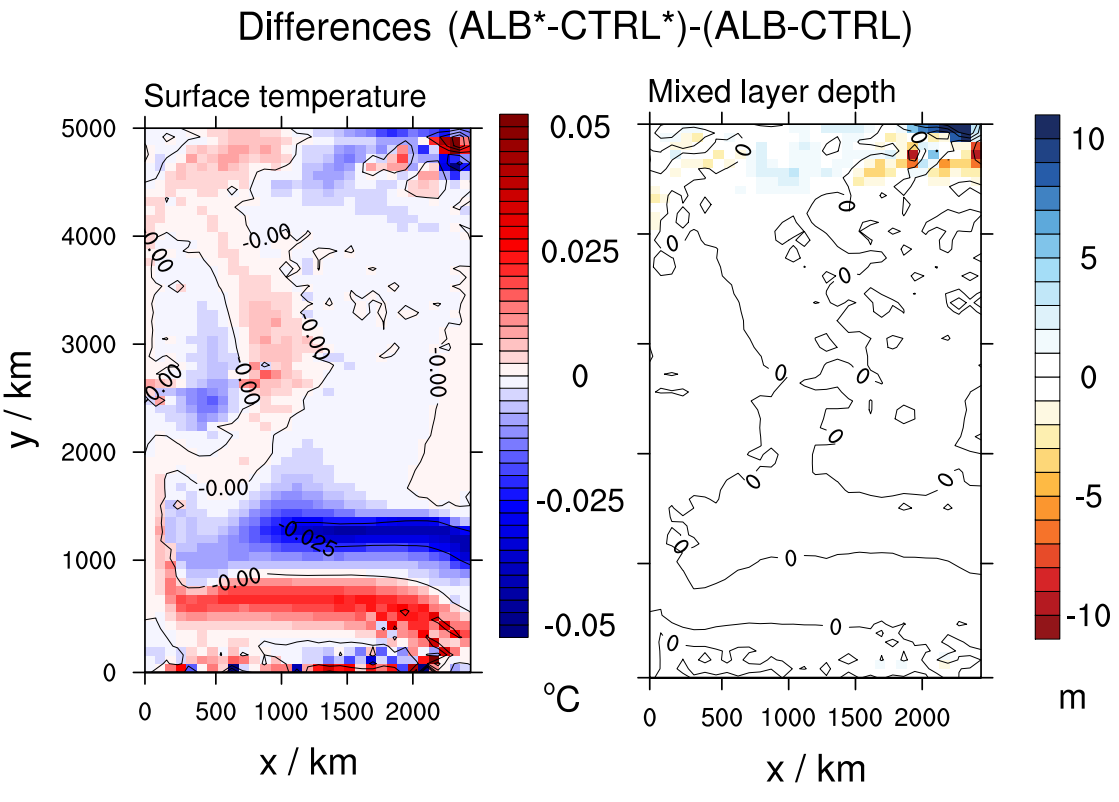

Figure 4.13.: Annual mean surface temperature and mixed layer depth differences between experiment ALB* and CTRL* in the warming scenario (a) and between experiment ALB and CTRL in the present-day scenario (b) as well as the corresponding differences between the differences (ALB*-CTRL*) and (ALB-CTRL) (c).

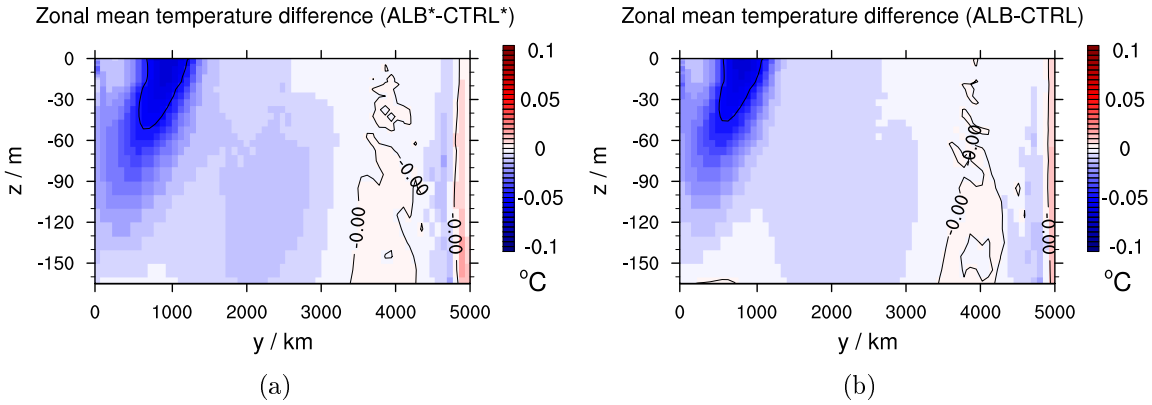

(a) (b)

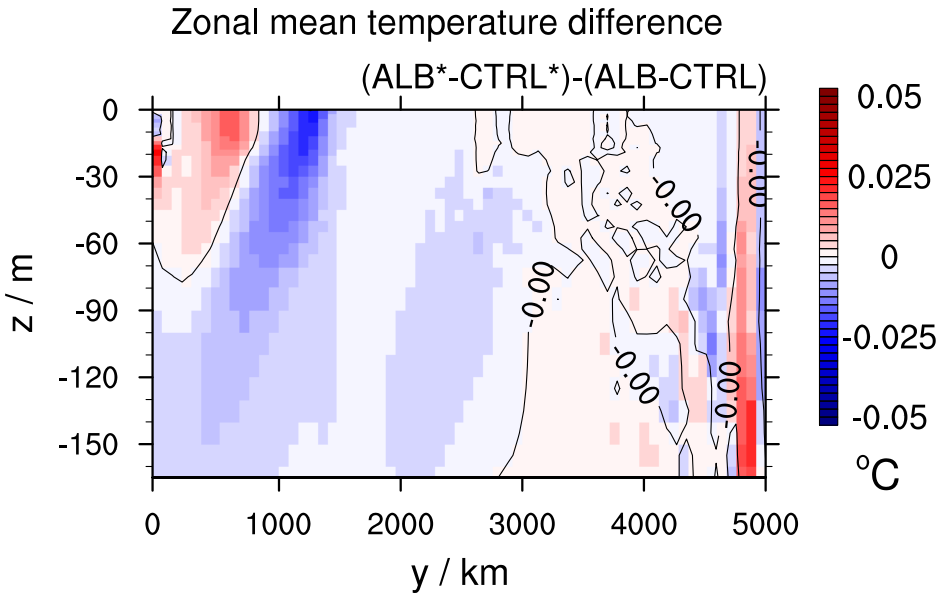

(c)

Figure 4.14.: Annual zonal mean temperature differences between experiment ALB* and CTRL* in the warming scenario (a) and between experiment ALB and CTRL in the present-day scenario (b) as well as the corresponding differences between the differences (ALB*-CTRL*) and (ALB-CTRL) (c).

4.3.3 | Wind feedback

Since the prescribed wind stress forcing is not changed, the surface wind stress is identical in the warming scenario and in the present-day scenario control simulations CTRL* and CTRL (Figure 4.15 (a)-(b)). The surface wind stress in the experiments including the wind feedback (WIND* and WIND) is similar in both scenarios (Figure 4.15 (a)-(b)). Yet, due to the altered cyanobacteria concentrations in the warming scenario, the surface wind stress in the southern subtropical region is locally higher in the warming scenario experiment WIND* compared to the present-day scenario experiment WIND (Figure 4.15 (c), left). The surface wind stress reduction relative to the control simulation is stronger in the northern part and weaker in the southern part of the subtropical region in WIND* compared to WIND (Figure 4.15 (c), right). The distortion of the wind-driven subtropical gyre due to the wind feedback is very similar in both scenarios (not shown).

The reduction of the wind-driven downwelling in the subtropical region and the confinement of the upwelling at the southern boundary of the ocean basin closer to the boundary due to the wind feedback is also similar in both scenarios (Figure 4.16 (a)-(b)). However, these effects are less pronounced in the warming scenario, since the cyanobacteria are shifted northward (Figure 4.16 (c)).

The subsequent changes in the circulation leading to higher zonal mean temperatures in the upper 400 m between the southern boundary and the subtropical region due to decreased upwelling of colder waters from deeper layers as well as to lower zonal mean temperatures in the upper 400 m in the subtropical region due to decreased downwelling of warmer surface water are also similar in both scenarios (Figure 4.17 (a)-(b)). Yet, both these local warming and cooling effects are less pronounced in the warming scenario (Figure 4.17 (c)).

The secondary effects on the biological components in the model due to the changes in circulation and the temperature field induced by the wind feedback are similar in both scenarios (Figure 4.18 (a)-(b)). Yet, the decrease at the southern boundary and the increase in a small strip at the southern boundary of the subtropical region, at the western boundary in the subtropical region, and in the northern part of the ocean basin in the phytoplankton surface concentrations due to the wind feedback are all less pronounced in the warming scenario (Figure 4.18 (c)). Also the increase in cyanobacteria surface concentrations due to the wind feedback is less pronounced in the southern subtropical region and in the southeastern corner of the ocean basin in the warming scenario (Figure 4.18 (c)). The reason for the less pronounced increases in the phytoplankton and cyanobacteria surface concentrations is the less pronounced reduction of the downwelling in the subtropical region and the upwelling at the southern boundary of the ocean basin in the warming scenario compared to the present-day case. The slight increase of the cyanobacteria surface concentration in the northern subtropical region in the warming scenario is due to a northward spread of the cyanobacteria distribution, which is not seen in the present-day scenario.

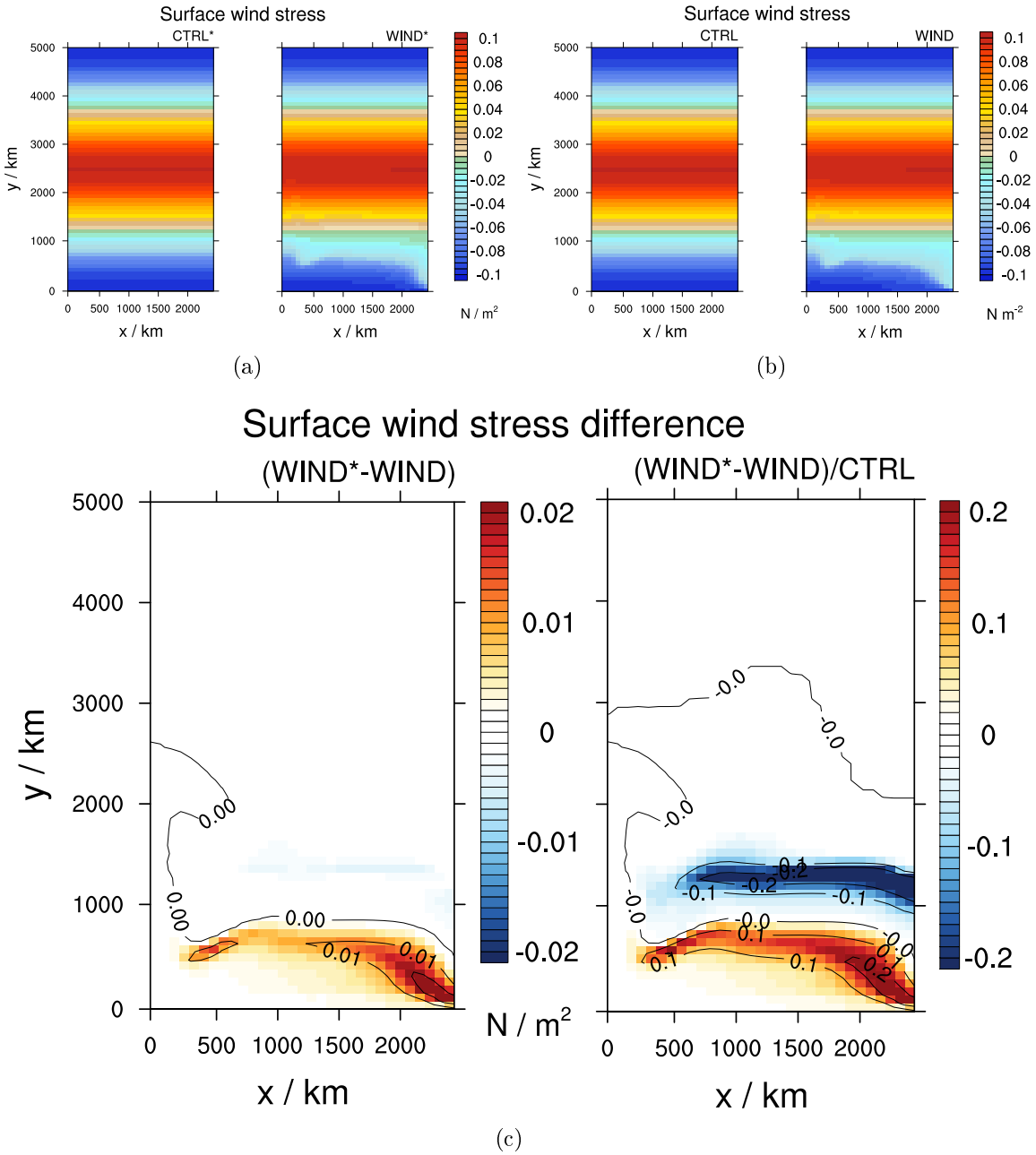

Figure 4.15.: Annual mean surface wind stress in experiments CTRL* and WIND* (a) and in experiments CTRL and WIND (b) as well as the magnitude differences and relative differences between experiments WIND* and WIND (c).

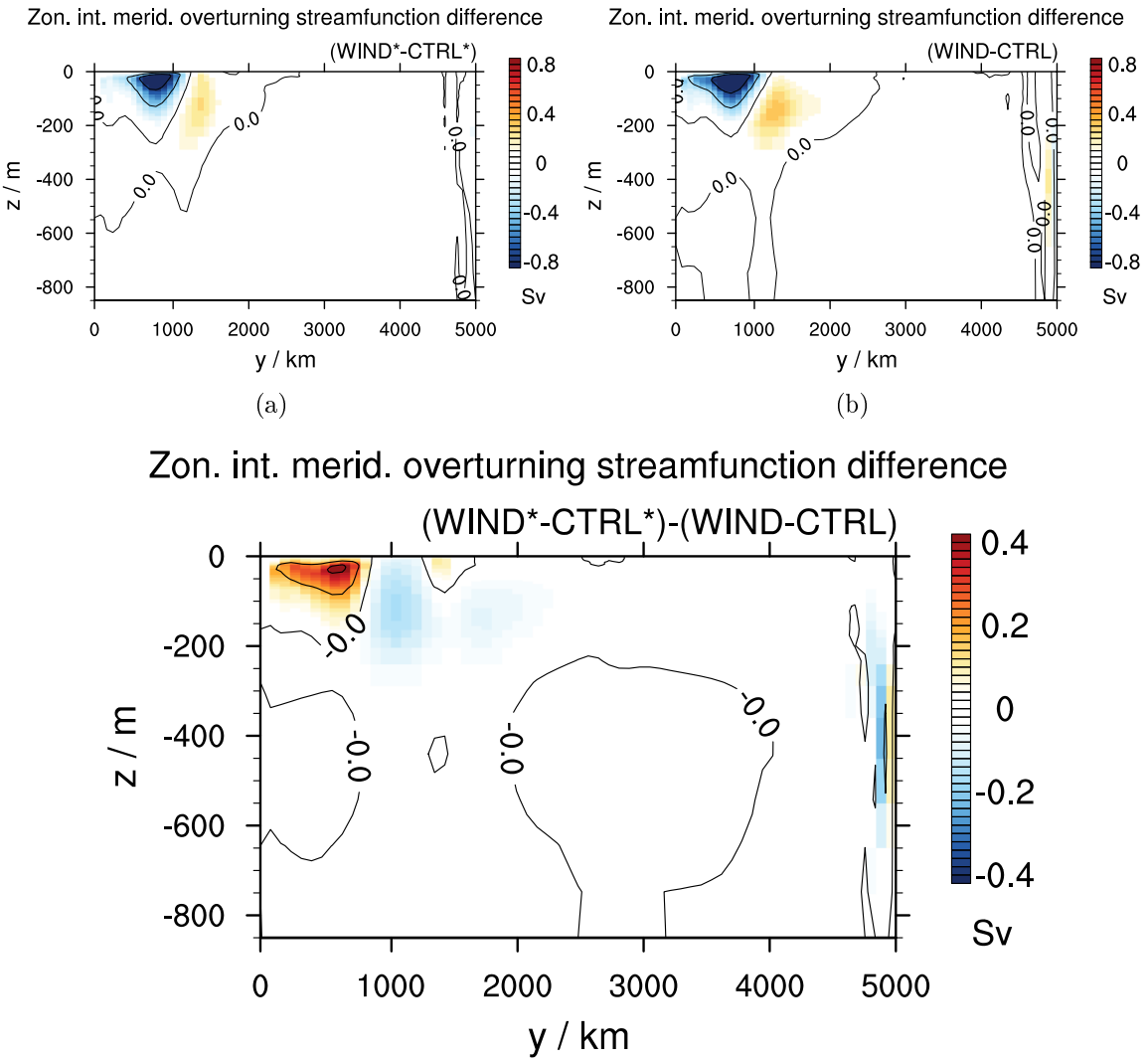

Figure 4.16.: Annual mean zonally integrated meridional overturning streamfunction differences between experiment WIND* and CTRL* in the warming scenario (a) and between experiment WIND and CTRL in the present-day scenario (b) as well as the corresponding differences between the differences (WIND*-CTRL*) and (WIND-CTRL) (c).

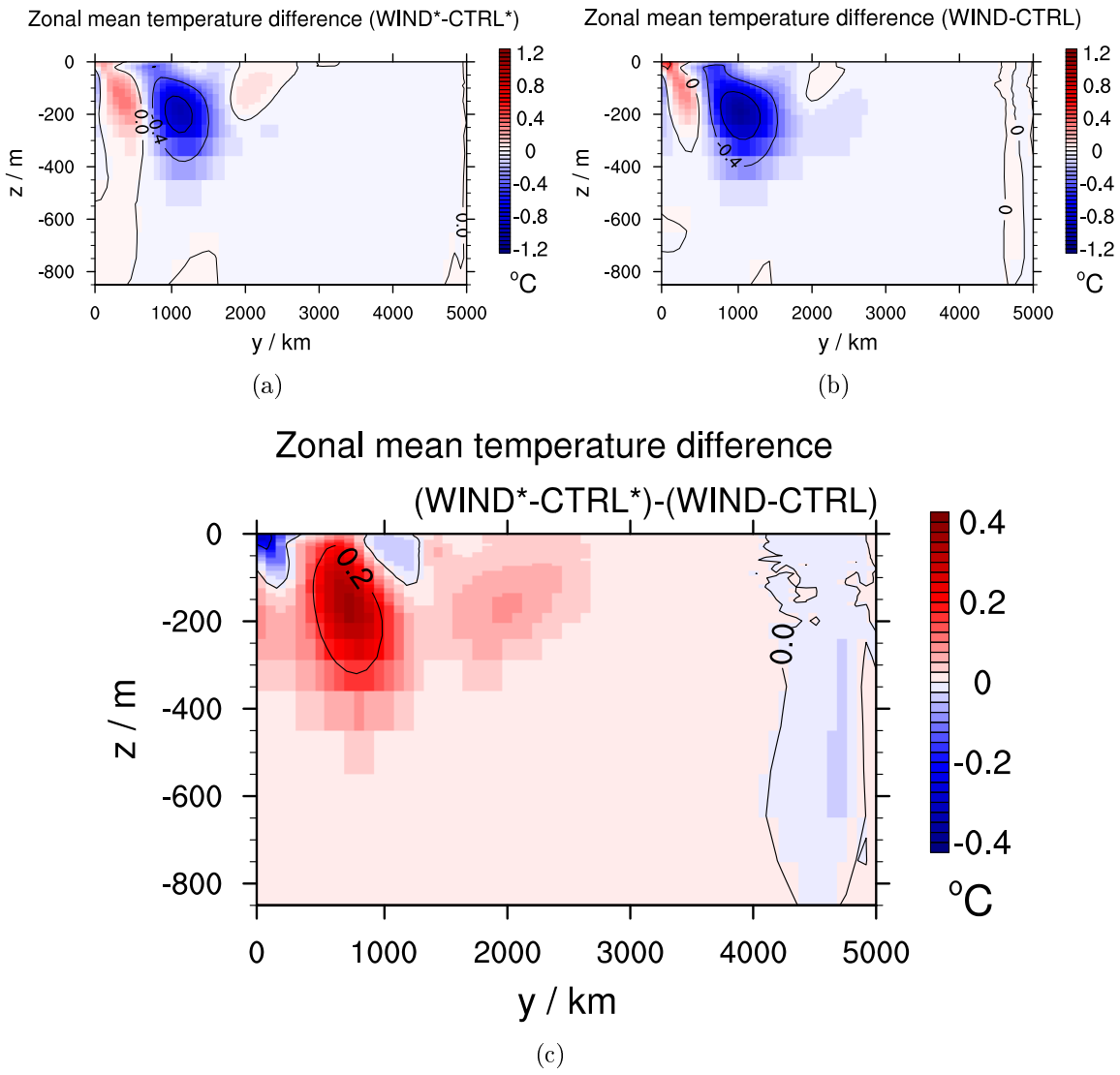

Figure 4.17.: Annual zonal mean temperature differences between experiment WIND* and CTRL* in the warming scenario (a) and between experiment WIND and CTRL in the present-day scenario (b) as well as the corresponding differences between the differences (WIND*-CTRL*) and (WIND-CTRL) (c).

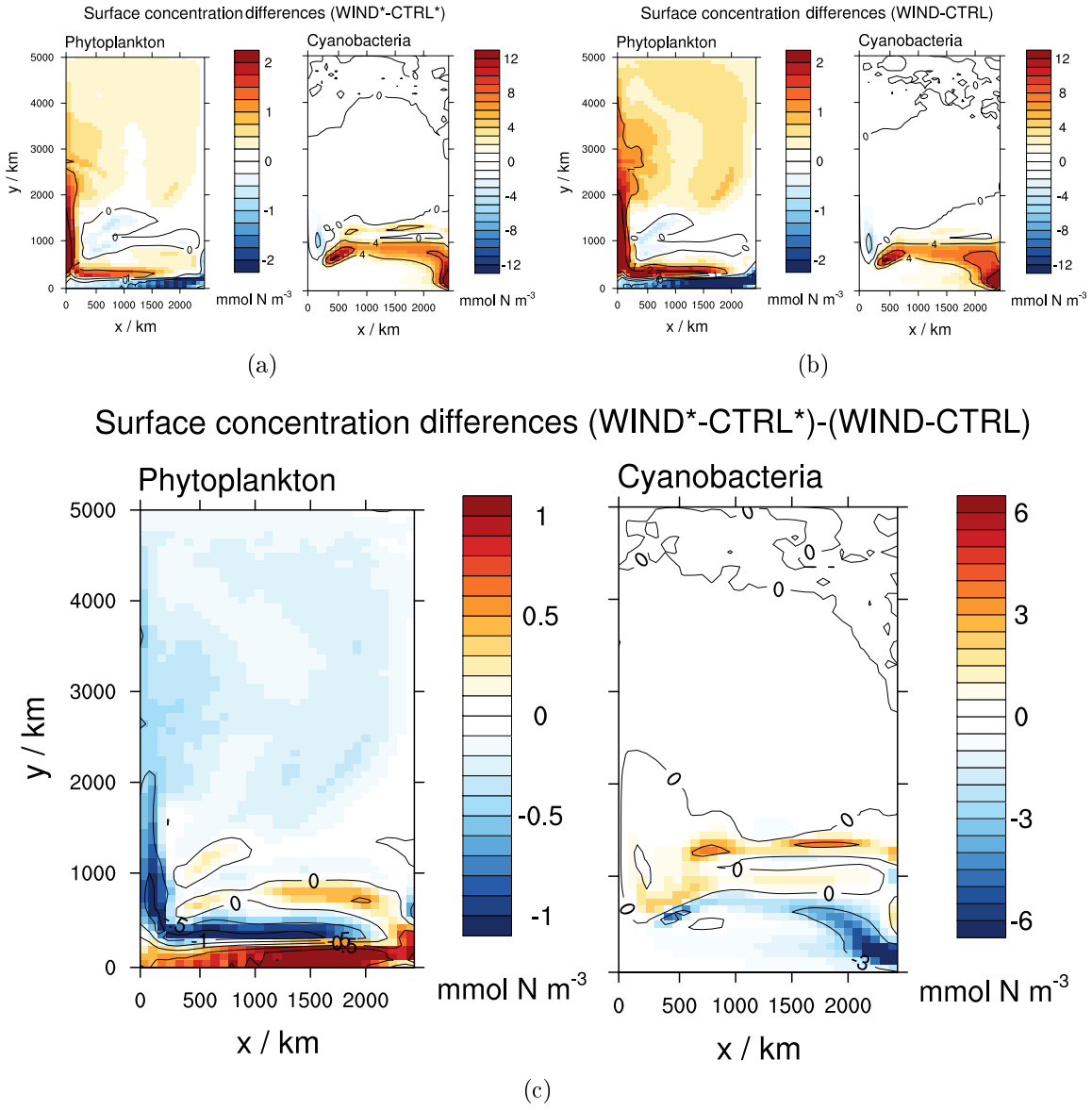

Figure 4.18.: Annual mean phytoplankton and cyanobacteria surface concentration differences between experiment WIND* and CTRL* in the warming scenario (a) and between experiment WIND and CTRL in the present-day scenario (b) as well as the corresponding differences between the differences (WIND*-CTRL*) and (WIND-CTRL) (c).

4.3.4 | Basin-wide and regional mean effects of the feedbacks

To further assess the effects of the different feedbacks, we also repeat the other additional model simulations described in Section 4.3 in the warming scenario. In experiment ABSALB* we include the absorption and the albedo feedback together and in experiment ABSALBWIND* we additionally include the wind feedback, In the following we compare the results of these two experiments and experiment ABS* with experiment CTRL* as well as with the corresponding present-day scenario experiments.

The cooling effect of including the absorption feedback on the basin mean temperature is similar in both scenarios, but slightly more pronounced in the warming scenario compared to the present-day scenario (Figure 4.19 (a)-(b)), whereas the additional cooling effect of including the albedo feedback is comparably small in both scenarios. Additionally taking into account the wind feedback leads to an overall cooling that is less pronounced in the warming scenario than in the present-day case. The effects of the different feedbacks on the basin mean surface temperature are very similar in both scenarios (Figure 4.19 (c)-(d)).

The subsequent effects of the different feedbacks on the biological model components are similar in both scenarios. Yet, the decrease in June and July and the increase in the rest of the year due to the absorption feedback, the decrease due to the albedo feedback, and the increase due to the wind feedback in the basin mean phytoplankton concentration are all less pronounced in the warming scenario than in the present-day scenario (Figure 4.20 (a)-(b)). The increase in the basin mean cyanobacteria concentration due to the absorption feedback is less pronounced in summer and early fall, but more pronounced in the rest of the year in the warming scenario than in the present-day scenario (Figure 4.20 (c)-(d)). The decrease in the basin mean cyanobacteria concentration due to the albedo feedback is less pronounced and is even turned into a slight increase in late summer and fall in the warming scenario. The increase in the basin mean cyanobacteria concentration due to the wind feedback is more pronounced from spring to mid summer, but less pronounced in the rest of the year in the warming scenario compared to the present-day scenario.

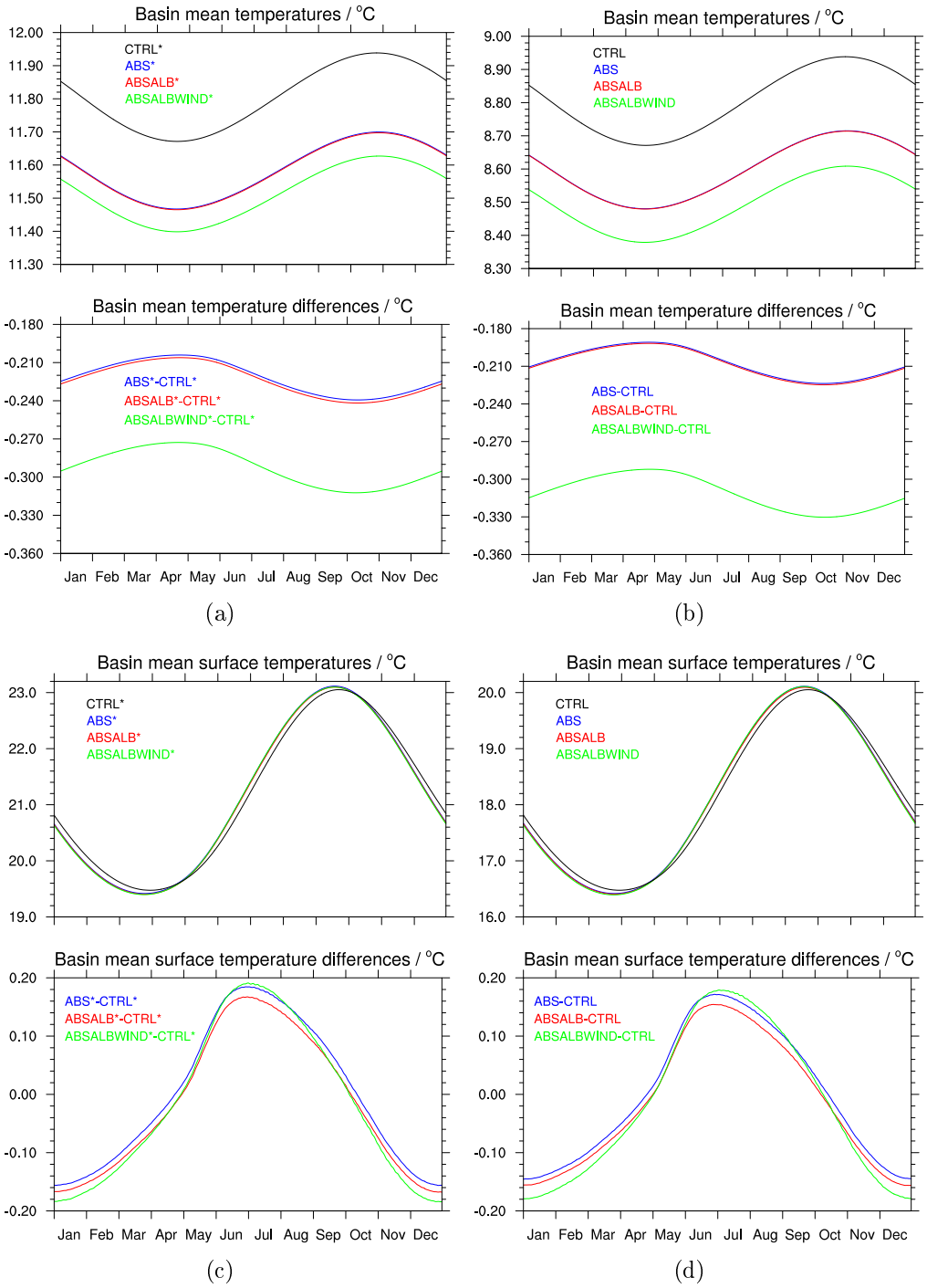

Figure 4.19.: Basin mean temperatures (a)-(b) and basin mean surface temperatures (c)-(d) and the differences of experiments ABS*, ABSALB* and ABSALBWIND* compared to CTRL*, and ABS, ABSALB and ABSALBWIND compared to CTRL, respectively.

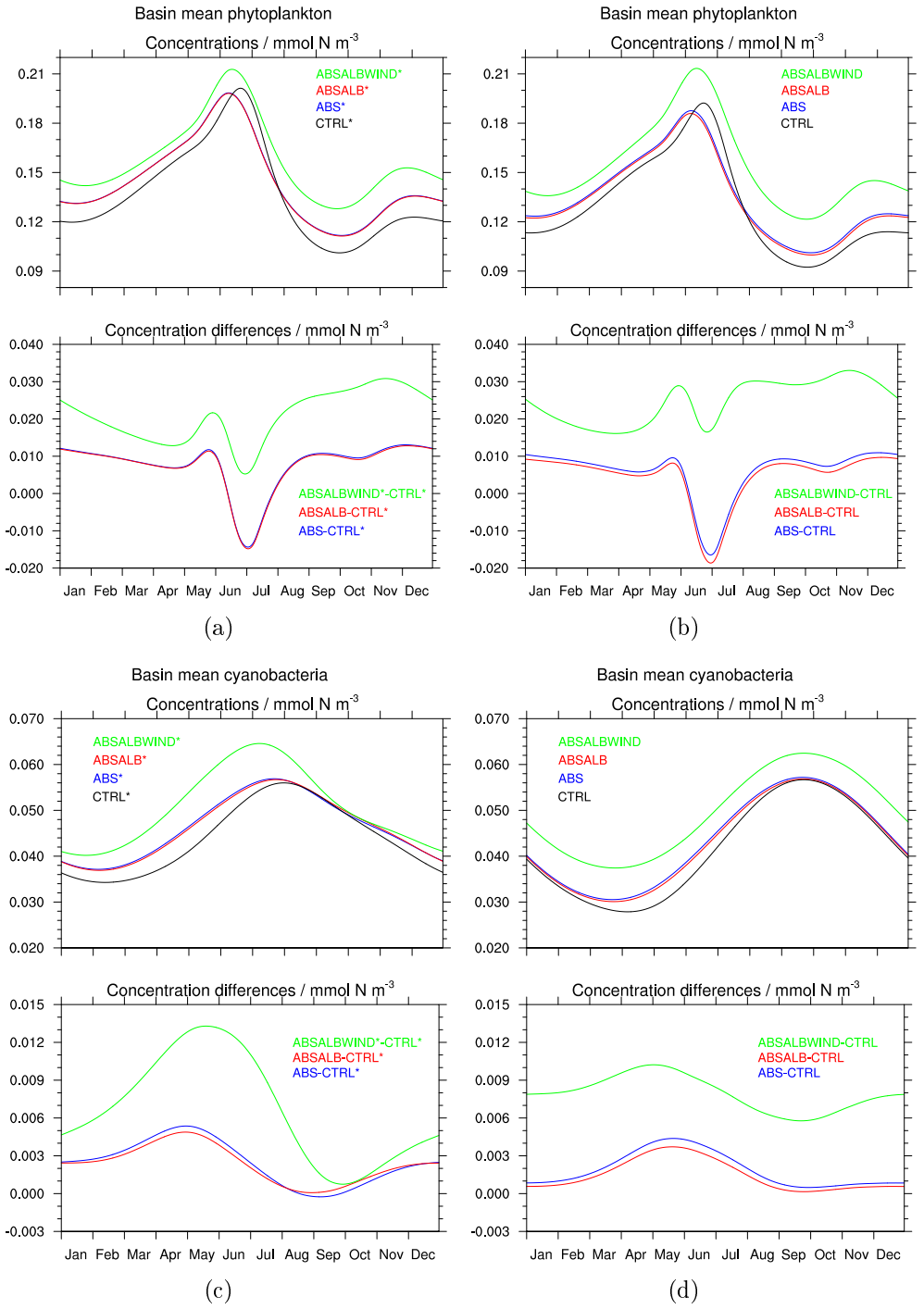

Figure 4.20.: Basin mean phytoplankton (a)-(b) and cyanobacteria (c)-(d) concentrations and the differences of experiments ABS*, ABSALB* and ABSALBWIND* compared to CTRL*, and ABS, ABSALB and ABSALBWIND compared to CTRL, respectively.

The regionally different effects of the different feedbacks in the two regions of interest – the equatorial region ranging from the southern boundary 240 km north and the subtropical region ranging from 240 km to 1440 km north – are also comparable in the two scenarios.

The absorption feedback has a cooling effect of around 0.3 °C and the albedo feedback has almost no effect on the equatorial mean surface temperature in both scenarios. Yet, the warming effect of the wind feedback on the equatorial mean surface temperature is reduced in the warming scenario compared to the present-day scenario, especially in fall and winter (Figure 4.21 (a)-(b).

In both scenarios, the effect of the absorption feedback on the subtropical mean surface temperature has a strong seasonal cycle (Figure 4.21 (c)-(d)). The cooling effect of the albedo feedback is comparable in both scenarios. However, the maximum of the warming effect of the absorption feedback in summer occurs about one month earlier and the cooling effect of the additional wind feedback is less pronounced in winter in the warming scenario than in the present-day scenario.

The effect of the absorption and albedo feedbacks on the equatorial mean mixed layer depth are very similar in both scenarios, except for a slightly stronger reduction due to the absorption feedback in January (Figure 4.22 (a)-(b)). The additional shallowing of the equatorial mean mixed layer due to the wind feedback is more pronounced in the first half of the year in the warming scenario than in the present-day scenario.

In the subtropical region, the reduction of the mixed layer depth due to the absorption feedback is more pronounced during the whole year, whereas the shallowing of the subtropical mixed layer due to the wind feedback is less pronounced in fall and winter, but more pronounced in spring and summer in the warming scenario than in the present-day scenario (Figure 4.22 (c)-(d)).

Also the effect of the biological-physical feedbacks on the equatorial and subtropical phytoplankton and cyanobacteria concentrations is comparable in both scenarios. Yet, the decrease in the phytoplankton surface concentrations due to the wind feedback varies seasonally in the equatorial region in the warming scenario, with a less pronounced reduction from late summer to early spring (Figure 4.23 (a)-(b)). In addition, the increase in the phytoplankton surface concentration due to the absorption feedback is more pronounced in summer and fall and the increase due to the wind feedback is less pronounced in spring and summer in the subtropical region in the warming scenario (Figure 4.23 (c)-(d)). Concerning cyanobacteria, the increase in the equatorial mean surface concentrations due to the wind feedback follows a strong seasonal cycle, with less pronounced increase from summer to early spring in the warming scenario (Figure 4.24 (a)-(b)). In the subtropical region, the increase in the cyanobacteria surface concentrations due to the absorption feedback is more pronounced in spring, whereas the increase due to the wind feedback is more pronounced in late spring and summer, but less pronounced in fall and winter, in the warming scenario (Figure 4.24 (c)-(d)).

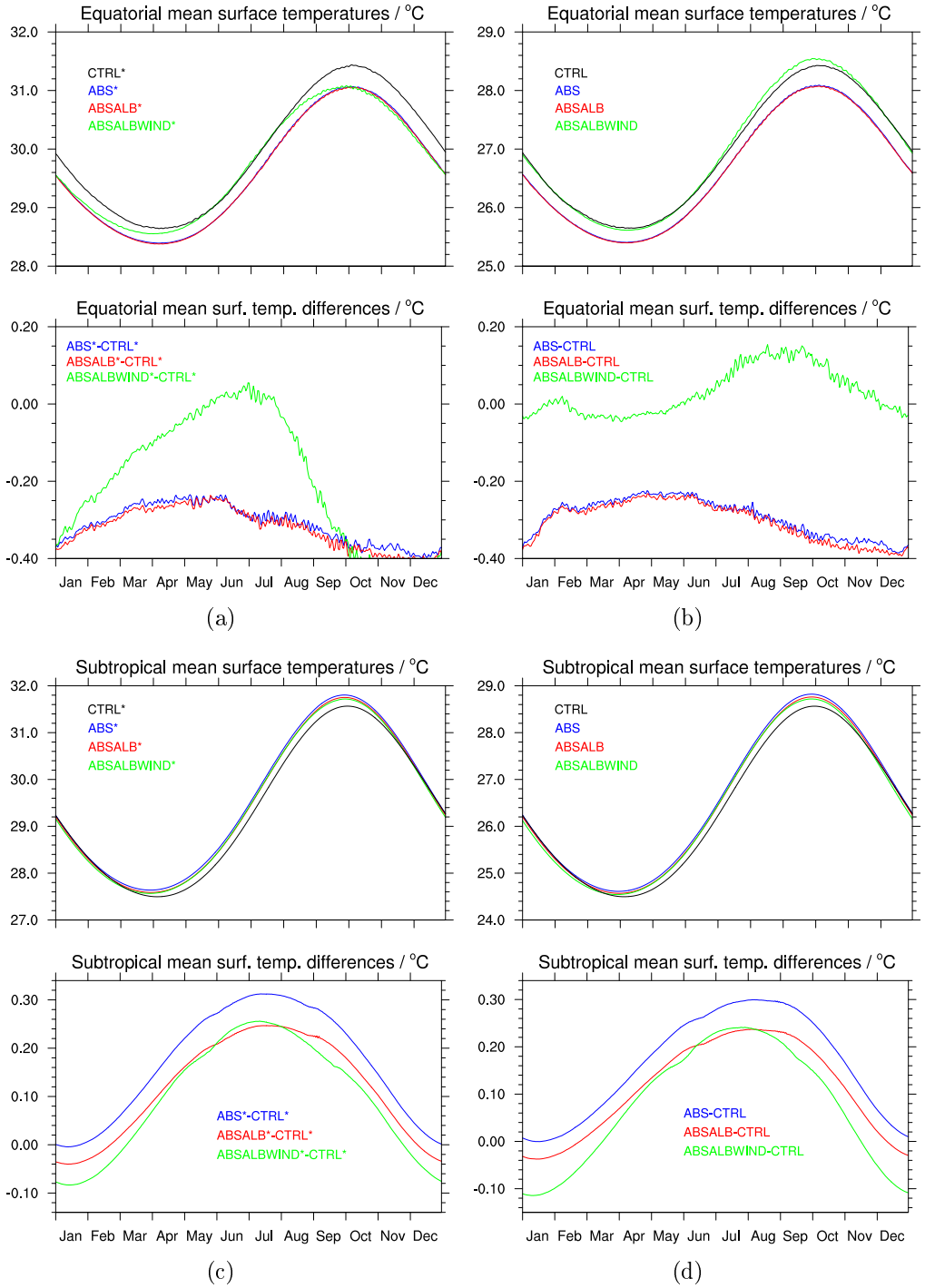

Figure 4.21.: Equatorial (a)-(b) and subtropical (c)-(d) mean surface temperatures and the differences of experiments ABS*, ABSALB* and ABSALBWIND* compared to CTRL*, and ABS, ABSALB and ABSALBWIND compared to CTRL, respectively.

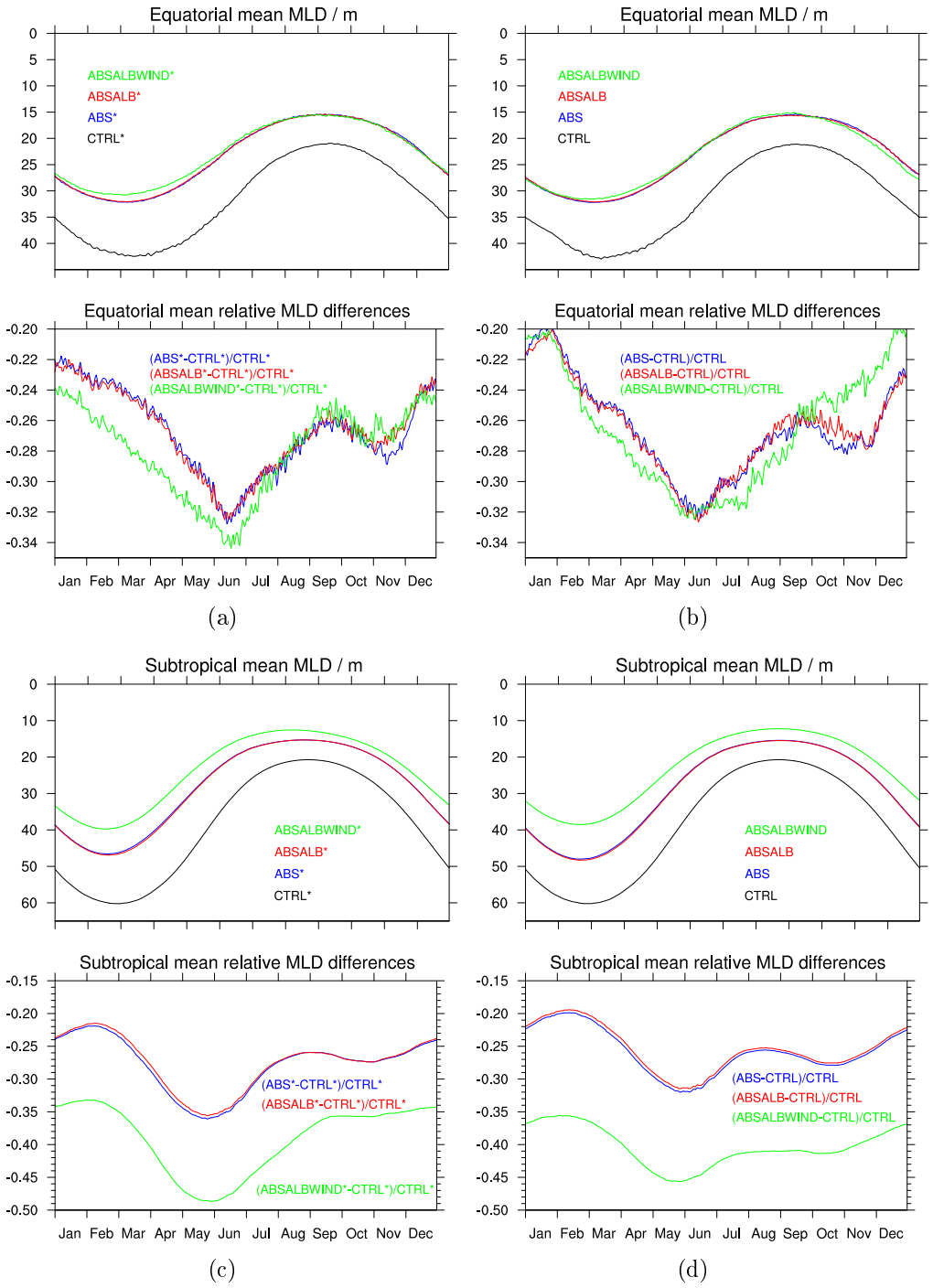

Figure 4.22.: Equatorial (a)-(b) and subtropical (c)-(d) mean mixed layer depths and the relative differences of experiments ABS*, ABSALB* and ABSALBWIND* compared to CTRL*, and ABS, ABSALB and ABSALBWIND compared to CTRL, respectively.

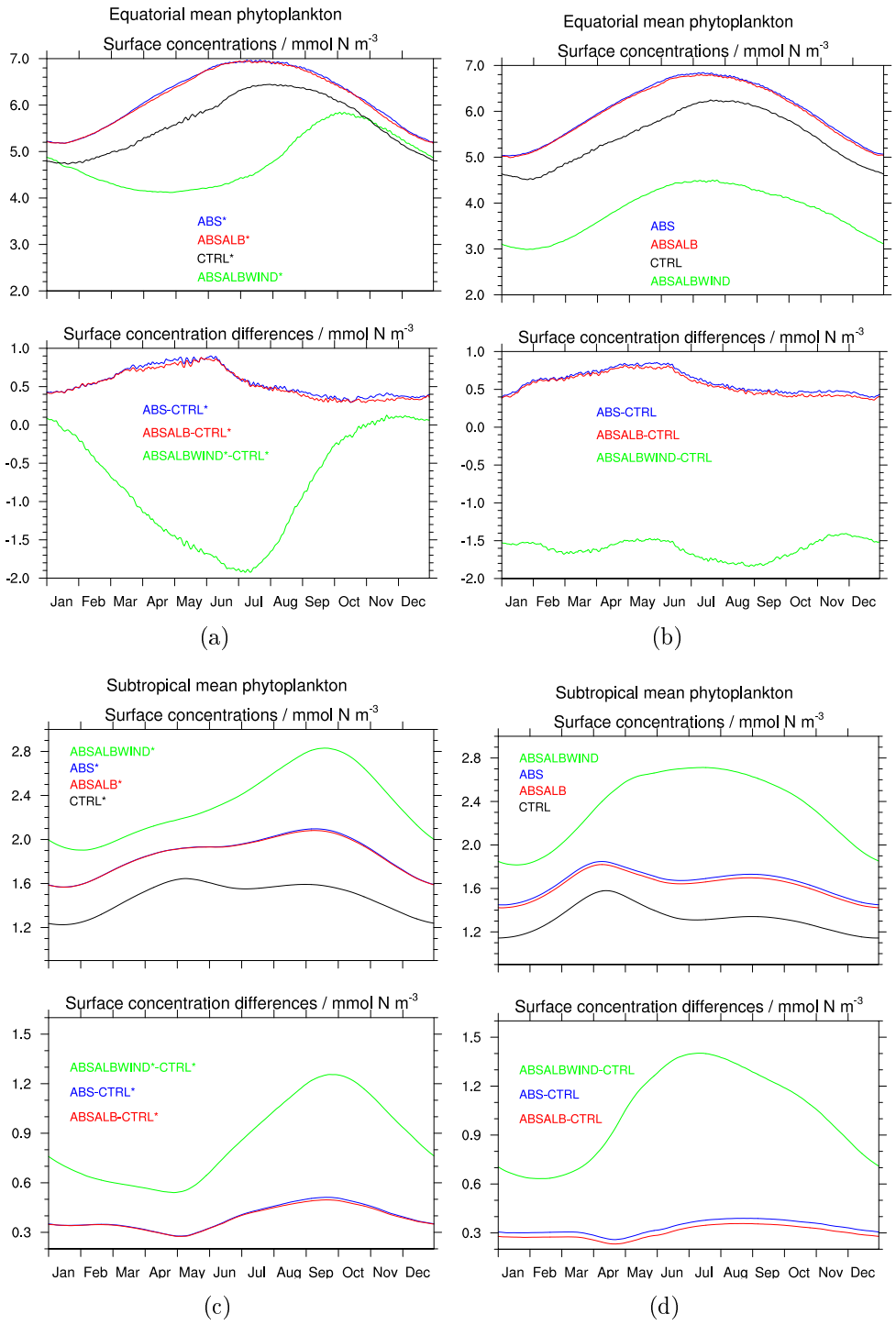

Figure 4.23.: Equatorial (a)-(b) and subtropical (c)-(d) mean surface phytoplankton concentrations and the corresponding differences of experiments ABS*, ABSALB* and ABSALBWIND* compared to CTRL*, and ABS, ABSALB and ABSALBWIND compared to CTRL, respectively.

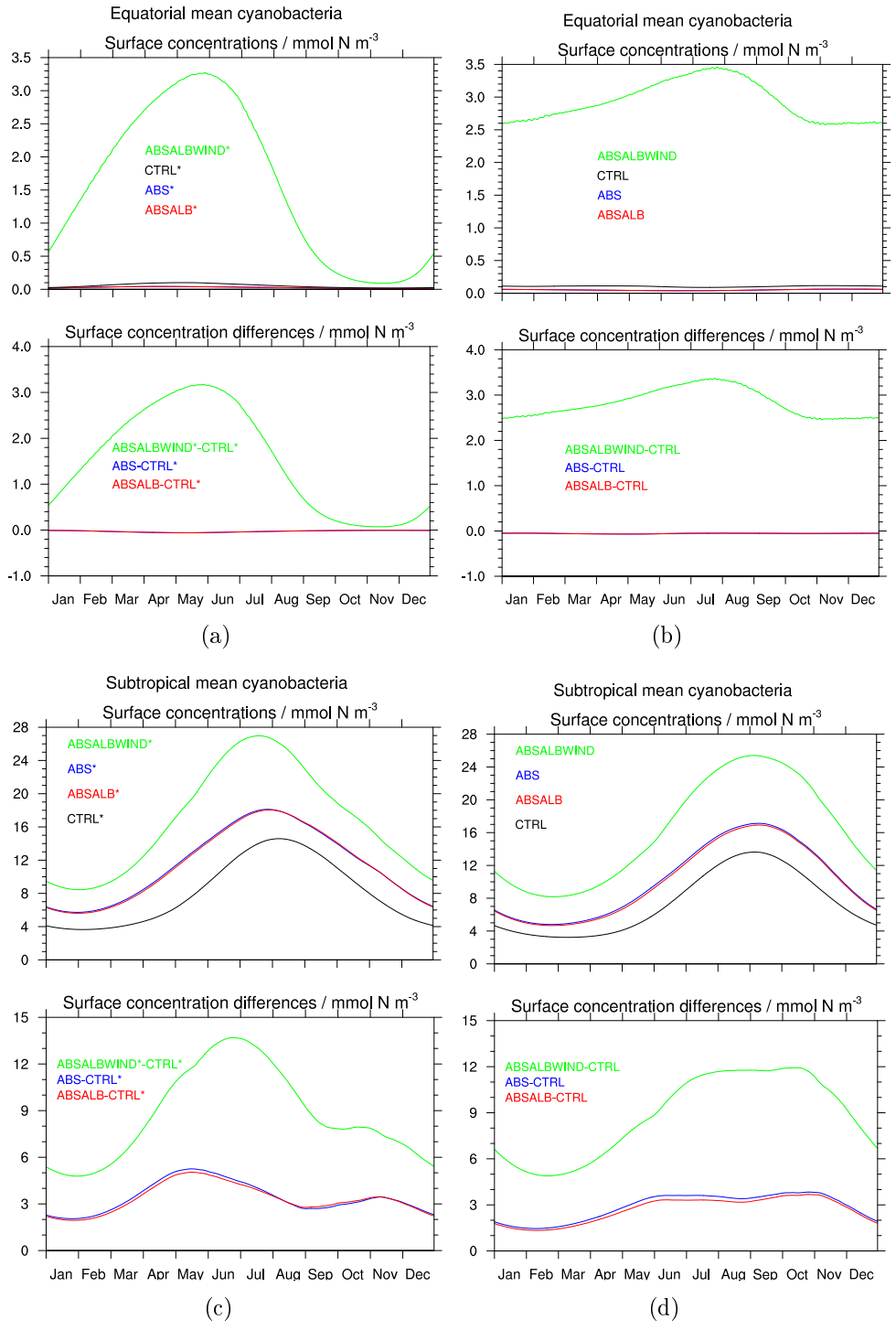

Figure 4.24.: Equatorial (a)-(b) and subtropical (c)-(d) mean surface cyanobacteria concentrations and the corresponding differences of experiments ABS*, ABSALB* and ABSALBWIND* compared to CTRL*, and ABS, ABSALB and ABSALBWIND compared to CTRL, respectively.

4.4 | Summary, discussion and conclusions

The three-dimensional warming scenario model studies presented in this chapter show how a warming environment alters the distribution of phytoplankton and cyanobacteria and leads to changes in the local and non-local effects mediated by physical-biological feedbacks in the model. We have studied the feedback via light absorption by phytoplankton and cyanobacteria as well as the specific feedbacks mediated by cyanobacteria through ocean surface albedo increase and wind stress reduction using a dynamically coupled three-dimensional ecosystem-ocean general circulation model simulating conditions comparable to the North Atlantic in a warming environment.

4.4.1 | Summary

The altered temperature forcing in the warming scenario leads to an almost completely homogeneous shift of the temperature field by 3 °C and essentially no changes in the mixed layer dynamics. Due to the higher temperatures in the warming scenario, the conditions for cyanobacteria growth are altered, since their growth rate depends on temperature. The surface area where temperatures do not limit cyanobacteria growth extends more to the north in the warming scenario compared to the present-day case. However, the surface temperatures increase beyond the temperature optimum for cyanobacteria growth in the southern part of the ocean basin in the warming scenario leading to a regional growth limitation north of the southern boundary upwelling region.

Due to the northward shift of cyanobacteria, the surface warming induced by the absorption feedback is stronger in the northern and weaker in the southern subtropical region, the maximum subtropical warming in summer occurs earlier, and the subsurface cooling and the subtropical shallowing of the mixed layer are more pronounced. The subsurface cooling due to the albedo feedback is less pronounced in the southern and more pronounced in the northern subtropical region. Also the effects of the wind feedback are altered in the warming scenario, with less pronounced equatorial warming and subtropical cooling, a shallowing of the subtropical mixed layer being less pronounced in fall and winter, but more pronounced in spring and summer, and a less pronounced distortion of the wind-driven subtropical gyre and changes in overturning circulation.

The effect of the absorption feedback on the phytoplankton concentrations is locally stronger or weaker in the warming scenario, whereas the increase in the cyanobacteria concentrations is stronger in the northern and weaker in the southern subtropical region. The local decreases and increases in the phytoplankton concentrations as well as the increase in the southern subtropical region cyanobacteria concentrations due to the wind feedback are less pronounced in the warming scenario, whereas the increase in the northern subtropical region cyanobacteria concentration is more pronounced.

4.4.2 | Discussion and conclusions

The warming scenario model results suggest that with potentially increasing atmospheric temperatures cyanobacteria shift northwards and lead to altered effects of the biological-physical feedbacks on upper ocean physics. Since the surface temperatures increase beyond the temperature optimum for cyanobacteria growth in the southern part of the ocean basin in the warming scenario, the question arises whether cyanobacteria can adapt also to these higher temperatures (e.g. Breitbarth *et al.*, 2007). We have performed additional model simulations to study possible scenarios of temperature adaptation of cyanobacteria growth. None of these model scenarios shows a substantial increase in the area covered by cyanobacteria. In our model, this is partly due to the competitive advantage of phytoplankton over cyanobacteria in the regions where nutrient availability does not limit phytoplankton growth, since in these regions phytoplankton have a larger growth rate than cyanobacteria. Another reason that our model does not show a spatial spread of cyanobacteria could be the strong downwelling in the central subtropical gyre preventing the cyanobacteria to build up accumulations at the surface.

Our coupled biological-physical ocean general circulation model study indicates potential consequences of a future rise in sea surface temperatures as well as the consequences of a changing geographical distribution of cyanobacteria induced by this warming. Our results do not allow for ultimate conclusions, whether the distribution of surface buoyant cyanobacteria will spread and increase in the future and thereby also lead to stronger effects on ocean physics via biological-physical feedbacks. Yet, our study suggests that the effects of marine biological feedbacks on the ocean's temperature structure, mixed layer dynamics, as well as circulation patterns are also substantial in a warming scenario. Thus, changes in surface ocean biota and their feedbacks to the physics of the upper ocean should no longer be neglected in climate scenario model simulations.

Chapter 5

Conclusions and outlook

In this thesis I have outlined how marine organisms can alter their physical environment and how the dynamic interaction between biology and physics in the ocean can be integrated in coupled biological-physical numerical models. In particular, I have shown how the specific changes of the absorptivity of light, the ocean surface albedo, and the surface wind stress by surface buoyant cyanobacteria can be described in ocean model frameworks. Furthermore, I have described potential feedback loops between cyanobacteria and upper ocean physics. For the first time, these feedback mechanisms and their effects on the upper ocean as well as changes in their effects in a warming climate have been assessed quantitatively using a one-dimensional water column model and a three-dimensional general circulation model framework.

5.1 | Main findings

I can now answer the research questions raised in Section 1.3:

- How do different distributions of phytoplankton groups affect the temperature structure of the upper ocean via the absorption feedback?

The results of the water column model studies suggest that the effect of taking into account the absorption of short wave radiation by biological matter on the upper ocean temperature structure depends on the characteristic growth limitation and vertical motility of a phytoplankton group. The effect of the absorption feedback depends on the vertical distribution and the concentrations of the phytoplankton group. The absorption feedback mediated by surface buoyant cyanobacteria leads to a sea surface warming of up to 1°C and a sub-surface cooling of more than 2°C compared to the feedback mediated by non-buoyant phytoplankton.

- What are the relative magnitudes of the effects mediated by the absorption, the albedo, and the wind feedback due to cyanobacteria?

The absorption and the wind feedback mediated by cyanobacteria have stronger effects on upper ocean physics than the albedo feedback. Cyanobacteria locally create environmental conditions that promote their own growth via local positive feedback mechanisms due to increased light absorption and decreased wind stress induced turbulence in the upper water column.

- How do the different feedbacks influence the ocean surface mixed layer thickness locally?

Surface buoyant cyanobacteria mediate a shallowing of 20 to 30% of the surface mixed layer due to the absorption feedback and of around 10% due to the wind feedback in the regions where they occur.

- What are the non-local effects of the different feedbacks through and on ocean circulation?

The general circulation model study suggests that increased absorption by biological matter affects the meridional overturning circulation and that a reduction of the surface wind stress mediated by cyanobacteria leads to a distortion of the subtropical gyre as well as a reduction of subtropical downwelling and equatorial upwelling. Cyanobacteria driven feedbacks lead to a local surface warming, but also to a surface cooling at other locations due to changes in the mixed layer dynamics and reduced up- and downwelling.

- What are potential changes in the effects of the feedbacks in the future?

The local effects of the absorption and the wind feedback on upper ocean physics are stronger than today in a warmer climate. Cyanobacteria shift northwards with increasing temperatures and lead to more pronounced effects of the biological-physical feedbacks in some regions, but less pronounced effects in other regions in the model. If cyanobacteria are able to adapt to temperatures higher than 30°C, increasing sea surface temperatures might lead to a spread of cyanobacteria and thus a larger region of the ocean will be affected by the induced feedbacks. However, model scenario simulations of temperature adaptation of cyanobacteria growth do not show a substantial increase in the area covered by cyanobacteria.

5.2 | Next steps and extensions of this work

Observational studies

The studies presented in this thesis simulate plausible distributions and biomass concentrations of surface buoyant cyanobacteria. However, more measurements of cyanobacteria biomass on a basin-wide to global scale are needed in order to better evaluate models for their distribution and the feedbacks induced by cyanobacteria.

To improve the feedback parameterizations, also measurements of biologically induced changes in temperature and in turbulence are needed. Although, strictly speaking, the strength of a feedback mechanism itself can only be assessed in a model study, since in an observation it is impossible to disentangle cause and effect, estimates for the separate direct effects of biological organisms on their physical environment need to be derived from measurements. In particular for the reduction of the wind stress due to cyanobacterial surface mats, measurements should be carried out to arrive at a better confidence in the magnitude of the resulting effects.

Model extensions

To further assess the relevance of cyanobacteria driven biological-physical feedbacks, several extensions building up on the model studies presented in this thesis can be proposed.

The model setups in this work give valuable first estimates of the potential effects of the feedbacks, but the physical model setups are idealized and simplified in some respects. Therefore, additional three-dimensional model studies including a more realistic geometry and bathymetry of the ocean basin and a more realistic atmospheric forcing might be interesting. These studies would allow for a larger internal variability in the model and a comparison of the feedback signals with this variability. While the vertical resolution of the model setups used in this work is rather high, the horizontal resolution of the three-dimensional model could be increased to study the effects of eddies on the surface phytoplankton distribution and the resulting changes in the feedbacks. Furthermore, an extension of the geographical model domain would allow for an estimation of the feedback effects on a global scale.

Since changes in the physics of the upper ocean are tightly linked to atmospheric processes, it would be interesting to assess the effect of a dynamic coupling of an ocean model including marine biological-physical feedbacks to an atmospheric model. Using this coupling would allow for an explicit representation of air-sea interactions in order to study potential amplifying or dampening atmospheric effects on the biological-physical feedbacks in the upper ocean.

Concerning the parameterizations of the biological-physical feedbacks, a more detailed description of the optical properties of different biological components, e.g., different absorption coefficients and albedo changes for different phytoplankton groups, would be interesting to study. Also a more detailed description of the changing mechan-

ical characteristics of the ocean surface due to cyanobacterial mats instead of directly altering the surface wind stress could be interesting. To get a more realistic description of the cyanobacterial surface mats, an explicit resolution, i.e., a description of mats of biogenic matter lying on the ocean surface, as well as the breakdown of these mats due to strong winds could be implemented in a model. Also more details in the physical processes altered by the feedbacks could be included in a model, e.g., a reduction of the heat loss to the atmosphere due to cyanobacterial surface mats.

To study the potential future evolution of nitrogen fixing surface buoyant cyanobacteria, an explicit description of nitrogen deposition into the ocean and also the role of other nutrients such as iron or phosphorus as well as the effects of ocean acidification could be included in model studies. These model scenario simulations could also be used to study a potential adaptation of cyanobacteria to higher temperatures.

5.3 | Concluding remark

The results presented in this thesis indicate potential consequences of a changing geographical distribution of cyanobacteria induced by a potential future rise in sea surface temperatures. A recent study on projected climate change effects on cyanobacteria in the Baltic Sea by Hense *et al.* (2013) suggests that biological-physical feedback mechanisms become more important with global warming. Since the model studies presented in this work suggest that marine biological feedbacks have an impact at least on the mixed layer dynamics and ocean circulation patterns, marine biota needs to be considered as an active component in ocean models used for future climate scenario model studies.

Appendix A

Coupled biological-physical ocean models

In this appendix, the theoretical basis for numerical models describing biological and physical processes in the ocean are outlined and approaches to model ecosystem dynamics are described. The underlying mathematical formulations, required assumptions and numerical approaches to solve the resulting equations are discussed. In particular, the Public Domain water column model GOTM (General Ocean Turbulence Model), which was originally published by Burchard *et al.* (1999) and regularly extended since then (see Umlauf *et al.*, 2005), and the general circulation model MITgcm (Massachussets Institute of Technology general circulation model, Marshall *et al.*, 1997) are presented.

The water column model GOTM is used in the one-dimensional model studies presented in Chapter 2 and the general circulation model MITgcm is used in the three-dimensional model studies presented in Chapters 3 and 4. I will only briefly describe the derivation of the needed equations and the main characteristics of the model frameworks used in this thesis. For further details the reader is referred to standard text books on geophysical fluid dynamics (e.g. Cushman-Roisin and Beckers, 2011) and ocean dynamics (e.g. Olbers *et al.*, 2012) and to the GOTM (http://www.gotm.net) and MITgcm (http://mitgcm.org) websites, where the model codes and documentations are available.

In the first section of this appendix, the basic approaches for marine physical and biological models are outlined. In Section A.2 and Section A.3 the specific model frameworks GOTM and MITgcm are presented.

A.1 | General considerations

Physical ocean models

The properties of the flow in the ocean can be described by well-defined mathematical equations for the dynamics of a fluid. However, ocean processes are nonlinear and

turbulent and the theory of nonlinear, turbulent flow with rotation in basins with complex geometry is not understood. Therefore, theories used to describe the dynamics of the ocean are much simplified approximations to reality. Even these approximative equations cannot be solved exactly, but need to be treated numerically involving even more approximations to the real ocean's behavior. Yet, a combination of theory and observations over the last decades has led to ever more realistic descriptions of ocean dynamics through numerical models.

Marine ecosystem and biogeochemical models

The major difficulty in finding an appropriate way of describing the dynamics of an ecosystem or a biogeochemical system by mathematical equations in a model is the missing analogue for biological processes to the fundamental equations describing fluid flow, like the Navier-Stokes equations. The choice for a suitable model therefore always depends on the application and the questions to be addressed.

Marine ecosystems and biogeochemistry The marine ecosystem can be described as the system of all living marine organisms and their interaction with the environment. The study of chemical, physical, geological, and biological processes governing the composition of the natural environment is referred to as biogeochemistry. In particular, biogeochemistry studies the cycles and interactions of chemical elements like carbon, nitrogen, phosphorus, or sulfur, how they are influenced by living organisms and transported through the whole Earth system. Since a focus of biogeochemistry lies on elemental cycles which are either driven by or have an impact on biological processes, the field of marine biogeochemistry is intimately connected to the study of marine ecosystems. In many cases, the methods to analyze, describe, or model a biogeochemical system are the same as those used for ecosystems and sometimes the two terms are even used interchangeably. The core scientific questions can, though, differ a lot between the two fields of study. For instance, one focus of biogeochemistry could be the quantification of the fate of carbon dioxide, whereas in ecosystem science rather the timing and environmental consequences of an algal bloom might be the main topic of interest.

The major biological components of an ecosystem are the producers, the consumers, and the decomposers. The interactions between these components are constituted by several different processes involving the exchange of matter or energy in between. These processes include, among others, light absorption, nutrient uptake, growth, grazing, predation, mortality, respiration, excretion, remineralization, and organism behavior. The processes are sometimes rather direct, relatively well known and straightforward to describe quantitatively, but more often they are not known in detail or hardly possible to measure or it is just not feasible to describe all the involved mechanisms. Light absorption and nutrient uptake are two fundamental processes which are of particular importance in determining the behavior of the whole marine biogeochemical and ecological system. One of the key biological components within the marine system is

phytoplankton. These passively drifting or wandering organisms are small, primarily microscopic, algae that carry out photosynthesis. They are the drivers of biogeochemical cycles and as primary producers form the basis of the marine food web. That is, the absorption of solar energy by photosynthetic pigments like chlorophyll enables them to convert inorganic material into new organic compounds. The links from this primary production to higher trophic levels are provided via the food web.

Marine ecosystem models In the following, I use the terms biogeochemical model, ecological model and ecosystem model interchangeably. Yet, one needs to keep in mind that although being described by similar or equal model equations, often ecosystem models focus on ecological aspects like, e.g., life cycles of organisms or trophic interactions, while biogeochemical models focus on elemental fluxes or cycles. Furthermore, I restrict the ecosystem model description to prognostic numerical Eulerian models in contrast to statistical or Lagrangian transport individual-based models. That is, I focus on models describing the dynamics of marine biota by providing prognostic equations for the spatio-temporal evolution of quantities in the ocean and the exchange processes of matter and energy without taking into account higher trophic levels, like fish or mammals, or the human influences, e.g., through fisheries, explicitly.

One of the most simple and earliest marine ecosystem models (see Riley, 1946) describes the system as consisting of three components: nutrients, phytoplankton, and zooplankton. Phytoplankton is the driver of biogeochemical cycles and the basis for the marine food web. Being primary producers, phytoplankton relies on the uptake of inorganic nutrients. The important nutrients for phytoplankton are primarily nitrate, ammonium, silicate and phosphate, but also the abundance of other substances like iron can be crucial for phytoplankton growth. Depending on the question, in a model only the most important nutrients dominating the dynamics of the system are considered.

The term zooplankton refers to the heterotrophic type of plankton, i.e., the type of drifting marine organisms that depend on the consumption of organic material. Zooplankton plays an important role in the marine ecosystem by being able to control the abundance of phytoplankton to some extent through grazing and linking the primary producers to the rest of the marine food web. In addition, zooplankton is a key component in the so-called biological pump. This mechanism refers to the transport of carbon to the ocean's interior and is mediated for instance by sinking fecal pellets produced by zooplankton. However, in a marine ecosystem model focusing on phytoplankton dynamics, grazing by zooplankton does not have to be taken into account explicitly, but can be considered implicitly by using an additional or a larger loss term for phytoplankton.

Many contemporary ecosystem model approaches include a distinct compartment for each so-called functional group of organisms, which is supposed to describe a group of organisms or species that plays a key role within the ecosystem or biogeochemical cycles. That is, the compartments for plankton are split up into two or more different

groups of species.

Often models also include one or more compartments for detritus describing non-living particulate organic material including excrements and dead organisms. This organic material sinks to the ocean's interior or the ground and can be remineralized by microorganisms, i.e., it can be transformed to inorganic material which can then act as a nutrient for the organisms again. By including several compartments of detritus, different elements as well as different sinking velocities and remineralization rates can be described. Depending on the question, the process of remineralization can be, and usually is, described implicitly without including microorganisms like bacteria explicitly in a model.

The types of models consisting of nutrient, phytoplankton, zooplankton and detritus are referred to as NPZD-type models and are widely used in ecosystem and biogeochemical modeling. The models' complexity has increased drastically in the past years involving, e.g., more and more different species and their physiological characteristics as well as ever more specific elements and compounds.

Adding a compartment for detritus to the system of one nutrient and one phytoplankton compartment, that is, a PND type of model, constitutes an ecosystem model which is very minimalistic. However, it represents a closed cycle of matter and for many applications is already suitable to describe the main characteristics of the phytoplankton dynamics. Furthermore, a system of only three compartments provides the possibility for easily controllable numerical experiments in order to understand the system's dynamics in conceptual model studies.

The components chosen for an adequate description of the ecosystem need to be quantified in some way in order to describe them in a mathematical model. This quantification can be realized as either numbers of organisms or particles, as dry or wet weight biomass, or as the inventory of some suitable chemical element, e.g., carbon, nitrogen, or phosphorus. In order to describe the quantities of a biogeochemical system or ecosystem within an Eulerian hydrodynamic model, they need to be described as a concentration or number density, i.e., per volume.

In addition to the set of components of the ecosystem model, the links between the components need to be specified by giving functional relationships for the dependence of the described processes on the components and other external factors. The various mathematical functions that can be used here are mostly based on empirical relationships expressing correlations between measurable variables. The real ecological or physiological processes underlying the observed correlation are usually not resolved explicitly. Often no sound statistical or physiological basis to reject one or the other parameterization exists, but one rather chooses them with respect to the model application and the whole purpose and context of the respective study. A collection of widely used parameterizations in marine ecosystem models can be found, e.g., in Tian (2006).

A.2 | The water column model GOTM

The basis of the physical part of GOTM are the Reynolds-averaged Navier-Stokes equations in a rotating frame of reference together with the corresponding tracer equations for temperature and salinity. With the Boussinesq approximation and the assumption that the effects of horizontal advective and turbulent transport are negligible, the one-dimensional forms of the momentum equations in cartesian coordinates read

$$\partial_t u - \nu \partial_{zz} u + \partial_z \left\langle u'w' \right\rangle = -\frac{1}{\rho_0} \partial_x p + fv \,, \tag{A.1}$$

$$\partial_t v - \nu \partial_{zz} v + \partial_z \left\langle v'w' \right\rangle = -\frac{1}{\rho_0} \partial_y p - fu \,, \tag{A.2}$$

where u and v are the horizontal velocities in x- and y-direction, respectively, and w is the vertical velocity in z-direction. The origin $z = 0$ is located at the mean sea surface elevation and z is pointing upwards. The angular brackets indicate ensemble averages of the fluctuating parts of the velocity components, denoted by the corresponding primed quantities, resulting from the Reynolds decomposition. The molecular viscosity is denoted by ν, ρ_0 is a constant reference density, p is pressure, and f is the Coriolis parameter.

With the hydrostatic assumption the pressure gradients can be expressed as

$$-\frac{1}{\rho_0} \partial_x p = -g \frac{\rho(\zeta)}{\rho_0} \partial_x \zeta + \int_z^\zeta \partial_x b \, \mathrm{d}z' \tag{A.3}$$

$$\text{and} \qquad -\frac{1}{\rho_0} \partial_y p = -g \frac{\rho(\zeta)}{\rho_0} \partial_y \zeta + \int_z^\zeta \partial_y b \, \mathrm{d}z' \,, \tag{A.4}$$

where g is the acceleration due to gravity, ρ is the potential density of water, ζ is the elevation of the free surface and $b := -g \frac{\rho - \rho_0}{\rho_0}$ is the buoyancy. The two terms on the right hand sides of the equations describe external and internal pressure gradients due to surface slopes and density gradients, respectively. The gradient of ζ needs to be specified and is treated as an input parameter here.

The tracer equation for the potential temperature θ, corresponding to the above momentum equations, reads

$$\partial_t \theta - \nu_\theta \partial_{zz} \theta + \partial_z \left\langle w'\theta' \right\rangle = \frac{1}{c_\mathrm{p} \rho_0} \partial_z I \,, \tag{A.5}$$

where ν_θ denotes the molecular diffusivity of heat and c_p is the specific heat capacity of water. The incoming solar shortwave irradiance I is treated as an inner source of heat and is parameterized as

$$I(z) := I_0 \left[a \exp\left(k'_\mathrm{w} z\right) + (1-a) \exp\left(k_\mathrm{w} z\right) B(z) \right] \,, \tag{A.6}$$

where I_0 is the downwelling irradiance at the surface, k'_w and k_w are absorption coefficients for seawater, and a is a dimensionless weighting parameter with $0 \leq a \leq 1$. On

the right hand side of the above equation the first term describes attenuation of the red part of the spectrum and the second term of the blue-green light. This second part can be further absorbed by particulate matter, described by the function B, which will be specified in the description of the biogeochemical part of the model. The absorption coefficients and the weighting parameter in Equation A.6 are assumed to be constant and taken from Paulson and Simpson (1977), who provided values for the parameters for 6 different types of oceanic water. These types are classified according to Jerlov (1968) and describe the turbidity of seawater from extremely clear to turbid, roughly corresponding to the range from clear open ocean water to turbid coastal waters.

The tracer equation for the salinity S reads

$$\partial_t S - \nu_S \partial_{zz} S + \partial_z \langle w' S' \rangle = \mathcal{F}_S \,, \tag{A.7}$$

where ν_S denotes the molecular diffusivity of salt and $\mathcal{F}_S$ is the freshwater flux, which is the difference of precipitation and evaporation.

The potential density ρ needs to be determined by an equation of state

$$\rho = \rho\,(\theta, S, p) \;, \tag{A.8}$$

which in this work, as it is done for many oceanic applications, is approximated by the UNESCO equation of state (see Fofonoff and Millard, 1983).

Together with initial and boundary conditions for the prognostic variables and closure assumptions for the turbulent transport terms, the physical part of the model system is complete.

For the calculation of the mean vertical turbulent fluxes appearing in the above momentum and tracer equations many different parametrization methods exist. Here I only briefly describe the method which is used in this work. A detailed description of the different types and levels of closure models that are implemented in GOTM is given in Umlauf *et al.* (2005).

The turbulent fluxes are expressed as

$$\langle u' w' \rangle = -A_\mathrm{v}\, \partial_z u \tag{A.9}$$
$$\langle v' w' \rangle = -A_\mathrm{v}\, \partial_z v \tag{A.10}$$
$$\langle w' \theta' \rangle = -K_\mathrm{v}\, \partial_z \theta \tag{A.11}$$
$$\langle w' S' \rangle = -K_\mathrm{v}\, \partial_z S \tag{A.12}$$
$$\tag{A.13}$$

with the vertical turbulent diffusivities given by

$$A_\mathrm{v} := c_\mu \sqrt{k}\, l \tag{A.14}$$
$$K_\mathrm{v} := c'_\mu \sqrt{k}\, l \tag{A.15}$$

g	=	$9.81\,\mathrm{m\,s^{-2}}$	ν	=	$1.3\cdot10^{-6}\,\mathrm{m^2\,s^{-1}}$	a	=	0.58
ρ_0	=	$1027\,\mathrm{kg\,m^{-3}}$	ν_θ	=	$1.4\cdot10^{-7}\,\mathrm{m^2\,s^{-1}}$	k_w	=	$0.04\,\mathrm{m^{-1}}$
c_p	=	$3985\,\mathrm{J\,kg^{-1}\,K^{-1}}$	ν_S	=	$1.1\cdot10^{-9}\,\mathrm{m^2\,s^{-1}}$	$k_{\mathrm{w}'}$	=	$2.86\,\mathrm{m^{-1}}$

Table A.1.: Parameter values for the physical part of the specific GOTM setup used in Chapter 2.

c_μ^0	=	0.5477	c_{ϵ_2}	=	1.92	σ_k	=	1.0
c_{ϵ_1}	=	1.44	c_{ϵ_3}	=	1.0	σ_ϵ	=	1.3

Table A.2.: Parameter values for the k-ϵ model according to Rodi (1987) in the specific GOTM setup used in Chapter 2.

respectively. Here, k denotes the turbulent kinetic energy and l is the integral length scale. The non-dimensional quantities c_μ and c'_μ are functions of two non-dimensional stability parameters describing the influence of shear and stratification on turbulent mixing. These functions can be constants or empirical functions or obtained in a consistent way from a second-moment turbulence closure model. Here, the stability functions according to Eifler and Schrimpf (1992) are used. The turbulent kinetic energy k and the length scale l, calculated from the dissipation rate

$$\epsilon = \left(c_\mu^0\right)^3 \frac{k^{3/2}}{l}\,, \tag{A.16}$$

are both computed prognostically from parameterized transport equations, corresponding to the so-called k-ϵ model. Here, the equations

$$\mathrm{D}_t\, k = \partial_z\left(\frac{c_\mu\left(c_\mu^0\right)^3}{\sigma_k}\frac{k^2}{\epsilon}\,\partial_z k\right) + \mathcal{P} + \mathcal{G} - \epsilon \tag{A.17}$$

$$\mathrm{D}_t\,\epsilon = \partial_z\left(\frac{c_\mu(c_\mu^0)^3}{\sigma_\epsilon}\frac{k^2}{\epsilon}\,\partial_z\epsilon\right) + \frac{\epsilon}{k}\left(c_{\epsilon_1}\mathcal{P} + c_{\epsilon_3}\mathcal{G} - c_{\epsilon_2}\epsilon\right) \tag{A.18}$$

according to Rodi (1987) are used, where D_t is the material derivative,

$$\mathcal{P} = A_\mathrm{v}\,\left((\partial_z u) + (\partial_z v)\right)^2 \tag{A.19}$$

is the shear production,

$$\mathcal{G} = -K_\mathrm{v}\,\partial_z b \tag{A.20}$$

is the buoyancy production, and c_μ^0, σ_k, σ_ϵ, c_{ϵ_1}, c_{ϵ_2}, and c_{ϵ_3} are constant parameters. For the turbulent kinetic energy and dissipation rate equations, Neumann-type logarithmic law of the wall upper and lower boundary conditions are used.

The parameter values for the physical part of the specific model setup used in Chapter 2 of this work are given in Tables A.1 and A.2.

Biogeochemical models in GOTM

Within GOTM, biogeochemical models can be coupled to the physical part of the model. This coupling allows the biogeochemical components to be transported and mixed according to the fluid flow and provides the possibility to describe interactions between the ecosystem components and their physical environment. The biogeochemical models need to be formulated in an Eulerian approach in which all state variables are expressed as concentrations. That is, the state variables are continuous fields even if they do not describe dissolved but particulate matter. In general, the equations of a biogeochemical model with n state variables expressed as ensemble averaged concentrations c_i with $i = 1, \ldots, n$ are given by

$$\partial_t c_i + \partial_z \left(m_i c_i - K_\mathrm{v} \partial_z c_i \right) = \mathcal{P}_i \left(\vec{c} \right) - \mathcal{D}_i \left(\vec{c} \right) , \tag{A.21}$$

where $\vec{c} := (c_1, \ldots, c_n)^\mathrm{T}$, m_i describes the autonomous motion of the component described by c_i, K_v is the vertical turbulent diffusivity, and $\mathcal{P}_i$ and $\mathcal{D}_i$ summarize the sources and sinks of the component i. These source and sink terms are composed of reactive flux contributions p_{ij} from c_j to c_i and d_{ij} from c_i to c_j. That is,

$$\mathcal{P}_i := \sum_{j=1}^{n} p_{ij} , \quad \mathcal{D}_i := \sum_{j=1}^{n} d_{ij} , \tag{A.22}$$

where for the type of models in which all state variables are based on the same measurable unit, e.g., nitrogen concentration, $p_{ij} = d_{ji} > 0$ for $i \neq j$ and $p_{ii} = d_{ii} = 0$. In this case and with this specification of the sources and sinks, mass conservation is assured.

One way in which the biological part of the model can feed back on the physical part is by altering the underwater light field. This change can be parametrized via a bioturbidity B entering the equation for the shortwave irradiance (see Equation A.6), which acts as an inner source of heat and thereby leads to altered temperature (see Equation A.5). The bioturbidity can be described as

$$B\left(z\right) := \exp\left[k_\mathrm{bio} \int_0^z c\left(z'\right) dz' \right] , \tag{A.23}$$

taking into account the attenuation at position z by particulate and dissolved matter in the water column above that position. The concentration c entering the integral can describe any organic matter with usually the dominant contribution from phytoplankton. The parameter k_bio describes the absorption coefficient by biogenic matter.

Numerics in GOTM

The numerical methods used in this work are discussed only very briefly here. For a detailed description of the different numerical schemes implemented in GOTM, I refer to Umlauf *et al.* (2005) for the physical equations and Burchard *et al.* (2003) for the reaction part of the biogeochemical tracer equations.

In order to meet the constraints of conservation and positivity of the biogeochemical tracer concentrations as well as stability and accuracy of the method to solve the corresponding prognostic equations, a split method is applied in GOTM. This method separates the numerical treatment of the transport and the reaction part. For the transport step, finite volume discretizations are used such that conservation of mass is guaranteed. The water column is discretized into not necessarily equidistant intervals with the state variables, represented by layer-averaged values, located in the centres of these intervals and the advective and diffusive fluxes located at the interfaces in between. The autonomous motion of the state variables is discretized by means of TVD (Total Variation Diminishing) advection schemes conserving positivity. To assure positivity also in the presence of strong gradients, so-called slope limiters are used for which different types can be chosen. For the diffusion, a central in space scheme is used which is slightly biased towards a backward in time scheme in order to avoid asymptotic instability.

By applying this operator splitting, positivity is obtained, the schemes are practically second order in time and space and only ordinary differential equations (ODE) need to be treated numerically for the reaction part. Basically, three classes of schemes for this ODE part are considered. Explicit schemes are conserving mass, but not positivity, unless the time step is sufficiently small, which may lead to impracticably high computational costs. These schemes include the first-order Euler-forward and the higher-order Runge-Kutta schemes. A second class of schemes, referred to as Patankar schemes, is unconditionally positive. However, these are not fully mass conserving, since the numerical treatment of terms for sources and sinks are different from each other. The equal treatment of source and sink terms results in implicit linear systems of equations that can be solved directly by Gaussian elimination. This third class of schemes, which are fully conservative and non-negative, is referred to as Modified Patankar schemes. The (Modified) Patankar schemes can also be formulated in higher orders in which case they are referred to as (Modified) Patankar-Runge-Kutta schemes.

Within this work I use a TVD scheme for the vertical autonomous motion of the state variables with the so-called ULTIMATE QUICKEST slope-limiter and a second-order Modified Patankar-Runge-Kutta scheme for the source and sink dynamics of the biological reactions.

A.3 | The general circulation model MITgcm

The MITgcm is a highly flexible and portable circulation model that can be used for simulating both ocean and atmosphere on a wide range of scales. The model is based on the inviscid, incompressible Navier-Stokes equations and can be used in a hydrostatic and a non-hydrostatic mode. Here, only the case of hydrostatic equations for oceanic motion is discussed. Together with the hydrostatic, the Boussinesq (or anelastic) and the so-called traditional approximations, the inviscid, incompressible Navier-Stokes equations are referred to as the hydrostatic primitive equations, which

in z-coordinates read

$$\mathrm{D}_t \vec{v}_\mathrm{h} + f \left(\hat{k} \times \vec{v}\right)_\mathrm{h} = -\frac{1}{\rho_0} \nabla_\mathrm{h} p \qquad \text{(horizontal momentum)} \tag{A.24}$$

$$\partial_z p = -g\rho \qquad \text{(vertical momentum)} \tag{A.25}$$

$$\nabla \cdot \vec{v} = 0 \qquad \text{(continuity)} \tag{A.26}$$

$$\rho = \rho(\theta, S, p) \qquad \text{(equation of state)} \tag{A.27}$$

$$\mathrm{D}_t \theta = 0 \qquad \text{(potential temperature)} \tag{A.28}$$

$$\mathrm{D}_t S = 0 \qquad \text{(salinity)} \tag{A.29}$$

where $\mathrm{D}_t := \partial_t + \vec{v} \cdot \nabla$ is the material derivative, $\vec{v} := (u, v, w)$ is the velocity, $\vec{v}_\mathrm{h} := (u, v)$ is the horizontal velocity, u, v, and w are the velocity components in x, y, and z-directions, respectively, $\hat{k}$ is the unit vector in z-direction, f is the Coriolis parameter, ρ_0 is a constant Boussinesq reference density and ρ is the deviation from that reference density, $\nabla_\mathrm{h} := (\partial_x, \partial_y)$ is the horizontal gradient, p is the deviation from the Boussinesq reference pressure, g is the acceleration due to gravity, θ is potential temperature, and S is salinity.

Together with initial and boundary conditions for the prognostic variables and assumptions for the scales which are not resolved in the discretized form of the equations, the physical part of the model system is complete.

Forcing, mixing and dissipation

The interaction of the ocean with the atmosphere as well as dissipation and mixing within the ocean at unresolved spatial scales can be described via additional terms in the momentum, temperature and salinity equations.

Commonly used forms of momentum dissipation are expressed via a mixing term including the Laplacian and biharmonic operators

$$D_{\vec{v}} = A_\mathrm{h} \nabla_\mathrm{h}^2 \vec{v} + A_\mathrm{v} \partial_{zz} \vec{v} + A_4 \nabla_\mathrm{h}^4 \vec{v}, \tag{A.30}$$

where A_h and A_v are (constant) horizontal and vertical viscosity coefficients and A_4 is the horizontal coefficient for biharmonic friction.

The mixing terms for the temperature and salinity equations can be written in a similar form to those of momentum, except that the diffusion tensor can be non-diagonal and have varying coefficients:

$$D_\theta = \nabla \cdot \left(\underline{\underline{K}} \nabla \theta\right) + K_4 \nabla_\mathrm{h}^4 \theta \tag{A.31}$$

$$D_S = \nabla \cdot \left(\underline{\underline{K}} \nabla S\right) + K_4 \nabla_\mathrm{h}^4 S \tag{A.32}$$

Here, $\underline{\underline{K}}$ is the diffusion tensor and K_4 is the horizontal coefficient for biharmonic diffusion. In the simplest case where the subgrid-scale fluxes of heat and salt are parameterized with constant horizontal and vertical diffusion coefficients, $\underline{\underline{K}}$ reduces to

a diagonal matrix with constant coefficients:

$$\underline{\underline{K}} = \begin{pmatrix} K_\mathrm{h} & 0 & 0 \\ 0 & K_\mathrm{h} & 0 \\ 0 & 0 & K_\mathrm{v} \end{pmatrix} ,$$

where K_h and K_v are the horizontal and vertical diffusion coefficients.

Additional optional parameterizations

Several different options for specifying additional parameterizations of physical processes are available in MITgcm via so-called packages. These packages can be used to define, e.g., different boundary conditions at the ocean surface, like prescribed or dynamic fluxes of heat, salt and momentum, or different horizontal and vertical mixing parameterizations.

Parameterizations that are implemented in MITgcm include the Redi scheme and the Gent-McWilliams parametrization for isopycnal mixing. The Redi scheme (Redi, 1982) aims to mix tracer properties along isentropes (neutral surfaces) by means of a diffusion operator oriented along the local isentropic surface. The Gent-McWilliams parametrization (Gent and Mcwilliams, 1990; Gent *et al.*, 1995) adiabatically re-arranges tracers through an advective flux where the advecting flow is a function of slope of the isentropic surfaces. For the vertical mixing, the so-called KPP scheme by Large *et al.* (1994) and the mixed layer closure scheme by Gaspar *et al.* (1990), which is based on turbulent kinetic energy and used in this study, are implemented in MITgcm. A description of the specific model setup and parameterizations used in this work is given in Chapter 3, the parameter values used in this work are given in Tables A.3, A.4, and A.5.

Biogeochemical models in MITgcm

In the model framework of MITgcm, ocean biogeochemical models can be coupled to the physical ocean model part via a package called "ptracers", which stands for "passive tracers". The term "passive" here means that the tracers do not directly affect the density of the water, as opposed to the so-called "active" tracers temperature and salinity. Sources and sinks of a biogeochemical model are provided via the additional package "gchem", which serves as an interface to the ptracers package and is a means to call functions used by the specific biogeochemical model.

Generally, the dynamics for the concentrations c_i of biogeochemical tracers is given by

$$(\partial_t + \vec{v} \cdot \nabla)\, c_i = \left(K_\mathrm{h}^\mathrm{bio}\, \partial_{xx} + K_\mathrm{h}^\mathrm{bio}\, \partial_{yy} + K_\mathrm{v}^\mathrm{bio}\, \partial_{zz}\right) c_i + \mathcal{Q}_i \,, \tag{A.33}$$

where $K_\mathrm{h}^\mathrm{bio}$ and $K_\mathrm{v}^\mathrm{bio}$ are the horizontal and the vertical biological tracer diffusivities and the term $\mathcal{Q}_i$ represents sources and sinks of the biological tracer i.

For the model simulations in this work, I use the Redi scheme and Gent-McWilliams parametrization for isopycnal mixing of the biological tracers.

f_0	=	2.5×10^{-5}	s^{-1}	Coriolis parameter at the southern boundary
β	=	1.5×10^{-11}	$\mathrm{s}^{-1}\,\mathrm{m}^{-1}$	meridional gradient of Coriolis parameter
L_x	=	2560	km	model domain size in meridional direction
L_y	=	5120	km	model domain size in zonal direction
H	=	900	m	model domain depth
Δx	=	80	km	grid size in meridional direction
Δy	=	80	km	grid size in zonal direction
Δz	=	$2 \ldots 100$	m	vertical grid size
Δt_{mom}	=	1200	s	time step for momentum equations
$\Delta t_{\mathrm{tracer}}$	=	7200	s	time step for tracer equations
t_α	=	2×10^{-4}	K^{-1}	thermal expansion coefficient in equation of state
A_h	=	2.5×10^4	$\mathrm{m}^2\,\mathrm{s}^{-1}$	lateral eddy viscosity
A_v	=	1×10^{-5}	$\mathrm{m}^2\,\mathrm{s}^{-1}$	vertical eddy viscosity
K_h	=	0	$\mathrm{m}^2\,\mathrm{s}^{-1}$	lateral tracer diffusivity
K_v	=	1×10^{-4}	$\mathrm{m}^2\,\mathrm{s}^{-1}$	vertical tracer diffusivity
$K_\mathrm{h}^{\mathrm{bio}}$	=	0	$\mathrm{m}^2\,\mathrm{s}^{-1}$	lateral diffusivity for biological tracers
$K_\mathrm{v}^{\mathrm{bio}}$	=	5×10^{-5}	$\mathrm{m}^2\,\mathrm{s}^{-1}$	vertical diffusivity for biological tracers
ρ_0	=	1000	$\mathrm{kg}\,\mathrm{m}^{-3}$	reference density
g	=	9.81	$\mathrm{m}\,\mathrm{s}^{-2}$	gravitational acceleration
T_E	=	86164	s	Earth's rotation Period
τ_T	=	103680	s	temperature restoring timescale

Table A.3.: Values and meanings of the physical model parameters used in the MIT-gcm model setup.

background isopycnal diffusivity	$1000\,\mathrm{m}^2\,\mathrm{s}^{-1}$
background GM skew flux diffusivity	$1000\,\mathrm{m}^2\,\mathrm{s}^{-1}$
minimum horizontal diffusivity	$50\,\mathrm{m}^2\,\mathrm{s}^{-1}$
epsilon used in slope calculation	10^{-20}
slope^2 cut-off value	10^{48}
type of tapering/clipping scheme	Danabasoglu and McWilliams, 1995
maximum slope of isopycnals	10^{-2}
minimum transition layer thickness (factor of dz)	1
maximum transition layer thickness (factor of MLD)	5
maximum transition layer thickness	$500\,\mathrm{m}$
vertical mode number for BVP wave speed	1
minimum wave speed for BVP	$0.1\,\mathrm{m}\,\mathrm{s}^{-1}$

Table A.4.: Model parameter values and settings for the Redi and Gent-McWilliams parametrization used in the MITgcm model setup.

viscosity parameter	0.1
dissipation parameter	0.7
TKE diffusivity parameter	30
wind stress to vertical stress ratio	3
minimum kinetic energy	$4 \times 10^{-6}\,\mathrm{m^2\,s^{-2}}$
minimum surface kinetic energy	$1 \times 10^{-4}\,\mathrm{m^2\,s^{-2}}$
bottom kinetic energy	$4 \times 10^{-6}\,\mathrm{m^2\,s^{-2}}$
upper limit for viscosity	$100\,\mathrm{m^2\,s^{-1}}$
upper limit for diffusivity	$100\,\mathrm{m^2\,s^{-1}}$
horizontal diffusivity for TKE	0
minimum mixing length	$10^{-8}\,\mathrm{m}$

Table A.5.: Model parameter values and settings for the TKE vertical mixing scheme after Gaspar *et al.* (1990) used in the MITgcm model setup.

Numerics in MITgcm

The MITgcm uses an Arakawa C-grid for placement of the model's physical arrays. Spatial discretization is carried out using the finite volume method with several different time stepping and advection schemes. For an overview of the different schemes I refer to the documentation on the MITgcm website (http://mitgcm.org).

In this work I use the semi-implicit pressure method for hydrostatic equations with a rigid lid with variables staggered in time and implicit time stepping for diffusion and viscosity as well as the third order upwind biased advection scheme. For the biological tracers I use the second order flux limiter method for advection.

Appendix B

Literature survey on biological-physical feedbacks in marine systems

When speaking about biological-physical interactions in marine systems, many studies refer to the effect physical properties of the ocean have on the biological component of the system. In biological-physical models, this interaction is implemented then using a one-way coupling taking into account the impact of physics on biology. There are, however, also feedbacks from marine biota on the physical environment. These feedbacks can only be described adequately by incorporating a two-way coupling into a model, which makes it possible to analyze the potential impact of these feedbacks.

An exception from the widespread view of a one-way coupling is the concept of "ecosystem engineers" (Jones *et al.*, 1994; Berke, 2010; Breitburg *et al.*, 2010), where organisms modify physical state changes and thereby adjust, maintain or create habitats for themselves or other organisms. This concept has also been applied to marine pelagic organisms engineering their physical environment, but has not seen considerable attention yet.

In the following sections, I give an overview of observational and modeling studies on the effect marine biota can have on the physics of the ocean via alterations in light absorption, the surface albedo, as well as turbulence and the surface wind drag.

B.1 | Absorption

Biologically induced changes in the absorption of light in the ocean is mainly mediated by phytoplankton. Phytoplankton use light as an energy source in the process of photosynthesis, which requires the absorption of solar radiation by pigments. One part of the absorbed light is used to build up organic matter and the rest is mostly converted to heat and released. The part of the solar energy which is used for the formation of

biomass generally is very small (see e.g. Lewis *et al.*, 1983, and references therein) and can be neglected.

The spectral range of solar irradiance at the ocean surface covers wavelengths λ of approximately $300\,\mathrm{nm} < \lambda < 2800\,\mathrm{nm}$, with an ultra-violet (UV) part with $\lambda < 400\,\mathrm{nm}$, a part in the humanly visible range with $400\,\mathrm{nm} < \lambda < 700\,\mathrm{nm}$, and an infrared (IR) part with $\lambda > 700\,\mathrm{nm}$. Approximately 50 % of the solar irradiation reaching the ocean surface is in the IR range and is largely absorbed in the first few centimeters of the upper ocean. The remaining part is predominantly in the visible and UV ranges, which represent the so-called photosynthetically active - or available - radiation (PAR), and is absorbed by water, phytoplankton, and other suspended particles.

In general, the absorption of solar energy in the ocean is dominated by the absorption from seawater itself. However, the variability in absorption and the distribution of solar energy into the upper layers of the open ocean is controlled primarily by phytoplankton pigment concentrations (e.g. Smith and Baker, 1978).

Observational studies

Lewis *et al.* (1990) showed that a large amount of solar radiation penetrates to below the mixed layer. In their study they noted the sensitivity of the sea surface temperature to variations in surface concentrations of phytoplankton and stated that an increase in the phytoplankton abundances in the western Pacific to levels usually found in the east resulted in an additional heating of the order of $10\,\mathrm{Wm}^{-2}$ in the surface layers. Their finding could explain the consistent overestimation of sea surface temperatures in the equatorial Pacific Ocean by ocean-atmosphere models at that time

Shortly after, the first evidence of a biological-physical feedback between light and phytoplankton was provided by Sathyendranath *et al.* (1991). Their satellite data for chlorophyll abundances in the Arabian Sea showed a surface warming by near surface chlorophyll. The finding that phytoplankton could increase the heating rate of the mixed layer was later confirmed by Siegel *et al.* (1995), who used in situ optical, physical, and biological oceanographic observations from the western equatorial Pacific.

A ship based study of Ramp *et al.* (1991) along the California coast and a satellite and buoy data based study by Strutton and Chavez (2004) in the central-eastern equatorial Pacific also showed a correlation between sea surface temperature and surface chlorophyll. In a ship and satellite data based study, Capone *et al.* (1998) found a large phytoplankton surface bloom of cyanobacteria covering an area as large as 20 % of the Arabian Sea surface. They noted a coinciding increase in local surface temperature by about 5 K and suggested a positive feedback due to the cyanobacteria leading to heat absorption and increased stability of the water column.

McClain *et al.* (2002) verified that in the tropical Pacific Ocean high surface chlorophyll concentrations correlate with high sea surface temperatures by analyzing various satellite data products. They reported that biologically driven variability of ocean turbidity is a significant term in the ocean heat budget, and that the magnitude of this effect shows significant temporal variability associated with the El Niño Southern

Oscillation (ENSO).

Conceptual and one- to two-dimensional local model studies

Lewis *et al.* (1983) were the first to demonstrate that nonuniform vertical distributions of phytoplankton pigments cause variations in local heating and can support the development of a thermal instability within the water column. In their local conceptual model study they documented an example of a short-term feedback from biological to physical processes. In particular, they showed that at an oligotrophic ocean station the chlorophyll maximum was sufficiently strong that the local heating of water due to absorption of solar radiation caused increased vertical mixing and deepening of the mixed layer. The study also indicated that the chlorophyll maximum decreased the rate of heating of the water immediately below it, thereby increasing the stability of that part of the thermocline. According to Mann and Lazier (2006) this phenomenon is probably widespread in the ocean.

Trevisan and Bejan (1986) investigated how horizontal variations in water turbidity, potentially resulting from phytoplankton, can induce circulation. Using scale analysis and asymptotic considerations, they describe the main features of a potential natural convection and compare the analytical results with numerical simulation results from a two-dimensional shallow water model. These theoretical considerations were later extended and validated through small water tank experiments by Coates and Patterson (1993). Their experiments showed that horizontally differential heating of the water established a pressure gradient which lead to an intrusion of warm surface water into the colder part of the tank, happening on a time scale in good agreement with the scale analysis.

Using a coupled thermodynamic mixed layer model, Simonot *et al.* (1988) showed that the sensitivity of computed sea surface temperatures to the inclusion of phytoplankton induced heating is not negligible. Yet, the magnitude of this modeled effect was in the same order as the error between observed and simulated sea surface temperatures in the eastern North Atlantic Ocean.

Sathyendranath *et al.* (1991) used a bulk mixed layer model to investigate the heating effect of phytoplankton in the surface layer of the Arabian Sea, which they detected by analyzing remotely sensed data. They indicated that the variations in phytoplankton biomass were a dominant contribution to the heating rate of the mixed layer.

Also Ramp *et al.* (1991) were able to reproduce their observed vertical thermal structure by using a mixed layer model and assuming increased light absorption due to increased chlorophyll concentration at constant albedo. They suggested a feedback mechanism starting with the formation of a phytoplankton patch that causes enhanced stratification of the water column. Thus phytoplankton cells are kept near the surface, which leads to accelerated growth and results in ever more inhomogeneous chlorophyll distributions.

To evaluate the impact of a phytoplankton bloom on the mixed layer depth and temperatures at a high latitude site near Iceland, Stramska and Dickey (1993) used a

one-dimensional hydrodynamic model. They estimated that increasing phytoplankton abundances in spring induced increasing sea surface temperatures by about 0.2 K, which caused stronger stratification and shallower mixed layers. They also indicated that the dependence of the upper layer thermal structure on biology was expected to be more important when vertical mixing was weaker and phytoplankton concentrations were higher.

By coupling a one-dimensional dynamic thermodynamic sea ice model to a bio-optical model, Zeebe *et al.* (1996) investigated the effects of microalgae on the thermal regime of sea ice. Their results indicate that high concentrations of phytoplankton enhance ice melting, leading to an earlier breakup of sea ice and an onset of the spring bloom.

Using a bulk mixed layer model, Lefèvre *et al.* (2001) showed that taking into account the effect of physiological processes triggering internal elemental ratios in phytoplankton cells can lead to differences in sea surface temperatures by about 1 K in mid-latitudes.

Edwards *et al.* (2001) indicated that biologically induced vertical and horizontal along-frontal velocities contribute to the overall flow field in frontal ocean regions. They used a conceptual two-dimensional steady state hydrodynamic model, solved the corresponding equations analytically, and analyzed the effect of a horizontal gradient in phytoplankton concentration on the temperature gradient and subsequently on the pressure gradient. In an extension of this study using similar methods (Edwards *et al.*, 2004), they also considered a case of a long band of phytoplankton and investigated the circulations that could arise by differential heating effects. They found that biologically induced heating could produce circulation cells and speculate about a feedback mechanism related and complementary to the one suggested by Ramp *et al.* (1991), whereby biologically induced circulation could bring nutrient-rich water into the sunlit surface waters, enhancing phytoplankton production. In their study Edwards *et al.* (2004) suggested to perform more-sophisticated numerical experiments to determine if the effects of biologically induced circulation are important at larger scales.

Concerning the effect of marine biology on sea surface temperatures in the tropics, Timmermann and Jin (2002) conducted a study using a simplified coupled atmosphere-ocean model. They found that phytoplankton blooms can lead to a surface layer warming of about 20 Wm^{-2} thereby regulating the surface temperatures and influencing ENSO. Gildor *et al.* (2003) coupled a marine ecosystem model to a simple atmospheric model for the tropical Pacific region and suggested that the heating effect by phytoplankton could actually affect tropical intra-seasonal variability in the atmosphere. Later, Heinemann *et al.* (2011) used a modified version of the conceptual coupled atmosphere-ocean model by Timmermann and Jin (2002) and coupled it interactively to a three-component ecosystem model to study the interaction between marine biota and ENSO. They showed that bio-physical coupling may play a considerable role in modulating ENSO variability.

To study the potential local impact of biological heating on the upper tropical Indian Ocean, Babu *et al.* (2004) used a series of simulations with a one-dimensional hydrodynamic model. They found variations in mixed layer depth of up to 10 m in the

Arabian Sea, and an overall improvement of model results compared to observations when taking into account the biological heating in the model.

Using a one-dimensional coupled hydrodynamic-biological model simulating conditions for the Baltic Sea, Hense (2007) showed that cyanobacteria floating to the ocean surface could induce changes in the temperature field, which resulted in slightly more favorable conditions for the cyanobacteria. This positive feedback suggested that cyanobacteria gained from their own presence.

By using a one-dimensional analytical model, Zhai *et al.* (2011) studied the feedback of phytoplankton on the air-sea heat exchange. They showed that this feedback mechanism limits the effect of bio-optical heating to a short period and thus significantly decreases the effect of heating through light absorption by phytoplankton. Moreover, they argue that the net temperature increase is determined by the total absorption of light in the mixed layer, accumulated over a period of a few weeks.

Concerning the importance of resolving the vertical distribution of phytoplankton, Duteil *et al.* (2009) studied the effect of bio-optical heating using a one-dimensional coupled ocean-biogeochemical model with high vertical resolution. They found that a deep chlorophyll maximum (DCM) can influence the upper ocean thermal structure. They showed that the DCM increases the seasonal thermocline by 2 K in summer and decreases the permanent thermocline by up to 2 K, resulting in more stable stratification and a better fit compared to observations. They also suggested that using at least a 1 m vertical resolution model is mandatory to assess the energetical importance of the DCM.

Three-dimensional regional and global models with non-interactive biology

Changes in light absorption by marine phytoplankton have been studied quite intensively in the last years using three-dimensional models of different complexity and with different regional or thematic focus. Many of these studies, however, did not include an interactive biological component.

A particular focus of these studies has been the biological-physical feedback mechanism via absorption changes in the tropical Pacific (e.g. Miller *et al.*, 2003). Here, changes in absorption can result in a feedback between sea surface temperature, atmospheric circulation, and surface chlorophyll because of high solar irradiance, high surface chlorophyll concentrations and the strong sensitivity of the tropical atmosphere to changes in sea surface temperatures (Jochum *et al.*, 2010).

Schneider and Zhu (1998) were the first to note, with a coupled atmosphere-ocean general circulation model, that problems related to model coupling may be due to the inaccurate representation of solar transmission in the ocean. They investigated the effects of considering radiant heating beyond the top model level in the equatorial Pacific. They showed that mixed layer depth increases by 15 m and SST increases by as much as 1 K when solar energy is allowed to heat beyond the top model level. The

deeper mixed layer causes a decrease in the sensitivity of SST to upwelling, leading to lighter easterly winds and a reduction in zonal currents along the equator. Moreover, the modeled SST fields are much closer to observed values when solar heating is allowed beyond the top level.

Nakamoto *et al.* (2001) incorporated variable biological heating through absorption into an ocean general circulation model and found that this incorporation shoaled the mixed layer by trapping heat closer to the surface in the equatorial Pacific. They also showed that this ultimately leads to decreasing sea surface temperatures in the eastern Pacific because of enhanced westward surface currents, which strengthen the equatorial undercurrent and favor upwelling.

Using a global ocean general circulation model, Rochford *et al.* (2001) showed that incorporating realistic biological heating, derived from satellite data, improved the predictive skill of the model regarding sea surface temperatures, most prominently in the tropics.

Murtugudde *et al.* (2002) also used global ocean circulation models using constant versus variable biological absorption. In the eastern equatorial Pacific, including altered absorptivity by variable chlorophyll resulted in increased subsurface heating. This warming led to decreased, as apposed to increased in Nakamoto *et al.* (2001), upwelling because of weaker stratification, deeper mixed layers, and reduced divergence.

Using an ocean general circulation model with and without the radiative effects of phytoplankton to determine how phytoplankton change SST and prescribing these SST changes from the ocean model as boundary conditions for an atmospheric general circulation model, Shell *et al.* (2003) showed for the first time the response also of the extra-tropical region to the biophysical feedback through light absorption. In the mid latitudes they found a significantly amplified seasonal cycle in the near surface atmospheric temperature due to the prescribed SST changes.

Kara *et al.* (2004) investigated ocean turbidity through depth-dependent attenuation of solar radiation in an ocean general circulation model with an embedded bulk-type mixed layer model. They only found a minor impact of phytoplankton on the sea surface temperature in the equatorial Pacific.

Ueyoshi *et al.* (2005) conducted numerical experiments with an ocean general circulation model and found that due to phytoplankton-radiation forcing, equatorial Pacific sea surface temperature is decreased by 0.3 K on average annually and reaching 1.5 K in sub-surface layers in the eastern Pacific.

Gildor and Naik (2005) investigated the effect of inter-annually varying chlorophyll concentration on the sea surface temperature in the Atlantic Ocean. In their study, they did not find a relationship between inter-annual variability of surface phytoplankton biomass and sea surface temperature. They argued that in previous studies, the differences in modeled sea surface temperatures were not a result of the direct effect of ocean biota on light penetration, but rather a series of feedbacks amplified the initial anomaly.

Kara *et al.* (2005) used an eddy-resolving regional ocean general circulation model for the Black Sea to study the effects of biologically increased ocean turbidity on upper-

ocean circulation features. They found a shallower mixed layer with much stronger stratification at the base as well as much better agreement with observations when including the effect of biology on the absorptivity.

Using a statistical atmosphere model coupled to a reduced-gravity ocean general circulation model for the equatorial Pacific, Ballabrera-Poy *et al.* (2007) found that changes in the heat trapped in the surface mixed layer arose as a combination of the direct thermal term due to the change of the attenuation depth and an indirect dynamical term related to the ocean dynamical response. They argued that the relative amplitude of each term determined whether a warming or cooling would occur.

Wu *et al.* (2007) studied the impact of bio-optical heating in the Labrador Sea with the seasonal changes of chlorophyll distribution. They used a regional ocean general circulation model and found an average increase in sea surface temperature of around 1 K and up to 2.7 K in areas with shallow mixed layers and high chlorophyll concentrations. They also found heating rates that are comparable to those in the Arabian Sea (Sathyendranath *et al.*, 1991), an enhanced stratification of the upper ocean and a reduction of the mixed layer depth by up to 50 %. Near surface temperature changes of the same order of magnitude were also found in another regional study in the Gulf of St. Lawrence by Zhai *et al.* (2011), who used satellite-derived chlorophyll concentration and an optically-coupled circulation model to investigate the oceanic response to the light attenuation by phytoplankton. Their results also support the result of Shell *et al.* (2003) that the change of net air–sea heat flux induced by phytoplankton amplifies the seasonal cycle in the near surface air temperature.

Using a global ocean general circulation model, Subrahmanyam *et al.* (2008) found that variations of light-absorbing phytoplankton pigments changed the vertical distribution of solar heating in the mixed layer, thereby affecting upper-ocean circulation. Their model results showed a large seasonal variability in the strength of the meridional overturning circulation, meridional heat transports, and equatorial undercurrent.

Anderson *et al.* (2007) studied the impact of the dependence of shortwave radiation penetration into the surface ocean on chlorophyll concentrations using a coupled ocean-atmosphere-land-ice model. Their results indicated a potential positive feedback between chlorophyll concentration and a non-local coupled response in the fully coupled ocean-atmosphere system. Extending those results, Anderson *et al.* (2009) found that the mean state and variability of the tropical Pacific is highly sensitive to the concentration and distribution of ocean chlorophyll.

Also Zhang *et al.* (2009) found that the biologically induced feedback through changing absorptivity can have significant effects on ENSO behaviors, including its amplitude, oscillation periods and seasonal phase locking. They used a global ocean general circulation model and postulated a negative feedback to explain the weakening effect on inter-annual variability and the shortening effect on oscillation periods.

Gnanadesikan and Anderson (2009) examined how changes in ocean water clarity propagate through the climate system, how changes in sea surface temperatures affect ocean circulation as a whole, both directly and indirectly through changing the wind field, to which degree this response is linear in the chlorophyll concentration, and how

different regions have different impacts. The found that less short wave absorption in the surface layers in their global climate model leads to a warming south of the equator, a shift of the subtropical gyres toward the equator, a warming of the Pacific cold tongue, a weaker Walker circulation, and an increase in mode water formation from subtropical water.

Gnanadesikan *et al.* (2010) studied the effect of ocean color in the formation of tropical cyclones in the North Pacific and found biological heating to be responsible for increasing subtropical cyclone activity by a factor of 2/3, suggesting to take into account biologically induced changes in ocean absorptivity in models used for the prediction of tropical cyclone activity.

Using a coupled ocean-atmosphere forecasting system, Jolliff *et al.* (2012) compared model simulations with constant uniform solar shortwave ocean transparency and more realistic, spatially varying attenuation based on satellite estimates. They found consistently higher SST in the realistic case and an 88% increase in cumulative turbulent thermal energy transfer from ocean to atmosphere over a three month simulation period resulting in local air temperature differences approaching 2 K and suggesting that retention of shortwave solar flux by ocean flora may directly impact even short-term forecasts of coastal meteorological variables.

Turner *et al.* (2012) used a coupled atmosphere-ocean general circulation model with prescribed chlorophyll concentrations to study the role of local seasonal phytoplankton blooms on the mean climate of the Arabian Sea and the South Asian summer monsoon. They found that the inclusion of bio-optical heating leads to a bias reduction in mixed layer depth and an increased seasonality in SST.

In an ocean general circulation model study, Ma *et al.* (2012) found that high summer chlorophyll concentrations in the upwelling region of the South China Sea leads to enhanced upwelling and lower SST, whereas in the non-upwelling regions, surface warming and subsurface cooling are found.

In another regional study, Löptien and Meier (2011) address the question whether the heating effect by increased water turbidity needs to be included in Baltic Sea ocean models using hindcast experiments. They found that increased water turbidity can affect summer SST trends significantly, but the effect was too small to explain observed extreme summer trends in the Baltic Sea.

Three-dimensional regional and global models with interactive biology

The models used in all of the studies described so far do not take into account an interactive biological dependence. That is, they do not include biological components dynamically affected by physical components and affecting the absorptivity at the same time. Instead, all those models use observed or analyzed data from satellites prescribing the optical oceanic properties. Yet, general circulation model studies involving a two-way coupling of biology and physics regarding the dynamical changes in light absorption

have also been published in recent years.

Regarding the North Atlantic Ocean, Oschlies (2004) used a regional eddy-permitting ocean general circulation model coupled to an ecosystem model to study biological-physical feedbacks involving absorptivity changes by phytoplankton. He found a net cooling of the ocean by biota at a rate of about $1\,\mathrm{W\,m^{-2}}$. The simulated chlorophyll concentrations increased, indicating a positive feedback, only in the subpolar regions with a pronounced phytoplankton spring bloom. Furthermore, the biotically induced trapping of heat closer to the sea surface lead to a faster shoaling of the mixed layer and a more intense spring bloom in the model. However, on basin average, simulated surface chlorophyll concentrations decreased by 3 %, constituting a weak negative feedback of $0.03\,\mathrm{W\,m^{-2}}$, when heating by biotic absorption of solar radiation was accounted for.

The first attempt to quantify the global impact of the presence of phytoplankton on both physical and biogeochemical processes using a global ocean general circulation model coupled to a state-of-the-art ocean biogeochemistry model was presented by Manizza (2006). He found an increase in SST by up to 1.5 K, a reduction of mixed layer depths by 30 m, and a reduction of summer sea ice cover by 4% due to light absorption by phytoplankton in the extra-tropical oceans. Concerning the subsequent effect on the phytoplankton composition, he found an increase of coccolithophores by 10% and of diatoms by 15%. In addition, he found changes in air-sea fluxes of carbon dioxide and oxygen, which were, however, not as substantial as expected, and in oceanic production of the volatile organic sulfur compound dimethylsulfide (DMS). He also studied the direct feedback of climate change on ocean physics through surface phytoplankton biomass, showing that in the polar oceans the seasonal cycle was amplified stronger in the Arctic than in the Antarctic, when including the bio-physical feedback via light absorption. In Manizza *et al.* (2005) the model results showed that phytoplankton biomass amplified the seasonal cycle of temperature, mixed layer depths and ice cover by roughly 10 %. The authors indicated that the physical changes drove a positive feedback increasing phytoplankton biomass by 4-12 % and further amplified the initial physical perturbations. Manizza *et al.* (2008) showed that the phytoplankton-light feedback influenced the dynamics of the upper tropical and subtropical oceans. They also showed that a change in circulation enhanced the vertical supply in the tropics and the lateral supply of nutrients from the tropics to the subtropics thereby increasing subtropical productivity. Moreover, they indicated that the feedback had an impact on the ecosystem structure, but a small effect globally on air-sea fluxes of carbon dioxide and oxygen.

Another global ocean-biogechemical general circulation model study with the above mentioned two-way coupling was presented by Marzeion *et al.* (2005). They showed that both the surface layer concentration as well as the vertical profile of chlorophyll had a significant effect on the simulated mean state, the tropical annual cycle, and ENSO. They supported the previously suggested hypothesis by Timmermann and Jin (2002) that predicted an influence of phytoplankton concentration on the tropical Pacific climate mean state and its variability.

Also Wetzel *et al.* (2006) studied the influence of phytoplankton on the seasonal cycle

and the mean global climate in a fully coupled climate model. Their findings were in agreement with Murtugudde *et al.* (2002) concerning the rise in sea surface temperature and a warming in the upwelling regions of the Arabian Sea. They also found that the seasonal cycle in both hemispheres was amplified and less sea ice in the high latitudes, which is in agreement with Manizza *et al.* (2005). Additionally, they found a shift of the seasonal cycle by about two weeks caused by the influence of the phytoplankton spring bloom on the upper ocean surface heating and the mixed layer depth. They also found a reduction in the strength of inter-annual sea surface temperature variability by about 10–15 % as well as several changes in ENSO properties. In agreement with Shell *et al.* (2003), they also found temperature changes occurring over land.

Using a different global coupled atmosphere-ocean-biogeochemical general circulation model, Lengaigne *et al.* (2007) showed that biology acted to warm the surface eastern equatorial Pacific by about 0.5 K by two competing processes. A direct, one-dimensional biologically induced warming process in the top layers from strong chlorophyll concentrations in upwelling regions and a two-dimensional meridional cooling bringing cold off-equatorial anomalies from subsurface into the equatorial mixed layer.

Also using an Earth system model, Lengaigne *et al.* (2009) indicated that using an interactive biology resulted in a warming of the ocean surface along the coastal shelves of Alaska and Siberia. They also showed that including biophysical feedbacks brought modeled sea-ice characteristics close to the observed estimates and freshened the Arctic Ocean surface layer.

Löptien *et al.* (2009) used an eddy-permitting regional biogeochemical-ocean general circulation model and validated their model results with observations. They demonstrated that the explicit simulation of biophysical feedbacks had considerable effects on the simulated mean climate conditions of the eastern tropical Pacific and its intra-seasonal to inter-annual variability. They also showed that including the absorptivity feedback improved the model performance in comparison to observations. Additionally, they indicated that the details of this feedback seemed to be highly model-dependent and had to be fully resolved yet. They argued that contradictory results from previous model studies might be partly due to use of different reference simulations and that overall, the use of a biological component and the biophysical coupling brought the models closer to observations.

To study the contribution of interannual chlorophyll variability on ENSO, Jochum *et al.* (2010) used a fully coupled Earth system model including an interactive marine ecosystem. They showed that including the interactive ecosystem reduces tropical variability compared to the case with prescribed chlorophyll climatology.

Using a biogeochemical-ocean general circulation model, Park and Kug (2013) studied the influence of phytoplankton on the tropical climate variability in the Indian Ocean and found significant effects on the characteristics of the Indian Ocean Dipole.

Using a fully coupled atmosphere-ocean-biogeochemistry model, Patara *et al.* (2012) found that absorption of solar radiation by phytoplankton increases global mean SST by 0.2 K. In their study, they highlight the relevance of global atmosphere-ocean interactions in the response to phytoplankton solar absorption. They found an increase

in evaporation and atmospheric temperatures as well as decreased polar sea ice cover, changes in the North Atlantic Ocean meridional overturning circulation and in upper ocean heat content. Overall they showed that modeled effects of phytoplankton on the global climate are within the range of natural climate variability, suggesting the necessity to include phytoplankton as an active component in Earth system models.

Parametrization of absorptivity in previous model studies

The attenuation of light in the ocean can be parametrized using one or several, for different spectral ranges, exponential functions for the downwelling irradiance as a function of depth. The attenuation coefficients can be constant in space and time, dependent on the water-type of the respective regions, or varying spatially and temporally according to the particulate matter altering the absorptivity. These variations can be either determined by ocean color satellite data and prescribed in the model, or the attenuation is computed dynamically from a component within the model.

Various parameterization schemes have been presented for modeling ocean radiant heating (e.g. Denman, 1973; Paulson and Simpson, 1977; Morel, 1988; Morel and Antoine, 1994; Ohlmann and Siegel, 2000). For a discussion of schemes used in climate models see e.g. Ohlmann (2003).

In their simplified atmosphere-ocean model, Timmermann and Jin (2002) directly prescribe the temperature dependence of chlorophyll and use this calculated chlorophyll concentration to compute the contribution in the temperature through the scheme by Morel (1988).

Sweeney *et al.* (2005) tested the sensitivity of ocean physics to bio-optical parameterizations for the global ocean using the bio-optical models of Morel and Antoine (1994) and Ohlmann (2003). Their results suggested that ocean general circulation models are highly sensitive to the bio-optical parameterizations not only in the tropical but also in the subtropical zones of the ocean.

Lin *et al.* (2007) found that the discrepancies between previous investigations on the effect of phytoplankton on sea surface temperatures in the central and eastern equatorial Pacific were due to the fact that different models and different shortwave penetration parameterizations were used.

In a more recent study, Mobley and Boss (2012) present factors computed by a radiative transfer code that can be used to convert above-surface to in-water net irradiance, as needed for calculations of water heating.

B.2 | Albedo

The ocean surface albedo is defined as the ratio of upward to downward short-wavelength radiation right above the sea surface. Surface floating marine organisms can alter the total amount of solar radiation entering the ocean. The magnitude and the direction of the effect is species-dependent (Jin *et al.*, 2004), i.e., how much more or less light

can enter the water, depends on the color of the organisms located at the surface. In general circulation models the ocean surface albedo is only crudely parametrized by taking into account the influence of the sun zenith angle and the ratio of diffuse and direct sunlight.

Observational studies

Holligan *et al.* (1983) reported strong reflectance of visible light by phytoplanktonic coccolithophores in their ship- and satellite based study in the north-west European continental shelf. Later, Holligan *et al.* (1993) confirmed the increased reflectance in their study of an extensive bloom of coccolithophores in the north east Atlantic Ocean. In their ship-based measurements Balch *et al.* (1991) found a correlation between phytoplankton abundance and surface albedo in the Gulf of Maine. They could show that the surface light reflectance increases with the density of coccoliths, which are plates of calcium carbonate formed by coccolithophores. For an overview of optical properties of coccolithophorids see also Balch and Utgoff (2009) and references therein.

In a satellite and ship based study Kahru *et al.* (1993) showed that near-surface accumulations of cyanobacteria increase the ocean surface albedo.

Park *et al.* (2011) investigated the role of biologically induced ocean surface albedo changes in the equatorial Pacific. In their satellite based study, they found that surface chlorophyll variability associated with ENSO changes the surface shortwave albedo and thereby leads to a cooling of the ocean surface. However, their study did not allow for a quantitative estimation of the phytoplankton-albedo feedback.

Model studies

Regarding biological-physical feedbacks through altering ocean surface albedo, presently no ocean model studies have been published. In general circulation models the ocean surface albedo is only crudely parametrized by taking into account the influence of the sun zenith angle and the ratio of diffuse and direct sunlight.

However, using a multispectral, multicomponent Monte Carlo simulation, Tyrrell *et al.* (1999) showed how phytoplankton increase the ocean surface albedo. They indicated that biotically induced increases in the albedo could result in a net global cooling of the ocean by about $0.2\,\mathrm{Wm}^{-2}$. Frouin and Iacobellis (2002) used a radiation-transfer model for the biologically induced change in global ocean optical surface properties and found that oceanic phytoplankton could change the globally and annually averaged outgoing radiative flux by as much as $0.25\,\mathrm{Wm}^{-2}$ with respect to pure seawater. The actual magnitude and the sign of this change, however, depends on the characteristics of the dominating phytoplankton species. Yet, in their study, they only used average optical properties of many different phytoplankton species.

B.3 | Turbulence and surface wind drag

The effects of marine biota on turbulence in the ocean mixing are mediated by changes in the seawater viscosity.

The term viscosity is used to describe two fundamentally different phenomena. One refers to a measure of the resistance of a fluid to a deformation by stress and is more precisely called molecular viscosity. The molecular viscosity of seawater generally increases with particulate matter concentration. The other phenomenon that is referred to as viscosity is the turbulent or eddy viscosity, which characterizes the transport and dissipation of energy in the smaller-scale flow. This turbulent viscosity is mainly influenced by winds, waves and currents, but can also be altered by marine organisms (e.g. Huntley and Zhou, 2004). Typically, the turbulent viscosity is orders of magnitude larger than the molecular viscosity, which is why the latter is neglected in most marine studies. The part of the turbulent viscosity that is of main interest here is the vertical turbulent viscosity. Phytoplankton species floating to the surface can build up large mats with very high concentrations of matter. Thereby the viscosity of the seawater at the ocean surface is changed leading to a change in the surface wind drag an thus to a altered turbulent wind mixing in the water.

Observational studies

The molecular viscosity of seawater containing phytoplankton has been found to increase with increasing phytoplankton concentration (e.g. Jenkinson and Biddanda, 1995). Taking measurements of chlorophyll and molecular viscosity in the eastern English Channel and the southern North Sea, Seuront *et al.* (2007) showed that during a phytoplankton bloom molecular viscosity of the seawater increased by a factor of three.

Biological impacts on oceanic properties through changing turbulence were examined even some decades ago by Munk (1966) and have been reported in several recent studies. Based on an analysis of measured data characterizing the hydrodynamics of swimming, Huntley and Zhou (2004) found that expected levels of turbulence in schools and swarms of a range of species from krill to large fish are of comparable order of magnitude as turbulence generated by storms. Consistent with this finding, Kunze *et al.* (2006) observed that planktonic organisms can locally increase turbulence levels by three to four orders of magnitude compared to average levels in the stratified ocean. They subsequently noted shear fluctuations at length scales much larger than the individual organisms (Kunze *et al.*, 2007). They claimed that these fluctuations indicated that mixing actually was occurring, yet they did not provide an explanation of the mechanisms by which the turbulence can be created. Katija and Dabiri (2009) observed that large plankton populations generate turbulence potentially affecting large-scale ocean mixing significantly. The mechanism by which the organisms generate motion on length scales large enough for efficient ocean mixing is called Darwinian-drift mechanism (see Darwin, 1953). Its importance appears to increase with increasing viscosity, imply-

ing that smaller organisms might have an even bigger impact on ocean mixing than larger organisms, since the induced fluid motion is strongly influenced by viscosity for smaller organisms and the marine biomass is dominated by them (Subramanian, 2010). However, Subramanian (2010) argued that the importance of the drift-induced mixing mechanism was greatly overestimated and such a mechanism was rather unlikely to contribute to oceanic mixing on a global scale. Yet, the role and relevance of biogenic mixing has not been determined yet conclusively.

Deacon (1979) reports that biological surface films reduce the drag coefficient by a factor of up to three as compared to the open sea. Those surface films might be comparable to the cyanobacterial surface films, which were first described by Sieburth and Conover (1965). In another study using a water tank with algal colonies in a wind tunnel, Hutchinson and Webster (1994) found that a surface film, likely produced by the floating algae, dampens surface waves and decreases vertical mixing. However, their study did not allow for a quantification of the observed effect.

Model studies

Presently, no model studies involving a hydrodynamic component for the ocean have been published concerning biological-physical feedbacks through altering viscous and turbulent ocean properties by marine organisms.

Yet, using different approaches to estimate the global contribution to turbulent mixing of the ocean, Dewar *et al.* (2006) concluded that mixing by marine organisms is as effective as mixing by winds and tides. The role of this so-called biogenic mixing in helping to stir the ocean has been discussed critically in the last years. Visser (2007) for instance argued that in spite of the production of large dissipation rates by marine organisms only a very small fraction actually went into mixing. Because of the very low mixing efficiency of a large part of the organisms most of the mechanical energy they impart to the oceans is dissipated almost immediately as heat.

Performing simplified simulations, Dabiri (2010) suggested that in order to generate mixing at length scales significantly larger than the size of the organisms an additional mechanism may be necessary, namely vertical migration, introducing a bias across diapycnals. They argued that organisms migrating vertically could generate overturning length scales compatible with large-scale mixing and high mixing efficiency.

Regarding the reduction of the surface wind drag by biogenic surface mats up to now no model studies have been conducted.

Bibliography

Anderson, W., A. Gnanadesikan, and A. Wittenberg (2009). Regional impacts of ocean color on tropical Pacific variability. *Ocean Science*, **5**:313–327, doi:10.5194/os-5-313-2009.

Anderson, W. G., A. Gnanadesikan, R. Hallberg, J. Dunne, and B. L. Samuels (2007). Impact of ocean color on the maintenance of the Pacific Cold Tongue. *Geophysical Research Letters*, **34**:L11609, doi:10.1029/2007GL030100.

Babu, K. N., R. Sharma, N. Agarwal, V. K. Agarwal, and R. A. Weller (2004). Study of the mixed layer depth variations within the north Indian Ocean using a 1-D model. *Journal of Geophysical Research*, **109**:C08016, doi:10.1029/2003JC002024.

Balch, W. M., P. M. Holligan, S. G. Ackleson, and K. J. Voss (1991). Biological and optical properties of mesoscale coccolithophore blooms in the Gulf of Maine. *Limnology and Oceanography*, **36**:629–643.

Balch, W. M. and P. E. Utgoff (2009). Potential interactions among ocean acidification, coccolithophores, and the optical properties of seawater. *Oceanography*, **22**:146–159, doi:10.5670/oceanog.2009.104.

Ballabrera-Poy, J., R. Murtugudde, R.-H. Zhang, and A. J. Busalacchi (2007). Coupled ocean-atmosphere response to seasonal modulation of ocean color: Impact on interannual climate simulations in the Tropical Pacific. *Journal of Climate*, **20**:353–374, doi:10.1175/JCLI3958.1.

Berke, S. K. (2010). Functional groups of ecosystem engineers: a proposed classification with comments on current issues. *Integrative and Comparative Biology*, **50**:147–157, doi:10.1093/icb/icq077.

Bracher, A., M. Vountas, T. Dinter, J. P. Burrows, R. Röttgers, and I. Peeken (2009). Quantitative observation of cyanobacteria and diatoms from space using PhytoDOAS on SCIAMACHY data. *Biogeosciences*, **6**:751–764, doi:10.5194/bg-6-751-2009.

Breitbarth, E., A. Oschlies, and J. LaRoche (2007). Physiological constraints on the global distribution of *Trichodesmium* - effect of temperature on diazotrophy. *Biogeosciences*, **4**:53–61, doi:10.5194/bg-4-53-2007.

Breitburg, D. L., B. C. Crump, J. O. Dabiri, and C. L. Gallegos (2010). Ecosystem engineers in the pelagic realm: alteration of habitat by species ranging from microbes to jellyfish. *Integrative and Comparative Biology*, **50**:188–200, doi:10.1093/icb/icq051.

Briegleb, B. P., P. Minnis, V. Ramanathan, and E. Harrison (1986). Comparison of regional clear-sky albedos inferred from satellite observations and model computations. *Journal of Applied Meteorology and Climatology*, **25**:214–226, doi:10.1175/1520-0450(1986)025<0214:CORCSA>2.0.CO;2.

Brock, T. D. (1981). Calculating solar radiation for ecological studies. *Ecological Modelling*, **14**:1–19, doi:10.1016/0304-3800(81)90011-9.

Burchard, H., K. Bolding, W. Kühn, A. Meister, T. Neumann, and L. Umlauf (2006). Description of a flexible and extendable physical-biogeochemical

model system for the water column. *Journal of Marine Systems*, **61**:180–211, doi:10.1016/j.jmarsys.2005.04.011.

Burchard, H., E. Deleersnijder, and A. Meister (2003). A high-order conservative Patankar-type discretisation for stiff systems of production-destruction equations. *Applied Numerical Mathematics*, **47**:1–30, doi:10.1016/S0168-9274(03)00101-6.

Burchard, H., B. K., and V. M.R (1999). GOTM—a general ocean turbulence model. Theory, applications and test cases. Technical Report EUR 18745 EN, European Commission.

Campbell, L., H. Liu, H. A. Nolla, and D. Vaulot (1997). Annual variability of phytoplankton and bacteria in the subtropical North Pacific Ocean at Station ALOHA during the 1991-1994 ENSO event. *Deep-Sea Research Part I: Oceanographic Research Papers*, **44**:167–192, doi:10.1016/S0967-0637(96)00102-1.

Caperon, J. (1967). Population growth in micro-organisms limited by food supply. *Ecology*, **48**:715–722.

Capone, D. G., J. A. Burns, J. P. Montoya, A. Subramaniam, C. Mahaffey, T. Gunderson, A. F. Michaels, and E. J. Carpenter (2005). Nitrogen fixation by *Trichodesmium* spp.: An important source of new nitrogen to the tropical and subtropical North Atlantic Ocean. *Global Biogeochemical Cycles*, **19**:GB2024, doi:10.1029/2004GB002331.

Capone, D. G., A. Subramaniam, J. P. Montoya, M. Voss, C. Humborg, A. M. Johansen, R. L. Siefert, and E. J. Carpenter (1998). An extensive bloom of the N_2-fixing cyanobacterium *Trichodesmium erythraeum* in the central Arabian Sea. *Marine Ecology Progress Series*, **172**:281–292, doi:10.3354/meps172281.

Capone, D. G., J. P. Zehr, H. W. Paerl, B. Bergman, and E. J. Carpenter (1997). *Trichodesmium*, a globally significant marine cyanobacterium. *Science*, **276**:1221–1229, doi:10.1126/science.276.5316.1221.

Carpenter, E. and D. Capone (eds.) (1992). *Marine pelagic cyanobacteria: Trichodesmium and other diazotrophs*, vol. 362 of *NATO Science Series C: (closed)*. Springer. Proceedings of the NATO Advanced Research Workshop on Trichodesmium and other Marine Diazotrophs, Bamberg, Germany, May 26-31, 1991.

Carpenter, E. J. (1983). Nitrogen fixation by marine *Oscillatoria* (*Trichodesmium*) in the world's oceans. In Carpenter, E. J. and D. G. Capone (eds.), *Nitrogen in the Marine Environment*, pp. 65–103. Elsevier, New York, NY, USA.

Carpenter, E. J., A. Subramaniam, and D. G. Capone (2004). Biomass and primary productivity of the cyanobacterium *Trichodesmium* spp. in the tropical N Atlantic ocean. *Deep-Sea Research Part I: Oceanographic Research Papers*, **51**:173–203, doi:10.1016/j.dsr.2003.10.006.

Clark, N. E., L. Eber, R. M. Laurs, J. A. Renner, and J. F. T. Saur (1974). Heat exchange between ocean and atmosphere in the Eastern North Pacific for 1961–1971. Tech. Rep. NMFS SSRF-682, NOAA, U.S. Dept. of Commerce, Washington, D.C., USA.

Coates, M. J. and J. C. Patterson (1993). Unsteady natural convection in a cavity with non-uniform absorption of radiation. *Journal of Fluid Mechanics*, **256**:133–161, doi:10.1017/S0022112093002745.

Conkright, M., R. Locarnini, H. Garcia, T. O'Brien, T. Boyer, C. Stephens, and J. Antonov (2002). World Ocean Atlas 2001: objective analyses, data statistics, and figures, CD-ROM documentation. Technical report, National Oceanographic Data Center,

Silver Spring, MD, USA.

Cushman-Roisin, B. and J.-M. Beckers (2011). *Introduction to Geophysical Fluid Dynamics*. Academic Press.

Dabiri, J. O. (2010). Role of vertical migration in biogenic ocean mixing. *Geophysical Research Letters*, **37**:L11602, doi:10.1029/2010GL043556.

Darwin, C. G. (1953). Note on hydrodynamics. *Mathematical Proceedings of the Cambridge Philosophical Society*, **49**:342–354, doi:10.1017/S0305004100028449.

Deacon, E. L. (1979). The role of coral mucus in reducing the wind drag over coral reefs. *Boundary-Layer Meteorology*, **17**:517–521, doi:10.1007/BF00118614.

Denman, K. (1973). A time-dependent model of the upper ocean. *Journal of Physical Oceanography*, **3**:173–184, doi:10.1175/1520-0485(1973)003<0173:ATDMOT>2.0.CO;2.

Denman, K., G. Brasseur, A. Chidthaisong, P. Ciais, P. Cox, R. Dickinson, D. Hauglustaine, C. Heinze, E. Holland, D. Jacob, U. Lohmann, S. Ramachandran, P. da Silva Dias, S. Wofsy, and X. Zhang (2007). Couplings Between Changes in the Climate System and Biogeochemistry. In Solomon, S., D. Qin, M. Manning, Z. Chen, M. Marquis, K. Averyt, M. Tignor, and H. Miller (eds.), *Climate Change 2007: The Physical Science Basis. Contribution of Working Group I to the Fourth Assessment Report of the Intergovernmental Panel on Climate Change*. Cambridge University Press, Cambridge, United Kingdom and New York, NY, USA.

Devassy, V., P. Bhattathiri, and S. Qasim (1978). Trichodesmium phenomenon. *Indian Journal of Marine Sciences*, **7**:168–186.

Dewar, W., R. Bingham, R. Iverson, D. Nowacek, L. St. Laurent, and P. Wiebe (2006). Does the marine biosphere mix the ocean? *Journal of Marine Research*, **64**:541–561, doi:10.1357/002224006778715720.

Doney, S. C. (2006). Plankton in a warmer world. *Nature*, **444**:695–696, doi:10.1038/444695a.

Duteil, O., A. Lazar, Y. Dandonneau, I. Wainer, and C. Menkes (2009). Deep chlorophyll maximum and upper ocean structure interactions: Case of the Guinea Thermal Dome. *Journal of Marine Research*, **67**:239–271, doi:10.1357/002224009789051191.

Edwards, A. M., T. Platt, and D. G. Wright (2001). Biologically induced circulation at fronts. *Journal of Geophysical Research*, **106**:7081–7095, doi:10.1029/2000JC000332.

Edwards, A. M., D. G. Wright, and T. Platt (2004). Biological heating effect of a band of phytoplankton. *Journal of Marine Systems*, **49**:89–103, doi:10.1016/j.jmarsys.2003.05.011.

Eifler, W. and W. Schrimpf (1992). Ispramix, a hydrodynamic program for computing regional sea circulation patterns and transfer processes. Tech. rep. eur 14856 en, European Commission Joint Reseach Center, Ispra, Italy.

Fairall, C. W., E. F. Bradley, D. P. Rogers, J. B. Edson, and G. S. Young (1996). Bulk parameterization of air-sea fluxes for Tropical Ocean-Global Atmosphere Coupled-Ocean Atmosphere Response Experiment. *Journal of Geophysical Research*, **101**:3747–3764, doi:10.1029/95JC03205.

Fofonoff, N. P. and R. Millard (1983). Algorithms for the computation of fundamental properties of seawater. *Unesco technical papers in marine sciences*, **44**:1–53.

Follows, M. J., T. Ito, and J. Marotzke (2002). The wind-driven, subtropical gyres and the solubility pump of CO_2. *Global Biogeochemical Cycles*, **16**:1113, doi:10.1029/2001GB001786.

Frouin, R. and S. F. Iacobellis (2002). Influence of phytoplankton on the global radiation

budget. *Journal of Geophysical Research*, **107**:4377, doi:10.1029/2001JD000562.

Gaspar, P., Y. Grégoris, and J.-M. Lefevre (1990). A simple eddy kinetic energy model for simulations of the oceanic vertical mixing: Tests at station Papa and long-term upper ocean study site. *Journal of Geophysical Research*, **95**:16179–16193, doi:10.1029/JC095iC09p16179.

Geider, R. and J. La Roche (2002). Redfield revisited: variability of C:N:P in marine microalgae and its biochemical basis. *European Journal of Phycology*, **37**:1–17, doi:10.1017/S0967026201003456.

Geider, R. J. (1987). Light and temperature dependence of the carbon to chlorophyll ratio in microalgae and cyanobacteria: Implications for physiology and growth of phytoplankton. *New Phytologist*, **106**:1–34, doi:10.1111/j.1469-8137.1987.tb04788.x.

Gent, P. R. and J. C. Mcwilliams (1990). Isopycnal mixing in ocean circulation models. *Journal of Physical Oceanography*, **20**:150–155, doi:10.1175/1520-0485(1990)020<0150:IMIOCM>2.0.CO;2.

Gent, P. R., J. Willebrand, T. J. McDougall, and J. C. McWilliams (1995). Parameterizing eddy-induced tracer transports in ocean circulation models. *Journal of Physical Oceanography*, **25**:463–474, doi:10.1175/1520-0485(1995)025<0463:PEITTI>2.0.CO;2.

Gildor, H. and N. H. Naik (2005). Evaluating the effect of interannual variations of surface chlorophyll on upper ocean temperature. *Journal of Geophysical Research*, **110**:C07012, doi:10.1029/2004JC002779.

Gildor, H., A. H. Sobel, M. A. Cane, and R. N. Sambrotto (2003). A role for ocean biota in tropical intraseasonal atmospheric variability. *Geophysical Research Letters*, **30**:1460–1463, doi:10.1029/2002GL016759.

Gnanadesikan, A. and W. G. Anderson (2009). Ocean water clarity and the ocean general circulation in a coupled climate model. *Journal of Physical Oceanography*, **39**:314–332, doi:10.1175/2008JPO3935.1.

Gnanadesikan, A., K. Emanuel, G. A. Vecchi, W. G. Anderson, and R. Hallberg (2010). How ocean color can steer Pacific tropical cyclones. *Geophysical Research Letters*, **37**:L18802, doi:10.1029/2010GL044514.

Gregg, W. W. and N. W. Casey (2007). Modeling coccolithophores in the global oceans. *Deep-Sea Research Part II: Topical Studies in Oceanography*, **54**:447–477.

Gruber, N. and J. L. Sarmiento (1997). Global patterns of marine nitrogen fixation and denitrification. *Global Biogeochemical Cycles*, **11**:235–266, doi:10.1029/97GB00077.

Haney, R. L. (1971). Surface thermal boundary condition for ocean circulation models. *Journal of Physical Oceanography*, **1**:241–248, doi:10.1175/1520-0485(1971)001<0241:STBCFO>2.0.CO;2.

Heinemann, M., A. Timmermann, and U. Feudel (2011). Interactions between marine biota and ENSO: a conceptual model analysis. *Nonlinear Processes in Geophysics*, **18**:29–40, doi:10.5194/npg-18-29-2011.

Hense, I. (2007). Regulative feedback mechanisms in cyanobacteria-driven systems: a model study. *Marine Ecology Progress Series*, **339**:41–47, doi:10.3354/meps339041.

Hense, I. and A. Beckmann (2008). Revisiting subsurface chlorophyll and phytoplankton distributions. *Deep-Sea Research Part I: Oceanographic Research Papers*, **55**:1193–1199, doi:10.1016/j.dsr.2008.04.009.

Hense, I., H. Meier, and S. Sonntag (2013). Projected climate change impact on Baltic Sea

cyanobacteria. *Climatic Change*, doi:10.1007/s10584-013-0702-y.

Hense, I. and B. Quack (2009). Modelling the vertical distribution of bromoform in the upper water column of the tropical Atlantic Ocean. *Biogeosciences*, **6**:535–544, doi:10.5194/bg-6-535-2009.

Holligan, P. M., E. Fernández, J. Aiken, W. M. Balch, P. Boyd, P. H. Burkill, M. Finch, S. B. Groom, G. Malin, K. Muller, D. A. Purdie, C. Robinson, C. C. Trees, S. M. Turner, and P. van der Wal (1993). A biogeochemical study of the coccolithophore, *Emiliania huxleyi*, in the North Atlantic. *Global Biogeochemical Cycles*, **7**:879–900, doi:10.1029/93GB01731.

Holligan, P. M., M. Viollier, D. S. Harbour, P. Camus, and M. Champagne-Philippe (1983). Satellite and ship studies of coccolithophore production along a continental shelf edge. *Nature*, **304**:339–342, doi:10.1038/304339a0.

Hood, R. R., V. J. Coles, and D. G. Capone (2004). Modeling the distribution of *Trichodesmium* and nitrogen fixation in the Atlantic Ocean. *Journal of Geophysical Research*, **109**:C06006, doi:10.1029/2002JC001753.

Huntley, M. and M. Zhou (2004). Influence of animals on turbulence in the sea. *Marine Ecology Progress Series*, **273**:65–79, doi:10.3354/meps273065.

Hutchins, D., M. Mulholland, and F. Fu (2009). Nutrient cycles and marine microbes in a CO_2-enriched ocean. *Oceanography*, **22**:128—145, doi:10.5670/oceanog.2009.103.

Hutchins, D. A., F.-X. Fu, Y. Zhang, M. Warner, Y. Feng, K. Portune, P. W. Bernhardt, and M. R. Mulholland (2007). CO_2 control of *Trichodesmium* N_2 fixation, photosynthesis, growth rates, and elemental ratios: Implications for past, present, and future ocean biogeochemistry. *Limnology and Oceanography*, **52**:1293–1304, doi:10.4319/lo.2007.52.4.1293.

Hutchinson, P. A. and I. T. Webster (1994). On the distribution of blue-green algae in lakes: Wind-tunnel tank experiments. *Limnology and Oceanography*, **39**:374–382.

Jenkinson, I. R. and B. A. Biddanda (1995). Bulk-phase viscoelastic properties of seawater relationship with plankton components. *Journal of Plankton Research*, **17**:2251–2274, doi:10.1093/plankt/17.12.2251.

Jerlov, N. G. (1968). *Optical oceanography*. Elsevier.

Jin, Z., T. P. Charlock, J. Smith, William L., and K. Rutledge (2004). A parameterization of ocean surface albedo. *Geophysical Research Letters*, **31**:L22301, doi:10.1029/2004GL021180.

Jochum, M., S. Yeager, K. Lindsay, K. Moore, and R. Murtugudde (2010). Quantification of the feedback between phytoplankton and ENSO in the Community Climate System Model. *Journal of Climate*, **23**:2916–2925, doi:10.1175/2010JCLI3254.1.

Jöhnk, K. D., J. Huisman, J. Sharples, B. Sommeijer, P. M. Visser, and J. M. Stroom (2008). Summer heatwaves promote blooms of harmful cyanobacteria. *Global Change Biology*, **14**:495–512, doi:10.1111/j.1365-2486.2007.01510.x.

Jolliff, J. K., T. A. Smith, C. N. Barron, S. deRada, S. C. Anderson, R. W. Gould, and R. A. Arnone (2012). The impact of coastal phytoplankton blooms on ocean-atmosphere thermal energy exchange: Evidence from a two-way coupled numerical modeling system. *Geophysical Research Letters*, **39**:L24607, doi:10.1029/2012GL053634.

Jones, C. G., J. H. Lawton, and M. Shachak (1994). Organisms as ecosystem engineers. *Oikos*, **69**:373–386.

Kahru, M., J. Leppänen, and O. Rud (1993). Cyanobacterial blooms cause heating of the sea surface. *Marine Ecology Progress Series*, **101**:1–7.

Kara, A. B., H. E. Hurlburt, P. A. Rochford, and J. J. OBrien (2004). The impact of water turbidity on interannual sea surface temperature simulations in a layered global ocean model. *Journal of Physical Oceanography*, **34**:345–359, doi:10.1175/1520-0485(2004)034<0345:TIOWTO>2.0.CO;2.

Kara, A. B., P. A. Rochford, and H. E. Hurlburt (2000). An optimal definition for ocean mixed layer depth. *Journal of Geophysical Research*, **105**:16803–16821, doi:10.1029/2000JC900072.

Kara, A. B., A. J. Wallcraft, and H. E. Hurlburt (2005). A new solar radiation penetration scheme for use in ocean mixed layer studies: An application to the Black Sea using a fine-resolution hybrid coordinate ocean model (HYCOM). *Journal of Physical Oceanography*, **35**:13–32, doi:10.1175/JPO2677.1.

Karl, D. M. (1999). A Sea of change: Biogeochemical variability in the North Pacific subtropical gyre. *Ecosystems*, **2**:181–214, doi:10.1007/s100219900068.

Karl, D. M., A. Michaels, B. Bergman, D. Capone, E. Carpenter, R. Letelier, F. Lipschultz, H. Paerl, D. Sigman, and L. Stal (2002). Dinitrogen fixation in the world's oceans. *Biogeochemistry*, **57-58**:47–98, doi:10.1023/A:1015798105851.

Katija, K. and J. O. Dabiri (2009). A viscosity-enhanced mechanism for biogenic ocean mixing. *Nature*, **460**:624–626, doi:10.1038/nature08207.

Kromkamp, J., M. De Bie, N. Goosen, J. Peene, P. Van Rijswijk, J. Sinke, and G. C. Duinevel (1997). Primary production by phytoplankton along the Kenyan coast during the SE monsoon and November intermonsoon 1992, and the occurrence of *Trichodesmium*. *Deep Sea Research Part II: Topical Studies in Oceanography*, **44**:1195–1212, doi:10.1016/S0967-0645(97)00015-5.

Kunze, E., J. F. Dower, I. Beveridge, R. Dewey, and K. P. Bartlett (2006). Observations of biologically generated turbulence in a coastal inlet. *Science*, **313**:1768–1770, doi:10.1126/science.1129378.

Kunze, E., J. F. Dower, R. Dewey, E. A. D'Asaro;, and A. W. Visser (2007). Mixing it up with krill. *Science*, **318**:1239, doi:10.1126/science.318.5854.1239b.

Large, W. G., J. C. McWilliams, and S. C. Doney (1994). Oceanic vertical mixing: A review and a model with a nonlocal boundary layer parameterization. *Reviews of Geophysics*, **32**:363–403.

LaRoche, J. and E. Breitbarth (2005). Importance of the diazotrophs as a source of new nitrogen in the ocean. *Journal of Sea Research*, **53**:67–91, doi:10.1016/j.seares.2004.05.005.

Lefèvre, N., A. H. Taylor, and R. J. Geider (2001). Phytoplankton physiology can affect ocean surface temperatures. *Geophysical Research Letters*, **28**:1251–1254, doi:10.1029/2000GL011509.

Lengaigne, M., G. Madec, L. Bopp, C. Menkes, O. Aumont, and P. Cadule (2009). Bio-physical feedbacks in the Arctic Ocean using an Earth system model. *Geophysical Research Letters*, **36**:L21602, doi:10.1029/2009GL040145.

Lengaigne, M., C. Menkes, O. Aumont, T. Gorgues, L. Bopp, J.-M. André, and G. Madec (2007). Influence of the oceanic biology on the tropical Pacific climate in a coupled general circulation model. *Climate Dynamics*, **28**:503–516, doi:10.1007/s00382-006-0200-2.

Lewis, M. R., M.-E. Carr, G. C. Feldman, W. Esaias, and C. McClain (1990). Influence of penetrating solar radiation on the heat budget of the equatorial Pacific Ocean. *Nature*, **347**:543–545, doi:10.1038/347543a0.

Lewis, M. R., J. J. Cullen, and T. Platt (1983). Phytoplankton and thermal structure in the upper ocean: Consequences of nonuniformity in chlorophyll profile. *Journal of Geophysical Research*, **88**:2565–2570, doi:10.1029/JC088iC04p02565.

Lin, P., H. Liu, and X. Zhang (2007). Sensitivity of the upper ocean temperature and circulation in the equatorial Pacific to solar radiation penetration due to phytoplankton. *Advances in Atmospheric Sciences*, **24**:765–780, doi:10.1007/s00376-007-0765-7.

Liu, H., H. Nolla, and L. Campbell (1997). *Prochlorococcus* growth rate and contribution to primary production in the equatorial and subtropical North Pacific Ocean. *Aquatic Microbial Ecology*, **12**:39–47, doi:10.3354/ame012039.

Lochte, K., H. Ducklow, M. Fasham, and C. Stienen (1993). Plankton succession and carbon cycling at 47°N 20°W during the JGOFS North Atlantic Bloom Experiment. *Deep Sea Research Part II: Topical Studies in Oceanography*, **40**:91–114, doi:10.1016/0967-0645(93)90008-B.

Löptien, U., C. Eden, A. Timmermann, and H. Dietze (2009). Effects of biologically induced differential heating in an eddy-permitting coupled ocean-ecosystem model. *Journal of Geophysical Research*, **114**:C06011, doi:10.1029/2008JC004936.

Löptien, U. and H. M. Meier (2011). The influence of increasing water turbidity on the sea surface temperature in the Baltic Sea: A model sensitivity study. *Journal of Marine Systems*, **88**:323–331, doi:10.1016/j.jmarsys.2011.06.001.

Luo, Y.-W., S. C. Doney, L. A. Anderson, M. Benavides, I. Berman-Frank, A. Bode, S. Bonnet, K. H. Boström, D. Böttjer, D. G. Capone, E. J. Carpenter, Y. L. Chen, M. J. Church, J. E. Dore, L. I. Falcón, A. Fernández, R. A. Foster, K. Furuya, F. Gómez, K. Gundersen, A. M. Hynes, D. M. Karl, S. Kitajima, R. J. Langlois, J. LaRoche, R. M. Letelier, E. Marañón, D. J. McGillicuddy Jr., P. H. Moisander, C. M. Moore, B. Mouriño-Carballido, M. R. Mulholland, J. A. Needoba, K. M. Orcutt, A. J. Poulton, E. Rahav, P. Raimbault, A. P. Rees, L. Riemann, T. Shiozaki, A. Subramaniam, T. Tyrrell, K. A. Turk-Kubo, M. Varela, T. A. Villareal, E. A. Webb, A. E. White, J. Wu, and J. P. Zehr (2012). Database of diazotrophs in global ocean: abundance, biomass and nitrogen fixation rates. *Earth System Science Data*, **4**:47–73, doi:10.5194/essd-4-47-2012.

Ma, J., H. Liu, H. Zhan, P. Lin, and Y. Du (2012). Effects of chlorophyll on upper ocean temperature and circulation in the upwelling regions of the South China Sea. *Aquatic Ecosystem Health & Management*, **15**:127–134, doi:10.1080/14634988.2012.687663.

Manizza, M. (2006). *Modelling phytoplankton-light feedback and its ocean biochemical implications*. Ph.D. thesis, School of Environmental Sciences of the University of East Anglia.

Manizza, M., C. Le Quéré, A. J. Watson, and E. T. Buitenhuis (2005). Bio-optical feedbacks among phytoplankton, upper ocean physics and sea-ice in a global model. *Geophysical Research Letters*, **32**:L05603, doi:10.1029/2004GL020778.

Manizza, M., C. Le Quéré, A. J. Watson, and E. T. Buitenhuis (2008). Ocean biogeochemical response to phytoplankton-light feedback in a global model. *Journal of Geophysical Research*, **113**:C10010, doi:10.1029/2007JC004478.

Mann, K. and J. Lazier (2006). *Dynamics of Marine Ecosystems: Biological-Physical Interactions in the Oceans*. Wiley-Blackwell, Boston, USA, 3rd ed.

Marañón, E., P. M. Holligan, M. Varela, B. Mouriño, and A. J. Bale (2000). Basin-scale variability of phytoplankton biomass, production and growth in the Atlantic Ocean. *Deep Sea Research Part I: Oceanographic Research Papers*, **47**:825–857, doi:10.1016/S0967-0637(99)00087-4.

Marshall, J., A. Adcroft, C. Hill, L. Perelman, and C. Heisey (1997). A finite-volume, incompressible Navier Stokes model for studies of the ocean on parallel computers. *Journal of Geophysical Research*, **102**:5753–5766, doi:10.1029/96JC02775.

Marzeion, B., A. Timmermann, R. Murtugudde, and F.-F. Jin (2005). Biophysical feedbacks in the tropical Pacific. *Journal of Climate*, **18**:58–70, doi:10.1175/JCLI3261.1.

McClain, C. R., J. R. Christian, S. R. Signorini, M. R. Lewis, I. Asanuma, D. Turk, and C. Dupouy-Douchement (2002). Satellite ocean-color observations of the tropical Pacific Ocean. *Deep-Sea Research Part II: Topical Studies in Oceanography*, **49**:2533–2560, doi:10.1016/S0967-0645(02)00047-4.

McClain, C. R., G. C. Feldman, and S. B. Hooker (2004). An overview of the SeaWiFS project and strategies for producing a climate research quality global ocean bio-optical time series. *Deep Sea Research Part II: Topical Studies in Oceanography*, **51**:5–42, doi:10.1016/j.dsr2.2003.11.001.

Miller, A. J., M. A. Alexander, G. J. Boer, F. Chai, K. Denman, D. J. Erickson, R. Frouin, A. J. Gabric, E. A. Laws, M. R. Lewis, Z. Liu, R. Murtugudde, S. Nakamoto, D. J. Neilson, J. R. Norris, J. C. Ohlmann, R. I. Perry, N. Schneider, K. M. Shell, and A. Timmermann (2003). Potential feedbacks between Pacific Ocean ecosystems and interdecadal climate variations. *Bulletin of the American Meteorological Society*, **84**:617–633, doi:10.1175/BAMS-84-5-617.

Mobley, C. D. and E. S. Boss (2012). Improved irradiances for use in ocean heating, primary production, and photo-oxidation calculations. *Applied Optics*, **51**:6549–6560, doi:10.1364/AO.51.006549.

Monteiro, F. M., M. J. Follows, and S. Dutkiewicz (2010). Distribution of diverse nitrogen fixers in the global ocean. *Global Biogeochemical Cycles*, **24**:GB3017, doi:10.1029/2009GB003731.

Morel, A. (1988). Optical modeling of the upper ocean in relation to its biogenous matter content (case I waters). *Journal of Geophysical Research*, **93**:10749–10768, doi:10.1029/JC093iC09p10749.

Morel, A. and D. Antoine (1994). Heating rate within the upper ocean in relation to its bio-optical state. *Journal of Physical Oceanography*, **24**:1652–1665, doi:10.1175/1520-0485(1994)024<1652:HRWTUO>2.0.CO;2.

Munk, W. H. (1966). Abyssal recipes. *Deep Sea Research and Oceanographic Abstracts*, **13**:707–730, doi:10.1016/0011-7471(66)90602-4.

Murtugudde, R., J. Beauchamp, C. R. McClain, M. Lewis, and A. J. Busalacchi (2002). Effects of penetrative radiation on the upper tropical ocean circulation. *Journal of Climate*, **15**:470–486, doi:10.1175/1520-0442(2002)015<0470:EOPROT>2.0.CO;2.

Nakamoto, S., S. P. Kumar, J. M. Oberhuber, J. Ishizaka, K. Muneyama, and R. Frouin (2001). Response of the equatorial Pacific to chlorophyll pigment in a mixed layer isopycnal ocean general circulation model. *Geophysical Research Letters*, **28**:2021–

2024, doi:10.1029/2000GL012494.

Ohlmann, J. C. (2003). Ocean radiant heating in climate models. *Journal of Climate*, **16**:1337–1351, doi:10.1175/1520-0442-16.9.1337.

Ohlmann, J. C. and D. A. Siegel (2000). Ocean radiant heating. Part II: Parameterizing solar radiation transmission through the upper ocean. *Journal of Physical Oceanography*, **30**:1849–1865, doi:10.1175/1520-0485(2000)030<1849:ORHPIP>2.0.CO;2.

Olbers, D., J. Willebrand, and C. Eden (2012). *Ocean Dynamics*. Springer, Heidelberg, doi:10.1007/978-3-642-23450-7.

Oschlies, A. (2004). Feedbacks of biotically induced radiative heating on upper-ocean heat budget, circulation, and biological production in a coupled ecosystem-circulation model. *Journal of Geophysical Research*, **109**:C12031, doi:10.1029/2004JC002430.

Paerl, H. W. and J. Huisman (2008). Climate: Blooms like it hot. *Science*, **320**:57–58, doi:10.1126/science.1155398.

Park, J.-Y. and J.-S. Kug (2013). Marine biological feedback associated with Indian Ocean Dipole in a coupled ocean/biogeochemical model. *Climate Dynamics*, doi:10.1007/s00382-012-1640-5.

Park, J.-Y., J.-S. Kug, J. Park, S.-W. Yeh, and C. J. Jang (2011). Variability of chlorophyll associated with El Niño Southern Oscillation and its possible biological feedback in the equatorial Pacific. *Journal of Geophysical Research*, **116**:C10001, doi:10.1029/2011JC007056.

Patara, L., M. Vichi, S. Masina, P. Fogli, and E. Manzini (2012). Global response to solar radiation absorbed by phytoplankton in a coupled climate model. *Climate Dynamics*, **39**:1951–1968, doi:10.1007/s00382-012-1300-9.

Paulson, C. A. and J. J. Simpson (1977). Irradiance measurements in the upper ocean. *Journal of Physical Oceanography*, **7**:952–956, doi:10.1175/1520-0485(1977)007<0952:IMITUO>2.0.CO;2.

Payne, R. E. (1972). Albedo of the sea surface. *Journal of the Atmospheric Sciences*, **29**:959–970, doi:10.1175/1520-0469(1972)029<0959:AOTSS>2.0.CO;2.

Ramp, S. R., R. W. Garwood, C. O. Davis, and R. L. Snow (1991). Surface heating and patchiness in the coastal ocean off central California during a wind relaxation event. *Journal of Geophysical Research*, **96**:14,947–14,957, doi:10.1029/91JC01140.

Redi, M. H. (1982). Oceanic isopycnal mixing by coordinate rotation. *Journal of Physical Oceanography*, **12**:1154–1158, doi:10.1175/1520-0485(1982)012<1154:OIMBCR>2.0.CO;2.

Reed, R. K. (1977). On estimating insolation over the ocean. *Journal of Physical Oceanography*, **7**:482–485, doi:10.1175/1520-0485(1977)007<0482:OEIOTO>2.0.CO;2.

Riley, G. (1946). Factors controlling phytoplankton populations on Georges Bank. *Journal of Marine Research*, **6**:54–73.

Rochford, P. A., A. B. Kara, A. J. Wallcraft, and R. A. Arnone (2001). Importance of solar subsurface heating in ocean general circulation models. *Journal of Geophysical Research*, **106**:30923–30938, doi:10.1029/2000JC000355.

Rodi, W. (1987). Examples of calculation methods for flow and mixing in stratified fluids. *Journal of Geophysical Research*, **92**:5305–5328, doi:10.1029/JC092iC05p05305.

Rosati, A. and K. Miyakoda (1988). A general circulation model for upper ocean simulation. *Journal of Physical Oceanography*, **18**:1601–1626, doi:10.1175/1520-

0485(1988)018<1601:AGCMFU>2.0.CO;2.

Sathyendranath, S., A. D. Gouveia, S. R. Shetye, P. Ravindran, and T. Platt (1991). Biological control of surface temperature in the Arabian Sea. *Nature*, **349**:54–56, doi:10.1038/349054a0.

Sathyendranath, S., V. Stuart, A. Nair, K. Oka, T. Nakane, H. Bouman, M. Forget, H. Maass, and T. Platt (2009). Carbon-to-chlorophyll ratio and growth rate of phytoplankton in the sea. *Marine Ecology Progress Series*, **383**:73–84, doi:10.3354/meps07998.

Schneider, E. K. and Z. Zhu (1998). Sensitivity of the simulated annual cycle of sea surface temperature in the equatorial Pacific to sunlight penetration. *Journal of Climate*, **11**:1932–1950, doi:10.1175/1520-0442(1998)011<1932:SOTSAC>2.0.CO;2.

Seuront, L., C. Lacheze, M. Doubell, J. Seymour, V. Van Dongen-Vogels, K. Newton, A. Alderkamp, and J. Mitchell (2007). The influence of *Phaeocystis globosa* on microscale spatial patterns of chlorophyll. *Biogeochemistry*, **83**:173–188, doi:10.1007/s10533-007-9097-z.

Shell, K. M., R. Frouin, S. Nakamoto, and R. C. J. Somerville (2003). Atmospheric response to solar radiation absorbed by phytoplankton. *Journal of Geophysical Research*, **108(D15)**:4445, doi:10.1029/2003JD003440.

Sieburth, J. M. and J. T. Conover (1965). Slicks associated with *Trichodesmium* blooms in the Sargasso Sea. *Nature*, **205**:830–831, doi:10.1038/205830b0.

Siegel, D. A., J. C. Ohlmann, L. Washburn, R. R. Bidigare, C. T. Nosse, E. Fields, and Y. Zhou (1995). Solar radiation, phytoplankton pigments and the radiant heating of the equatorial Pacific warm pool. *Journal of Geophysical Research*, **100**:4885–4891, doi:10.1029/94JC03128.

Simonot, J.-y., E. Dollinger, and H. Le Treut (1988). Thermodynamic-biological-optical coupling in the oceanic mixed layer. *Journal of Geophysical Research*, **93**:8193–8202, doi:10.1029/JC093iC07p08193.

Smith, E. (1936). Photosynthesis in relation to light and carbon dioxide. *Proceedings of the National Academy of Sciences of the United States of America*, **22**:504–511, doi:10.1073/pnas.22.8.504.

Smith, R. C. and K. S. Baker (1978). The bio-optical state of ocean waters and remote sensing. *Limnology and Oceanography*, **23**:247–259.

Sohm, J. A., C. Mahaffey, and D. G. Capone (2008). Assessment of relative phosphorus limitation of *Trichodesmium* spp. in the North Pacific, North Atlantic, and the north coast of Australia. *Limnology and Oceanography*, **53**:2495–2502, doi:10.4319/lo.2008.53.6.2495.

Sonntag, S. and I. Hense (2011). Phytoplankton behavior affects ocean mixed layer dynamics through biological-physical feedback mechanisms. *Geophysical Research Letters*, **38**:L15610, doi:10.1029/2011GL048205.

Stal, L. J. (2009). Is the distribution of nitrogen-fixing cyanobacteria in the oceans related to temperature? *Environmental Microbiology*, **11**:1632–1645, doi:10.1111/j.1758-2229.2009.00016.x.

Stramska, M. and T. D. Dickey (1993). Phytoplankton bloom and the vertical thermal structure of the upper ocean. *Journal of Marine Research*, **51**:819–842, doi:10.1357/0022240933223918.

Strutton, P. G. and F. P. Chavez (2004). Biological heating in the equatorial Pacific:

Observed variability and potential for real-time calculation. *Journal of Climate*, **17**:1097–1109, doi:10.1175/1520-0442(2004)017<1097:BHITEP>2.0.CO;2.

Subrahmanyam, B., K. Ueyoshi, and J. M. Morrison (2008). Sensitivity of the Indian Ocean circulation to phytoplankton forcing using an ocean model. *Remote Sensing of Environment*, **112**:1488–1496, doi:10.1016/j.rse.2007.05.021.

Subramanian, G. (2010). Viscosity-enhanced bio-mixing of the oceans. *Current Science*, **98**:1103–1108.

Sweeney, C., A. Gnanadesikan, S. M. Griffies, M. J. Harrison, A. J. Rosati, and B. L. Samuels (2005). Impacts of shortwave penetration depth on large-scale ocean circulation and heat transport. *Journal of Physical Oceanography*, **35**:1103–1119, doi:10.1175/JPO2740.1.

Tian, R. C. (2006). Toward standard parameterizations in marine biological modeling. *Ecological Modelling*, **193**:363–386, doi:10.1016/j.ecolmodel.2005.09.003.

Timmermann, A. and F.-F. Jin (2002). Phytoplankton influences on tropical climate. *Geophysical Research Letters*, **29**:2104, doi:10.1029/2002GL015434.

Trevisan, O. V. and A. Bejan (1986). Convection driven by the nonuniform absorption of thermal radiation at the free surface of a stagnant pool. *Numerical Heat Transfer, Part B: Fundamentals*, **10**:483–506, doi:10.1080/10407788608913530.

Turner, A., M. Joshi, E. Robertson, and S. Woolnough (2012). The effect of Arabian Sea optical properties on SST biases and the South Asian summer monsoon in a coupled GCM. *Climate Dynamics*, **39**:811–826, doi:10.1007/s00382-011-1254-3.

Tyrrell, T., P. M. Holligan, and C. D. Mobley (1999). Optical impacts of oceanic coccolithophore blooms. *Journal of Geophysical Research*, **104**:3223–3241, doi:10.1029/1998JC900052.

Tyrrell, T., E. Marañón, A. J. Poulton, A. R. Bowie, D. S. Harbour, and E. M. S. Woodward (2003). Large-scale latitudinal distribution of *Trichodesmium* spp. in the Atlantic Ocean. *Journal of Plankton Research*, **25**:405–416, doi:10.1093/plankt/25.4.405.

Ueyoshi, K., R. Frouin, S. Nakamoto, and B. Subrahmanyam (2005). Sensitivity of equatorial Pacific Ocean circulation to solar radiation absorbed by phytoplankton. In *SPIE Proceedings, Remote Sensing of the Coastal Oceanic Environment*, vol. 5885. SPIE, San Diego, CA, USA.

Umlauf, L., H. Burchard, and K. Bolding (2005). General Ocean Turbulence Model. Scientific documentation. v3.2. Marine Science Reports 63, Baltic Sea Research Institute Warnemünde, Warnemünde, Germany.

Uppala, S. M., P. W. Kållberg, A. J. Simmons, U. Andrae, V. D. C. Bechtold, M. Fiorino, J. K. Gibson, J. Haseler, A. Hernandez, G. A. Kelly, X. Li, K. Onogi, S. Saarinen, N. Sokka, R. P. Allan, E. Andersson, K. Arpe, M. A. Balmaseda, A. C. M. Beljaars, L. V. D. Berg, J. Bidlot, N. Bormann, S. Caires, F. Chevallier, A. Dethof, M. Dragosavac, M. Fisher, M. Fuentes, S. Hagemann, E. Hólm, B. J. Hoskins, L. Isaksen, P. A. E. M. Janssen, R. Jenne, A. P. Mcnally, J.-F. Mahfouf, J.-J. Morcrette, N. A. Rayner, R. W. Saunders, P. Simon, A. Sterl, K. E. Trenberth, A. Untch, D. Vasiljevic, P. Viterbo, and J. Woollen (2005). The ERA-40 re-analysis. *Quarterly Journal of the Royal Meteorological Society*, **131**:2961–3012, doi:10.1256/qj.04.176.

Visser, A. W. (2007). Biomixing of the Oceans? *Science*, **316**:838–839,

doi:10.1126/science.1141272.

Wasmund, N. (1997). Occurrence of cyanobacterial blooms in the Baltic Sea in relation to environmental conditions. *Internationale Revue der gesamten Hydrobiologie und Hydrographie*, **82**:169–184, doi:10.1002/iroh.19970820205.

Westberry, T. K. and D. A. Siegel (2006). Spatial and temporal distribution of *Trichodesmium* blooms in the world's oceans. *Global Biogeochemical Cycles*, **20**:GB4016, doi:10.1029/2005GB002673.

Wetzel, P., E. Maier-Reimer, M. Botzet, J. Jungclaus, N. Keenlyside, and M. Latif (2006). Effects of ocean biology on the penetrative radiation in a coupled climate model. *Journal of Climate*, **19**:3973–3987, doi:10.1175/JCLI3828.1.

Wu, Y., C. C. Tang, S. Sathyendranath, and T. Platt (2007). The impact of bio-optical heating on the properties of the upper ocean: A sensitivity study using a 3-D circulation model for the Labrador Sea. *Deep-Sea Research Part II: Topical Studies in Oceanography*, **54**:2630–2642, doi:10.1016/j.dsr2.2007.08.019.

Zeebe, R. E., H. Eicken, D. H. Robinson, D. Wolf-Gladrow, and G. S. Dieckmann (1996). Modeling the heating and melting of sea ice through light absorption by microalgae. *Journal of Geophysical Research*, **101**:1163–1181, doi:10.1029/95JC02687.

Zehr, J. P. (2011). Nitrogen fixation by marine cyanobacteria. *Trends in Microbiology*, **19**:162–173, doi:10.1016/j.tim.2010.12.004.

Zhai, L., C. Tang, T. Platt, and S. Sathyendranath (2011). Ocean response to attenuation of visible light by phytoplankton in the Gulf of St. Lawrence. *Journal of Marine Systems*, **88**:285–297, doi:10.1016/j.jmarsys.2011.05.005.

Zhang, R.-H., A. J. Busalacchi, X. Wang, J. Ballabrera-Poy, R. G. Murtugudde, E. C. Hackert, and D. Chen (2009). Role of ocean biology-induced climate feedback in the modulation of El Niño-Southern Oscillation. *Geophysical Research Letters*, **36**:L03608, doi:10.1029/2008GL036568.

Acknowledgments

I would like to thank my advisor Inga Hense for giving me the opportunity to work on this topic, for her guidance, support, and confidence, and for always having time and being open for discussions. I also thank Carsten Eden for giving useful advice and feedback and for serving as a reviewer of this thesis. Special thanks go to Katharina Six for being part of my advisory panel and giving valuable advice and feedback as well as to Michael Schatzmann for serving as my advisory panel chair. I thank Nils Brüggemann and Lars Czeschel for lots of support concerning the physical model setup in MITgcm and Christoph Völker for help with setting up the biological model in MITgcm. Thanks also to Jorn Bruggeman for helpful discussions on the feedback parameterizations and to Jef Huisman for the helpful review of the article Chapter 2 is based on.

I thank Aike Beckmann, Nils Brüggemann, Florian Rauser, Katharina Six, Irene Stemmler, and Bettina Walter for proof-reading and making very helpful comments on this thesis.

I thank the School of Integrated Climate System Science and the Cluster of Excellence CliSAP of the University of Hamburg, funded through the German Research Foundation (DFG), for financial support.

Special thanks go to Florian and all others involved in YESS community and/or ICYESS 2013 activities. Working with you guys was and still is great fun.

Many thanks go to my former office mate Alexandra Warns (aka Kroll) for a great balance of work and distractions (from my side). I also thank all other fellow PhD students, colleagues and friends at IHF for a relaxed atmosphere, enjoyable lunch breaks in the GE kitchen or at the Elbe aquarium, table tennis sessions, and great Christmas parties! Thanks also go to all other people I had the pleasure to meet during my PhD time.

I thank the Blau-Gelb/Max-Planck tennis team for lots of nice matches and fun times on and next to the tennis court.

I thank Jutta, Klaus, Lisa, Maren, Bernd, Tim, and Mats, and especially my family, Gabi, Valentin, Philipp & Cemsy, for always supporting me and being there.

Thank you, Laura, for always being there!

Erklärung

Hiermit versichere ich, dass ich die vorgelegte Dissertation selbständig angefertigt habe, keine anderen als die angegebenen Quellen und Hilfsmittel benutzt habe und die den benutzten Werken wörtlich oder inhaltlich entnommenen Stellen als solche kenntlich gemacht habe.

Sebastian Sonntag